Doctoral Dissertation
Doctoral Program in Environmental and Civil Engineering (32.th cycle)

A new flat jack test for evaluating shear properties on unreinforced masonry

Nicola Viale
* * * * * *

Supervisors
Prof. G. Ventura - Polytechnic University of Turin
Prof. P. B. Lourenço - University of Minho

Doctoral Examination Committee:
Prof. M. Fagone, Referee, University of Florence
Prof. G. Mirabella Roberti, Referee, University of Bergamo
Prof. M. Corrado, Polytechnic University of Turin
Prof. L. Jurina, Polytechnic University of Milan
Prof. D. V. Oliveira, University of Minho

Politecnico di Torino
September, 2020

I hereby declare that the contents and organisation of this dissertation constitute my own original work and does not compromise in any way the rights of third parties, including those relating to the security of personal data.

. . . . . .

Nicola Viale
Turin, September, 2020

Summary

Unreinforced masonry structures represent the large part of the existing buildings in many countries. Some of these countries belong to regions were high seismic hazard is present. Due to the high mass of these structures, the seismic action can be the most demanding [104]. If the out-of-plane failure mechanisms of a structure are avoided, the resisting mechanism to horizontal action has to be assured. The distribution of the forces in the resisting elements is dependent on the shear capacity of the media [181] and the failure of these elements is characterized by diagonal tension cracking [16]. These structures may need retrofitting, conservation, safety assessments, etc. For these reasons, the mechanical characterization of the shear modulus and of the tensile strength is necessary. These properties are usually measured using destructive tests that can be incompatible with some structures and are quite expensive. Therefore, the necessity of a minor destructive test for evaluating the shear modulus and the tensile strength of masonry structures is clear.

To achieve this goal, a new minor destructive test (Shear *FJ* test) was conceived using the flat jack technique. *FEM* analyses were utilized in order to define the best geometrical configuration that was defined considering the destructiveness, costs and effectiveness of each layout. Once the best layout was found, a parametric study of the test was performed giving as result tools to evaluate principal stresses of the sample and a method to measure the shear modulus.

The test method was then designed and successfully applied on five in situ experiments.

Linear and non-linear numerical analyses were performed to analyze the experimental results. In particular, the analyses were performed to understand the ability of the Shear *FJ* test to measure the tensile strength and the shear modulus.

Further tests and the analyses of the results obtained here will give a definitive response to understand the effectiveness of the Shear *FJ* test.

Acknowledgements

Vorrei ringraziare il Professor Ventura che mi ha seguito, aiutato e consigliato in questo lavoro. Non conoscevo il Professore prima di iniziare questa esperienza e sono stato rimasto molto colpito.

I would like to thank Professor Lourenço that hosted me in UMinho. He taught to me many things and he let me found a beautiful academic environment.

Many thanks also to Javier. I was really lucky to have you as a supervisor.

I am also thankful to Cismondi SRL, Arcos Engineering SRL, the city of Boves, the "Agenzia del Demanio" and to the *MiBAC*.

Grasie a Mare, Pare, Giulia, Nonu, Nona e Eloy. Smia nen ma m'eve giutà tantu. Chi 'n nà manera chi 'n nauta ma seve stet empurtant per pusè finii stu travaj. *Ma ura travaies o studies en co?*

I am really really thankful to Mara. She was an important part of the end of this work. Your suggestions and support were extremely important as well as the tips to go back on track without losing my mind. Muito Obrigado.

Thank you to all the persons that in Portugal made me felt like I was at home and that did the same here in Torino: Aaron, Abide, Alban, Alberto, Alessandra, Alessandro, Alice, Anna Maria, Antonio M., Antonio R., Arezu, Bea, Carolina, Chandan, Claudia, Claudio, Daniele, Dmytro, Duaa, Elesban, Elisabete, Fabio, Federico A., Federico R., Franceso M., Franceso P., Giacomo, Giovanni, Giulia, Giuseppe, Jennifer, Kee, Lidia, Luis, Maria Jose, Maria Pia, Mariacarla, Maxime, Matteo, Meera, Nicoletta, Pilar, Pratik, Rafael, Reza, Satya, Telma, Thais, Thomas, Xinyu and all the ones that I forgot.

I would like to dedicate this thesis to my loving parents

The time to repair the roof is when the sun is shining.

John F. Kennedy

Sábio é o que se contenta com o espectáculo do mundo

Ricardo Reis

Contents

List of Figures

List of Tables

Chapter 1

Introduction

Unreinforced masonry (*URM*) represents one of the most diffuse construction system. In addition, this technique is also one of the oldest methods for humanity to build a shelter. This construction system was used (and many times it is still adopted) to build from small residential/civil houses to bridges, temples, churches, aqueducts, theaters, royal palaces, etc. Examples of the application of this material can be found in a large number of countries around the world.

1.1 Overview

As introduced, *URM* was used in history but also in present time. A lot of old structures made with this material are still present and many of them are still used. Italy can be chosen as an example. The National Institution of Statistic (*ISTAT*) evaluated the residential buildings present in Italy. Figure 1.1 presents the evolution in the last century of the constructions in Italy. This graph shows the age and the percentage of the structures divided by typologies of construction: masonry, concrete and others (wood, steel, etc.). It is possible to observe that the existing masonry structures in Italy represent the 57% of the constructions. 24% of the Italian masonry structures (representing 14% of all of the buildings) have more than a century. Moreover, 73% of the masonry constructions (40% of the total) have more than 50 years. It has to be said that, in addition to these residential buildings, there are many structures with even bigger value. It can be understandable that, by extension, a similar situation can be found it the Mediterranean area and not only there (e.g. [50]).

As it can be observed in Figure 1.1 many of these structures are old. For this reason *URM* structures may need conservation, retrofitting, safety assessments, evaluations of seismic vulnerability, etc. (e.g. [45, 50, 54, 96, 97]). It is now clear the importance of a good mechanical characterization.

Masonry has many characteristics that make it, at the same time, interesting and difficult to study it. For example, masonry is usually made with two elements: the resisting element (masonry unit) and the mortar. However, in literature many combinations of different materials used for these elements are present and each combination brings different characteristics of the media. In parallel to this, the behavior of the masonry could depend on texture, aging, humidity, strain rate, load history, manufacturing, etc. [23,

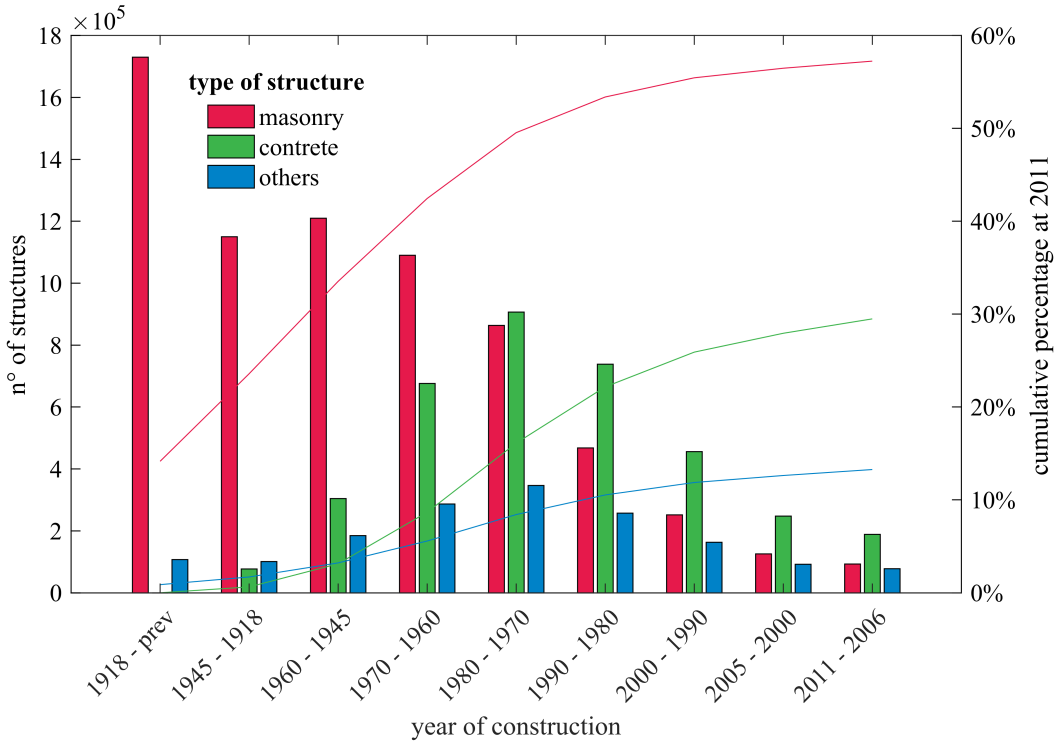

Figure 1.1: Summary of the Italian residential structures from Census in 2011 (*ISTAT*). The bars indicate the number of structures in 2011 subdivided by their built decade. The lines represent the cumulative percentage of structures with respect to the total number of structures present in 2011.

113, 180]. It has to be underlined that all of these boundary/initial conditions influence directly the mechanical characteristics of the media.

URM constructions are vulnerable to seismic actions [104]. This problem is due to the low tensile strength of the material and that these buildings are usually massive. In Figure 1.2 It is possible to appreciate that the Mediterranean area shows a high seismic hazard. This combination, of old *URM* structures and seismic hazard, leads to a high risk. Moreover, this issue is not only present in the Mediterranean area, in fact, high risk appears in other regions and countries of the world (e.g. Kashmir, Iran, Pakistan, Himalaya, Turkey, Andes, etc.).

The low tensile strength of masonry is usually displayed with diagonal cracks in panels after earthquakes actions [16]. These fissures are present in load-bearing windows piers or walls [181, 184]. The diagonal failure of a panel can be reached with two different mechanisms: sliding shear and diagonal tension-shear. The first mechanism is characterized by the relative sliding of the resisting elements over the mortar joints (bed and vertical). This mechanism is not controlled by the resistance of the blocks because the failure takes place in the mortar joints. The diagonal tension-shear mechanism, on the contrary, depends from both resisting elements and joints. It has to be underlined that the shear failure can also happen due to a third mechanism that consists in the shear slide in a single bed joint [181]. All these mechanisms can take place only if the masonry does not disintegrate (meaning that all the elements are well bonded together) and

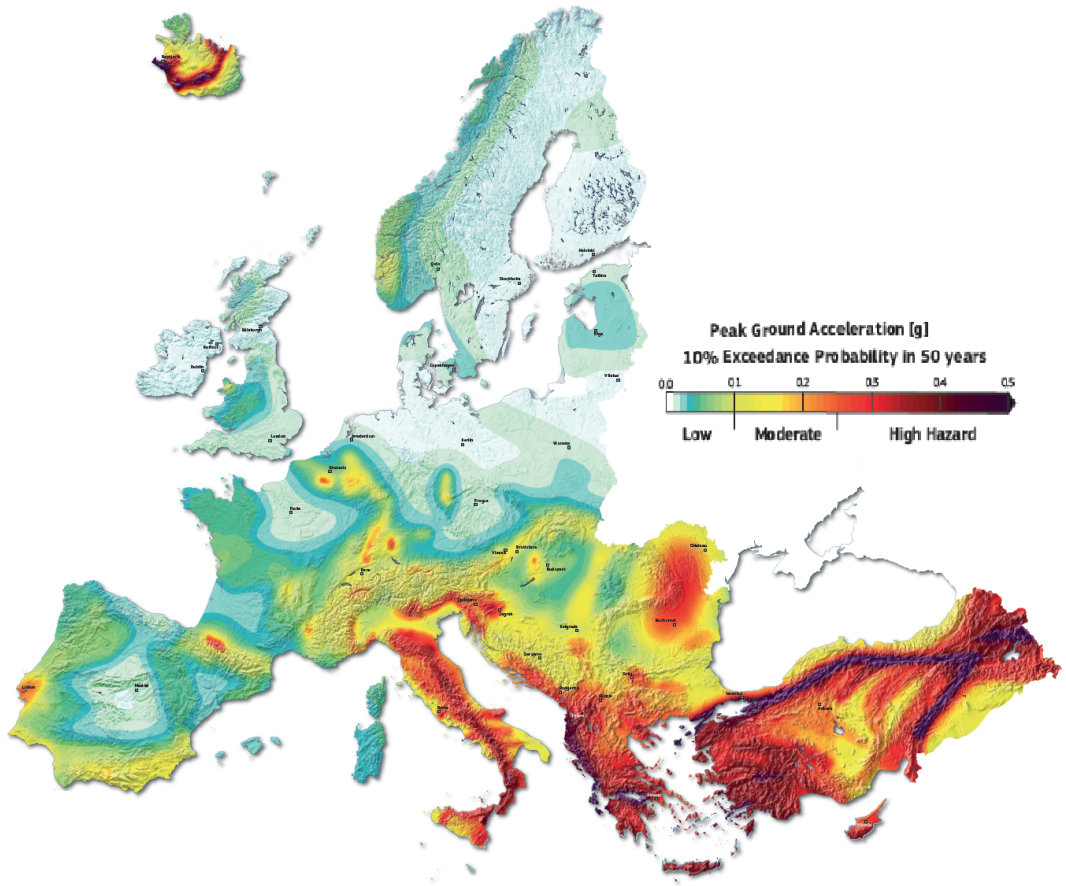

Figure 1.2: European seismic hazard considering 10% exceedance probability in 50 years [75].

if out-of-plane mechanisms do not take place.

The shear-tensile characteristics can be improved with different techniques, for example, improving the quality of the mortar and/or of the existing elements [184], confining the walls at the top and at the end [184], enlarging the cross area of the wall [184], using mortar rendering (e.g. [60]), using Fiber Reinforced Polymers (*FRP*) (e.g. [119]), etc. These retrofitting methods are expensive and sometimes they have an important impact in the aesthetic of the structure. Thus, it is important to measure the tensile strength and shear modulus of masonry in order to understand if a retrofitting is needed or to design it. Attention should be paid to costs, to the aesthetic impact and to the functionality of the structure.

The evaluation of the shear modulus and of the tensile strength in existing masonry structures is usually performed with two standard tests. These tests, namely, the Shear-compression test and the Diagonal test, are characterized by a massive impact on the structure. In fact, to carry out these tests, large masonry panels ($\sim 1-2$ m sides) have to be partially isolated from walls. After that the isolation is performed, the test is usually carried out at high stresses giving as result a high damage in the sample. Furthermore, the isolation can damage the sample and it surely damages the aesthetic of the wall. It results understandable that these tests are not suitable in all the structures and in all

situations.

1.2 Objectives

The present work aims to design a new moderate destructive test dedicated to the evaluation of the shear mechanical properties. In particular, the objectives were to measure the shear modulus, to evaluate the tensile strength in a 45° inclined plane, to reduce invasiveness and to limit costs of the test. To achieve these goals, it was decided to use the Flat Jack (*FJ*) technique. This method is known as a low impacting test and it is used not only for masonry structures.

1.3 Thesis content

A brief summary of the thesis content is present in this Section. In particular, the thesis is developed as follows:

- Chapter 2. In this Chapter, a state of the art is presented. In particular, are discussed aspects related to the importance of the shear-tensile properties, usually adopted tests for the mechanical characterization, bases of numerical modeling and codes.
- Chapter 3. The design of the test is here presented as well as the numerical results of the parametric analysis and the tools needed to evaluate the shear modulus and the tensile strength.
- Chapter 4. This Chapter reports the proposed test method and the results obtained with the in situ experiments. In addition, Acoustic Emission results are also shown.
- Chapter 5. The linear and non-linear analyses performed in order to understand the experimental results are here presented. In particular, these analyses were performed on micro and macro-models.
- Chapter 6. In this Chapter the conclusions about the work performed are presented.
- Appendix A. In the Appendix some details and more information about the results of the in situ tests and of the test design are given.

Chapter 2

Literature review

As introduced, the shear modulus and the tensile strength affect the behavior of masonry constructions. It has to be underlined that the shear (tension) failure of a masonry panel could be reached by diagonal (tension) shear cracking or by horizontal bed joint failure [16, 48, 181]. However, the diagonal (tension) shear failure is the most critical [181].

This Chapter is a partial review on the state of the art regarding the studies on masonry structures. A summary of all the efforts done until now which has the scope of increasing the knowledge in masonry constructions would be a huge work and partially useless considering the topic of the present dissertation. These facts justify why a large study on the state of the art is not presented. However, this Chapter provides a brief but exhaustive review on basic information, main features of this material, mechanical characterization, numerical modeling, standards and codes. Some of the following Sections give only a general overview of this construction material. On the contrary, the other Sections focus the attention on the main object of the work giving the opportunity of exploring deeper the tools that played an important role in the present work.

2.1 Background information

Masonry structures represent one of the more complex and diffused construction systems. Unreinforced masonry was (and still is) used for a large number of purposes, from simple houses and civil buildings to bridges and cathedrals. Therefore, the structural performances of the material were designed in accordance with the scope of the structure. The behavior of this laid structural system varies in dependence on a large number of parameters. Therefore, it is necessary to know the main types of *URM*, some nomenclature [13] and classifications basics even if a universal classification of all the different masonry types is absent [94]. These are briefly presented in the following paragraphs.

One of the possible classifications divides the masonry typologies considering their mechanical behavior. Binda et al. [24] suggest that a first idea of the behavior of a masonry wall can be deduced considering:

- the geometry;

- the characteristics of the following aspects: texture, cross-section, connections between the leaves; joints (empty or filled with mortar); physical, chemical and mechanical characteristics of the components (bricks, stones, mortar);
- the characteristics of masonry as a composite material.

This classification is already very difficult to apply. Considering, for example, a historical structure, it is hard to have the possibility of characterizing its components because this implies the removal of some resisting elements and/or joints. This operation can influence the aesthetic of the structure. Moreover, this classification considers as a key aspect the mechanical behavior but this cannot be useful for all the applications. In addition to this, the great number of materials, technologies, abilities and cultures has generated a large number of different masonry typologies.

The *ASTM* [13] defines masonry as a type of construction made of masonry units laid with mortar, grout or other methods of joints. A possible interpretation of this definition is that a material that joints the resisting elements is always present in the masonry. This is not true. In fact, in one of the oldest methods of masonry construction, named dry stack, the joints are void [59, 98, 172, 185]. Moreover, there is another method of construction named rammed earth (walls made in frameworks compacting moldable materials like clay added with gravel and sand) where joints are not even present or at least it is difficult to define them as such unlike other typologies of masonry. Therefore, the only feature that is common to all types of masonry is the presence of resisting elements that can be used for the classification. In fact, the resisting elements can be made only of natural or artificial elements that are stones and bricks. Carbonara [76] presents a classification that takes into account the resisting elements and divides them into stones, un-fired bricks, fired bricks and formacei walls. It must be considered now the not remote possibility of masonry composed by both artificial and natural elements and the combination with different joint techniques.

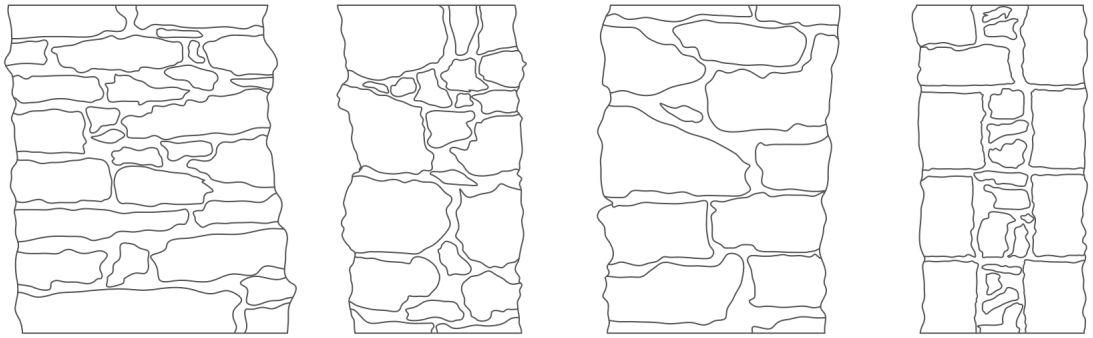

Figure 2.1: The image illustrates examples of different cross-section in stone masonry. Starting from the left it is possible to distinguish single-leaf, double-leaf without and with interlocking and three leaves.

The differences in the types of masonry constructions are not only given by the usage of different materials (that for some structures is imposed by the local possibilities) but they also depend on the different techniques used [24]. Considering as an example

the cross-sections of different stone walls (Fig. 2.1), it is possible to classify four principal techniques that are single-leaf, double-leaf (without and with interlocking) and three leaves. These different cross-sections lead to different mechanical behaviors. In fact, the presence of multiple leaves leads to a non-monolithic behavior of the wall for the out-of-plane actions (Fig. 2.2). However, the presence of some transverse connection elements (called header) can restore a single-leaf behavior.

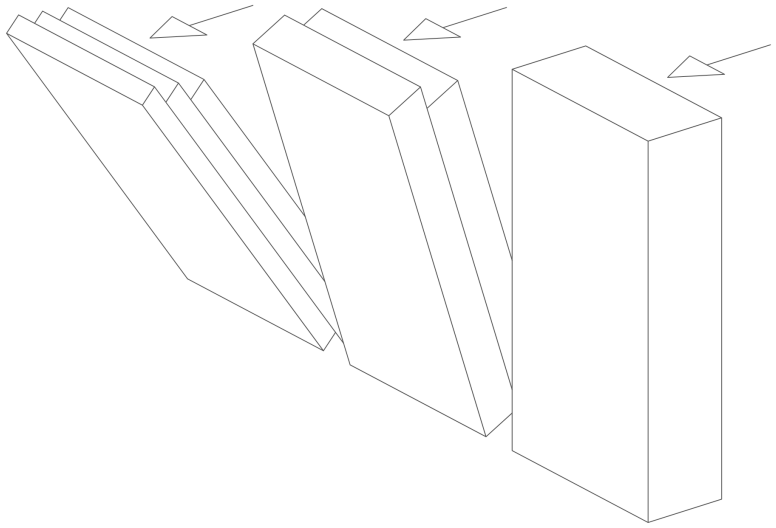

Figure 2.2: In the image an exemplification of out-of-plane behavior for walls having different cross-sections is displayed.

The disposition of the resisting elements (or texture) is usually related to aesthetic choices. For the large part of the historical rural and residential buildings, the texture was imposed by the local available materials and by the manual skills of the construction workers. The texture plays also an important role in the mechanical behavior. For example, not continuous horizontal bed joints can modify the lateral compressive strength of a masonry wall panel [30].

There is also a classification regarding the typologies of elements that compose civil masonry structures. This classification is based on the presence of openings because they play an important role in the behavior of structures especially under seismic actions. Three bi-dimensional elements (Fig. 2.3) are defined considering the different behaviors that they play into the structure [17]. The pier panels are included between two openings on the same floor. Their main function is to bear the vertical loads. The spandrel panels are included between two openings on two different floors. They are connected to the slab and they bear its load. The last typology of element is the cross panels. They connect the pier and spandrel panels. The cross panel bears both the slab and the stress due to the vertical loads coming from the piers.

This brief Section was more focused on some characteristics, components and nomenclature of masonry. These basics give an elementary knowledge of masonry and masonry elements. It has to be remarked that the perfect understanding of a masonry

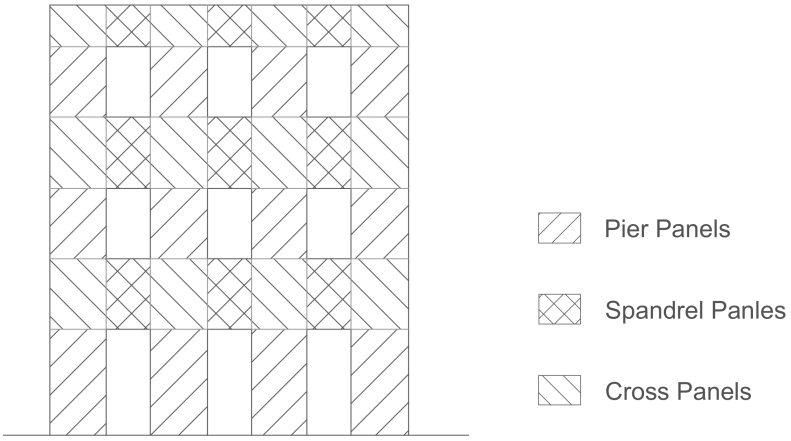

Figure 2.3: The image gives an example of a façade in a civil masonry construction considering the different typologies of elements that compose it.

structure is more difficult to obtain because factors such as building history and evolution (consequently load history and evolution), disposition of resisting elements, connection between walls and floors, crack patterns, materials degradation, loading rates, boundary conditions, strain rates, etc., play an important role in the structural/material behavior [23, 77, 81, 180].

2.2 Overview of in situ characterization

Masonry constructions are widespread. Looking at the architectural heritage, *URM* is the most used construction system. In almost all the Mediterranean countries masonry structures still represent the largest number of the presents buildings. The knowledge of the mechanical behavior of this type of structure plays the key role for prevention, renovations, maintenance, retrofitting, etc. The mechanical parameters allow to understand the behavior of the constructions under different actions. Countries like Italy, Portugal, Turkey, Nepal, etc., need tools to determine the seismic vulnerability of their structures. These are only some of the objectives that spurred generations of engineers and architects to improve and create characterization tests.

Masonry characterization can be performed both in laboratory and/or in situ. Lab tests are usually performed for the characterization of samples realized directly in laboratory. In these tests variables like dimensions, materials composition, curing, etc., are easy to control. However, it is not unusual to test in laboratory specimens coming from existing structures. These tests present a limitation in the validity of the results because the specimens could be damaged during the isolation from the structure and/or during the transportation to the laboratory. The in situ characterization gives the opportunity to test specimens reducing the risk of damaging them and the structure from where they were taken. These are remarkable advantages for existing structures especially if they have a historical and/or architectural value.

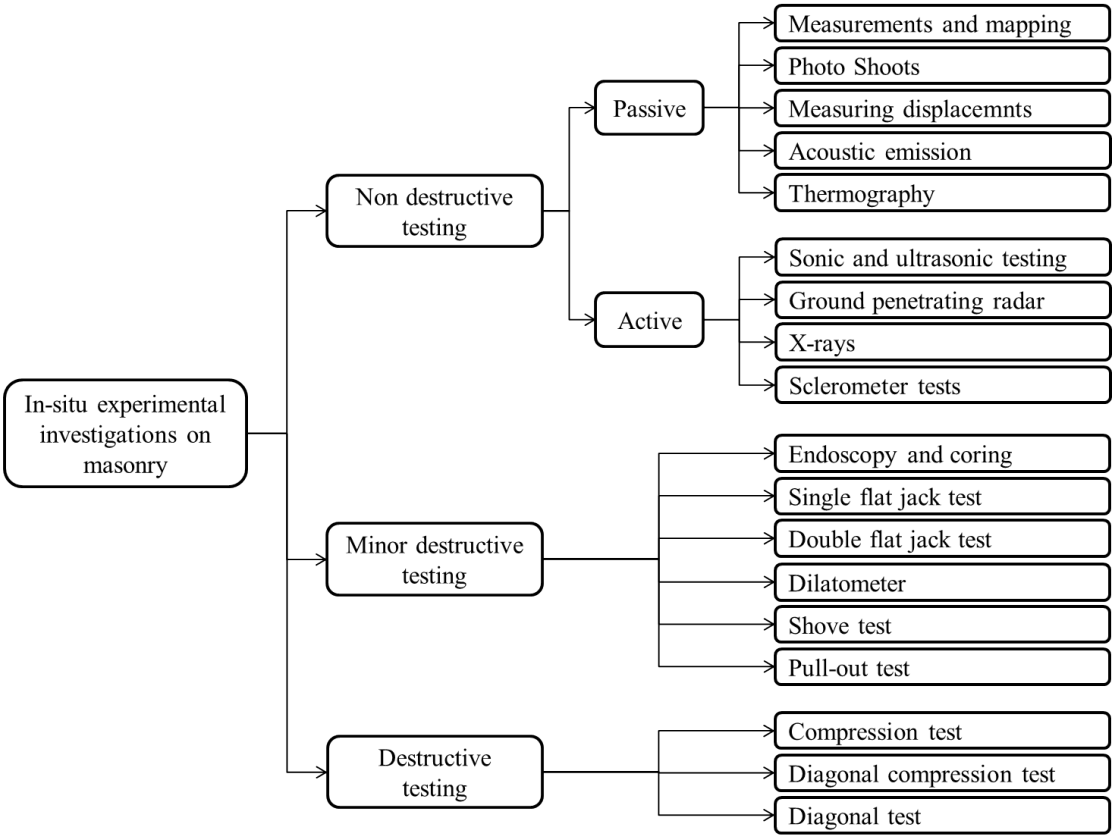

Figure 2.4: The chart illustrates the classification of the principal in situ tests fro masonry testing [57].

This Section gives an overview of the tests used for the characterization of masonry. In particular, attention is paid to the mechanical characterization of the existing buildings. Some of these tests do not contemplate a contact with the structure. However, other tests destroy a portion of the structure. These differences in the interaction with the material give a classification of the characterization methods. These are divided according to their destructiveness in Non Destructive Testing *NDT*, Minor Destructive Testing *MDT* and Destructive Testing *DT* methods (Fig. 2.4) [57]. It is important to remember that a large number of these tests was not only created for masonry structures but (as happens very often for tests) they were already employed for different materials (like concrete [132]) and different applications (for example oil and mineral exploration, manufacturing quality control, physiological evaluation, etc. [132]).

A second classification exists. Tests can be divided into direct and indirect tests. In a direct test the mechanical property is physically measured (for example flat jack tests, compression test, diagonal test, etc.). On the contrary, in an indirect test, the mechanical property is estimated via correlation to other direct measures (for example sclerometer, sonic and ultrasonic tests).

2.2.1 Non Destructive Testing methods

Non Destructive Testing (*NDT*) methods do not cause any damage or alteration to the masonry [57]. *NDT* cannot eliminate the necessity of conducting other tests but offers a mean to reduce the number of more destructive tests [131, 167]. Some of the *NDT* techniques are always used and are the starting point to study all kinds of structures. In fact, measurements, mapping, photo shooting and the measure of displacements are the base for every work done in all types of existing structures. These first operations give the basic information that is needed for deeper investigations. These tests are usually performed in parallel (and not in substitution) to more destructive tests because *NDT* can help to identify the uniformity of the results obtained with the others tests.

NDT methods can be divided into two sub-categories that are active and passive tests. The distinction between them is given by the interaction that they have with the sample. In passive tests, no energy is given to the sample. On the contrary, in the active *NDT*, the energy is usually introduced in form of mechanical or electromagnetic waves. This energy departs the from the instrumentation through the sample and the measure is an evaluation of the behavior of the specimen toward this introduced energy (Fig. 2.4).

The acoustic emission (*AE*) test is presented in a following Section (2.6) because this test is used in the present work and for this reason, a deeper view on the technique was presented.

Sonic and ultrasonic tests consist in monitoring stress waves through a medium [37, 101, 123]. Mechanical waves are transmitted on the media and are then reflected by the opposite side of the sample or in flaws, cracks, voids. A receiver finds these imperfections by measuring the transmission velocity of the waves. The main difference between sonic and ultrasonic test is the frequency of the waves used. These techniques give a simple evaluation of the condition of the masonry [123].

The Ground Penetrating Radar (*GPR*) uses electromagnetic waves instead of mechanical waves. This method provides results similar to the sonic and ultrasonic tests; in fact, it is based on the study of the reflection of electromagnetic waves [101]. *GPR* technique has received a lot of attention in the last decades. For example, it is used to study from simple walls to historical masonry bridges [175] or to control the effectiveness of masonry reinforcements [9].

Electromagnetic waves are also used in radiography (X-rays) test. These electromagnetic waves can penetrate the solid media and are partially adsorbed by it because they have shorter wavelengths than the *GPR* ones. The radiation that is not totally absorbed can be displayed on a screen, monitored by electronic equipment or recorded on special papers or films [123, 142].

Thermography is a passive technique that has applications in a lot of fields. This method consists in a camera that measures the infra-red waves per unit of area coming out from the structure [101, 124, 142]. This special camera captures a part of the structure giving a thermal imagine that is used to define the presence of different thicknesses, voids, cracks and presence of water leaks. These defects are detected because they cause variations on the heat flow [142].

The scleometer (or Schmidt hammer rebound test) was firstly applied on concrete structures and later also to rocks [169] and masonry. The test consists in a mass impacting the mortar surface. The equipment measures the mass rebound and gives a

measurement of the superficial hardness [57].

Digital Image Correlation (named *DIC*) is a non-contact and non-interferometric optical method for the assessment of displacements and strains of a sample surface [135, 165]. The first optical methods were developed since the early 1950's but the *DIC* is a more recent method conceived four decades ago by a group of researches at the University of South Carolina [49, 140, 177, 178]. The main advantage of *DIC* measurement is the fact that the measures are taken without contact with the sample. This characteristic is very important when the monitored object has hight temperature or is in some way impossible (or not recommended) interact with it. A second big advantage is that with this method it is possible to monitor displacements/strains of an entire area of a sample.

Noland et al. [131] consider *NDT* very important when more invasive investigations are not allowed, for example, in structures that have architectural and/or historical value. This affirmation can be accepted reminding that Noland et al. [131] consider other more destructive tests like the flat jack tests or the shove test belonging to the *NDT* techniques.

The descriptions here presented of some *NDT* methods highlight the impossibility of using these tests for an exhaustive characterization of the media especially from the point of view of the mechanical properties.

2.2.2 Minor Destructive Testing methods

Minor Destructive Testing (*MDT*) methods, as their name states, are less destructive than *DT* but at the same time, they allow to obtain more precise and qualitative results with respect to *NDT*. The big advantage of *MDT* is the possibility of a more direct mensuration of mechanical characteristics maintaining at the same time a low level of invasiveness. In fact, after the execution of a *MDT* technique it is possible to obtain a total (or almost total) reparation of the tested zone and the impact on the aesthetic is very limited in comparison to the *DT*. This last aspect is the feature that allows the use of minor destructive tests also in architectural heritage and historic structures. Some of these tests are now presented.

One of the most important and utilized *MDT* techniques is the flat jack method [122]. These tests are not presented here because a following Section is extensively dedicated to them (Sec. 2.3).

The coring technique consists in boring a hole in a wall using a drill and extracting a cylindrical sample. This test allows to determine the wall stratigraphy [57]. It is very important to know the stratigraphy of a wall because the presence of leaves can be detected and these leaves change the mechanical behavior of the structure. The cored samples are usually damaged due to the vibration of the drill and/or to the water used to core [26]. These samples should not be used for mechanical characterization but sometimes they are used for this purpose.

The endoscope is a small camera that can be inserted in small holes. It is not unusual to use the coring technique and this instrument. In this case, the endoscope is inserted into the hole in order to take photos of the wall section and to verify the presence of anomalies or voids [57, 101].

The pull-out test, also known as screw (helix) pull-out method, measures the shear strength of a small cylinder of material [63]. After the helix is inserted into the mortar

joint, it is then pulled out whilst monitoring the force by means of a test load unit [153]. This force is a measure of the mortar strength.

In the dilatometer technique, a drill is used to create a hole in a wall in which a cylindrical tube is then introduced. The cylinder expands radially in the perforation and, by monitoring the pressure of the cylinder and the radial deformation of the masonry, it is possible to estimate the modulus of deformation of the wall [57, 101].

The shove test is a methodology to test the shear strength of the bed mortar joints of brickwork. For the test, a brick is removed in order to create a void in which a small jack can be inserted. The jack pushes the adjacent brick that is the tested one. At the opposite side of the tested brick (relative to where the jack is placed) the vertical mortar joint is removed in order to allow the displacement of the tested brick [2, 57]. Once the applied force and the displacement of the brick are known, it is possible to evaluate the shear strength of the mortar.

The few *MDT* methods described here show a different interaction with the structure in contrast to the *NDT* techniques. The major difference is that *MDT* can give information about mechanical characteristics that are measured directly on the masonry.

2.2.3 Destructive Testing methods

Destructive testing (*DT*) causes the damage or the failure of a part of the masonry [57]. These tests are very similar to characterization tests performed in laboratory. *DT* allows direct measurements of the mechanical characteristics of the masonry. They are performed in situ and in samples obtained by isolating part of the structure. Cuts are usually used to isolate the sample from the rest of the structure. This isolation should be carefully performed in order to avoid/reduce damages of the sample.

In masonry characterization three major *DT* methods are present. These aim to determine the mechanical behavior of the media under shear and compression.

The compression test is designed in a specific way in order to determine the Young's modulus, Poisson's ratio and eventually the compression strength if the test is conducted up to the failure [28, 55, 57]. A rectangular part of a wall (180 cm height, 90 cm width and same depth of the tested wall) is isolated from the wall in order to apply on the top of it a vertical load by means of hydraulic jacks. The rectangle is not completely isolated from the wall. In fact, its base remains connected to the structure which gives the reaction necessary to apply the vertical load.

The other two *DT* techniques are presented in Section 2.4 in which more attention is paid. This choice was taken because these in situ tests are the ones usually conducted to characterize the shear behavior of existing *URM* structures.

The main advantage of all of these *DT* methods, in contrast to laboratory tests, is the possibility of investigating directly investigate a part of the studied masonry without transporting it to the laboratory so that by this way the risk of alterations is reduced. Another important characteristic of these tests is that they are directly derived from laboratory testing. This fact allows comparisons between tests performed in lab and tests performed in situ. It has to be remarked that a codification of this test is not present yet but some of these tests are indicated by the Italian codes [86, 87, 143]. As already said, the disadvantage of these tests is the destructiveness related to the isolation that has to be performed in the sample. There are also other issues related to the isolation

that are the time and the costs needed to create the sample, the risk of damaging the sample during its realization, and the reparation costs.

2.3 Flat jack tests

This Section gives a focus on the use of the Flat Jack (*FJ*) method as this technique is the pivot of part of the present thesis work. At the beginning, a short historical review of the utilization of this equipment for the mechanical characterization of masonry structures is presented. Whereupon, a deep technical view and the advanced applications of these *MDT* techniques are discussed.

A flat jack consists of two thin steel sheets welded together along the edges; two small tubes are also welded with the sheets in order to allow a liquid to flow inside the flat jack. The flat jack is positioned in a slot obtained in the masonry. After the connection with the hydraulic system is performed, a liquid flows into the *FJ* blowing it. This *MDT* technique offers the possibility to determine some mechanical properties of existing structures for subsequent evaluations [138]. Some authors classify these techniques as a *NDT* method [25, 40, 78, 130, 138]. However, in the opinion of the author and also the one of Dalla Benetta [57], non destructive tests do not cause any damage or alteration to the masonry. For this reason, the flat jack tests do not belong to this category even if their destructiveness is very low.

At almost four decades from the first application in the structural field, the *FJ*s are still some of the most employed *MDT* methods. This method was applied for the first time in the rock mechanics field (e.g. [21, 61, 70]). In the early 1980s the Italian researchers L. Jurina, P. Bonaldi and P. P. Rossi were the first to adopt this technique in the structural field. These researchers evaluated the stress state and the deformability of a masonry structure by means of flat jacks [91, 158, 157].

In a very short time, the flat jack method raised attention due to both its possible applications and its adaptability. For example, interest was given to the possibility of varying the geometry of the *FJ*. In fact, in 1983, Abdurn tested very small circular flat jacks [1, 78]. For a better understanding of the behavior of the flat jack and of the tested masonry, first non-linear *FEM* analyses were carried out [162]. Other important contributions came from Atkinson-Noland & Associates [130]. They evaluated the applicability of the *FJ* test in structures in the USA. Modifications on the technique were also performed. For example, thicker flat jacks were developed by W. Qinglin and W. Xiuyi. This special equipment was designed with the scope of applying larger displacements in order to test soft masonry in China [147].

This technique offers different possible applications in existing structures. Its best characteristic is that it is probably the only *MDT* technique (at the moment) that can give reliable information about the following parameters [26]:

- compression stress status of masonry structures;
- Young's modulus in compression;
- compressive strength.

The importance of this technique is that it can give reliable information about the masonry by directly testing it and at the same time avoiding its destruction. These *FJ* tests have two principal standards, one that was born in the United States and the other one in Europe. The European one is the *RILEM*. The first recommendations for the flat jack testing were released in 1990. Nowadays, these recommendations are the MDT.D.4 for the in situ stress test [154] and the MDT.D.5 for the in situ evaluation of deformability test [155]. The other standards organization that developed standards for the flat jack testing is the *ASTM*. This organization also released two standards that are the C1196-14a regarding the stress in situ [11] and the C1197-14a that treats the deformability test [12]. These standards are quite similar one to the other one. The principal limits and recommendations for both *ASTM* and *RILEM* are presented in the following Section where the tests are exposed. It has also to be said that there are some recommendations given by the Italian consortium named *ReLUIS* [150, 151].

Flat jack tests are considered by the Italian codes as tests for measuring the mechanical properties of masonry [74] and these codes consider the double flat jack test one of the tests adoptable to obtain extensive in situ investigations [86]. This means that *FJ* tests have an important impact on the characterization of masonry structures. In fact, the possibility of having extensive in situ investigations guarantees the possibility of using reduced safety coefficients for the mechanical characteristics. This fact highlights the reliability of these tests.

2.3.1 Stress test (single *FJ* test)

The evaluation of the vertical stress of a structure, also called stress test, is performed using a single flat jack. The knowledge of the stress state of a structure is important because it can help calibrating a numerical/analytic model, determining the applied load and identifying the stress gradient across the wall section [138, 167].

The first step to perform this test is the individuation of the location where it is possible to obtain a slot (perpendicular to the masonry surface) for the *FJ*. If the masonry texture is regular, it is preferable to create the slot in a bed joint (Fig. 2.5). In this case, the reparation after the test will be easy to perform and less visible in comparison to a slot made directly in bricks or stones. On the contrary, if the mortar bed joints are more than 2 cm thick, the best choice is to create the slot through the bricks. However, this solution is not applicable in structures that have historical heritage and on valuable buildings [27]. Before creating the slot it is necessary to apply gauge points across the zone in which the slot will be created. The distances between the gauge points are recorded. Afterward, a circular saw blade or a drill is used for creating the cut that represents the slot. The choice between these two pieces equipment is made considering the type of flat jack that will be used. In fact, if the flat jack is circular or semi-rectangular it is better to use the circular saw because the created slot has a shape that fits better this type of flat jacks [78]. On the contrary, if the flat jack is rectangular it is better to use a drill. Water is usually used to cool down the blade and to eliminate the dust produced by the circular saw blade during the cut.

The creation of the slot produces a stress release of the masonry and a consequential closure of the cut [27, 91]. The test consists in the identification of the pressure necessary for the flat jack to restore the closure of the slot. Some assumptions are inevitable,

Figure 2.5: The image presents a slot created with a circular saw for the single *FJ* test. The picture shows also the three couples of measuring points and a thin remaining layer of water used to cool the saw.

for example, there is a compressive stress, the masonry is assumed to be homogeneous, the deformation of the masonry to be symmetrical around the slot, the stress that the flat jack acts on the masonry is supposed to be uniform and the value of the present stress is small compared to the compressive strength. This last assumption is made because in this way the masonry will be tested in the elastic regime [78].

A hydraulic system is then connected to the *FJ*. This equipment has a pump that is used for the pressurization of the liquid inside of the flat jack. The liquid pressure is then gradually increased until the distance between the measured points is equal to the initial one meaning that the closure that took place after the realization of the cut is restored. At this point, the pressure of the oil p is proportional to the masonry stress status. As said before, the principle of the test is to restore the deformations caused by the stress release created by the slot but it is important to take into account that creep deformations can be present. For this purpose, it is recommended that the time needed for the pressurization should be the same time used to prepare the cut and the test itself [154]. It is assumed that this time symmetry eliminates the creep deformations in the measurements.

The pressure p inside of the *FJ* is not perfectly equal to the stress σ that applies to the masonry. This because the *FJ* has its own rigidity and the area of the slot is not coincident with the flat jack area. Two constants k_m and k_a are used to take into account these factors.

k_m is a dimensionless constant (< 1) that takes into account the stiffness of the flat jack [11, 12]. This constant gives the proportionality between the oil pressure p and the stress applied to the masonry σ [154, 155]. The k_m is obtained by putting the *FJ* in a compression machine. This calibration is performed raising the liquid pressure inside of the *FJ*, by keeping a constant thickness of it and by monitoring the equivalent force that the flat jack applies to the compression machine. More details about this procedure

can be found in [11, 12, 132]. The k_m is given by the flat jack producer and sometimes a curve of the k_m is given in function of the hydraulic pressure.

The other dimensionless constant is k_a (< 1). This is a ratio between the area of the flat jack A_{FJ} and the area of the obtained slot A_{slot}:

$$k_a = \frac{A_{FJ}}{A_{slot}} \tag{2.1}$$

A_{FJ} is given by the producer of the *FJ*. The area of the slot is directly measured in situ. The length of the visible part of the cut is measured and is then divided into segments of $10-20$ mm. For each segment, the depth of the cut is measured and the total area A_{slot} is obtained by summing the area of all the strips [154, 155]. In the *FJ* tests, the stress applied by the *FJ* to the media is considered uniform and applied to the whole slots. This is the reason why the geometrical constant k_a is adopted.

The compressive stress σ transferred by the *FJ* to the sample is then evaluated using the equation:

$$\sigma = -pk_ak_m \tag{2.2}$$

where compressive stress is considered negative.

There are some characteristics concerning the equipment that have to be known in order to perform reliable tests. The hydraulic system consists in a manual or electrical pump connected to the flat jack and to a pressure gauge. Following the *ASTM* and *RILEM* recommendations, this system must have an accuracy of 1% of the full scale [11, 12, 154, 155] and it must be capable of maintaining a constant pressure (within the 1% of the full scale) for at least 5 min [11, 12]. This last recommendation is given because if the measurement of the gauge points is performed manually the operator spends at least a few minutes to take the measures.

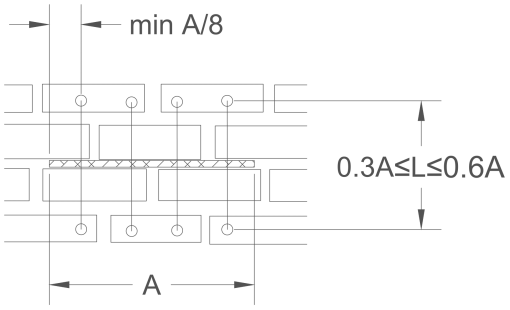

Figure 2.6: The image provides the *RILEM* specifications for the position of the four gauge points in the single *FJ* test are indicated [154].

The recommendations give also some limits in the number, distances and positions of the gauges. For example, *RILEM* [154] recommends four pairs of points that have to respect geometrical conditions represented in Figure 2.6. Another advice given by *RILEM*. is that the sensitivity and the precision of the mechanical strain gauge (or electrical like *LVDT*) must be the highest possible and that a sensitivity of approximately 0.0025 mm is normally sufficient [154]. The *ASTM* [11] recommends the same geometrical conditions of *RILEM* and also the same number of gauge points but gives more

specifications about the measuring device. This must have the capability of measuring deformations up to 5 mm and the accuracy should be at least of $\pm 0.005\%$ [11]. Some additional test specifications (in Italian) are given by the *ReLUIS* [151].

2.3.2 Compression deformability test (double *FJ* test)

This test allows a direct measure of the Young's modulus in compression [130]. This is a key property that has to be known for a large number of further analyses (for example *FEM* analyses, analytic models). In this short Sub-section the main features and the principal suggestions to perform an optimal test are exposed.

A large number of the recommendations used for the single *FJ* test are also valid for this test [11, 154]. These are referred to the compression deformability test [12, 155]. As for the single flat jack test, the *ReLUIS* adds some specifications [150].

Figure 2.7: The picture shows a double flat jack test. This photo was taken at the end of the test. In the picture, the measure points are highlighted in blue and the cracks in green. Position 1 "ex Teatro dei Nobili".

The double flat jack test consists in the partial isolation of a prism of the wall. This isolation is obtained by creating two cuts parallel to each other and perpendicular to

the wall surface. In this test, the *FJ*s placed in the slots are used to apply a load to the masonry included between them. The masonry between the two cuts is assumed to be unstressed before pressuring the oil [78]. The two flat jacks are mutually connected in order to allow the liquid to flow from one to the other one and to guarantee equal pressure for both *FJ*s. Following the *ASTM* [12] recommendation, the reciprocal distance between the flat jacks must be larger than the masonry unit but not less than 200 mm and, at the same time, the distance must be lower than 1.5 times the length of the flat jack. *RILEM* recommendations [155] suggest that the distance between the two *FJ*s should be at least five courses of masonry (in the case of a unit height equal or less than 100 mm) or three courses of masonry in the case of a unit larger than 100 mm. The distance between the *FJ*s must be inferior to 1.5 times the length of the flat jack but also not less than 2.5 times the *FJ* width.

The *ASTM* recommends the use of only three equally spaced pairs of gauge points (or *LVDT*s) [12]. On the other hand, the *RILEM* recommends four pairs of gauge points that have to cover the $75-90\%$ of the distance between the flat jacks [155]. Usually, an additional pair of gauge points (or an additional *LVDT*) is used for monitoring the displacement along the transverse direction of the load (e.g. [24, 25, 27, 47, 158, 157]).

The stress acting on the masonry is evaluated by using the same equation of the single flat jack test (Eq. 2.2). However, in this test the geometrical ratio k_a is different because the slots are two. In fact, in the double flat jack test k_a is the ratio between the area of the flat jack A_{FJ} and the mean area of the obtained slots A_{av} [12, 155]:

$$k_a = \frac{A_{FJ}}{A_{av}} = \frac{A_{FJ}}{(A_1 + A_2)/2} \tag{2.3}$$

where A_1 and A_2 are the areas of the two slots. For what regards the mechanical coefficient k_m, if the used *FJs* have two different values the average of them can be adopted.

Similarly to the single *FJ* test, after a first measure of the distances of the gauge points, the pressure is slowly increased. In the case of mechanical measurements, at every incremental step the pressure must be held for at least a few minutes before measuring the displacements. This operation is performed because the record of the displacements takes some minutes as the pressure and the deformations must be steady [12, 150, 155]. During the experiment, several steps of pressure are tested both loading and unloading the sample. Usually, for every cycle, the maximum pressure reached is increased with respect to the previous one. The first steps have to be performed at a low pressure in order to have information regarding the elastic parameters [27]. The average of the vertical strains ε_v and the horizontal strain ε_h are usually plotted versus the applied stress σ. In the case of low rise buildings, it may happen that the flat jacks do not have sufficient reaction from the upper part of the structure [26, 27]. For these buildings, it is impossible to explore the behavior of the masonry for high stress levels and probably only the elastic range can be characterized [26].

From the test, it results possible to obtain the Poisson's ratio ν, the tangent Young's modulus E_t and the secant modulus of elasticity E_s.

The tangent modulus of elasticity is evaluated at different levels of stress and is given by:

$$E_t = \frac{\delta\sigma_i}{\delta\varepsilon_{vi}} \tag{2.4}$$

where $\delta\sigma_i$ is the increment of stress and $\delta\varepsilon_{vi}$ is the corresponding increment of vertical strain [12, 155].

In a similar way it is possible to obtain the secant modulus of elasticity [12, 155]:

$$E_s = \frac{\sigma_i}{\varepsilon_{vi}} \tag{2.5}$$

where in this case σ_i is the cumulative stress at the general load step i and ε_{vi} is the cumulative vertical averaged strain at the load step i.

The Young's modulus E is usually evaluated as the linear interpolation of measures taken in the elastic range of the sample. Usually, some cycles of loading are performed in this range and then the Young's modulus of the media is calculated as an average of linear interpolations determined in these cycles.

The Poisson's ratio can be evaluated thanks to both the vertical and horizontal measurements [139]. In fact:

$$\nu = -\frac{\varepsilon_h}{\varepsilon_v} \tag{2.6}$$

where ε_h is the horizontal strain and ε_v is the averaged vertical strain.

At the end of the test, *FJ*s should be removed and the cuts repaired. However, in this test and in the evaluation of the compressive strength, this operation can be not very easy to be accomplished. These difficulties are related to the extraction of the *FJ*s because the high pressures could deform and block them inside of the slot.

One of the important characteristics of this test is the reliability of the results compared to other tests. It is important to make another confrontation with other possible adoptable techniques. If it is necessary to carry out a laboratory compression test, the sample has to be extracted directly from the wall. During the extraction and transportation it is very probable that some damages occur [27, 157]. There is a possible solution to this problem that consists in the construction of an equivalent masonry sample to test in laboratory. However, this technique is not very convenient because it is very difficult to reproduce a specimen without knowing the mechanical characteristics, the state of degradation and the (usually unknown) load history of the structure. Another possible solution is the application of the in situ compression test but the disadvantages of this *DT* technique were presented in Section 2.2.

The double flat jack test seems to be the best strategy to assess the mechanical characteristics of existing structures because it guarantees reliable results and a reduced destructiveness.

2.3.3 Evaluation of the compressive strength

The estimation of the compressive strength is performed using the same configuration of the double flat jack test [27, 39, 103, 130] and it is usually evaluated after this test. In fact, after the identification of the Young's modulus, the pressure inside of the *FJs* can be raised to higher values allowing the evaluation of the compressive strength.

Some researches focused the attention on the compressive strength evaluation. For example, Gregorczyk et al. [78] state that the compressive strength can be measured if an acceptable extended damage is obtained in the specimen. Similarly, Nobile et

al. [129] consider that the compressive strength can be evaluated through double *FJ* testing by increasing the applied load until the appearance of cracks in bricks.

Other authors tried to understand the discrepancy between the real compressive strength of the material and the measured one. Binda et al. [27] consider that this test can estimate only roughly the compressive strength. Jurina [90] states that the compressive strength evaluated using the *FJ* method overestimates the real strength of about the $10-15\%$. Lombillo [100] quantifies the ratio between the expected compressive strength $f_{c,exp}$ and the theoretical $f_{c,teo}$ for different types of masonry (Tab. 2.1).

These discrepancies are due to two main facts. One of these is that in the flat jack method the stress acting on the masonry is idealized as homogeneous on the surface. A second possible issue is that in the in *FJ* tests the masonry surrounding the specimen confines the specimen itself [90].

Table 2.1: The table gives the ratios between the expected $f_{c,exp}$ and the theoretical $f_{c,teo}$ compressive strength for different masonry typologies [100].

Type of masonry	$f_{c,exp}/f_{c,teo}$
Brick	1.00 ± 0.19
Ashlar	0.90 ± 0.23
Rubble stone	1.16 ± 0.64

In the present work, the estimation of the compressive strengths by means of *FJ* testing was performed following [95, 179]. This method relies on a logarithmic regression curve that fits the envelope curve in the plastic regime of the sample and the stress associated with a deformation of the $3‰$ in the fitting curve is considered the compressive strength of the material. This methodology is often adopted (e.g. [102, 103, 141, 173]).

As for the single *FJ* test, in the case of structures that are no very high, the reaction of the upper part of the building can be insufficient to allow a high level of applied stress. For this reason, it is possible that the test must be stopped at a stress inferior to the compressive strength (reasoning as absolute values) leaving unknown this mechanical characteristic.

2.4 *DT* methods for shear characterization

This section gives a focus on the two *DT* methods that are usually performed for the evaluation of the shear characteristic of masonry. The main advantages and disadvantages of *DT* techniques are already presented in Section 2.2. It has to be highlighted that the destructiveness of these tests usually yields to their unsuitability for investigations in historical and architectural heritage.

The two *DT* methods are the shear-compression and the diagonal tests. The results obtained with these two tests highlight a significant problem. In fact, the ratio between the shear resistance evaluated using the shear-compression test τ_s and the one evaluated with the diagonal test τ_d, is always different from the unit and can range between 1.23 and 1.89 in numerical simulations and between 2.44 and 3.67 for masonry panels tested

in laboratory [29]. This high difference between the results could lead to the problem of deciding which test adopt and to the problematic of the reliability of the results.

2.4.1 Shear-compression test

The shear-compression test (Fig. 2.8) is usually carried out after the compression test in order to have also information about the Young's modulus and the Poisson's ratio [56]. During the test, a vertical load V is guaranteed by the same equipment of the compression test. The difference between these two tests is that in the shear-compression test another hydraulic jack is used to create shear stress in the panel. In fact, this jack creates a horizontal force P_s at half of the height of the sample [28, 55, 57] which usually has dimensions of 1.8×0.9 m. In this test, a horizontal reaction is also needed in the upper part of the sample in order to concentrate the shear stress in two squared panels, one under the horizontal jack and the other above it.

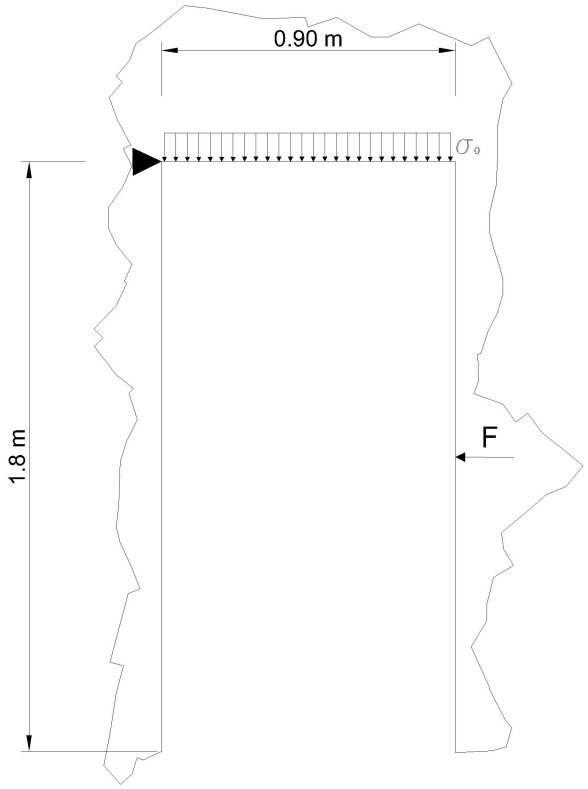

Figure 2.8: The image displays an Illustration of the set-up of the shear-compression test. The flag with the "F" is the point where the horizontal jack acts the horizontal force P_s. At the top of the sample is also represented the applied vertical stress σ_0.

The evaluation of the tensile strength is performed using the formulation proposed by Turnšek and Čačovič [183]. This formulation is also adopted by the Italian code (C8.7.1.1 [86, 87]). By reversing this formulation it is possible to obtain the tensile

strength referred to the bottom panel [28, 56] :

$$f_{t,s} = \sigma_0 \left[-\frac{1}{2} + \sqrt{\left(\frac{bP_{su}}{A_s \sigma_0} \right)^2 + \frac{1}{4}} \right] \tag{2.7}$$

where: P_{su} is the maximum horizontal force, A_s is the cross area of the specimen calculated as $A_s = lt$ in which t is the specimen thickness and l is its width, b is a shape factor that takes into account the stress distribution and σ_0 is the vertical stress calculated as:

$$\sigma_0 = \frac{V}{A_s} \tag{2.8}$$

Usually b is assumed as the ratio between l and the height h of the sample and is limited to the values 1 and 1.5.

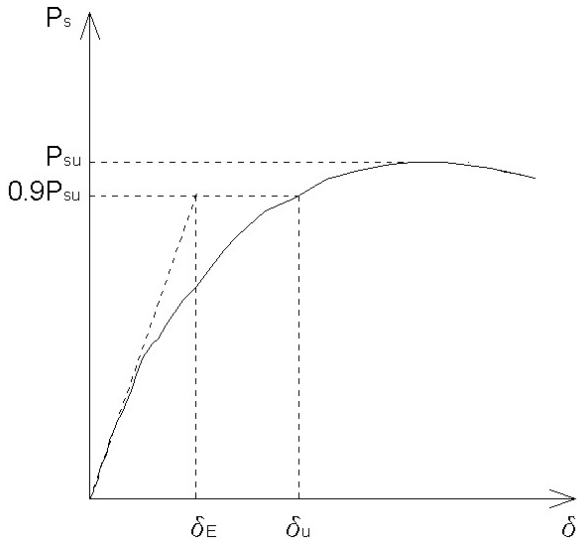

Figure 2.9: The graph plots the behavior of the horizontal force and the displacement at half of the height of the panel in the shear-compression test. In Figure it is also indicated how to evaluate δ_E.

The shear-compression test also allows the determination of the shear modulus of the sample. Sometimes for this scope, only the results coming from the lower half panel are used because this is the most stressed. Considering this panel in elastic regime and fully restrained at the top and at the bottom it is possible to evaluate its deformability by taking into consideration the combination of vertical and horizontal forces [170]:

$$\frac{\delta_E}{0.9P_{su}} = \frac{1.2h}{2GA} \left[1 + \frac{G}{1.2E} \left(\frac{h}{2t} \right)^2 \right] \tag{2.9}$$

where δ_E is the relative displacement between the base and the middle point of the panel assuming a linear and elastic behavior at $0.9P_{su}$ as shown in Figure 2.9. The shear modulus G results as the only unknown of Equation 2.9.

2.4.2 Diagonal test

The diagonal test (or diagonal compression test) derives directly from the laboratory test [15, 156]. This method aims at determining the shear (or tensile) strength of masonry. The squared panel has edges of 120 cm and depth equal to the masonry depth (Fig. 2.10). The sample has to be partially isolated from the structure and it remains connected to it with a limited part of its base. At two opposite vertexes of the sample, a couple of forces are applied by means of a hydraulic jack [28, 55, 57]. This test has not a clear and unique interpretation of the results yet [55] and, for this reason, some of these interpretations are presented in the following paragraphs (and in a summary in Tab. 2.2).

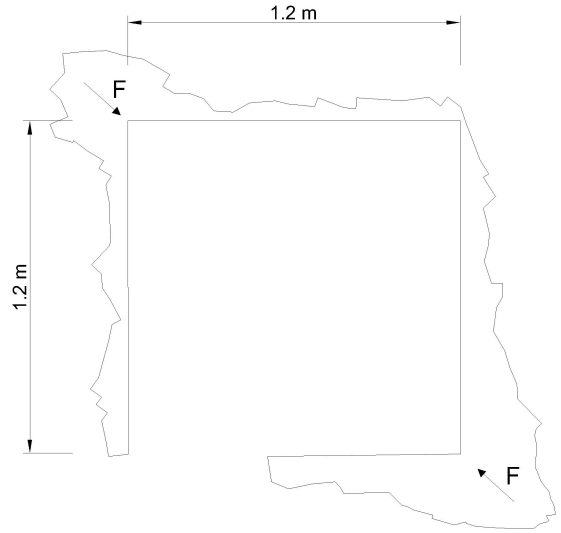

Figure 2.10: The image reports an illustration of the in situ configuration of the diagonal compression test.

The standards *ASTM* [15] and *RILEM* [156] assume a state of uniform shear stress ($\tau_{d,std}$) in the specimen (Fig. 2.11a). If this assumption is taken into account the shear stress is evaluated as:

$$\tau_{d,std} = f_{t,d,std} = \frac{1}{\sqrt{2}} \frac{P_d}{A_d} \tag{2.10}$$

where: P_d is the applied load and A_d is the net area of the specimen calculated using:

$$A_d = \frac{l+h}{2} tn \tag{2.11}$$

in which: l is the width of the specimen, h the height, t is the thickness of the specimen and n is the percent of the gross area of the unit that is solid and it is expressed as a decimal [15]. The shear strength $\tau_{du,std}$ is then evaluated for the maximum diagonal force P_{du}. Considering the assumption made by these standards, the shear stress is coincident with the tensile stress $f_{t,std}$ of the specimen. Equation 2.11 is used by all the authors, on the contrary Equation 2.10 is the object of different interpretations.

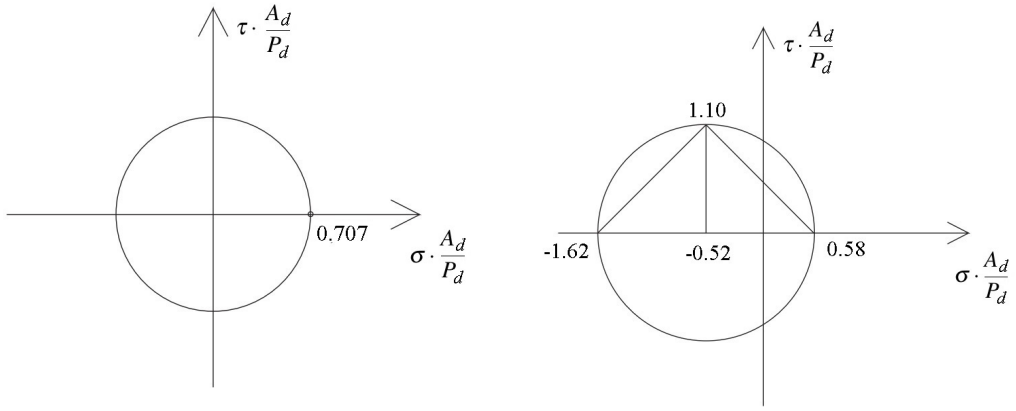

(a) (b)

Figure 2.11: The image represents the Mohr's cycles of the diagonal compression test: in 2.11a hypothesis of pure shear stress (*ASTM* and *RILEM*); in 2.11a hypothesis of not uniform stress.

In 1931, Frotch [69] evaluated the stress state of the panel in this load configuration. In this case, the hypotheses of an elastic, homogeneous, isotropic and continuum material were assumed leading to a not uniform stress field in the panel [31] (Fig. 2.11b). If these hypotheses are taken into account, the shear and the tensile stress are calculated as:

$$\tau_{d,F} = 1.10\frac{P_d}{A_d} \tag{2.12}$$

$$f_{t,d,F} = 0.58\frac{P_d}{A_d} \tag{2.13}$$

Brignola et al. [31] have analyzed the stress field in the sample by *FEM* linear analyses. The results show a shear stress field which is not uniform confirming Frotch's results (with a maximum error of 3%). Another finding of these linear analyses is the influence of the orthotropy on the diagonal compression test results. The last important contribution of the work of Brignola et al. [31] is a new formulation meant to define the tensile strength of masonry:

$$f_{t,d,B} = \alpha_f \frac{P_{du}}{A_d} \tag{2.14}$$

where the coefficient α_f depends on the masonry typology and varies from 0.35 for rubble stone to 0.56 for solid brick and lime mortar masonry. This formula is obtained by means of non-linear analyses. This coefficient α can also be used for the comparison of the different formulations because it is the value of the normalized stress (shear or tensile) by the diagonal force P_d and the area A_d of the specimen.

$$\alpha_\tau = \tau_d \frac{A_d}{P_d} \tag{2.15}$$

$$\alpha_f = f_{t,d} \frac{A_d}{P_d} \tag{2.16}$$

In the Italian code (C8.7.1.5 [86]) the diagonal compression test is also used for the assessment of the tensile strength and the given formulation is:

$$f_{t,d} = \frac{1}{2}\frac{P_{du}}{A_d} \tag{2.17}$$

Table 2.2: The table summarizes of the interpretations of: *ASTM* [15] and *RILEM* [156], Frocht M. [69], Brignola et al. [31] and the Italian code [86] of the shear and the tensile strength obtained from the diagonal compression test. The formulation is presented using the coefficients α.

Author	α_τ	α_f
ASTM & RILEM	0.707	0.707
Frocth	1.100	0.580
Brignola et al.	-	0.350-0.560
NTC08	0.333	0.500

The shear modulus is also an important characteristic to be evaluated in a structure. The following steps for the evaluation of the shear modulus G are valid for all of the interpretations of the test discussed before. In order to evaluate the shear modulus, it is necessary to monitor the shear strain γ. For this purpose, two measure bases are applied to the diagonals of the specimen. Sometimes the measure bases are four, two for each side of the sample. The shear strain is evaluated (following [15, 31]) as:

$$\gamma = \frac{\Delta_y - \Delta_x}{g} = \varepsilon_y - \varepsilon_x \tag{2.18}$$

where: Δ_x is the shortening in the direction parallel to the load, Δ_y is the extension in the perpendicular direction and g is the length of the measure bases (if four measure bases are used, Δ_x and Δ_y are the mean values of the two sides measurements). ε_x and ε_y are the strains in the directions just explained. The evaluation of the shear strain is necessary when the identification of the shear modulus G is requested because:

$$G = \frac{\tau_d}{\gamma} \tag{2.19}$$

Sometimes also the secant shear modulus at $1/3$ of the peak load is calculated. This is evaluated as:

$$G_{1/3} = \frac{\tau_{d,1/3}}{\gamma_{1/3}} \tag{2.20}$$

where: $\tau_{d,1/3}$ is the shear stress at $1/3$ of the peak load and $\gamma_{1/3}$ is the corresponding shear deformation [56].

It results now clearer that the two destructive tests for the evaluation of the shear properties on existing masonry structures have a huge impact on structures due to large dimensions of the samples. Moreover, discrepancies among the results are present. Furthermore, there are also different interpretations of the stress field inside of the specimen.

2.5 *MDT* methods for shear characterization

Many efforts done to employ the *FJ* technique for other objectives are described in literature. These works are justified by the high flexibility of the *FJ* technique. This characteristic is quite visible in a lot of works. Some of these studies and applications were focused on the development of new equipment or procedures [166]. For example, the creation of flexible flat jacks for irregular slots and to have an easier removal [82, 192]. The tube-jack test is another example of the development of this technique. In this case, the authors want to mitigate the destructiveness of the *FJ* by using a series of tube-jacks [116, 117, 118, 148, 149]. In other works, the goals are totally different. In these cases, the geometry of the flat jack test is changed in order to obtain different mechanical parameters. An example is the study, in presence of orthotropy, of Young's modulus, shear modulus, existing of normal and shear stress, tensile and compressive strengths and fracture energy. These evaluations are performed using two *FJ*s. The first is horizontal and the second, symmetrically positioned under the first, is vertical [73].

This Sub-section presents some studies, applications and variations of the *FJ* technique in which this method was used in order to obtain the shear characteristics of masonry. The particular attention focused on just one field of these advanced techniques is justified considering the main subject of the thesis work.

The first applications of *FJ* for the assessment of the shear parameters are already dated. In fact, three decades ago both *ASTM* and *RILEM* defined the standards for the in situ testing of the masonry bed joint shear strength method [14, 152]. This test considers the utilization of a jack (or a small flat jack) positioned in a slot obtained by removing a brick (or a head joint) in order to put a horizontal force to the brick after. A third brick positioned at the opposite side of the jack is also removed in order to allow displacements (it is possible to remove only the head joint instead of the brick). Two *FJ*s positioned at a certain distance under and above the tested brick can control the vertical load during the test. This procedure aims only at evaluating the shear characteristic of the bed joint (in [83] a relationship between the bed joint shear strength and the wall shear strength is presented) but it is mentioned because some of the following tests have a similar concept.

The other crucial applications/researches of the use of *FJ*s for evaluating shear characteristics are more recent and they were developed in the last fifteen years. These are more focused on evaluating the shear characteristics of the masonry as a homogeneous media and not just analyzing the shear properties of the single component of the material (for example the mortar in [14, 152]).

In 2007 Jurina [90] made the first experiments (to the author's the knowledge) with the objective of evaluating the shear characteristics of a masonry panel using flat jacks (Fig. 2.12). In order to achieve this scope, a partial isolation of a masonry prism was utilized to create the sample having dimensions of 800×400 mm. Four vertical and two horizontal flat jacks were employed. The test was performed in cycles and for every cycle the vertical stress was maintained constant and the horizontal stress was varied. In fact, the pressure was raised in one couple of the vertical *FJ*s (3-4 or 5-6) meanwhile in the other couple the pressure was set to zero. This test allows to determine the variation of the shear strength by varying the vertical stress with this alternated pressurization of couples of vertical *FJ*s [90].

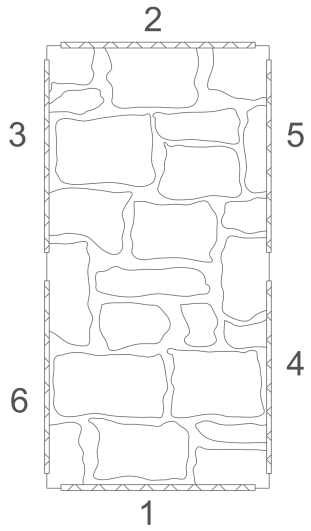

Figure 2.12: In the image the geometrical configuration of cuts, flat jacks and measuring points proposed by Jurina [90] for the evaluation of the shear strength is reported.

Caliò [34] presented other two methodologies. The first test consisted of two vertical cuts having length and depth close to the flat jack dimension. One of the cuts was used to insert the flat jack and the other cut was created to permit the horizontal displacements caused by the expansion of the *FJ*. A series of gauge points was used to monitor the displacements on the masonry sample. In this test, the vertical load acting on the sample was constant and consisted of the in situ vertical stress. The second methodology is more interesting because it is very similar to the in situ shear-compression test. In fact, a prism of masonry was partially isolated by means of two vertical cuts of 200 cm length positioned at a distance of 100 cm one from the other one. A flat jack was placed in the center of one cut and the other cut was made in order to allow displacements of the prism. In this case, the set-up allows to monitor and test two samples one above the *FJ* and the other under it. In fact, the horizontal stress created by the flat jack was balanced by two masonry panels that were partially loaded in diagonal by the *FJ* force and partially load by the vertical stress. The difference, between these tests and the in situ shear-compression test, is that, in this last one, the vertical stress is hydraulically controlled. On the contrary, in the test proposed by Caliò, the vertical load is fixed because it corresponds to the vertical load present in the wall.

Similar to the set-up designed by Jurina [90] is the one proposed in 2016 by Gambirasio et al. [71]. In this work, a numerical study of two different configurations for the evaluation of the shear characteristic was presented. This study was performed also considering different vertical load distributions. These configurations were similar between them and they considered the creation of two parallel vertical cuts in which two *FJ*s were placed (Fig. 2.13). The adopted approach is interesting because numerical *FEM* models were employed to optimize the geometry of the test before the in situ experimentation.

In 2016 also Simões et al. [173] worked with the configuration proposed by Caliò [34] in a masonry building in Lisbon.

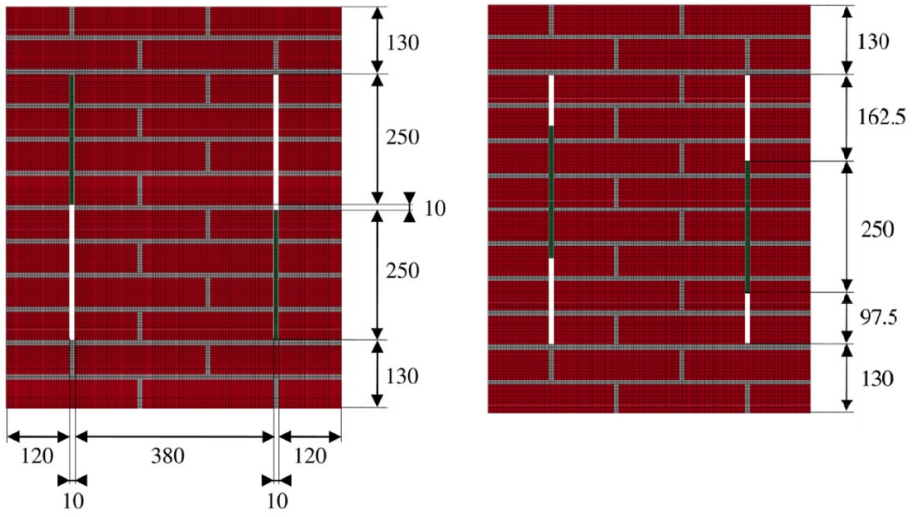

Figure 2.13: The image reports the two geometrical configurations of cuts and *FJ*s proposed by Gambirasio et al. [71]. The flat jacks are in green, the bricks in red and the mortar in gray. Inderscience retains copyright of figures.

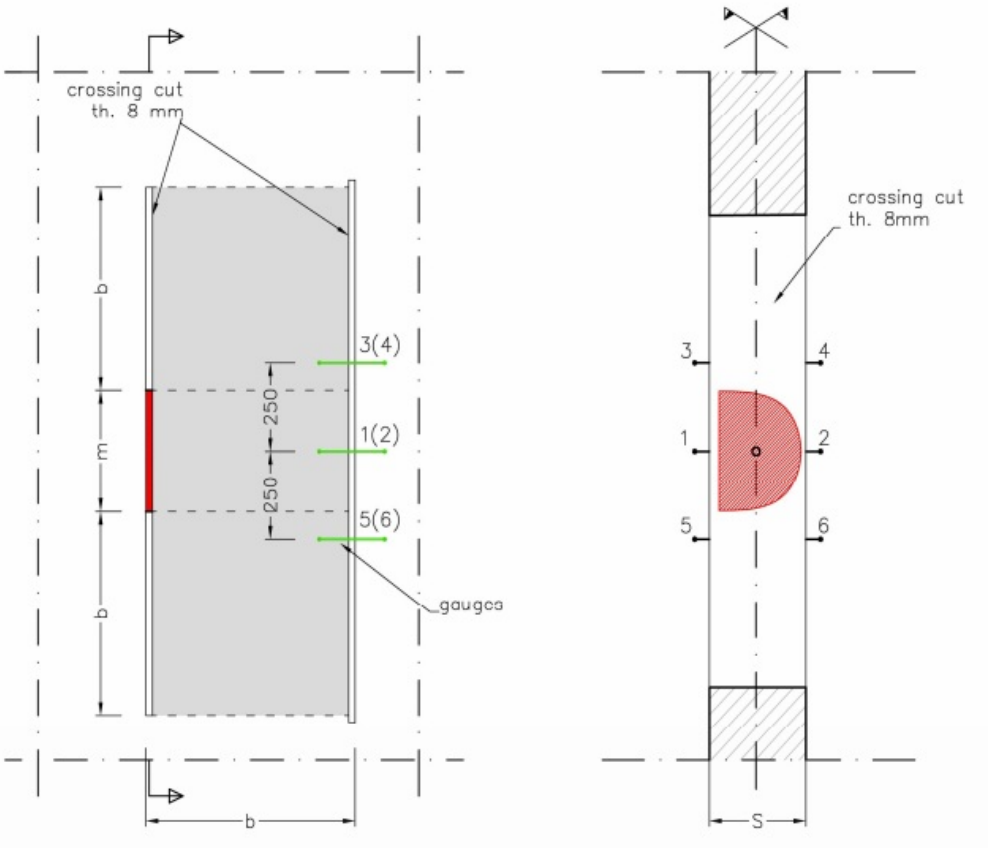

Figure 2.14: The image shows the layout of the shear characterization through flat jacks designed by Foppoli et al. [68].

The last effort (to the author's knowledge) for the assessment of the shear characteristics using *FJ* is the one proposed by Foppoli et al. [66, 67, 68] in 2016 and named *FJ-SCT* Method (Fig. 2.14). The geometrical configuration is similar to the one proposed by Gambirasio et al. [71]. In this case, only one flat jack was used. It was placed in the center of a vertical cut and the other cut was created in order to allow displacements of the sample. These vertical cuts were $160 - 200$ cm long, had a depth equal to the wall thickness and the distance between them was of $60 - 80$ cm. This geometrical configuration was adopted with the intention of testing two panels one above the flat jack and the other under it (similarly to the shear-compression test). The authors performed both laboratory and in situ tests. In the laboratory tests, real scale samples were used. These samples were tested in a specific frame which guaranteed the vertical and the horizontal reaction. The vertical load was provided by a large flat jack placed between the frame and the top of the specimen. In the in situ test the vertical load consisted in the actual vertical stress that was determined by means of a single flat jack test carried out next to the shear test. In addition, the authors performed a calibration with an in-scale diagonal compression test [66, 67]. These shear *FJ* tests showed a good agreement with the standard tests and with the Mohr-Coulomb criterion proposed by the Italian code [88]. This *FJ-SCT* method showed a disadvantage that consisted in the isolation of the sample. This isolation was inferior to the one of the *DT* methods but the dimensions of the specimen and of the cuts were relevant. In addition, these vertical cuts, where the *FJ*s are placed, pass through the whole thickness of the wall.

These works performed in the last 15 years highlighted the remarkable efforts done with the aim of obtaining shear characteristics of masonry. This fact underlines the dramatic necessity of obtaining a reliable *MDT* technique for the shear characterization. Furthermore, these efforts focus the attention on the possible utilization of the *FJ*s for this scope.

2.6 Acoustic emission

Acoustic Emission (also known as *AE*) is a passive *NDT* technique named after the homonym phenomena which consists in the propagation of elastic waves in solids. These waves are caused by the release of energy occurring during nucleation, propagation and coalescence of micro-cracks [79, 163, 171]. The first studies were performed in Germany by Kaiser in the '50s [92]. This method is applied to many fields such as monitoring and fatigue assessment and for a large number of different materials. In the present work, the *AE* technique was used to evaluate the damage evolution during the flat jack tests (not for the single *FJ* tests). In fact, this method can also give a quantitative non-destructive evaluation of the damage progression [43].

In the *AE* technique there are two methods used to record and to analyze signals. There are the parameter-based approach and the signal-based approach [19, 163]. In the signal-based approach, the waveform is recorded giving the opportunity of a deeper but more complicated and time consuming analysis. On the contrary, only some parameters of every single wave are recorded in the parameter analysis. This approach records a few data of each single waveform allowing also a real time monitoring [19]. In the present work the first approach was used and then through the analysis of the waves

parameters like the ones obtained in the parameter-based approach were evaluated.

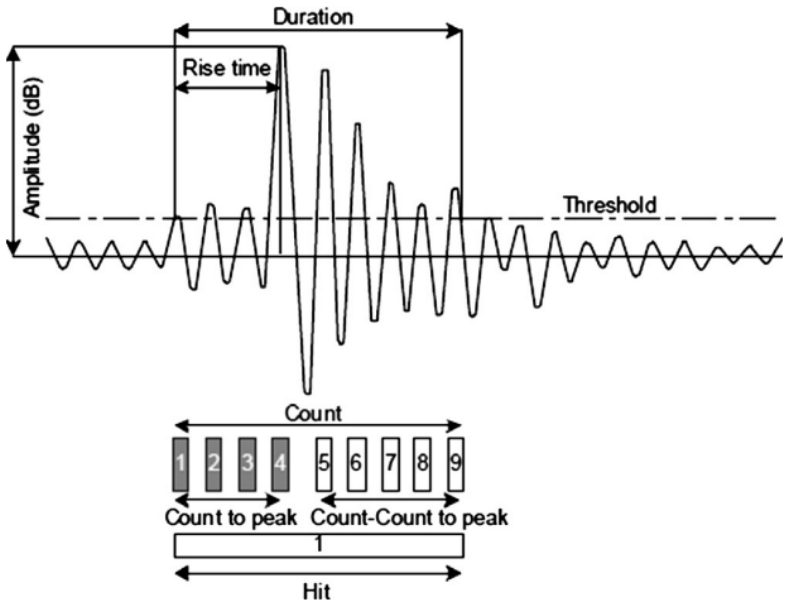

Figure 2.15: The image reports the schematization of the parametric analysis of an electric signal after its amplification and filtration [19]. http://www.sciencedirect.com/science/article/pii/S0950061814004292.

The *AE* measurement system is composed basically of three elements: transducers, amplifier and storage. Piezoelectric transducers are used in order to transform the mechanical waves into electric waves. These are applied to the surface of the sample by gluing them. The electric signal is then amplified and recorded. In both approaches, the recorded signal is passed through a filter that eliminates unwanted frequencies [38].

In the parameter-based method, the electrical signal is filtered and analyzed using a threshold level (Fig. 2.15) and just after the analysis is completed only the parameters are recorded. Many parameters can be analyzed and the same parameters can also be evaluated in the signal-based method. For example, for each event (signal) a parameter called oscillations counter (or counts) N_c increments every time that the electrical wave exceeds the threshold level. Each event is then characterized by the number of counts N_c that in a first approximation is correlated to the energy released during the event [38]. The number of events (N_{AE}) is also sometimes evaluated as well as the number of counts, the amplitude of the signal A_{dB} (the maximum value of the waveform) is correlated to the released energy. Other more sophisticated analyses record also additional parameters such as the rise time, the rise angle, the counts to peak, frequencies of the signal, the energy of the event and the duration between the first and the last part of the signal that exceeds the threshold [19].

One of the advantages of this technique is the possibility of localizing the *AE* sources. It results then possible to identify where the damage process takes place. The localization requires the knowledge of the sensors position, the speed propagation of waves through the medium and the time difference between the arrival of the signal to each sensor [41]. These parameters allow the triangulation of the signal sources. The

main problem in the source location in masonry is the speed of the waves. The path of the elastic waves and their attenuation depends on the heterogeneity of the medium. Consequently, the position of voids, cracks, bricks and joints may interfere in the localization [186].

As anticipated, the *AE* technique can be used to evaluate the damage evolution in the sample. One method to assess the damage is called the *b*-value analysis. This analysis is directly related to the Gutenberg and Richter empirical formula (Eq. 2.21) that is used in earthquake seismology [80]. This formula defines a logarithmic relationship between the magnitudes of events end their frequencies of occurrence:

$$log_{10}[N(\geq m)] = a - bm \tag{2.21}$$

where: m is the events magnitude, $N(\geq m)$ is the cumulative number of earthquakes having magnitude $\geq m$, a and b are positive empirical constant (varying from region to region [42] for what concerns earthquakes). The same formula (Eq. 2.22) is applied to the *AE* method to study cracking processes in structures or in samples:

$$log_{10}[N(\geq A_{dB})] = a - bA_{dB} \tag{2.22}$$

where: A_{dB} that is the amplitude of *AE* events in decibels. This possibility of using the same formula for different fields can be better understood considering that the magnitude m of a seismic event is a measure of the energy released and, similarly, also the amplitude A_{dB} is a measure of the same characteristic. During the damage process the *b*-value changes [42, 44, 52]. Maximum levels of *b*-value (around 1.5) are correlated to micro-cracks growth (critical condition) and minimum levels of *b*-value (around 1.0) highlight the imminent final failure (macro-cracks have formed) [42, 52].

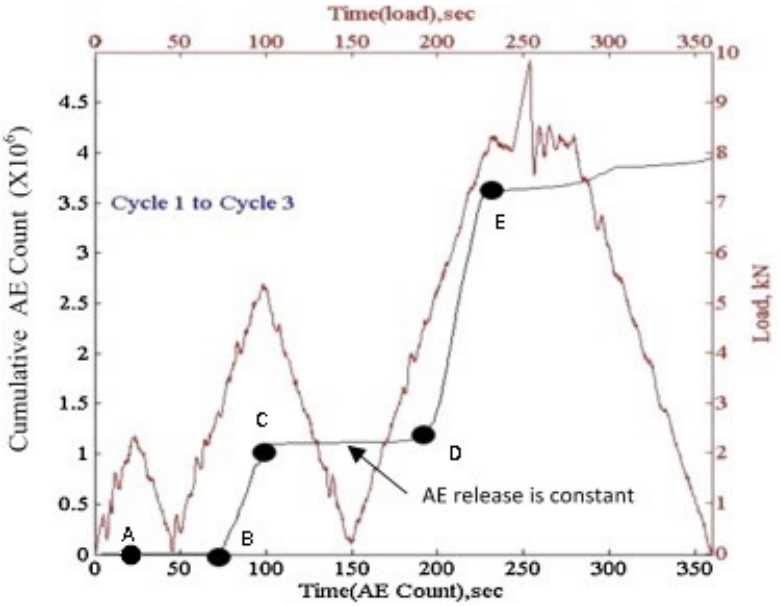

Figure 2.16: The graph displays in red different load cycles of a reinforced concrete beam and the cumulative *AE* counts line is plotted in black [164]. http://www.sciencedirect.com/science/article/pii/S1644966514000831.

There are other interesting characteristics of *AE* applications that can be used for damage control and evaluation. One of these is the Kaiser-effect [92] which consists in a reduction of the *AE* during a reload phase until the previous maximum load is achieved. This effect can be interpreted as a memory that "stores" the maximum previous load at which the sample/structure has been subjected [53]. An example of Kaiser-effect is present in Fig. 2.16 at point B. In fact, only at this point of the second cycle the *AE* activity starts highlighting that this load was already achieved in a previous cycle.

The Kaiser-effect is not always valid but for these cases the Felicity-ratio (named *FR*) can be used. This is the ratio between the load in which emissions restart and the previous maximum load. In Fig. 2.16, for example, *AE* restarts in point B and the corresponding load is the same as the one at point A. In this case the felicity-ratio is $FR = (load_B)/(load_A) \simeq 1.0$ indicating a perfect Kaiser-effect. On the contrary, in the third cycle, the *AE* activity starts in point D for a load of 4 kN. In this case in the previous cycle the load was stopped at 5 kN. The resulting Felicity ratio is $FR \simeq 4/5 = 0.8$.

Both the Felicity ratio and the Kaiser-effect are mutually connected. In fact, for very low levels of stress with respect to the material strength (up to the $70/85\%$ of the strength in concrete [128]) results easier to notice the Kaiser-effect ($FR = 1.0$). On the contrary, it is possible to observe a decrease in the Felicity-ratio for larger loads. Summarizing, both Kaiser-effect and felicity-ratio are tools used for the damage evaluation of structures and specimens.

It results now clearer that the *AE* method gives a tool to monitor and assess the damage. The fact that *AE* is a passive, non-invasive and non-destructive technique justifies the rising attention that, in the last fifteen years, has been paid to the application of this method also in masonry structures.

2.7 Numerical modeling

The numerical modeling of masonry is one of the important tools necessary to understand the behavior of this material and of the structure made using this media. As mentioned in previous Sections, this material is characterized by a pronounced non-linearity which is caused by the mechanical behavior of the joints (if they are present), the mechanical behavior of the resisting elements, the behavior dependence on the geometry of the resisting element, the presence of voids/defects/cracks, the anisotropy caused by the horizontal and vertical joints, etc. These non-linear behaviors lead to high computational efforts. This fact underlines why the study of masonry structures is usually performed numerically and inevitability results that, in some cases, simplified analytic model/handmade-evaluations could be hardly performed or might not be representative.

The studies of the last decades developed different numerical strategies for masonry modeling. These strategies can be divided into two different approaches which are the Finite Element Method (*FEM*) and the macro-elements approach (Fig. 2.17). The first is based on the use of bi or three-dimensional finite elements [36]. These can be used to model a structure from a detail of it to the whole of it, detail of a test, bricks, mortars, interfaces, etc. The macro-element is a simplified approach that aims at reducing the

computational efforts. Both approaches are described in the following Sub-sections where also a few brief notions of some numerical strategies are introduced.

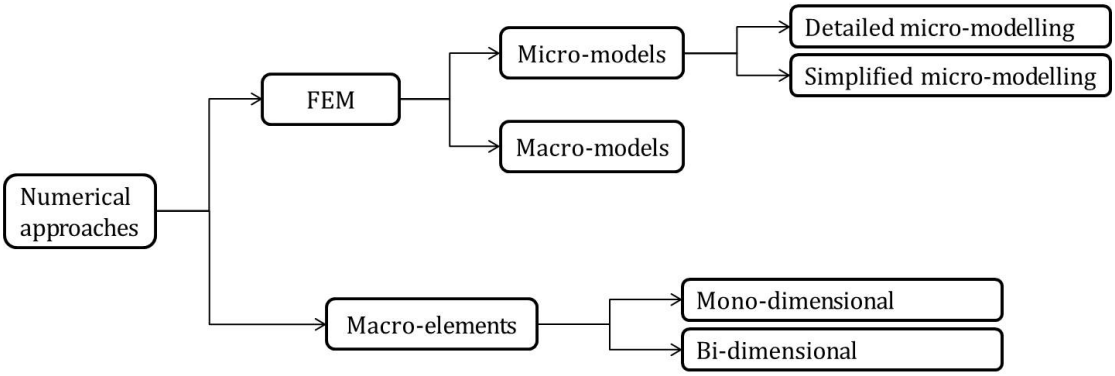

Figure 2.17: The chart summarizes the different numerical approaches used in masonry models.

2.7.1 *FEM*

As for the classification of the different masonry typologies, a univocal and universally accepted classification of the different types of *FEM* strategies existing for this material is not present yet [146]. However, following [106, 137, 161], it is possible to divide the *FEM* strategies into micro and macro-modeling (Fig. 2.17). The names of these two categories underline the potential applications of each technique. In fact, a micro-model can give a better comprehension of a local behavior of a structure but it fails if used to represent the whole structure and vice versa for the macro-model. The following paragraphs give some basic information and highlight the principal differences between these approaches.

Despite the *FEM* modeling approach is presented as a simple and unique technique, this is not true. In general *FEM* analyses could be performed by using a large number of methods like, for example, the generalized finite element method or the mixed finite element method. In masonry modeling, the most used techniques are the standard-*FEM* and eXtended Finite Element Method (*XFEM*) but they are not the only ones.

Micro-modeling

In the micro-modeling approach, particular attention is given to both the resisting elements (bricks/stones) and the joints. In this technique, these elements are modeled separately and considering dedicated constitutive laws. The first attempts of modeling independently joints and bricks (have almost five decades) and started with linear modeling (e.g. [174, 176]). These attempts were soon followed by non-linear modeling (e.g. [7, 72]). The use of this strategy must be adopted to only some parts of the structure because larger models lead to huge numerical efforts. Using this approach to model an entire structure can create problems considering that every single brick and joint has to be meshed. In addition, this technique can be utilized only when the exact

geometry of the element exists [108, 126]. On the other hand, these disadvantages become advantages when a more refined and detailed knowledge is necessary. In fact, it can be applied to model a small test, for example, the ones executed on masonry panels.

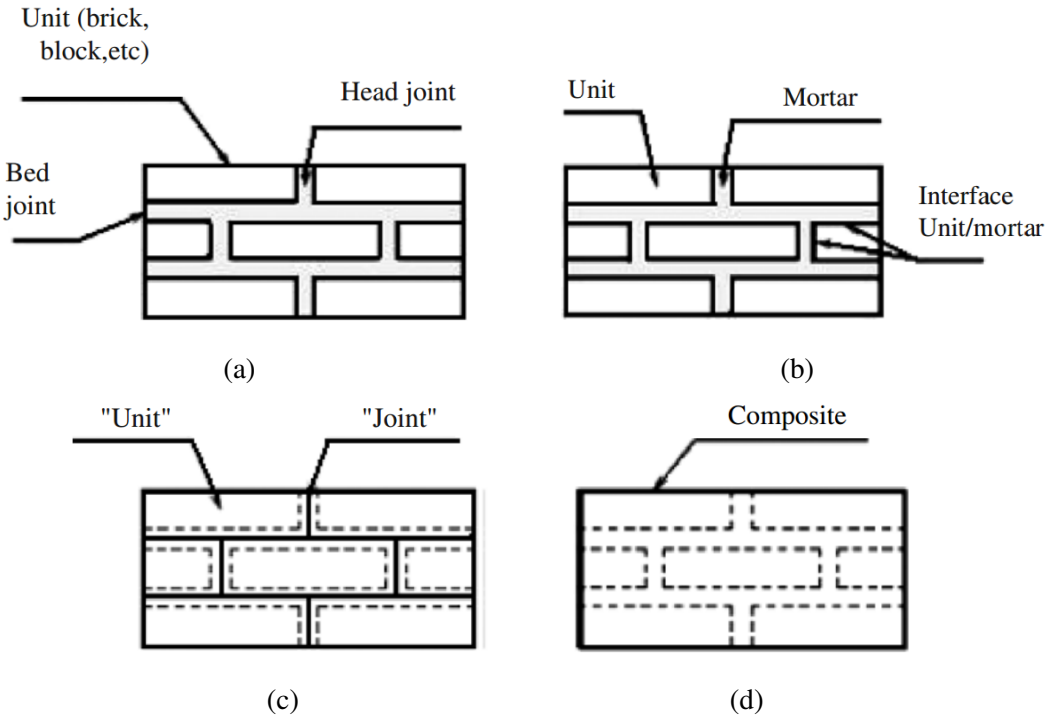

Figure 2.18: In the image different *FEM* modeling strategies are presented [168]. In particular, it is represented the masonry sample in Figure 2.18a, Figure 2.18b represents the detailed micro-modeling, in figure 2.18c the simplified micro-modeling is shown and in Figure 2.18d the macro-modeling is represented where the masonry is considered as a composite media. http://www.sciencedirect.com/science/article/pii/S0141029609000753.

This strategy can be divided into two distinct subcategories that are the detailed micro-modeling and the simplified micro-modeling [10, 168]. These categories are briefly presented.

The detailed micro-modeling (Fig. 2.18b) is the most accurate numerical approach used to model masonry. This strategy consists in modeling the masonry as a three-phases material [10]. These three phases are the resisting elements (bricks or stones), the mortar joints and the interfaces between the resisting elements and the joints. In this modeling typology, resisting elements and joints are modeled considering specific linear or non-linear constitutive laws and the interfaces are considered using special joint, contact or interface elements [126, 168]. The joint-brick interfaces are an important part of the masonry because they represent a plane of weakness in which cracks are often located [5]. The micro-modeling is rarely used in field applications [20] but it is applied when a high quality of the results is requested. For example, this strategy is used when specimens are modeled. The main difficulties of this numerical technique are the correct modeling of the geometry, the knowledge of the mechanical characteristics of the three different materials and of the knowledge/model of the three constitutive

laws. Sometimes the interfaces are not modeled and this results in a simplification in the creation of the model.

The simplified micro-model (Fig. 2.18c) considers masonry as a two-phase material [10]. The mortar joints are represented by discontinuous elements [168] which have zero thickness. For the sake of geometry, the bricks have a dimension expanded in comparison to the reality in order to compensate the zero thickness of the joints. The joint elements must represent the behavior of the mortar considering both the normal and shear stiffness properties [98] and they also have to represent the properties of the joint interface. These properties are lumped together in a unique element that allows a reduction of the computational efforts. Thanks to this technique the possibility of modeling part of structures or small structures is enabled [10, 126].

Macro-modeling

The macro-modeling (Fig. 2.18d) assumes that masonry can be represented as a unique phase material and for this scope the properties of bricks, joints and interfaces are smeared together in a homogeneous continuum. This continuum can be considered isotropic, orthotropic or anisotropic [168]. An advantage of this approach is the possibility of modeling entire structures and complicated geometries by using automatic or user-friendly mesh generators [106]. The macro-models are widely adopted for the global assessment of structures but are also used for more detailed analyses.

The material properties for the macro-model are obtained with three main approaches. The first consists in collecting experimental data directly from masonry specimens without considering the characteristics of each material [5, 108]. The second approach considers masonry as a composite material and evaluates its characteristics through homogenization techniques. These techniques consist in a mathematical process that examines the geometry, some materials parameters and the behavior of an elementary volume in order to obtain averaged parameters for the composite material [108, 125, 194]. The last approach to obtain these parameters is the search in codes and literature. This search has to be performed carefully and paying attention to the typology, texture, types of mortar and bricks, etc.

2.7.2 Macro-elements

The macro-element approach is a simplified methodology. The nomenclature of this method is not well defined and different names are used for example structural component models [107], macroblock approaches [108], or just simplified approaches. It is clear that the main characteristic of these numerical approaches is the simplification of the model which leads to a drastic reduction of the computational efforts. This is the most important feature of this approach because it speeds up the global assessment of structures.

In the macro-element models, the computational times are reduced in comparison to the *FEM* models because a lower number of unknowns is present. In the finite element models each wall of the structures is discretized into a large number of bi- and/or three-dimensional finite elements [93, 107]. In the macro-element approach, a

masonry panel is modeled using a few (or only one) elements. In fact, single structural components such as piers, spandrels, arches and vaults are modeled using beams, trusses, panels, shells and rigid elements [107]. As a result, the structure is modeled as a bi- tri-dimensional frame or is discretized into mono- and bi-dimensional discrete elements [33, 120]. This numerical method allows to speed up the computational times but leads to a disadvantage which consists in the loss of accuracy of the model [106].

The macro-elements approach groups a large number of different strategies. Considering the type of macro-element used, these strategies can be divided into mono- and bi-dimensional methods. A focus on all the different strategies is not presented in this work.

As their name state, in the bi-dimensional methods the structure is modeled using bi-dimensional elements. An example of this strategy is the one proposed by Caliò et al. [35]. In this method, the elementary element is represented by an articulated quadrilateral constituted by four rigid edges connected by four hinges and two diagonal non-linear springs [32, 35].

In literature a large number of different mono-dimensional macro-elements approaches are present but the most important of these is the equivalent frame method. The name of this method derives directly from the strategy used to model the structure. In fact, every wall with or without openings is properly simplified (Fig. 2.19), the result is a frame consisting of spandrels and piers connected together by rigid links [4, 115].

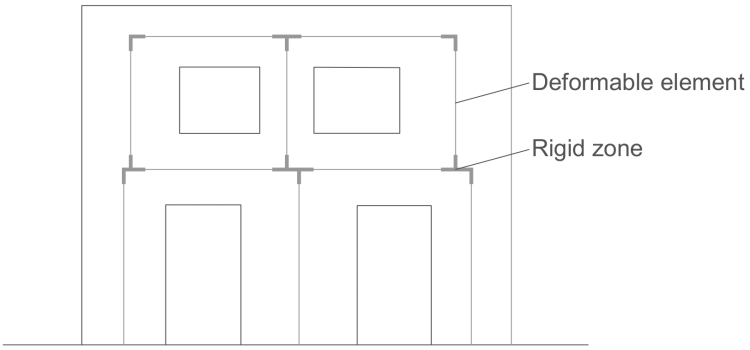

Figure 2.19: The image represents a wall and its representation using the equivalent frame method.

As mentioned, there are many methods and software operating with the approach of the equivalent frame model. It is important to cite the *POR* method [182] born in the '70s for its impact and for historical reasons. Another important contribution to this numerical technique was given by the *SAM* method [112, 114].

The differences between the *FEM* and the macro-elements approaches were analyzed by different authors (e.g. [33, 93, 115, 136]). Calderoli et al. [33] considered the results obtained by an equivalent frame model quite reliable compared to others obtained using *FEM* analyses. However, in the case of complex geometries, the quality of the results is influenced by the modeler capacity. Also Mallardo et al. [115] highlighted the fact that attention has to be paid by the modeler in order to obtain reliable results from equivalent frame models.

2.8 Building codes

This section gives an overview of recommendations and codes referred to the masonry constructions. In particular, attention is paid to the Italian building codes [88, 85] (known as *NTC08* and *NTC18*) and to the circulars of these codes [86, 87]. In parallel to these codes, another Italian code focused on the evaluation and reduction of the seismic risk for the cultural heritage [143] has to be cited. Other codes are also important because they are helpful and can help finding solutions in some situations and/or for specific problems. At the European level it can be cited the Eurocode 6 [46] and for the *USA* in the *FEMA* [62].

The topics reported in this Section are two and are both related to the existing *URM* structures. The first is dedicated to the type of analyses more frequently used to assess structures under seismic action. The second topic is related to the material properties for models. For the sake of simplicity and brevity, only some aspects are presented notwithstanding the possibility for the reader to investigate these, other codes and literature.

2.8.1 Analysis of masonry structures

In literature a large number of possible strategies proposed to analyze masonry structures are present. In this Sub-section a brief overview of the Italian recommendations regarding the methods of analysis of these structures under seismic actions is introduced. The analyses regarding self-weight, variable loads, snow, wind, etc., are not treated. This choice was made considering that these vertical loads (excluding wind) lead mainly to a compressive stress. The wind was not considered in this dissertation assuming that the level of stress caused by this action is very low compared to the strength of the material. This assumption is not totally wrong because normally masonry constructions (residential buildings) are not very tall and at the same time are very massive (if chimneys, some church façades and bell towers are excluded). The main horizontal action that can interfere with the global behavior of *URM* structures is the seismic one.

The possible failures in civil structures under seismic actions are of two types, the local and the global mechanisms. The local mechanisms affect only a part of the structure. On the contrary, global mechanisms involve the whole construction (e.g. [86, 87]). In global mechanisms, it is almost always assumed that the masonry panels work in their own plane. In contrast, in local mechanisms the out-of-plane behavior is more often studied. This dissertation is focused on the global behavior of structures and for this reason local mechanisms are not studied and evaluated.

The *NTC08* and the *NTC18* [85, 88] define four different analyses for structures under seismic action. Considering the type of analyses, these are divided into linear and non-linear. In this last one, the materials and non-linearities (and not always also the geometrical non-linearities) are taken into account. There is also another level of classification. This divides the methods of analyses considering the two possible ways to treat the equilibrium which can be static or dynamic. Therefore, the analyses are: the linear and dynamic analysis, the linear and static analysis, the non-linear and dynamic analysis and the last one is the non-linear static analysis. Of these four types of analyses, the last one is the one more used to assess *URM* structures.

The non-linear static analysis (push-over) consists in the application of the gravity loads and later of a system of horizontal forces. The horizontal actions are increased in order to have a monotonic growth of the displacement d_c of a controlling point (sometimes coincident with the center of the mass of the upper level of the construction). The horizontal forces have an equivalent lateral force (or base shear) named F_b and the graph F_b-d_c represents the capacity curve of the structure. The structure is then associated with an equivalent system having one degree of freedom from which the structural behavior is evaluated.

It is another time underlined the noticeable importance of the assessment of structures under horizontal actions. This puts in evidence how important is the characterization of the shear modulus and of the tensile strength.

2.8.2 Mechanical properties

In this small Sub-section some code recommendations [86, 87] about mechanical properties required for the numerical-analytic models of masonry structures are introduced. At the same time, also some works present in literature are cited. It is important to highlight that these properties are referred to the historical *URM* (unreinforced masonry).

First of all, it has to be known that this media has a behavior that is characterized by a strain softening. This feature is in common with other ceramic materials (e.g. rocks, concrete, bricks, etc.) [108]. This softening behavior can be described, in a sample or a structure, as a decrease of the mechanical resistance associated with the increase of deformations [108]. This decrease of resistance is due to the growth and development of cracks. For this reason, the softening is described with the fracture energy of the media (Fig. 2.20). If the heterogeneity of masonry is taken into account it is understandable that the mensuration of the fracture energy results not easy to be performed. Lourenço [108] suggested to use the ductility index d_{uc} in order to evaluate the fracture energy under compression [111]. Adopting this index, the evaluation of the fracture energy in compression G_{fc} is performed with the following equation:

$$G_{fc} = d_{uc} f_c \tag{2.23}$$

where f_c is the compressive strength of the material. The usually adopted ductility index is $d_{uc} = 1.600$ mm [108, 111] that is taken from the Model Code 90 [51] and it is valid for $f_c < 12$ MPa.

The masonry fracture energy in tension G_{ft} is more controversial and the values of this characteristic vary sometimes of an order of magnitude among authors. As an example, it is possible to find in literature values of $G_{ft} \sim 100$ N/m (e.g. [6]) or, more frequently, of $G_{ft} \sim 10$ N/m (e.g. [105, 133, 134]). In the opinion of the author it is better to utilize the ductility index given by Lourenço [108]:

$$G_{ft} = d_{ut} f_t \tag{2.24}$$

In which $d_{ut} = 0.028$ mm.

Following the codes, the mechanical parameters necessary to model structures are treated in two different ways in dependence on the type of analysis performed. In the

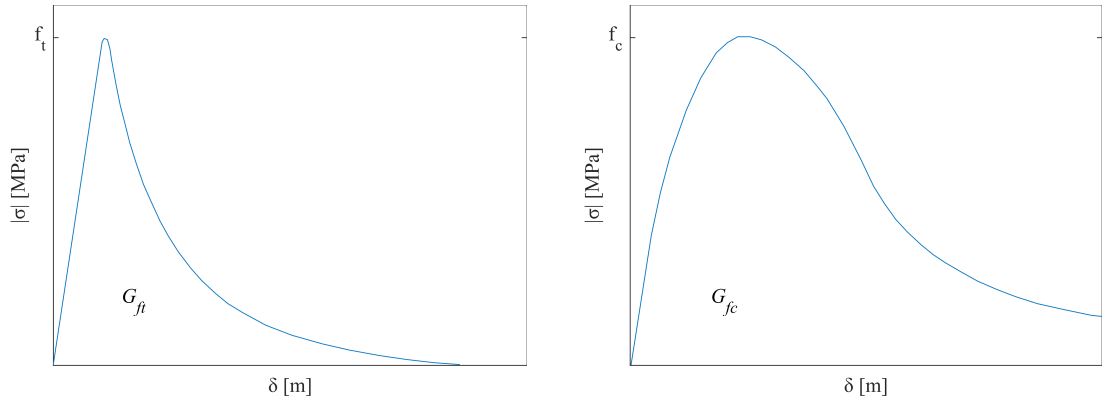

(a) (b)

Figure 2.20: In the graphs the representation of the softening behavior is reproduced. Figure 2.20a shows the tension softening and Figure 2.20b shows the compression softening behavior.

case of elastic analyses, these parameters are calculated dividing the average strengths by the confidential factor (*FC fattore di confidenza*) and then divided by the partial material safety coefficients. For non-linear analyses, the properties used for modeling are calculated dividing the average strengths by only the confidential factor *FC* (C8.7.1.5 [86]).

The confidential factors are safety coefficients related to the level of knowledge *LC* of the structure under examination. For masonry structures three different levels of knowledge from, *LC1* to *LC3*, are present. For each level the mechanical parameters are defined in the following way:

- *LC1*. This is the lowest level of knowledge and the corresponding confidential factor is $FC = 1.35$. This level is associated with a limited investigation of the construction details and of the mechanical characteristics. For this level, the average strengths and the elastic moduli (assumed from Tab. 2.3) are then elaborated as here reported:
  - elastic moduli: the average values;
  - strengths: the minimum values.
- *LC2*. A confidential factor of $FC = 1.20$ is assigned to this level. This level implies an exhaustive and extended knowledge of construction details and extended investigations of the mechanical properties. For this level, the average strengths and the elastic moduli (assumed from Tab. 2.3) as:
  - elastic moduli: the average values;
  - strengths: the average values.
- *LC3*. This level is assigned to the best investigations on the structure. A confidential factor of $FC = 1.00$ corresponds to this level. This level implies exhaustive and extended knowledge of construction details and exhaustive investigations of

the mechanical properties. For this level of knowledge, the average strengths and the elastic moduli are assumed with another method that also takes into account the experimental values.

- elastic moduli: the average experimental values or the average values of Tab. 2.3;
- strengths:
  - Case *a* (Three or more experimental strength values): the averages of the experimental values;
  - Case *b* (Two experimental strength values):
    - if the averages of the experimental values are larger than the maximum values of Tab. 2.3 these maximum values are then used;
    - if the averages of the experimental values are between the values of Tab. 2.3, the averages of these values are then used;
    - if the averages of the experimental values are inferior to the minimum values on Tab. 2.3, the averaged experimental values are then used.
  - Case *c* (Only one experimental values are present):
    - if the averages of the experimental values are larger or in between the values of Tab. 2.3, the mean table values are used;
    - if the averages of the experimental values are inferior respect to the minimum values of Tab. 2.3, the averaged experimental values are used.

(For the definitions of the terms limited, extended and exhaustive please refer to the Italian code C8A.1.A.3 [86])

Two tables of mechanical properties of masonry are presented. The first one is referred to the circular of the Italian code 2008 [86] (Tab. 2.3) and the other one refers to the newest circular [87] (Tab. 2.4). In these tables, the properties are referred to values (min and max) of the mechanical parameters for historical masonry that have poor mortar characteristics, absence of courses, leaves not connected, absence of consolidation and texture (in case of regular resisting elements) executed in accordance with the best practice. (For the translation of the masonry types Brignola et al. [31] was followed).

Tables 2.3 and 2.4 refer only to some specific characteristics of masonry. However, it is possible to consider constructions with other features and in these cases it is possible to correct the mechanical properties according to these characteristics (Tab. C8A.2.2 [86] for *NTC08* and Tab. C8.5.II [87] for the *NTC18*). The coefficients indicated in these tables can increase or decrease the values of the mechanical parameters. These coefficients change also in function of the type of masonry and they take into account the presence of joints of small thickness, courses, connections between leaves, consolidation and the presence of joints that have good mechanical characteristics.

It is important to know how these properties are then used in the evaluation of the behavior of the masonry structure. In particular, due to the main topic of the thesis, a

Table 2.3: Table of the values of mechanical parameters for historical masonry (part of the Tab. C8A.2.1 [86]). $f_{c,m}$ is the mean compressive strength, τ_0 is the mean shear strength, E is the mean Young's modulus, G is the mean shear modulus and w is the specific weight.

Masonry type	$f_{c,m}$ MPa	τ_0 MPa	E MPa	G MPa	w kN/m^3
Rubble stone	1.0 1.8	0.020 0.032	690 1050	230 350	19
Multiple-leaf hewn stone	2.0 3.0	0.035 0.051	1020 1440	340 480	20
Stone masonry with good texture	2.6 3.8	0.056 0.074	1500 1980	500 660	21
Soft stone (tuff)	1.4 2.4	0.028 0.042	900 1260	300 420	16
Solid stone blocks	6.0 8.0	0.090 0.120	2400 3200	780 940	22
Solid brick and lime mortar	2.4 4.0	0.060 0.092	1200 1800	400 600	18

focus is given to the shear resistance of masonry panels. The author refers to the latest version of the Italian code (*NTC18* and circular [86, 88]) to do this.

Following the Italian code, the shear failure of a masonry panel can be achieved in two ways:

- Masonry with irregular texture. In this case, the failure is reached with a diagonal tensile failure and the resistance of the panel is dependent on the shear strength τ_0. The strength of the masonry element is evaluated with the formulation proposed by Turnšek and Čačovič [183]:

$$V_{t,d} = A_s \frac{1.5\tau_{0d}}{b}\sqrt{1+\frac{\sigma_0}{1.5\tau_{0d}}} = A_s \frac{f_{td}}{b}\sqrt{1+\frac{\sigma_0}{f_{td}}} \tag{2.25}$$

  where (as in Eq. 2.7): A_s is the cross area of the specimen calculated as $A_s = lt$ in which t is the specimen thickness and l its width, b is a shape factor that takes into account the stress distribution, σ_0 is the mean vertical stress and f_{td} is the tensile strength.

- Masonry with regular texture. The previous failure typology can be considered because it is precautionary. However, the equation that is more suitable for these panels is:

$$V_{t,d} = \frac{A_s}{b}\left(\widetilde{f}_{v0d} + \widetilde{\mu}\sigma_0\right) = \frac{A_s}{b}\left(\frac{f_{v0d}}{1+\mu\phi} + \frac{\mu\sigma_0}{1+\mu\phi}\right) \leqslant V_{t,lim} \tag{2.26}$$

Table 2.4: Table of mechanical parameters for historical masonry (part of Tab. C8.5.I [87]). $f_{c,m}$ is the mean compressive strength, τ_0 is the mean shear strength with no perpendicular stress (case 1), f_{v0} is the mean shear strength with no perpendicular stress (case 2), E is the mean Young's modulus, G is the mean shear modulus and w is the specific weight.

Masonry type	$f_{c,m}$ MPa	τ_0 MPa	f_{v0} MPa	E MPa	G MPa	w kN/m^3
Rubble stone	1.0	0.018	-	690	230	19
	2.0	0.032	-	1050	350	
Multiple-leaf hewn stone	2.0	0.035	-	1020	340	20
		0.051	-	1440	480	
Stone masonry with good texture	2.6	0.056	-	1500	500	21
	3.8	0.074	-	1980	660	
Soft stone irregular (tuff)	1.4	0.028	-	900	300	13-16
	2.2	0.042	-	1260	420	
Soft stone regular (tuff)	2.0	0.040	0.10	1200	400	13-16
	3.2	0.080	0.19	1620	500	
Solid squared stone blocks	5.8	0.090	0.18	2400	800	22
	8.2	0.120	0.28	3300	1100	
Solid brick and lime mortar	2.6	0.050	0.13	1200	400	18
	4.3	0.130	0.27	1800	600	

where: f_{v0d} is the shear strength of the masonry with no vertical stress acting on it, μ is the friction factor, ϕ is the internal grip of the masonry. The limit of this shear resistance is dependent on the block tensile strength f_{btd} and is evaluated by:

$$V_{t,lim} = \frac{A_s}{b}\frac{f_{btd}}{2}\sqrt{1+\frac{\sigma_0}{f_{btd}}} \tag{2.27}$$

The tensile strength of the resisting element can be estimated considering the 10% of the compressive strength of the same element.

As can be noticed in the two Tables 2.3 and 2.4, in the *NTC08* the shear failure of a masonry panel was evaluated only with the formulation of Equation 2.25. In the newest code (Tab. 2.4), a column of f_{v0} is present. This strength considers the shear failure in mortar joints, is present.

2.9 Summary

The present Chapter provided an overview of the materials, structures and codes required for the comprehension of this dissertation. The inherent topics that are closer and more related to the objective of the thesis were deeply explored. On the contrary, other

subjects were treated more superficially. This choice was made considering the main topic of the thesis in order to provide a functional state of the art of *URM*. The main effort of this Chapter was oriented to define and explain the methods and tests adopted for the characterization of this material. This focus is required considering the main topic of the thesis. At the same time, some bases on material properties and numerical methods were also presented. In some cases, this Chapter provides references and examples in order to give the opportunity to the reader to better understand problems and/or methods that are only treated superficially for reasons of time and brevity.

Chapter 3

Shear *FJ* test

As said in the previous Chapters, some efforts were already performed in order to obtain shear mechanical properties through a *MDT* method [66, 67, 68, 71, 90, 173]. A definitive *MDT* technique for the evaluation of these characteristics is still not present.

The present Chapter aims to explain the steps performed to obtain the proposed *MDT* method, the "shear *FJ* test method". To be more precise, the Chapter explores the design procedure, the analysis of the chosen test set-up and the creation of models that represents the stress-strain status of the sample under test.

Some of the results obtained in the present Chapter were published in [188].

3.1 Test design

In this Sub-section the design procedure adopted to create the new shear *FJ* test is introduced. This design was developed through two main phases. In the first phase different geometrical configurations were defined considering literature and the objectives sought, and then numerically modeled and in the second phase considerations about the results were used to choose the final set-up.

As introduced, the first part of the design consisted in *FEM* analyses. These were performed on six different flat jack configurations by taking into consideration different geometries of cuts and *FJs* positions. The main purpose of these numerical simulations was the evaluation of the direction of the principal stress in order to obtain a 45° inclination with respect to the horizontal. It was taken into consideration not only the principal stress inclination but also the values of the stresses.

The second part of the design had as purpose the choice of the final test configuration. This choice was affected by the stress orientation and magnitude but also by parameters like costs and destructiveness. These technical considerations were an important part of the design because they guarantee the cost convenience and, even more important, the low impact on the building integrity and aesthetic.

3.1.1 Numerical models

The *FEM* models were created using two software: *LUSAS* [109, 110] and *DIANA* [65]. In this first part of test design, a single simple geometrical element that

represents a generic wall was used to evaluate the six configurations of cuts and *FJs*. This wall was defined as a rectangular cuboid of 2 m height, 2 m length and 0.5 m thickness (Fig. 3.1) and was analyzed using *LUSAS*.

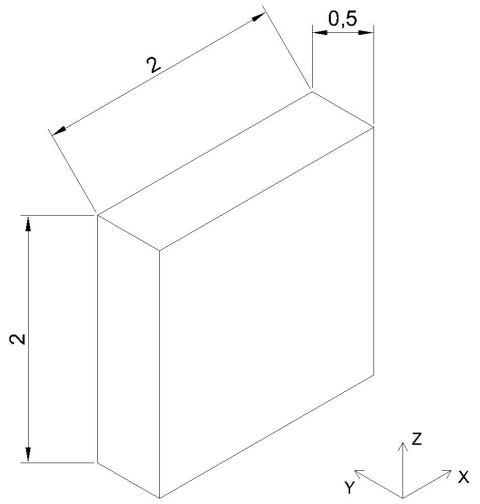

Figure 3.1: The image displays the wall dimensions used for *FEM* investigations.

The modeled wall was considered elastic, isotropic and homogeneous. These are strong assumptions for a material like masonry but the aim of this modeling part was only to find the best configuration for the test. Still, these assumptions are often taken. The micro-modeling would lead to more correct results. Still, it wouldn't be worthwhile considering the time needed for creating this model and also the fact that it is just a first part of the design process. The investigations of the walls were performed using simple linear analysis. It was then supposed that the wall was composed of bricks with lime mortar. These hypotheses were taken into consideration in order to find the elastic characteristics in the Italian Code (Tab. C8A.2.1 [86]). The mechanical characteristics used for the models were $E = 2000$ MPa and $\nu = 0.25$.

The base of the wall was fully restrained. On the other hand, in a first phase of the analysis, the translations along the vertical axis of the top of the model were released. However, all the other degrees of freedom of this face were restrained. This choice was taken because a vertical stress of $\sigma_0 = -0.20$ MPa was put on the top of the wall which represents the vertical stress coming from the superstructure.

Six different configurations (named *a*, *b*, *c*, *d*, *e* and *f*) were considered. These configurations were made using distinct geometries of slots, flat jack dimensions and different flat jack positions. The slots were obtained by subtracting thin cuboids from the wall. These subtractions, that represent the cuts made in situ, were supposed to have different lengths and depths. The width of these cuts was the only dimension that was fixed at 10 mm for all the configurations. Rectangular loads were then assumed to represent the flat jack stress in the slots. A brief description of the six configurations is here presented.

Configuration *a* (Fig. 3.2). This set-up, that uses four flat jacks, is very similar to the one presented by Jurina [90] and to the one proposed by Simões et al. [173].

The configuration presented shows two main advantages. The first is the possibility of performing the shear test after a double flat jack test. This double *FJ* test should be performed just in the elastic range in order to not damage the sample. The second advantage is the possibility of performing the shear test by varying the vertical stress that acts on the tested part of the masonry. The horizontal cuts had lengths of 400 mm and of depths 200 mm that were chosen in order to allow the access to two *FJs* that have the same dimensions of the cuts. The distance between these two cuts was imposed at 600 mm following the recommendations for the double *FJ* test [12, 155]. This distance corresponds to 1.5 times the flat jack length. The vertical cuts, with a depth equal to 120 mm, were positioned at the vertex of the horizontal ones. In these slots two flat jacks (240×120 mm) were positioned. These jacks create the inclined stress inside of the sample. In this set-up the possibility of varying the load in the horizontal *FJs* was considered. This means that there is the necessity of two different hydraulic systems.

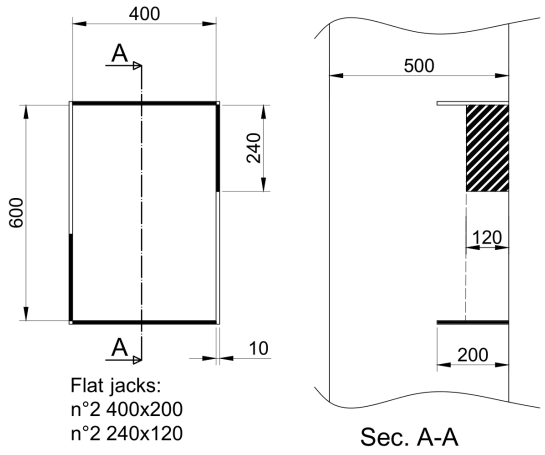

Figure 3.2: The image shows the cuts and flat jacks configuration *a*.

Configuration *b* (Fig. 3.3). Only two *FJs* were considered for this geometry in which the cuts (of 400 mm length and 200 mm depth) were inclined of 45° with respect to the vertical axis. As for configuration *a*, the distance between the two slots was taken as 1.5 times the length of the flat jack length. The proposed configuration perfectly corresponds to the standard double *FJ* test [12, 155], with the only difference being the 45° inclination. Flat jacks having length of 400 mm and depth of 200 mm were used in the model. No others cuts were present in this configuration.

Configuration *c* (Fig. 3.4). This configuration is very similar to the previous one. The two shortest cuts (of 400 mm length and 200 mm depth) were considered inclined of 45° with respect to the vertical axis. The difference between *b* and *c* is that other two cuts were modeled in the latter one. These were placed perpendicularly at the external edges of the other two cuts already described. The two longer slots, of 600 mm length and 200 mm depth, were conceived in order to partially isolate a cuboid in which the test was performed. This separation was conceived in order to have a sample that is not (or not completely) subjected to the vertical stress.

Configuration *d* (Fig. 3.5). It is possible to notice that the *d* set-up was modeled starting from the diagonal compression test [15, 156]. The differences between the two

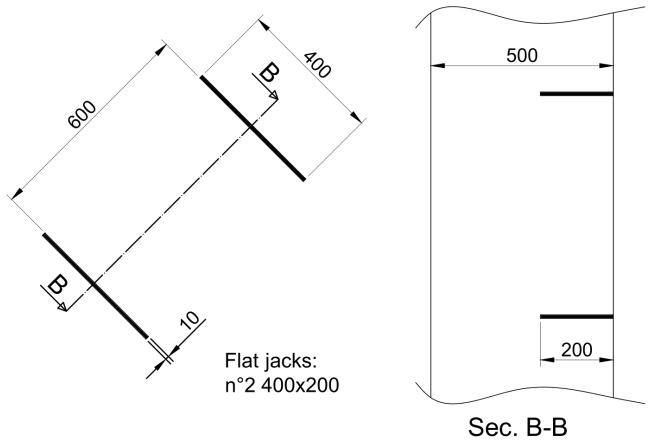

Figure 3.3: In the image are displayed cuts and flat jacks configuration *b*.

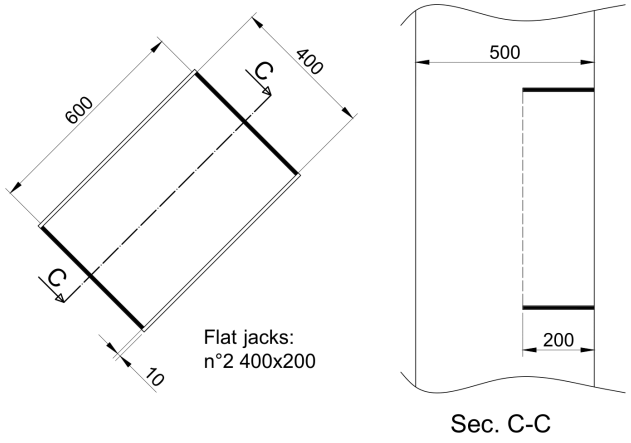

Figure 3.4: The image shows the cuts and flat jacks configuration *c*.

tests are the dimensions of the sample and the fact that in the proposed configuration the sample is not completely isolated. In the proposed layout the four cuts had lengths of 800 mm. This dimension was decided in order to slightly decrease the size of the specimen with respect to the standard diagonal test. A 120 mm depth of the slots was imposed. This measure was chosen in order to accommodate the 240×120 mm flat jacks. As in configuration *c*, also in this case the choice of creating long cuts was taken in order to provide a partial insulation from the rest of the wall.

Configuration *e* (Fig. 3.6). This set-up took in consideration only two cuts and two flat jacks. The slots were vertically oriented and they have a depth of 120 mm, a length 880 mm and a relative distance of 400 mm. The two *FJs* were assumed to be 240×120 mm. The principal aim of this configuration was to obtain a squared sample where the stresses are concentrated. To this purpose, the total length of the cuts is equal to the sum of the two lengths of the flat jacks (240 mm) plus the space between the cuts (400 mm). Placing one *FJ* on the bottom of the first cut and the other flat jack in the top of the other slot, the squared sample in which the stresses are concentrated was obtained.

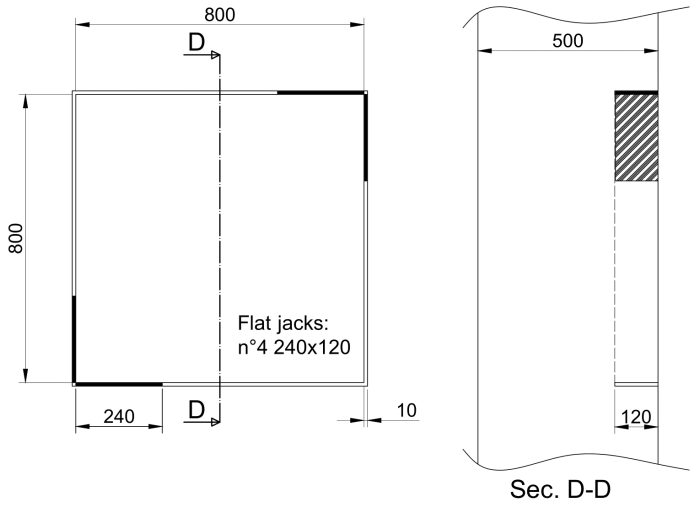

Figure 3.5: In the image cuts and flat jacks configuration *d* are displayed.

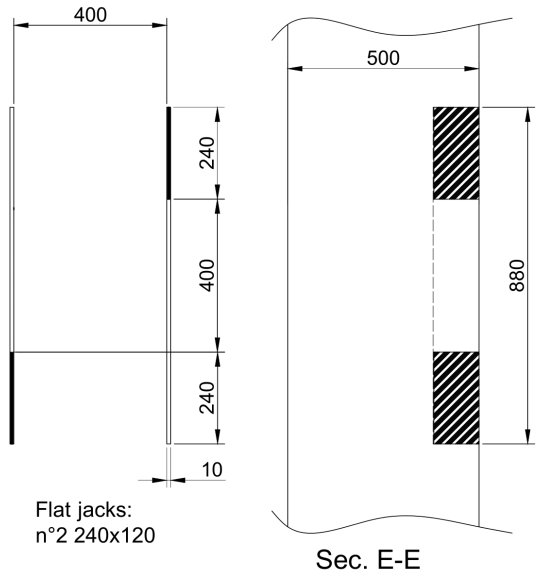

Figure 3.6: The image shows cuts and flat jacks configuration *e*.

Configuration *f* (Fig. 3.7). This last configuration is very similar to the method proposed by Foppoli et al. [68]. The present configuration was developed in a similar way to the previous one (conf. *e*). In fact, the purpose was to create two squared samples where the stresses are concentrated. In order to achieve this goal, two cuts spaced 400 mm were modeled. Their length (1040 mm) is equal to two times the space between the cuts plus the length of the *FJs* used (240 mm). This configuration seems to be the most effective because it can test two specimens at the same time (one in the zone above the flat jack and the other one in the zone under it) and use only one *FJ* (dimension of 240×120 mm). The stress states of these two specimens are not perfectly identical due to the self-weight of material. In fact, the lower sample has additional stress coming

from the dead load of the upper specimen. It can be stated that this difference is very small and that can be neglected considering the magnitude of the acting vertical stress modeled (or present) in the wall.

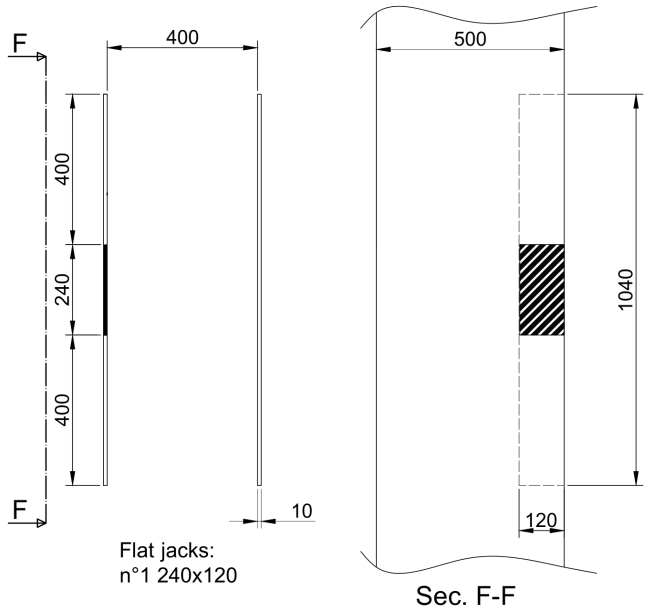

Figure 3.7: In the image cuts and flat jacks configuration *f* are displayed.

As mentioned before, for all configurations a vertical stress of $\sigma_0 = -0.20$ MPa was considered. As already said, the *FJs* were simulated using rectangular loads that represent the pressure exchanged between the actuator and the masonry. The load was supposed to be perpendicular to the cuts surface. Each configuration was studied through three different load steps (*FJ* stress of 0.10, 0.20 and 0.50 MPa).

It was impossible to obtain a perfect regular mesh due to the presence of cuts. Linear tetrahedral elements named TH4 [109, 110] were used for the models. Considering that the zones included between the slots were the ones where more attention was paid, the wall was divided into two different meshed zones. The zones outside the slots were meshed using elements of moderate dimensions (element size 0.10 m). In the slots zones, a refined mesh was used (element size 0.05 m) in order to better understand the behavior of the zone where the stresses are concentrated (Fig. 3.8). The number of elements utilized for each model was approximately 14000.

3.1.2 *FEM* results

In this Section the results obtained from the six different analyses are presented (Fig. 3.9 and 3.10). The results are also compared in order to obtain a first idea of the best configuration. The confrontations were performed looking at the principal stresses and their orientations.

Some results are presented using the images taken directly from *LUSAS*. For each configuration, four images were obtained. The first three are the contour plots of the shear stress in the three load cases and the fourth images are the vectors indicating

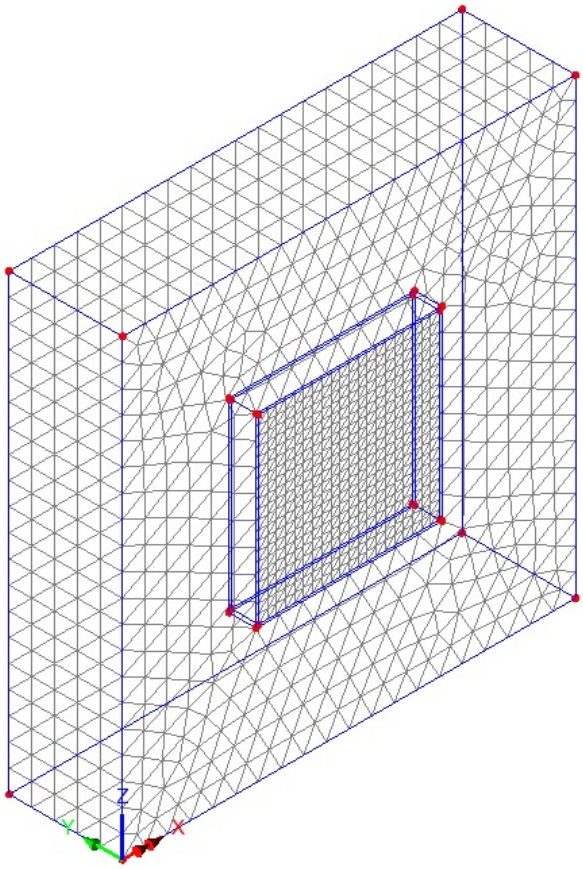

Figure 3.8: The image reports the *FEM* mesh of the configuration *d*.

the orientation of the principal stresses. All of these images were taken looking at the surface of the wall.

The main goals of the present work are the measurements of the shear modulus and of the tensile strength on a 45° inclined plane. This is the reason why particular attention was given to the orientation of the principal stresses. These stresses were evaluated on the surface of the sample and in the plane of the wall.

The contour plots of the six layouts were scaled starting from the maximum and minimum values of the shear stress obtained in all of the *FEM* analyses. This choice was taken in order to compare all the combinations in an easy and efficient way. The maximum and minimum values (-0.251 MPa and 0.306 MPa) were obtained in configuration *c*.

From the orientations of the principal stresses (Fig. 3.9 and 3.10), it can be easily noticed that configurations *b*, *c* and *d* present an inclination of approximately 45° of the principal stresses. Set-ups *a* and *f* yield to lower inclinations of the stresses and, on the contrary, configuration *e* presents a higher inclination.

From both the contour plots and the directions of the principal stresses, it is possible to notice some other peculiarities. Configurations *a*, *d*, *e* and *f* present directions of the principal stresses that are almost parallel to the direction of the dead load. The only part in which the direction is different is near to the location of the flat jacks. Encouraging

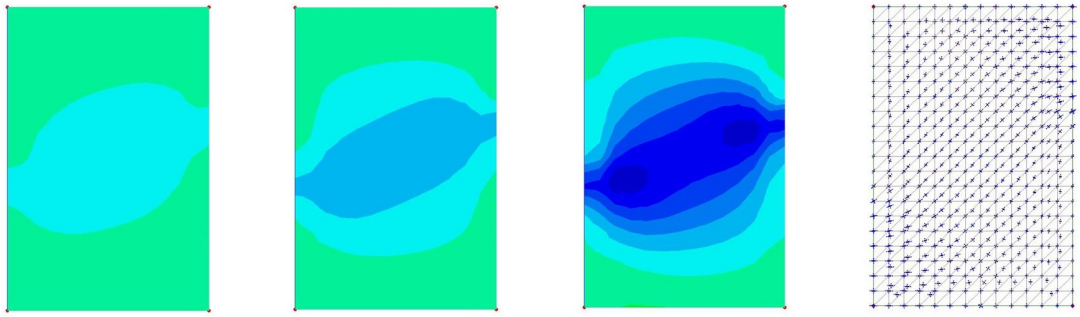

(a) Configuration *a*

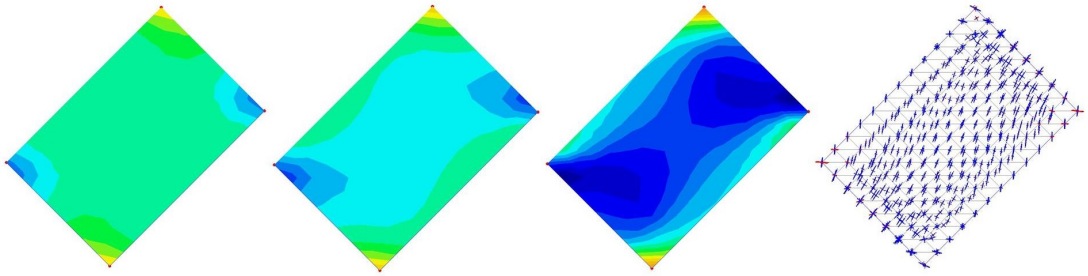

(b) Configuration *b*

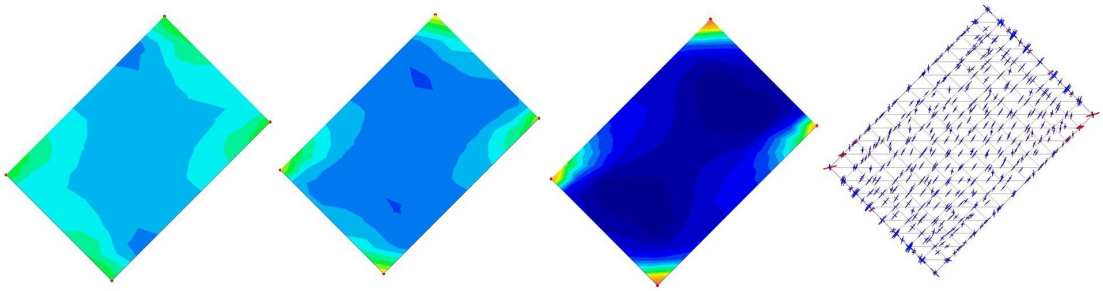

(c) Configuration *c*

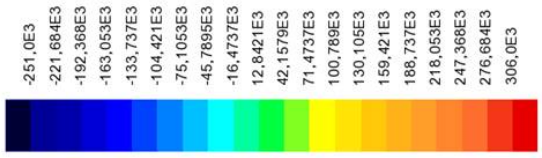

Component: SZX (N/m^2)

Figure 3.9: In the images are plotted the contour plots of configurations *a, b* and *c*. Starting from the left, the three load cases (*FJ* stress $\sigma = -0.10, -0.20$ and -0.50 MPa) are shown. In the last column on the right the vectors of the principal stress are plotted.

results were obtained in *c*. Due to the high isolation of the sample, performed with long cuts, the orientation of the principal stresses is more consistent with the main purpose of this work. In addition, this configuration shows also the highest stresses. Configuration *b* shows similar results. Both configurations *b* and *c* seem to be the best configurations despite the inclination of the principal stress not being perfectly equal to 45°.

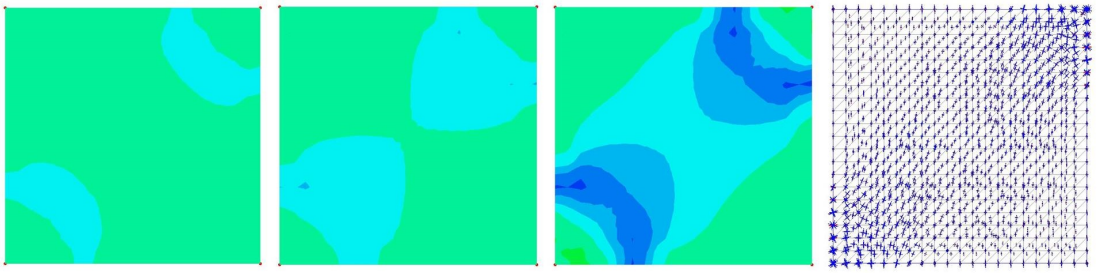

(a) Configuration *d*

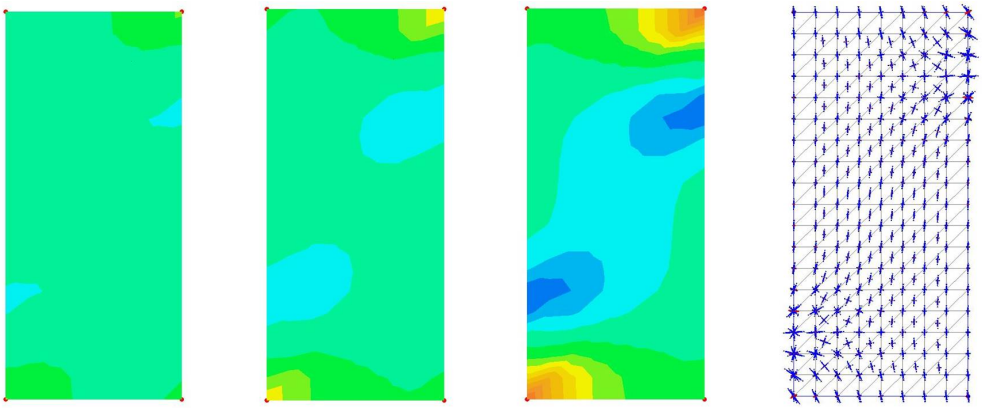

(b) Configuration *e*

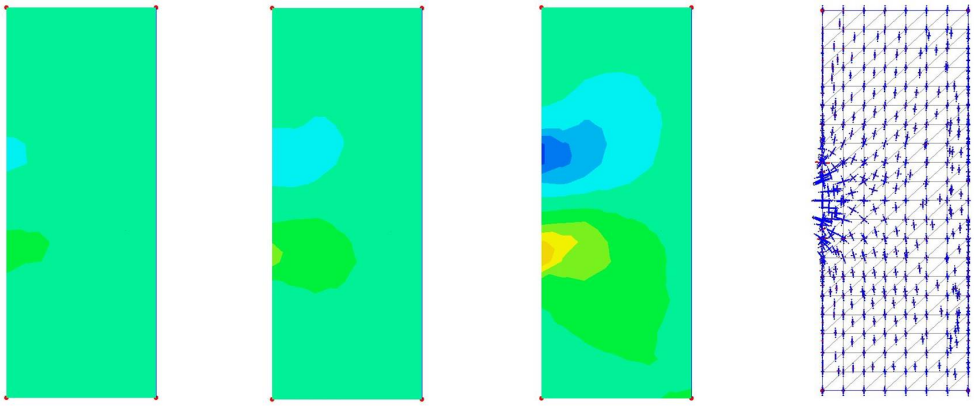

(c) Configuration *f*

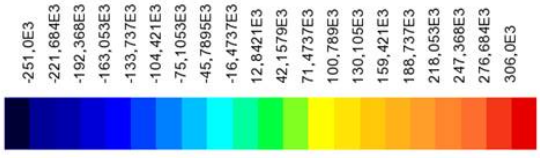

Component: SZX ($\mathrm{N/m^2}$)

Figure 3.10: The images reports the contour plots of configurations *d, e* and *f*. Starting from the left, the three load cases (*FJ* stress $\sigma = -0.10$, -0.20 and -0.50 MPa) are shown. In the last column on the right the vectors of the principal stress are plotted.

3.1.3 Criteria used to choose the set-up

In the following paragraphs the characteristics taken into account to choose the best configuration are presented.

Costs and simplicity of execution of the flat jack configurations were evaluated taking into account different possibilities that are as follows:

- Time needed to create the slots. The time needed to create the slot is not very relevant if compared to the whole time of the test but it was nevertheless considered because no other action can be performed at the same time. In addition, subsequently to the creation of the cuts these have to be cleaned and measured.
- Number of flat jacks used. The *FJs* have a cost that has to be taken into account. Despite these devices are commonly used, they have a limited life that could be correlated to the times of utilization. The use of an "elevated" number of flat jacks raises a lot the costs of the whole test. Moreover, after the test the *FJs* have to be extracted from the wall in order to restore it. In the case that high pressures are reached, it is possible that the *FJs* extraction results not easy to perform because it is possible that it can get stuck in the slot due to its plastic deformations. This time has to be taken into account for this possible phase.
- In a configuration it was also considered to have two separate hydraulic systems. In this case the cost of the additional equipment, the time needed to connect and maneuver it has to be taken into account.
- Reparation of the cuts. This is usually required after the test is performed. A high number of cuts and/or their great length raises the time as well as the costs needed for the reparation.

The time consuming operations mentioned above do not take into account the placement of the measure bases (or *LVDT* sensors). This operation can be problematic and time consuming due to the heterogeneity of the material and to the fact that the samples usually do not show a perfect plane surface. This phase was not evaluated because the positions and number of measure bases have to be designed in order to estimate it. It has to be said that, especially for manual readings, the time dedicated to position the measuring points and the time needed to acquire the measurement can be noticeable.

The standard flat jack tests are considered as *MDT* method. This characteristic is probably one of the most important features that has contributed to their wide use (e.g. their use for historical constructions). The importance of limiting the destructiveness of the test results clear. To evaluate the destructiveness, the following characteristics were monitored:

- Size of the sample. One of the principal aims of the test is to investigate the tensile strength of masonry. To accomplish this, the specimen must be submitted to intense stress and therefore the appearance of some cracks is very likely to occur. Considering this, it is understandable that larger specimens will ruin a larger part of the tested wall. In historical heritage buildings this problem is empathized because the preservation of both the aesthetic and the structural behavior is required. The possibility of reducing the specimen dimensions has to be examined

considering also that specimens too small will not be representative of the wall properties. This because the sample cannot be considered homogeneous.

- Integrity of the wall. The use of circular saws is very common in order to obtain the slots. Sometimes these saws use water to eliminate the dust, to cool themselves and to remove the debris in the slot. The water can compromise or even ruin the wall. For these reasons, decreasing the number and length of cuts decreases the destructiveness of the test. Another fact to consider is that the water could also disturb the mechanical behavior of the specimen because it could interact with the joints and the resisting elements.

- Aesthetic of the wall. The number and length of the cuts are one of the principal problems. A large number of cuts raises the possibility of compromising the aesthetic of the wall. Moreover, also the orientation of the cuts is important. Considering a brick wall, it is possible that there are some bed joints that are perfectly horizontal. In these joints the creation of cuts can be easily performed as well as the restoration. For vertical or inclined slots it is more complicated because the cuts interest both joints and resisting elements. In this case, the restoration is more complicated.

The most important criterion used to choose the best configuration is the stress-strain status of the sample. This feature is significant because the goal of the test is to investigate the mechanical properties of the sample. As mentioned before, it is important to have the principal stresses inclined of 45° in order to achieve a diagonal cracking or, at least, the concentration of the plastic deformations on an inclined plane.

3.1.4 Summary of the test design

The principal aim of the whole section was to investigate different flat jacks configurations. This investigation was performed in order to obtain the layout of the *MDT* method for assessing the shear modulus and the tensile strength on a 45° inclined plane of the media. In order to reach this purpose, *FEM* analyses of the configurations were performed. The results of these numerical models and the criteria defined were guidelines adopted to choose the final geometrical configuration.

As reported in Fig. 3.9 and 3.10, the *FEM* analyses highlighted the effectiveness of some configurations from the point of view of the stresses. The results of *b*, *c* and *d* pointed out an optimal orientation of the stresses. At the same time, plots of the directions of the principal stresses of configurations *a*, *d*, *e* and *f*, exclude these configurations for other insights. In fact, none of these four configurations shows principal stresses inclined of 45°.

At this point, the criteria of costs and destructiveness helped to take the final choice.

Configuration *d* shows a good inclination of the principal stresses. In addition, its similarity to the standard diagonal compression stress could lead to simpler comparisons with the diagonal compression test. The disadvantages of this configuration are more related to the destructiveness and to the costs. The sample has the biggest dimensions and two of the cuts are vertically oriented. The utilization of four *FJs* can also

raise the costs. Moreover, the vertical cuts would require a lot of time to be repaired because both joint and resisting elements are interested.

Configurations *b* and *c* show very similar results for what concerns the stresses and their orientation. Configuration *c* could be considered the best solution because it shows a uniform orientation of the stresses. However, due to the additional cuts this configuration results more invasive and the realization of these cuts can also interact more with the sample and might compromise it.

For these reasons configuration *b* was chosen as the optimal configuration. In addition to this choice, it has to be said that instead of using rectangular *FJs* the semicircular ones represent the best solution. In fact, these are more widespread as well it is the equipment to use them. Moreover, slots for these *FJs* can be easier created with a circular saw. These *FJs* have dimensions of 350×260 mm and an area of $A_{FJ} = 77506$ mm^2. The adoption of this more diffuse type of *FJ* could also help to have other researches on the proposed test. Actually, it would be more probable to have other possibilities to perform the test if the equipment was more diffuse.

3.2 Analysis of the shear *FJ* test configuration

After the definition of the best configuration, deeper numerical analyses were performed. The main aims of these analyses were two. The first aim is to understand if the chosen set-up (configuration *b*) is adoptable to measure the shear characteristics (tensile strength and shear modulus). The second aim is the creation of piecewise linear laws (and other tools) which should give the sample stress status knowing the applied stress.

For these scopes a parametric analysis was performed using *FEM* models. This analysis was conducted considering a homogeneous, isotropic, linear and elastic material. This analysis and its results are reported in the following.

3.2.1 Model strategies

Not every numerical model is suitable to represent the behavior of the masonry sample. In addition, the numerical model should also be able to give results that are directly comparable with the in situ measurements. That is why attention was paid in order to identify the more suitable *FEM* model.

In the large part of the analyses usually performed to assess the behavior of masonry buildings, the mechanical behavior of the material is simplified. Usually, masonry is modeled as a homogeneous, elastic and isotropic material. The material can be better modeled with more complicated constitutive laws and considering its non-linear behavior. However, in these analyses, the material was considered isotropic and homogeneous because in this way it should be easier to comprehend how the sample behaves. In addition, not too many mechanical properties have to be guessed and a more efficient way of reading the results can be used. In addition, it is not infrequent to consider masonry as a homogeneous, elastic and isotropic material in the models created to study test set-ups.

As already introduced it was decided to use semicircular *FJs*. For this reason, in these more detailed models it was decided to use this semicircular shape for both cuts

and *FJ* loads. This choice was taken in order to create more representative numerical models.

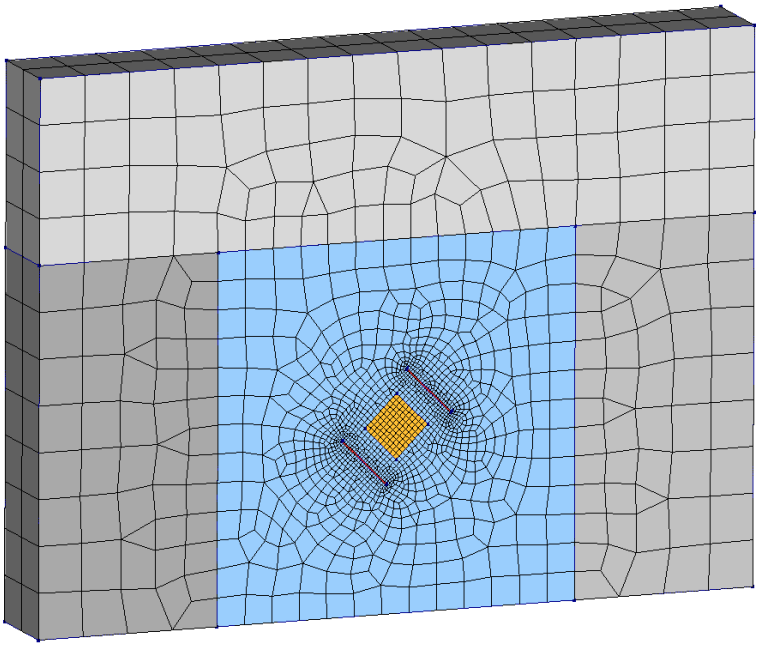

Figure 3.11: The image displays the mesh of the numerical model used for the analysis of shear *FJ* configuration. In this case the wall has dimension of $4.0 \times 3.0 \times 0.5$ m. It is possible to notice the cuts in red and the central prism in yellow (which has a base of 250×250 mm).

As far as possible, recommendations given for standard *FJ* tests were used [11, 12, 154, 155]. The distance between the two *FJs* was set at 500 mm. The standard equipment for a *FJ* test is also composed of a manual strain gauge having a base length of 250 mm. For this reason it was decided to create a prism that crosses at the center the whole thickness of the wall which has a squared base of 250 mm (Fig. 3.11). The position and the orientation of the prism were decided trying to imitate the sensor set up of the diagonal compression test [15]. In this way, the nodes on the numerical wall surface that have a relative distance of 250 mm can be tracked as well as the points in real samples (Fig. 3.12). The model had approximately 34000 elements that were quadratic bricks named CHX60 [65]. *DIANA* software was used in this case, given the subsequent extension to nonlinear analysis and support available for the work.

The numerical models had a precise sequence of steps that was applied before the application of the *FJ* loads. At first, the entire model was subjected to a vertical stress. Secondly, lateral constraints were applied to the wall. Then, the two cuts were realized creating the one that is above the sample before the other one. At this point, the *FJ* loads were finally applied to the slots surfaces. As already introduced they consist in semicircular stresses coincident with the slots surfaces which are perpendicular to these surfaces.

This sequence of steps is realized in order to better reproduce what happens in the sample during the test. In fact, in an in situ test, the above part of the structure applies a

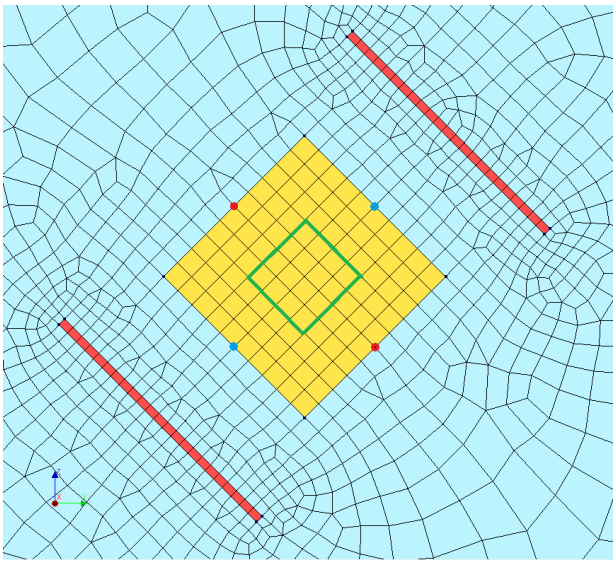

Figure 3.12: The image represents the mesh used to analyze the shear *FJ* configuration. In this image it is possible to notice the cuts in red, the central prism in yellow, the nodes monitored to evaluate the strains (in blue the perpendicular nodes and in red the parallel nodes) and finally the nodes monitored to evaluate the stress of the sample in green.

vertical stress on the sample. This load acts on the sample before and after the creation of the cuts.

Stress analysis

In order to understand the stresses inside of the sample the nodes in the center of the sample were analyzed, in particular the stresses of five nodes belonging to the center (100 mm side, highlighted in green in Figure 3.12) were studied (Fig. 3.13). The stresses on these nodes were evaluated by extrapolating the stresses from the Gaussian nodes of the nearby elements.

In these models, the vertical stress was always considered. It represents the vertical stress coming from the upper part of the structure. It was decided to consider the stress created by the vertical load as uniform. For this reason, at the moment of the vertical stress application, supports were applied at the base of the wall. Specifically, an edge was fixed for the horizontal displacements in the main direction of the wall and another edge for the horizontal displacement in the direction perpendicular to the wall plane.

The analysis of these nodes was performed looking at the principal stresses. Stresses in the direction of the referring system were taken from the softwares (*DIANA* and *LUSAS*). They were then processed in order to obtain the principal stresses and their orientation. Since the nodes studied belong to the wall surface, they are under a bi-axial stress status. This is due to the fact that there is no stress in the direction perpendicular to the wall plane ($x' = 0$). For this reason, the present stresses are three: the stress in the horizontal direction σ_x, the stress in the vertical direction σ_y and the shear stress τ_{xy}.

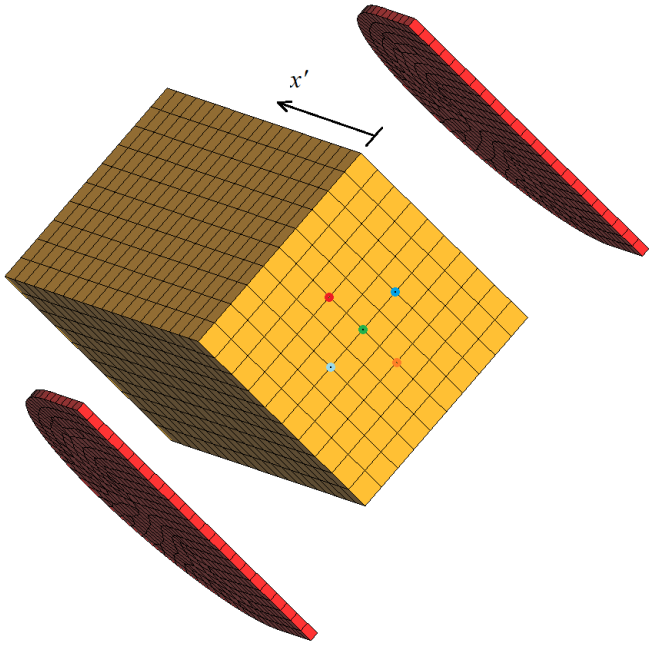

Figure 3.13: The image shows the center and the slots of the numerical model. The nodes analyzed to understand the stress distribution are highlighted: the center in green, the node above in blue, the node above in light blue, the node on the left in red and the node on the right in orange. It is also presented the referring system (x') used for the analysis of the distribution of the stresses inside of the wall.

From these three stresses it is possible to evaluate the two principal stresses:

$$\sigma_{1,2} = \frac{\sigma_x + \sigma_y}{2} \pm \sqrt{\left(\frac{\sigma_x - \sigma_y}{2}\right)^2 + \tau_{xy}^2} \tag{3.1}$$

The angle that the largest principal stress has with respect to the vertical is:

$$\psi = \frac{1}{2} tan^{-1}\left(\frac{2\tau_{xy}}{\sigma_x - \sigma_y}\right) \tag{3.2}$$

The analysis of the principal stresses of five nodes was performed (Fig. 3.13) and then compared to the average of the nodes belonging to the center of the central prism of the sample (Fig. 3.12). For this analysis, the model was taking into consideration a $4.0 \times 3.0 \times 0.5$ m wall with a vertical stress $\sigma_0 = -0.35$ MPa. The elastic properties used do not change the stress status of the sample but only the strain of it. Since displacements were not taken into account, it is not important to know these properties.

The results of this analysis are presented in Figure 3.14. Here, σ is the stress applied by the *FJs* to the masonry sample. It is possible to notice that the nodes belonging to the sample axis of symmetry have stresses that are similar among each other for both the largest principal stress σ_1 and the smallest σ_2. The other two nodes show, as absolute values, smaller principal stresses. The averaged values of the principal stresses of the nodes belonging to the center of the prism are, as expected, in between the results of

the five nodes. Since these mean values show an identical trend and that the difference among them is not too large, it was decided to use them as the stress status of the sample.

This choice was made considering that the principal stresses of a single node (e.g. the node in the sample center) is not representative of the sample stress state as well as the average of the principal stresses of all the nodes belonging to the sample surface. The failure of the material starts from in the zone where the principal stresses are larger. Nevertheless, when the principal stresses reach the material strength in a single node it is impossible to consider the sample failed. In contrast, the sample cannot be considered intact when the mean principal stresses of all the nodes of the samples are slightly inferior to the material strengths because in many zones the strengths would have been reached much before. Thus, it was decided to monitor a central part of the sample that has a dimension comparable to the dimensions of the resisting elements and, at the same time, to the dimensions of the sample.

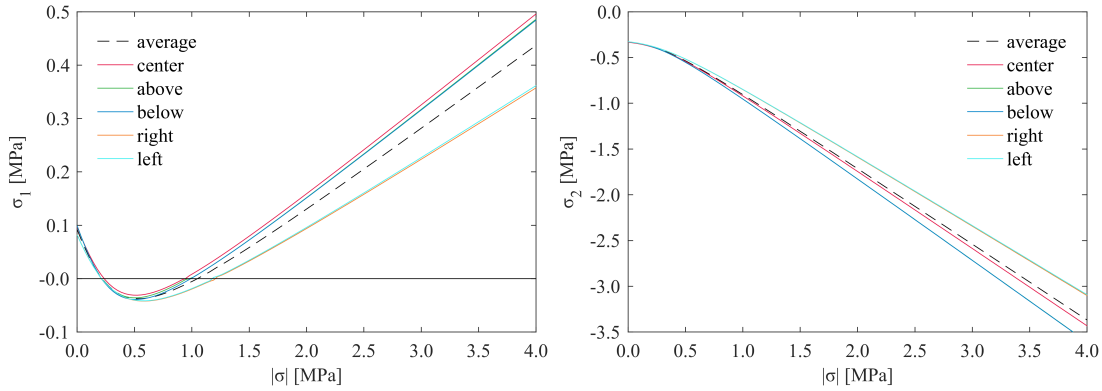

(a) (b)

Figure 3.14: In the two plots the analyses of the principal stresses of the nodes (highlighted in Figure 3.12) are presented. In Figure 3.14a the largest principal stresses and in Figure 3.14b the smallest one are plotted.

Strain analysis

The strain field of the sample, together with the applied stress, is important to evaluate the shear modulus of the material under test. Indeed, the knowledge of this strain status is essential in both numerical and real walls. This is why, as explained at the beginning of this Sub-section, the numerical models have to imitate the real experiment as much as possible.

Some considerations have to be performed in order to understand the strain field of the sample. It is possible to consider a 2D wall with a generic vertical stress σ_0, with the cuts already realized and crossing the whole thickness t of the wall, with zero pressure in the *FJs*. The media of this wall is considered homogeneous, linear, elastic and isotropic. With these premises it is possible to analyze the wall as a plane stress problem.

The present stress-strain statuses of the wall are considered as the initial ones. It is applicable the superposition principle due to the hypotheses of a linear and elastic

material. For this reason, the generic final status of the sample (with $\sigma \neq 0$) can be obtained summing the initial status (with $\sigma = 0$) to the one created only by the *FJs* stress. In particular, this partial strain status of the sample is the one that is measured during the in situ experiments. In order to be coherent, this strain status was taken into account in the numerical models.

The strain-stress status of the sample created only by means of *FJs* is the one that is taken into consideration starting from now. It results definable a local coordinate system (distinguished by the subscripts $\perp$ and $\parallel$) placed in the center of the sample. This local system has directions that are parallel ($\parallel$) and perpendicular ($\perp$) to the *FJs* planes. The stress status of the sample can be written with this tensor:

$$[\sigma_{\perp,\parallel}] = \begin{bmatrix} \sigma & 0 \\ 0 & 0 \end{bmatrix} \tag{3.3}$$

where σ is the stress applied by means of *FJs*. In the global coordinates this tensor (Eq.3.3) corresponds to:

$$[\sigma] = [R][\sigma_{\perp,\parallel}][R]' = \begin{bmatrix} \sigma/2 & -\sigma/2 \\ -\sigma/2 & \sigma/2 \end{bmatrix} \tag{3.4}$$

where $[R]$ is the rotation matrix that considers an angle of 45°. The tensor $[\sigma]$ (Eq. 3.4) shows that the *FJs* apply a shear stress τ (members of the matrix in position 1,2 and 2,1) in the sample that is equal to $\sigma/2$.

In the local system the strain status results to be:

$$\vec{\varepsilon}_{\perp,\parallel} = \begin{bmatrix} \varepsilon_{\perp} \\ \varepsilon_{\parallel} \\ \gamma_{\perp,\parallel} \end{bmatrix} = \frac{1}{E} \begin{bmatrix} 1 & -\nu & 0 \\ -\nu & 1 & 0 \\ 0 & 0 & 2(1+\nu) \end{bmatrix} \vec{\sigma}_{\perp,\parallel} = \frac{1}{E} \begin{bmatrix} \sigma \\ -\nu\sigma \\ 0 \end{bmatrix} \tag{3.5}$$

in which $(\vec{\sigma}_{\perp,\parallel})^T = [\sigma,0,0]$.

Similarly to what was done for the stress tensor, it is possible to write the strains in a tensor and then to rotate it in the global system. From this rotated tensor it is possible to write the strain vector in the global system (v = vertical, h = horizontal):

$$\vec{\varepsilon} = \begin{bmatrix} \varepsilon_v \\ \varepsilon_h \\ \gamma \end{bmatrix} = \frac{1}{2E} \begin{bmatrix} \sigma - \nu\sigma \\ \sigma - \nu\sigma \\ \sigma + \nu\sigma \end{bmatrix} \tag{3.6}$$

The shear modulus of a linear elastic isotropic solid is evaluated in the same way how it is evaluated in a plane stress problem:

$$G = \frac{\tau}{\gamma} \tag{3.7}$$

As highlighted previously, the shear stress applied by means of *FJs* to the sample is $\tau = -\sigma/2$ (Eq. 3.4). For what concerns the shear strain, some other considerations have to be taken. It has to be proved that it is possible to evaluate this strain with the mensuration of the displacement of the monitored points (Fig. 3.12).

A general strain of the sample (both numerical and experimental) is evaluated as:

$$\varepsilon_{i,j} = \frac{d_{i,j} - d_{i,0}}{l_i} \tag{3.8}$$

where: $i = \perp$ refers to the direction perpendicular to the *FJs* planes and $i = \parallel$ refers to the direction is parallel to the same plane; j refers to the general load step when the displacement and the applied stress is recorded ($j = 0$ refers to the moment after the creation of the slots when $\sigma = 0$); $d_{i,j}$ is the distance between the measured points of the basis having direction i and at the step j; l_i is the length of the measure basis at the moment $j = 0$.

Let's consider the shear strain evaluated following [15, 31] (maintaining the consistency in the load steps):

$$\gamma = \varepsilon_{\parallel} - \varepsilon_{\perp} \tag{3.9}$$

it is possible to prove that this evaluation is legit. In fact, from Equation 3.4, 3.5 and 3.6, Equation 3.9 is confirmed:

$$\gamma = \varepsilon_{\parallel} - \varepsilon_{\perp} = -\sigma\frac{1+\nu}{E} = \frac{1+\nu}{E}2\tau = \frac{\tau}{G} \tag{3.10}$$

which is equal to Equation 3.7.

Since the characteristics measured during a test are evaluated without taking in to account the initial status before the cuts creation, the shear modulus should be evaluated with the three monitored characteristics as:

$$G = \frac{\tau}{\gamma} = \frac{\sigma/2}{\varepsilon_{\perp} - \varepsilon_{\parallel}} \tag{3.11}$$

However, this shear modulus (evaluated numerically) has to be compared to the usual evaluation of the shear modulus:

$$G = \frac{E}{2(1+\nu)} \tag{3.12}$$

in order to prove that the hypotheses taken are valid.

The error between the numerical evaluation of the shear modulus (Eq. 3.11) performed using all the 3D models analyzed in this Chapter and the shear modulus calculated using Equation 3.12, is less than the 4%. This level of error in in situ masonry testing can be completely accepted. For this reason, it is possible to affirm that Equation 3.12 can be used also for the in situ test to evaluate the shear modulus of the media.

Models analysis

The models analyzed until now were 3D. Since it is very likely that the slots would not cross the whole thickness of the wall, the choice of using 3D model seemed to be the best solution. Nevertheless, two 2D models were analyzed (Fig. 3.15). The choice of examining this option is related to the possibility of having results similar to the one obtained with the 3D models with a smaller mesh size and, at the same time, speeding

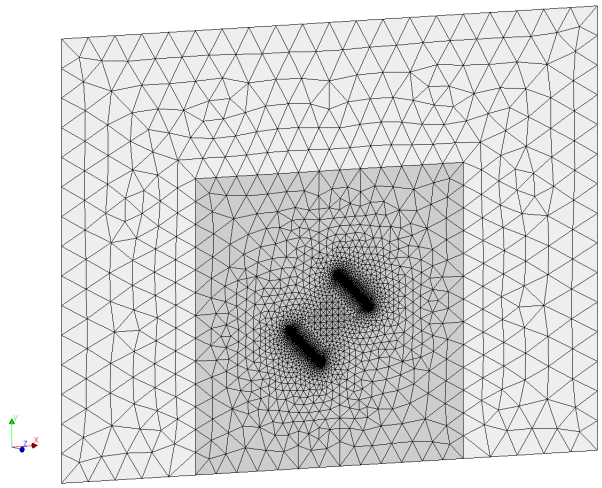

Figure 3.15: In the image the mesh used for the 2D *FEM* models is represented. In this *FEM* model a plane stress is considered and the wall has dimensions of $4.0 \times 3.0 \times 0.50$ m.

up the time of the analyses. This fact would be helpful considering that the parameters of the test set-up have to be analyzed and also non-linear analyses have to be performed.

The analyzed wall had dimensions of $4.0 \times 3.0 \times 0.5$ m. The material was considered homogeneous, isotropic, linear and elastic with a Young's modulus of $E = 2000$ MPa, Poisson's ratio of $\nu = 0.20$ and a vertical stress of $\sigma_0 = -0.35$ MPa. The sequence of phases used in the analyses performed before was kept.

The same model created for the previous stress analyses was used for the 3D analyses.

The two 2D models were created considering a plane stress status of the wall and using linear triangular elements (T3MEM [65]).

In the first model the cuts were realized erasing completely the material. This is equivalent to create cuts that perfectly cross the thickness of the wall.

The second model (called 2D modified) was created afterward and looking at the numerical results (Fig. 3.16a). Actually, it is possible to notice a big difference, that is present in the strains of the sample between the 2D and the 3D model. For this reason, instead of completely erasing the material from the cuts, it was decided to insert a synthetic material that simulates the media that in the real wall is present behind the cuts. This synthetic material was designed in order to have displacements close to the 3D model and also to have an initial largest principal stress close to the one obtained in the 3D model. In order to fulfill these two goals, the synthetic material having a Young's modulus $E = 984$ MPa (0.492 times in comparison to the Young's modulus of the rest of the wall) was inserted in the cuts at their realization.

From the results of these analyses (Fig.3.16) it is understandable that the 2D model is not suitable to model the physical problem. For what concerns the 2D modified model, it is possible to notice that strains and the initial tensile stress represent quite well the stress status obtain with the 3D model (Fig. 3.16). The main reason for which the 2D modified model was not used is the behavior of the principal stresses associated with the large absolute values of *FJs* stresses. It results clear that also this 2D model is

not suitable to replicate the behavior of the sample.

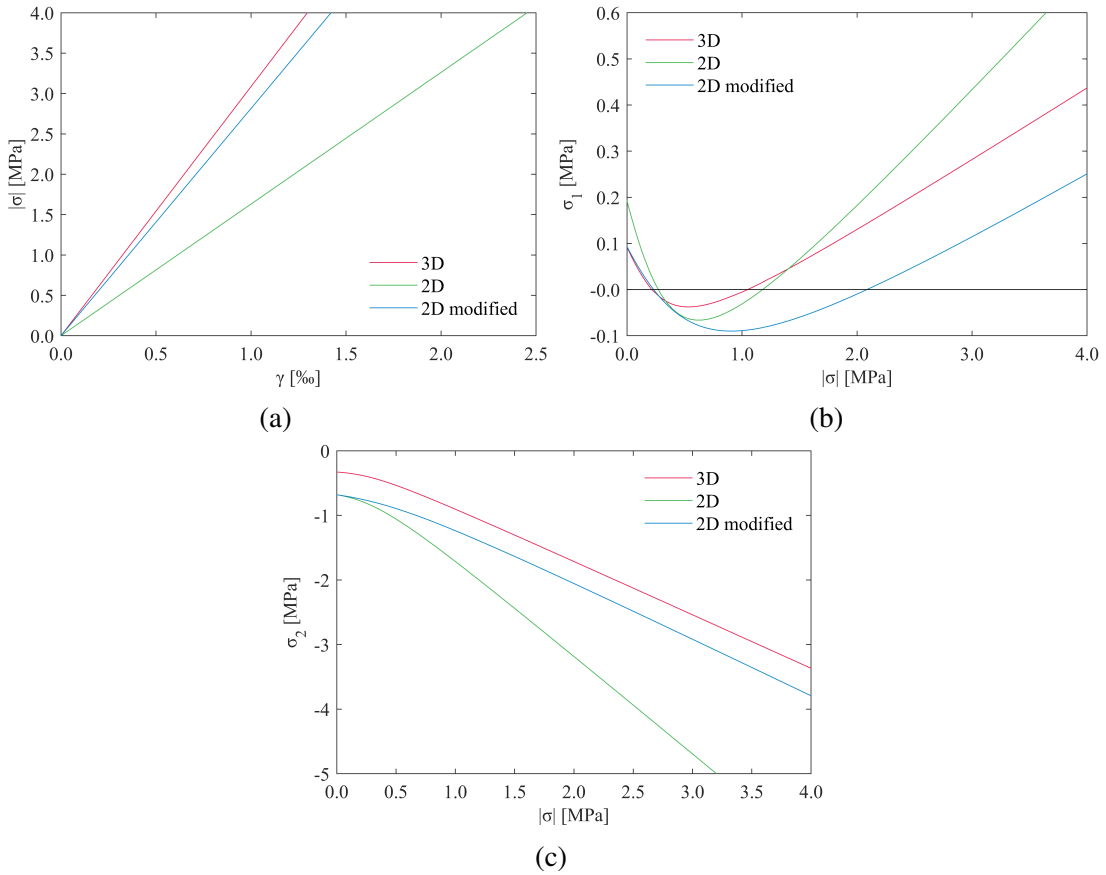

Figure 3.16: The graphs show the study performed in order to evaluate the possibility of using a simplified model. In Fig. 3.16a the absolute applied stress vs. the measured shear strain is plotted, in Fig. 3.16b and 3.16c the principal stresses are plotted vs. the absolute applied stress.

For this reason, it was decided that the best option was the utilization of 3D models. This kind of model, associated with the mentioned sequence of phases, were the ones used from this point to evaluate the behavior of the sample and to create the piecewise linear laws.

3.2.2 Parametric analysis

In order to fully understand the behavior of the sample under test, a parametric analysis was carried out. Before starting this parametric analysis, a study meant to understand the most suitable numerical model was performed. In this study the influences of different combinations of bearings and different dimensions of the wall were examined.

This analysis was carried out examining the elastic properties, the thickness and dimension of the wall, bearings and the vertical stress.

Bearings/Dimensions

As introduced, a study of the influence of the wall dimensions and of different combinations of constrains was performed before starting the parametric analysis. The goal is to study which combination of bearings changes the stress status of the sample and which one is more represen tative of a real wall.

For this study, it was taken into consideration a wall having: height of 3.0 m, thickness of 0.5 m, Young's modulus of $E = 2000$ MPa, Poisson's ratio $\nu = 0.20$ and a acting vertical stress $\sigma_0 = -0.30$ MPa. These were the characteristics that were in common to all the models.

The phases sequence of the analyses was in common for all the models. However, after the application of the vertical stress and before creating the cuts, different bearings were applied. It was nevertheless considered that the vertical load leads to a uniform stress inside of the wall.

For two models, a length of 6.0 m was taken in consideration. For the other four models the length of the wall was fixed at 4.0 m.

With regard to the bearings, four different combinations were considered. They always had in common the constrains at the base. In order to better understand the results, the models have a codification that is here explained:

- Combination *b*. Only constraints at the base were modeled.
- Combination *bl*. Bearings were applied to the base and to the lateral faces of the wall.
- Combination *bt*. The constraints were supposed to be applied to the base and to the opposite face (top face) of the wall.
- Combination *blt*. In this case all the sides of the wall were constrained.

The number before the code identifies the length of the wall.

The graphs presented in Figure 3.17 show the results obtained from the analyses and the study of these results is then presented in the following paragraphs.

Figure 3.17a shows that the presence of bearings situated only at the base (combinations *4b* and *6b*) leads to larger strains. These strains are quite different from the ones obtained with other combinations of bearings. In a real wall belonging to a structure it is really difficult to have this combination of bearings. This is because in this test a contrast to the *FJs* forces has to be provided. It is difficult to imagine testing a wall that is either on the last floor or that does not have a reaction (for example walls at the sided of the tested wall). For these reasons, it is possible to exclude combinations *4b* and *6b* as possible models to analyze the sample behavior.

Looking at the smallest principal stress σ_2 (Fig. 3.17c) and at the orientation of the principal stresses ψ (Fig. 3.17d), it is possible to affirm that changes of bearings and of dimensions do not play almost any role.

With respect to the principal stress σ_1 (Fig. 3.17b), the differences between the models are really small.

Therefore, the strain and stress fields of the real sample can be modeled by one of these four remaining models.

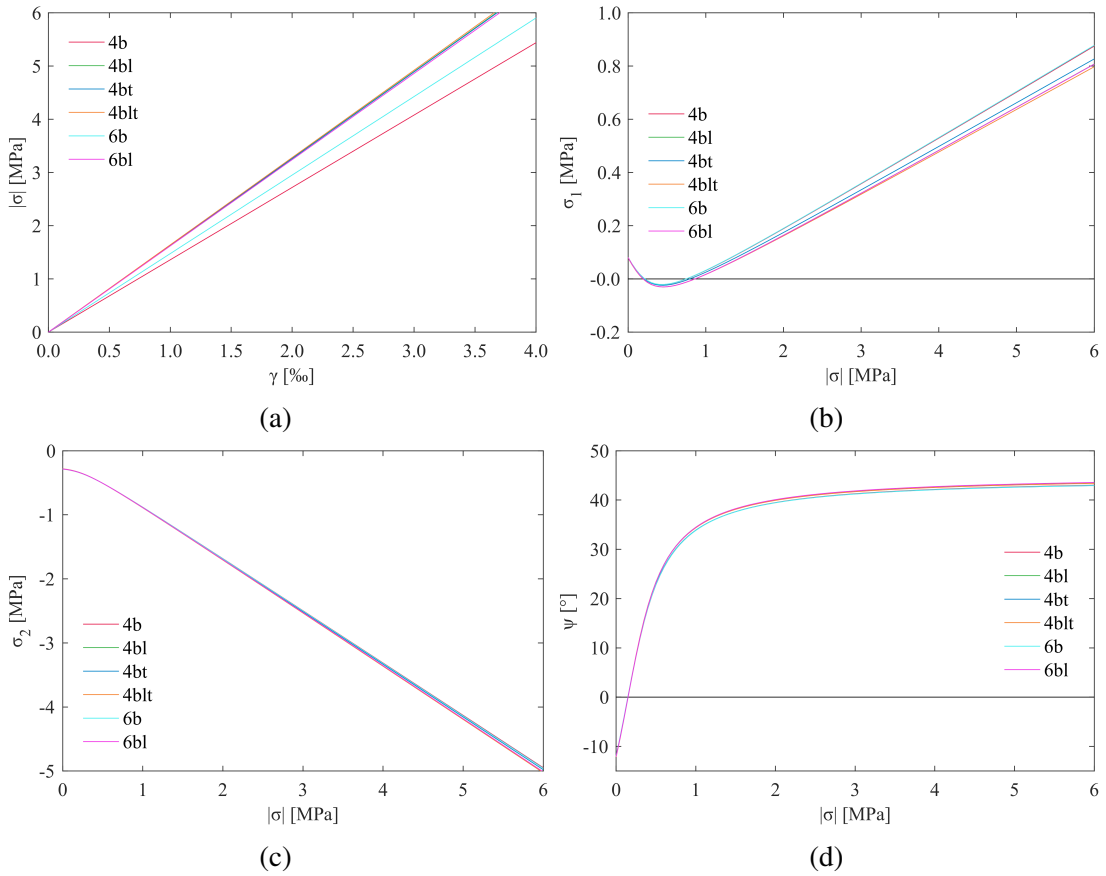

Figure 3.17: The plots display the results of the six linear analyses performed to investigate the influence of bearings and the wall dimensions. In Fig. 3.17a the absolute applied stresses vs. the measured shear strains are plotted, in Fig. 3.17b and 3.17c the principal stresses are plotted vs. the absolute applied stress and in Fig. 3.17d the orientations of the principal stresses are plotted.

For all of these reasons, it was decided to use combination *4bl* as a base model because the differences among the other suitable models are small.

The elements sizes of all the models were kept constant. In particular, the smallest elements, that were used for the cuts, had a dimension of 15 mm. This measure was chosen to avoid high aspect ratio considering that the thickness of the cut was modeled of 10 mm. This dimension was increased moving from the sample center (dimension of 25 mm) to the to sides and to the top of the modeled wall (where the seeding dimension was 250 mm). This seeding method leads to about 34000 elements for the model *4bl* having a thickness of 0.50 mm. The elements adopted were quadratic bricks named CHX60 [65].

These analyses were also useful to have a complete idea of the stress status of the sample. Moreover, it was possible to have a more important confirmation of the capability of the model to measure the tensile strength of the material. In fact, from the result presented in Figure 3.17 it is possible to have a comprehension of the stress trend during the tests.

The smallest principal stress σ_2 (Fig. 3.17c) results to be always a compressive

stress and it decreases monotonically. In a real test, attention should be paid to this stress during the test in order to avoid the compression failure of the media before that the tensile failure is reached.

The smallest principal stress σ_1 (Fig. 3.17b) has a behavior that is completely different. At the creation of the slots a tensile stress is present inside of the sample. Attention should be paid to this initial stress in order to avoid the failure of the material in the initial phases of the test. By increasing the pressure applied to the *FJs*, σ_1 decreases until it reaches the lowest point of the curve where a bi-axial compression is acting on the sample. After this minimum, the stress starts to increase monotonically and a tensile stress takes place in the sample. This second tensile branch is where the tensile strength should be measured.

It has to be recalled that one of the main purposes of the proposed test consists in measuring the tensile strength of the material on a 45° inclined plane. For this reason, attention has to be paid also to the inclination of the principal stresses. As stated, the tensile strength has to be measured in the second positive branch of the largest principal stress curve. It is possible to notice that this branch starts for a *FJ* stress of about $\sigma = -1.0$ MPa. For this value of applied stress it is possible to observe in Figure 3.17d that the inclination of the principal stress is already around 35°. If a tensile strength of the masonry larger than zero is taken in consideration, it is possible to assert that the test can give the measure of this characteristic on a plane that has an angle close to 45° (that anyway is an asymptote).

After the parametric analysis, these considerations have to be examined another time in order to understand if the possibility of testing the tensile strength is limited by some parameters.

Elastic properties

The investigation of the elastic properties was carried out in order to understand how deformations on the sample are related to these characteristics. In addition, along with the results obtained with an isotropic, homogeneous, linear and elastic material, it should be also possible to understand if in the real sample there is anisotropy and the role played by it in the deformations.

It is important to highlight that the elastic properties do not change the stress status of the sample during the test. In fact, variations of the elastic properties change the strains field but not the stress of the sample. As said in the previous section, the shear strain γ is calculated starting from the displacement measured after the creation of the slots. It results now clear that there is no relationship between the shear strain γ and the vertical stress σ_0.

Before starting this analysis it is important to take into account the field strain of the sample. The strain $\varepsilon_\perp$ (in the direction perpendicular to the *FJs* planes) results clearly dependent on the Young's modulus of the media during the application of the *FJ* load. It is possible to define the inclined Young's modulus E^* in this way:

$$E^* = \frac{\sigma}{\varepsilon_\perp} \tag{3.13}$$

This characteristic should be close to the Young's modulus of the media excluding the

fact that a confinement of the sample is present and that in a real sample anisotropy could be present.

The investigated Young's moduli were two $E = 1000$ and 2000 MPa, using a Poisson's ratio $\nu = 0.20$ and the optimal model found in the previous Sub-section (*4bl*). Using the properties of a homogeneous isotropic elastic media, it is possible to evaluate the shear modulus of the sample with Equation 3.11. They result to be $G = 416$ and 833 MPa.

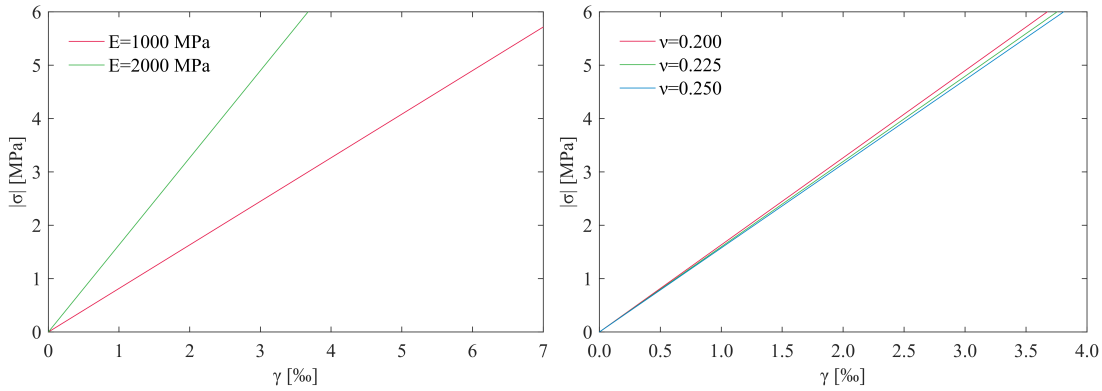

(a) (b)

Figure 3.18: The image gives the results of the analysis of the elastic properties.

In order to study the influence of the Poisson's ratio, the usual model was adopted using a Young's modulus $E = 2000$ MPa and exploring three values of Poisson's ratio $\nu = 0.200$, 0.225 and 0.250. Using the well known equation $G = E/[2(1+\nu)]$ it is possible to calculate the corresponding shear moduli $G = 833$, 816 and 800 MPa.

The results of the numerical analyses (Fig. 3.18) give the relationships between the moduli modeled and the ones measured. To the two Young's modulus investigated corresponds give as results $E^* = 1062$ and 2124 MPa and $G = 408$, 816 MPa. In parallel, to the three Poisson's ratio investigated correspond to $E^* = 2124$, 2106 and 2086 MPa and two shear moduli $G^* = 816$, 799 and 787 MPa.

The results of the inclined Young's moduli are interesting. The mean ratio E^*/E results to be 1.06. So, in a real test, if in parallel to the proposed test the Young's modulus of the media is measured (e.g. with a compression test), it is possible to have the ratio E^*/E and eventually have a measure of the anisotropy of the material (if the value is different from 1.06). It has also to be said that errors of magnitude 6% can be expected on field testing and it can be even more justified considering the characteristics of masonry.

For what regards the shear moduli, the differences between the shear moduli calculated with the equation $G = E/[2(1+\nu)]$ and the ones evaluated with the numerical results are of the order of the 2%. These results highlight, as said in the previous section, that the test set-up is valid for evaluating of the shear test with the hypotheses taken.

Vertical stress

The chosen configuration for the proposed test presents inclined cuts. In a hypothetical wall that has to be tested a vertical stress is present or, even more important, a vertical stress has to be present in order to guarantee a reaction to the *FJs* forces. If a wall has a present uniform vertical stress it is understandable that at the creation of cuts there is a redistribution of stresses. In fact, the faces of the slots become free, without stresses, and the vertical stress has to bend inside of the sample in order to guarantee the equilibrium. It results then clear that different vertical stresses lead to different stress statuses after the creation of the cuts and during the test.

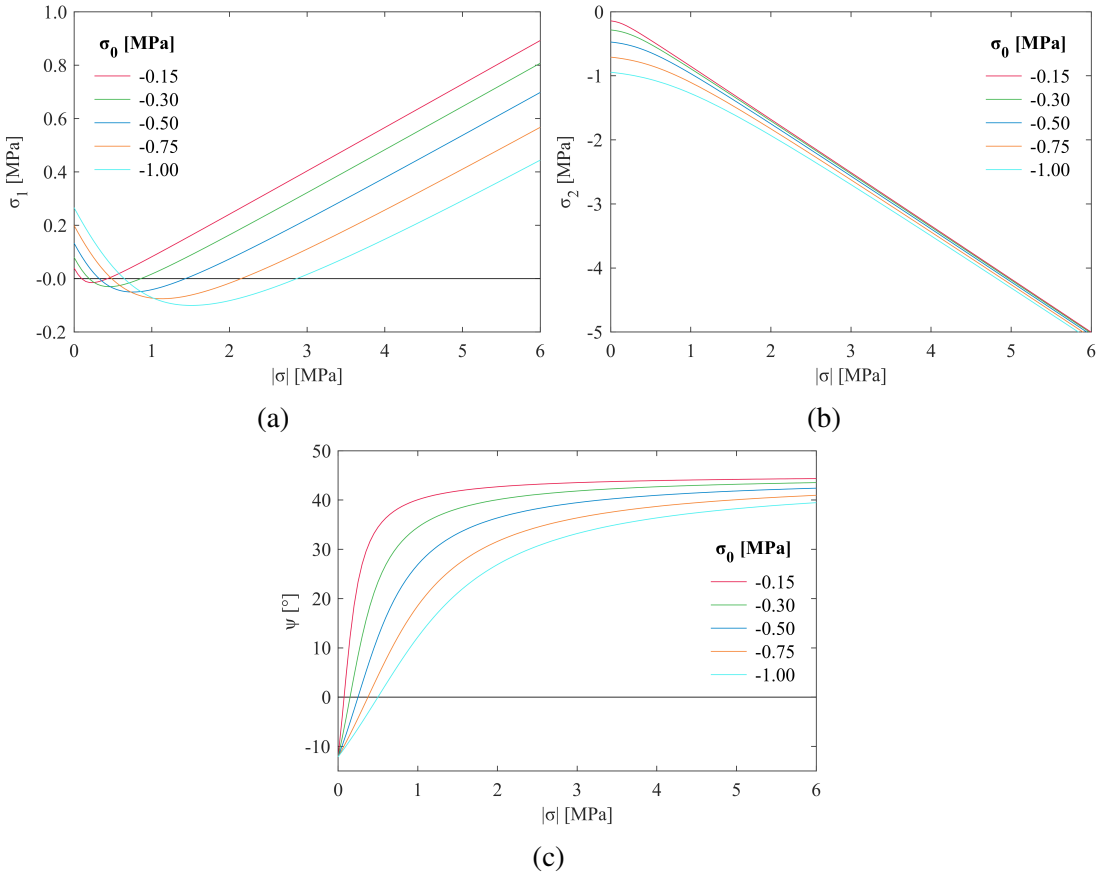

Figure 3.19: In the plots the results of the principal stresses (Fig. 3.19a and 3.19b) and in their orientation (Fig. 3.19c) are reported in function of different the vertical stresses $\sigma_0 = -0.15$, -0.30, -0.50 $-0{,}75$ and -1.00 MPa.

Due to the hypotheses taken, it is possible to affirm that the elastic properties of the sample do not influence its stress status.

In the present Sub-section a wall having $E = 2000$ MPa and $\nu = 0.20$ was modeled. As highlighted before, for the model it was always considered the precise sequence of steps in which the first step is the application of the vertical stress. The uniform vertical stresses investigated were five $\sigma_0 = -0.15$, -0.30, -0.50, -0.75 and -1.00 MPa.

The results obtained are reported in Figure 3.19. These results show a strong dependence on the stress status of the sample with respect to the vertical stress. For example,

larger vertical stress yield, after the creation of the cuts ($\sigma = 0.00$ MPa), to higher initial tensile stresses inside of the sample (Fig. 3.20a). Moreover, the second positive branch of σ_1 results to be shifted. In other words, by increasing the vertical stress, in order to obtain the same tensile status (in the second branch of largest principal stress) a higher stress has to be applied by means of *FJs*.

In parallel, the behavior of the smallest principal stresses is monotonic and is always deceasing (Fig. 3.20b). Moreover, for high levels of *FJs* stress, the smallest principal stresses seem to have a common asymptote.

To understand better this is interesting to use an example. Let's consider two walls with the same mechanical characteristics and subjected to two different vertical stresses $\sigma_0 = -0.30$ and 1.00 MPa. If the result obtained with $\sigma_0 = -0.30$ MPa is considered, it is possible to notice that the second branch of the tensile stress starts for a *FJs* stress $\sigma \simeq -1.00$ MPa. For this stress, the principal stresses are already oriented of 37° and this is almost optimal. The smallest principal stress results to be $\sigma_2 \simeq -0.70$ MPa. For the second wall (subjected to $\sigma_0 = -1.00$ MPa), it is possible to observe that the beginning of the second tensile branch is obtained for a *FJs* stress of $\sigma \simeq -3.00$ MPa. To this level of stress it corresponds $\psi = 32°$ and a compressive stress $\sigma_2 \simeq -2.50$ MPa. Therefore, too high vertical stresses can be associated with larger risks of the sample compressive failure. In fact, high stresses have to be applied in order to achieve the branch where the tensile strength has to be measured.

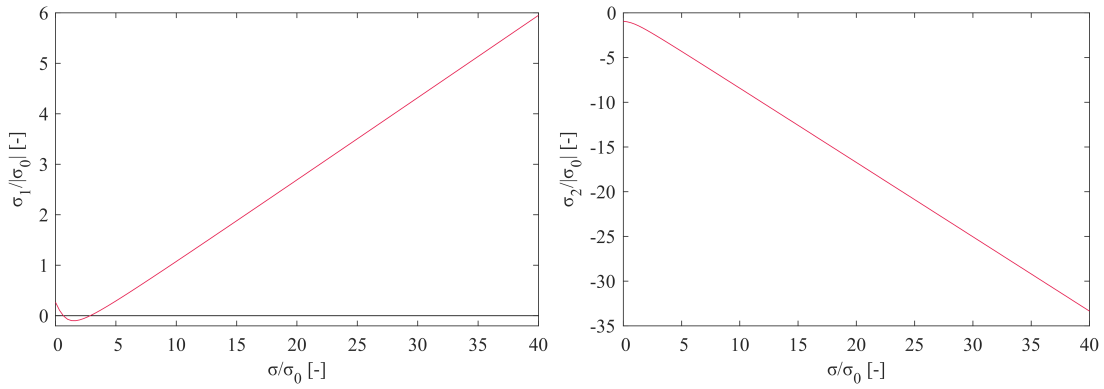

(a) (b)

Figure 3.20: The image shows the normalized results obtained in the analyses of the vertical stress influence. In particular the characteristics normalized (with respect to the vertical stress σ_0) are the stress applied σ and the two principal stresses σ_1 and σ_2.

The results highlight two main facts, the sample dependence on the vertical stress and the necessity of avoiding high vertical stresses in order to measure the tensile strength of the material.

Furthermore, it was also made a normalization of the results obtained with respect to the vertical stress. More in specific, the *FJs* stress σ and the two principal stresses σ_1 and σ_2 were divided by the corresponding vertical stress σ_0. The results (Fig. 3.20) show that the stress status of the sample is linearly dependent on the vertical stress. A deeper analysis of this relationship is presented in the Sub-section where the piecewise linear laws are developed.

Thickness of the wall

The thickness of the wall t was the last parameter examined. This geometrical characteristic plays an important role. In opposition to the elastic properties and to the vertical stress, the thickness of the masonry panel influences both the strain and the stress statuses of the sample.

As an example, two walls that have the same mechanical properties and vertical stress can be taken into consideration. In the first, the thickness of the panel is smaller than the slot depth. The thickness of the second wall is much larger than the depth of the cuts. In the thin wall, at the cut realization, a large part of the vertical stress has to pass through the sample in order to guarantee the equilibrium. On the contrary, in the thick wall a large part of the vertical stress is carried by the part of the panel that is behind the cuts and the sample. Moreover, when the *FJs* load is applied, the eccentricity of this stress, with respect to the thickness of the wall, plays a role in the status of the sample. Furthermore, it is possible to understand by this example that a larger thickness of the wall constraints more the sample and for this reason smaller displacements and strains should be expected.

In order to study deeper this geometrical influence, walls having $E = 2000$ MPa and $\nu = 0.20$ were modeled. The length and the height of the walls were kept constant (4.0×3.0 m) as well as the sequence of phases of the analysis and the vertical stress $\sigma_0 = -0.30$ MPa. The thicknesses of the walls examined were $t = 0.40,\ 0.50,\ 0.75,\ 1.00$ and 1.50 m.

The results of this part of the parametric analysis are presented in Figure 3.21. The measured shear strains (Fig. 3.21a) show a small dependence on the wall thickness. However, taking as a reference the wall of thickness $t = 0.50$ m, it is possible to demonstrate that the difference of the inclined Young's moduli range between -1.7 and 2.5%. It results possible to affirm that the analyzed parameter does not influence the strains of the sample. This affirmation can be considered true if all the approximations and uncertainties that are present in in situ tests are taken into account. In fact, it is legit to consider that approximations and uncertainties bring errors of the same magnitude of the differences numerically evaluated in the model.

The smallest principal stresses and the inclinations of the principal stress seem to be slightly affected by the thickness of the wall.

The thickness influences more the largest principal stresses σ_1 (Fig. 3.21b). It is possible to notice that these stresses at the cut realization (for $\sigma = 0.00$ MPa) are not influenced. On the other hand, the lowest points of these curves and the second tensile branches are quite dependent on this geometrical characteristic. Taking these branches as reference, it is possible to observe that for a fixed applied *FJ* stress, smaller tensile stresses are obtained with a larger thickness.

Summary of analyses

The linear elastic analyses performed were useful from many points of view. It was possible to find the most suitable model to be used in the analyses. In addition, it was demonstrated that the proposed test set-up is able to measure the tensile strength, the shear modulus and to give an estimation of an eventual anisotropy of the material.

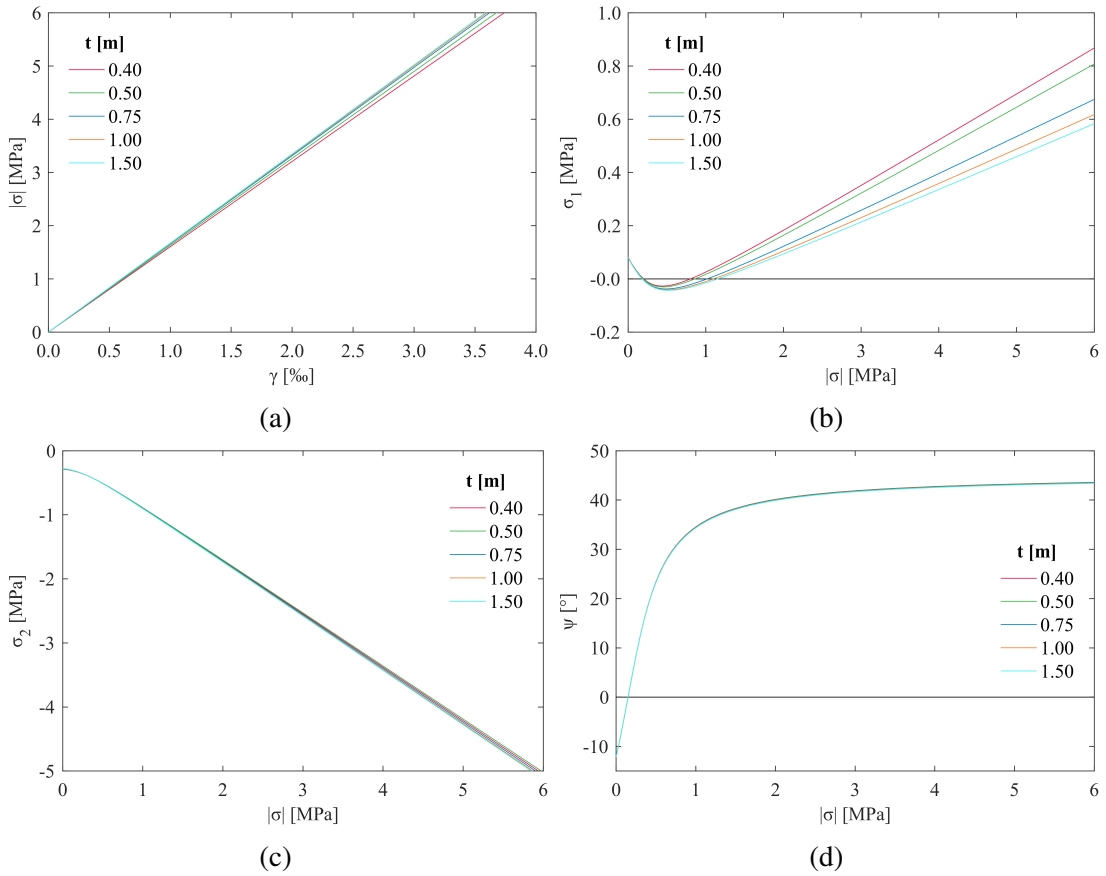

Figure 3.21: The image reports the results of the analyses of the wall thickness influence. In particular the plots of the shear strains (Fig. 3.21a), the principal stresses (Fig. 3.21b and 3.21c) and the inclination of the principal stresses (Fig. 3.21d) are presented.

As mentioned ahead, at the beginning of the parametric analysis, peculiar attention has to be paid to the second branch of the largest principal stresses. In particular, it has to be assured that the tensile strength is reached with an inclination of the principal stresses close to 45°. From the numerical results (Fig. 3.17d, 3.19c and 3.21d), it is possible to observe that the inclination of the principal stresses is already larger than 35° when the second branch of the principal stress starts to be positive. For this reason, it is proved that the evaluation of the tensile strength can be executed when the orientation of the principal stress is already close to the optimal value of 45°.

The parametric analysis leads to a deeper understanding of the strains and stress status dependence on the parameters analyzed. In particular, the independence of the sample stress status on the elastic characteristic was highlighted. On the other hand, the stress status dependence on the acting vertical stress and on the thickness of the wall was demonstrated.

3.2.3 Sample stress evaluation

The results obtained in the parametric analysis were used to create a piecewise linear regression model that aims at describing the stress status of the sample during the test and to evaluate the tensile strength of the media. In particular, the objectives of the piecewise linear laws are the knowledge of the initial stresses, the reproduction of the second branch of the largest principal stress and a good approximation of the smallest principal stress. It has to be underlined that the relation required to measure the shear modulus of the sample was already found (Eq. 3.12).

Starting from some random numerical results, it is possible to have a first idea of the suitable piecewise linear laws (Fig. 3.22). It was decided to simplify the largest principal stress with two lines of equation:

$$\sigma_1 = \begin{cases} \sigma_{1,1} \\ \sigma_{1,2} \end{cases} = \begin{cases} -(A\sigma_0 + B\sigma) & \text{if } \sigma > \frac{A\sigma_0}{B} \\ -(C\sigma_0 + D\sigma) & \text{if } \sigma \leq \frac{A\sigma_0}{B} \end{cases} \tag{3.14}$$

where the stresses will be considered in MPa.

Thanks to this model it is possible to know the initial tensile stress inside of the sample and to have a good approximation of the second tensile branch of the curve. The good match of these second branches is important because it is where the tensile strength has to be measured. The part of the model that has the worst approximation is the one in between the initial tensile stress (for $\sigma = 0.00$ MPa) and the second zero of the curve. This large approximation should not be a problem because this part of the test is not interesting from the point of view of the largest principal stress. Actually, if the loss of linearity of the material occurs in this branch, it means that the failure occurred either in a bi-axial compression, for orientations of the principal stresses that are not optimal or for compressive failure.

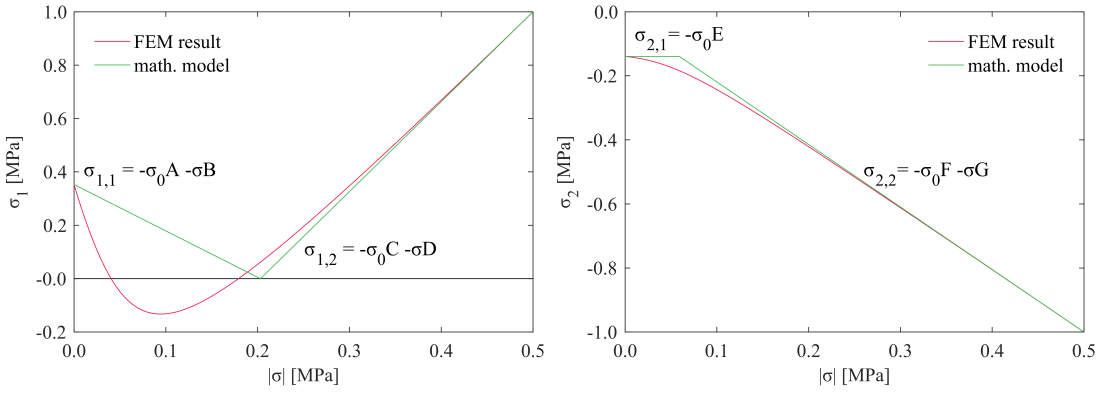

(a) (b)

Figure 3.22: The image shows two plots of the principal stresses of a numerical model and the proposition for the interpolations given by the supposed piecewise linear laws are presented.

The parametric analysis showed that the normalized (with respect to the vertical stress) intercept of the first line is a constant $A = 0.266$. The inclination of this first line

(B) was calculated afterwards, knowing the point where the second line has a value of zero.

The normalized (with respect to the vertical stress) intercept of the second line C is almost independent of the analyzed parameters and its value is $C = -0.516$. The inclination D of this second line is dependent on the thickness t of the wall. More precisely, the relation is inversely proportional and can be described with the following equation:

$$D = m + n\frac{1}{t} \tag{3.15}$$

where: t is the thickness of the wall in meters, the slope is $n = 0.0284$ m^{-1} and the intercept is $m = 0.102$.

Similarly to the largest principal stresses, also the smallest principal stress is modeled with two lines of equation:

$$\sigma_2 = \begin{cases} \sigma_{2,1} \\ \sigma_{2,2} \end{cases} = \begin{cases} -E\sigma_0 & \text{if } \sigma > \frac{(E-F)\sigma_0}{G} \\ -(F\sigma_0 + G\sigma) & \text{if } \sigma \leq \frac{(E-F)\sigma_0}{G} \end{cases} \tag{3.16}$$

where again the stresses are considered in MPa. Also in this case it is important to know the stress after the creation of the slots ($\sigma = 0.00$ MPa) which is obtained with the constant $E = -0.944$. The knowledge of this stress is necessary because if there is a compression that is too elevated it is possible to immediately have a compression failure. The second line has the normalized intercept (with respect to the vertical stress) F that is linearly dependent on the vertical stress:

$$F = r + s\sigma_0 \tag{3.17}$$

where: $r = -0.083$ and $s = -0.145$ MPa^{-1}. The slope of the line is independent of the parameters and its value is $G = -0.826$. This proposed well line reproduces the second branch of the smallest principal stress where attention has to be paid in order to be sure that the failure of the media is not reached in compression.

To summarize, it is possible to present the proposed piecewise linear laws:

$$\sigma_1 = \begin{cases} -0.266\sigma_0 + \left(0.0525 + 0.0144t^{-1}\right)\sigma & \text{if } \sigma > \frac{\sigma_0}{0.198+0.055t^{-1}} \\ 0.516\sigma_0 - \left(0.102 + 0.0284t^{-1}\right)\sigma & \text{if } \sigma \leq \frac{\sigma_0}{0.198+0.055t^{-1}} \end{cases} \tag{3.18}$$

$$\sigma_2 = \begin{cases} 0.944\sigma_0 & \text{if } \sigma > (1.04 + 0.175\sigma_0)\sigma_0 \\ (0.083 - 0.145\sigma_0)\sigma_0 + 0.826\sigma & \text{if } \sigma \leq (1.04 + 0.175\sigma_0)\sigma_0 \end{cases} \tag{3.19}$$

Before the application of these piecewise linear laws it was decided to test it. For this purpose, two numerical analyses were carried out. The common characteristics of these two *FEM* models are: $E = 2000$ MPa, $\nu = 0.20$ and two measures of the wall 4.0×3.0 m. In the first model a thickness $t = 0.5$ m and a vertical stress $\sigma_0 = -0.75$ MPa were taken into consideration. In the second model the thickness was supposed to be larger ($t = 1.0$ m) and, on the contrary, the vertical stress was supposed to be smaller ($\sigma_0 = -0.30$ MPa). The numerical results were then compared to the results obtained with the piecewise linear laws (Eq. 3.18 and 3.19). These comparisons (Fig. 3.23) show that, excluding small errors, the objectives of the model were fulfilled.

From the piecewise linear laws it also results possible to extrapolate some considerations of the test. As anticipated, it is important to avoid high levels of initial stress inside of the sample especially for what concerns the tensile stress. Secondly, particular attention should be paid to avoid high levels of compressive stress. In this way it is more probable to measure the tensile strength of the material.

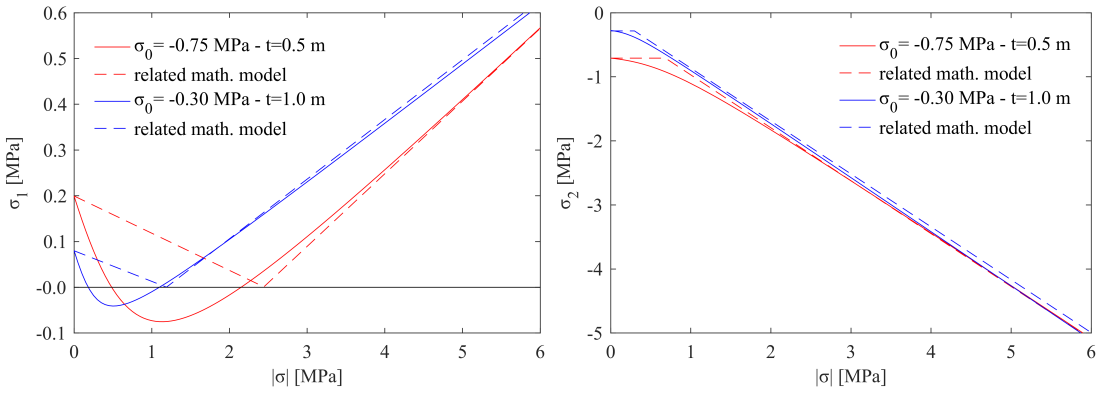

(a) (b)

Figure 3.23: In the graphs two tests on the piecewise linear laws are presented. These are performed comparing results of the piecewise linear laws and numerical results. In Fig. 3.23a is the largest principal stresses are plotted and in Fig. 3.23b the smallest.

It results then obvious that the knowledge of the thickness of the wall is important as well as the acting vertical stress. In order to optimize the test, thinner walls have to be preferred but it results also important to have a small vertical stress. This low stress helps to have higher values of tensile stress in the second branch of the curve and, contemporaneously, to have low initial stresses (for $\sigma = 0.00$ MPa). In addition, a small level of vertical stress reduces the compressive stress inside of the sample which is important in order to avoid the compressive failure of the sample. Resuming, the best conditions to test are a thin wall with a small vertical stress that ensures enough reaction to the *FJs* force.

Since the vertical stress plays an important role in the evaluation of the stress status of the sample, it is important to have a correct measurement of it. This can be easily carried out with the single *FJ* test.

The piecewise linear laws can also give some limits to be used in situ. It is possible to consider the stress status of the sample (Eq. 3.18 and 3.19) after the creation of the cuts ($\sigma = 0.00$ MPa):

$$\begin{cases} \sigma_1 = -0.266\sigma_0 \\ \sigma_2 = 0.944\sigma_0 \end{cases} \tag{3.20}$$

The vertical stress in a masonry structure is almost always (excluding peculiar cases) a compression so $\sigma_0 < 0$. Considering the compressive strength f_c and the tensile strength f_t as absolute values, to avoid the failure of the sample at the cuts creation the following inequalities have to be respected:

$$\begin{cases} f_t > 0.266|\sigma_0| \\ f_c > 0.944|\sigma_0| \end{cases} \tag{3.21}$$

Working on these inequalities it is possible to define two limits of the vertical stress:

$$|\sigma_0| < \begin{cases} 3.8 f_t \\ 1.1 f_c \end{cases} \tag{3.22}$$

These limits were created considering an isotropic failure criteria.

With an estimation of these strengths, for example taking them from building codes (e.g. [86, 87]), it is possible to understand if the vertical stress is too high in order to perform the shear *FJ* test. For what regards the compressive strength, instead of estimating the strength it is possible to perform a double *FJ* test that would give valuable information also for what regards the Young's modulus. However, for the tensile strength, an estimation from the codes is needed.

For a best estimation of the sample stress status, other two tools are given. These are meant to be used after the test execution in order to have a better evaluation of the sample stress status. These tools utilize the fact that for a fixed wall thickness the normalized principal stresses of the sample (normalized with the vertical stress) plotted versus the normalized applied stress collapse in single curves (see Fig. 3.20).

The first tool consists in two graphs of Figure 3.24. In these graphs the normalized principal stresses of walls with five different thicknesses are plotted and they can be used to evaluate the sample stress status.

The second tool is equivalent to the first one but it is probably more convenient while using datasheet. It consist in a Table (Tab. A.2) reporting the normalized applied stress and the normalized principal stresses for five different thicknesses of walls. For sake of space Table A.2 is reported in the Appendix A.

In conclusion, with the measure of the vertical stress, compressive strength, the thickness of the wall and with the estimation of the tensile strength, it is possible to decide if a test location is suitable or not for the application of the shear *FJ* test for the tensile strength evaluation.

3.3 Summary

In this Chapter a key phase of the creation of the new experimental test is presented.

At the beginning, the analysis of six different geometrical configurations was carried out by means of numerical models with the aim of finding the optimal configuration. The choice of the most suitable configuration was performed defining some criteria. These took into account costs, destructiveness and the stress status of the sample.

After the choice of the best configuration set-up, a deeper analysis of the stress-strain status was performed. This analysis is meant to control the ability of the shear *FJ* test to measure the shear modulus and the tensile strength of the material. This analysis was carried out after the optimal model was found. The possibility of using simplified 2D models was also explored. However, the performed analyses showed the impossibility of adopting this simplified model.

Once the most suitable model was found, a deep parametric analysis was carried out. This study gave a relationship between the measurable characteristics in situ and the shear modulus of the media (Eq. 3.11).

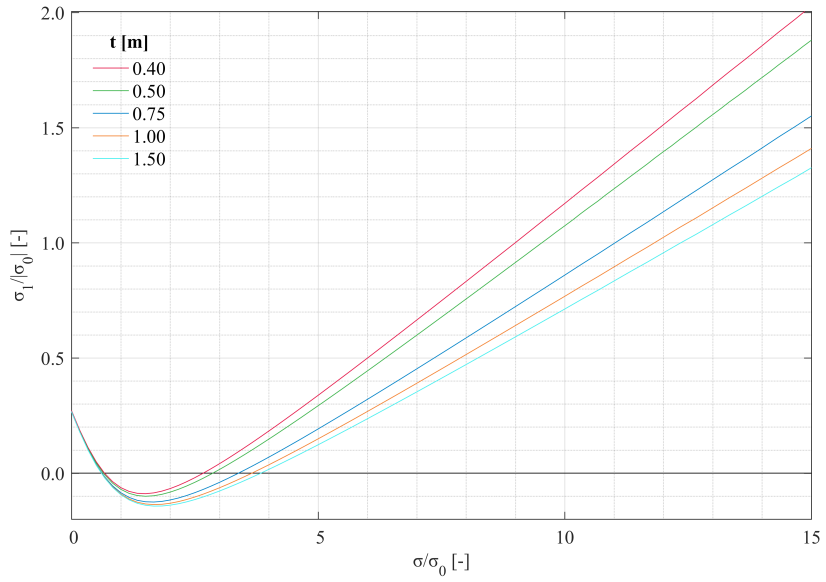

(a)

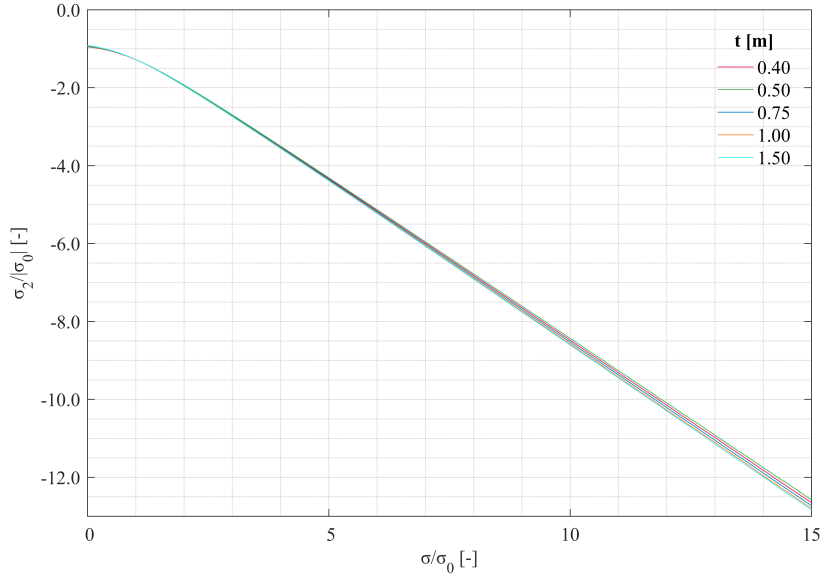

(b)

Figure 3.24: The image provides the two normalized principal stresses plotted versus the applied stress for different wall thicknesses. In Fig. 3.24a the normalized largest principal stress is plotted and in Fig. 3.24b the smallest principal stress.

It was also possible with the same parametric analysis to create piecewise linear laws. The purpose is to have the stress status of the specimen during the test without the necessity of running numerical analyses. This model approximates the stresses in some regions of the graphs. However, it ensures the knowledge of the initial principal stresses (after the cuts creation, $\sigma = 0.00$ MPa), the possibility of measuring the tensile strength and the opportunity of controlling the compression in order to know if a compressive failure takes place. These piecewise linear laws work thanks to the knowledge of the thickness of the wall and of the vertical stress. Moreover, two limits of the vertical stress

are also given (Eq. 3.22). These are meant to be used in order to optimize the position of the test. Other two tools were given in order to have a more precise evaluation of the sample principal stresses. The first one consists in two graphs having the normalized principal stresses ($\sigma_1/|\sigma_0|$ and $\sigma_2/|\sigma_0|$) plotted versus the normalized applied stress (σ/σ_0) for different wall thicknesses. The second tool is a table that summarizes the graphs just described.

All of these findings were successively used for creating the test method and in then they were used in five tests.

Chapter 4

Experimentation

The present Chapter is divided into two main parts. In the first, the test methodology created and used for performing the shear *FJ* test is presented and in the second part the results of the tests carried out are reported.

In particular, five shear *FJ* tests were performed as well as eight standard *FJ* tests (four single and four double *FJ* tests). These tests were executed in three different experimental campaigns in the "ex Teatro dei Nobili" (Vercelli, Italy), in the "Caserma Giovanni Cerutti" (Boves, Italy) and in the "Caserma Valfrè di Bronzo" (Alessandria, Italy).

In addition, the *AE* method was applied in two standard tests and in four shear *FJ* tests. However, in three tests the *AE* technique did not give acceptable results. This issue was due to the presence of a large noise that required to set a large threshold level that filtered out a large part of the *AE* signals. For what regards the other tests in which the *AE* data were acceptable, these data were processed using a self-made software. The results were compared with the ones obtained using another software [189]. Since the results were similar it can be concluded that the homemade software gives reliable results.

Some of the results were already presented by the author. The experimental results of the tests performed in the "ex Teatro dei Nobili" were presented in [187]. Some of the results obtained in the "Caserma Valfrè di Bronzo" and in the "Caserma Giovanni Cerutti" were published in [188] as well as a summary of the test methodology.

4.1 Test Method

In this section, the experimental set-up is presented giving a frame that aims at guiding eventual other shear *FJ* tests. Some recommendations for this set-up were already exposed in a previous part of the thesis. These recommendations are presented again here to provide clarity. For sake of completeness some data of the used equipment are given.

The chosen equipment was the one that is the most common in standard *FJ* testing. It consists of a manual pump and a manual extensometer. The oil pump, that can impose a pressure $p = 6.00$ MPa, has two gauges (the poorest sensitivity is 0.05 MPa). The recommendations for the sensitivity of the pressure gauges state that it has to be the 1%

of the hydraulic scale (that results to be 0.06 MPa) [11, 12, 154, 155]. The readings of the displacements are made with a mechanical extensometer that has a base length of 250 mm. Couples of gauge points have to be glued on the sample with a relative distance close to the base length and it is recommended to have at least two measure bases for each of the main directions of the sample (parallel and perpendicular to the *FJs* planes Fig. 4.1). The recommendations for the sensitivity of the extensometer state that it has to be the 0.005% of the base length (in the present case it results to be 12.5 μm) following the *ASTM* [11, 12] and 2.5 μm following the *RILEM* [154, 155]. The sensitivity of the extensometer adopted is 1 μm.

In order to optimize the results, the position of the test has to be chosen properly. It is preferable to test a thin wall where the vertical stress σ_0 is small but sufficient to guarantee the reaction to the *FJs* lifting force. Since the vertical stress plays an important role in the test results, it is recommended to perform a single *FJ* test in a wall with a similar vertical stress. This test is meant to give (or to allow the calculation of) the vertical stress. Moreover, a double *FJ* test should be performed in order to measure the Young's modulus and the compressive strength of the media. These two mechanical properties are useful in the second phase of the test when the analysis of the stresses is performed.

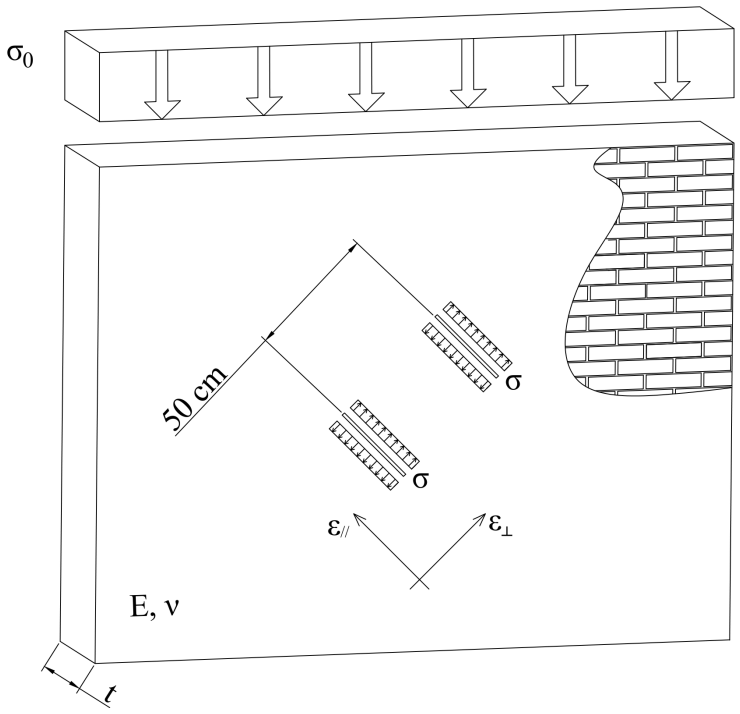

Figure 4.1: The image shows the layout of the proposed shear *FJ* test.

Once the wall that has been tested is defined, the location of the test on the wall has to be defined paying attention to avoid heterogeneities of the material (such as holes, voids, lack of vertical joints, etc.). The dimensions of the sample on a 45° plane are 0.50 m length, 0.35 m width and 0.25 m depth. These last two measures coincide with the chosen semicircular *FJs*. The location of the test has to be chosen considering also the possible positions of the measure bases. In fact, the standard equipment for

FJ testing has a base length of the extensometer of 250 mm. As introduced before, two measure bases for each direction are recommended. These should be applied on different bricks and symmetrically with respect to the center of the sample. In some cases, it can be not so simple to respect these two simple recommendations. This is why attention has to be paid to find the location of the test.

When the final location is found it is useful to draw the *FJs* position. This operation helps to find the positions of the measuring points. These points have to be glued before performing the cuts. The relative distances of couples of measuring points should be measured before and after the realization of each cut (Fig. 4.2a). These measurements are important to understand if the sample undergoes plastic deformations in these preliminary phases. To understand if the plastic regime is already attained, the strains of these initial phases have to be compared to the one obtained at the beginning of the *FJ* load that should be in the linear range of the material. Usually this linear range is present for small applied stresses. For this reason, if the initial strains are small in comparison to the one obtained in the elastic range, it is possible to confirm that no plasticization of the media was obtained during the cuts realization. Moreover, if the sample would be already damaged in the initial phases (in the realization of the cuts) the behavior of the sample would be non-linear even for small *FJ* loads.

After the application of the measure bases it is possible to realize the cuts. Due to the chosen equipment, a circular saw has to be used. The fact that the cuts are realized in both bricks and mortar joints does not help to create them. For this reason it is recommended to use a wood frame that has to be solidly placed on the wall (Fig. 4.2b). This frame helps to create perfect parallel cuts that have the correct relative distance. Due to the thickness of the frame, the cuts realized with it are not sufficiently deep to accommodate the *FJs*. For this reason, the frame has to be removed and the saw has to be used again to complete the slots. In order to reduce the stress acting on the sample, it is better to create the upper slots before the other ones. This sequence should isolate a bit more the sample from the vertical stress before the second cut creation.

After creating and cleaning the slots, their areas have to be measured. Following the recommendations for *FJ* testing, the length of the cuts should be divided every 20 mm. For each division, the depth of the cut has to be recorded and the area of the slot is then evaluated as the sum of triangles and trapezoids areas. The two areas of the slots are then averaged (A_{av}) in order to evaluate the geometric coefficient k_a as it is evaluated in standard *FJ* tests [11, 12]:

$$k_a = \frac{A_{FJ}}{A_{av}} \tag{4.1}$$

The mechanical coefficient of the *FJ* (k_m) is given by the *FJ* factory and, if the two *FJs* employed have different values of this coefficient, the mean value can be used. The level of stress applied by the *FJs* to the sample is then evaluated using the well known formula:

$$\sigma = -pk_ak_m \tag{4.2}$$

where p is the pressure of the liquid inside of the *FJs*.

Once the *FJs* are placed and the hydraulic circuit is created, it is possible to do a last operation before starting testing. The upper plug of the upper *FJ* should be kept open meanwhile the pump is used to fill the *FJs*. The plug has to be placed back in its place

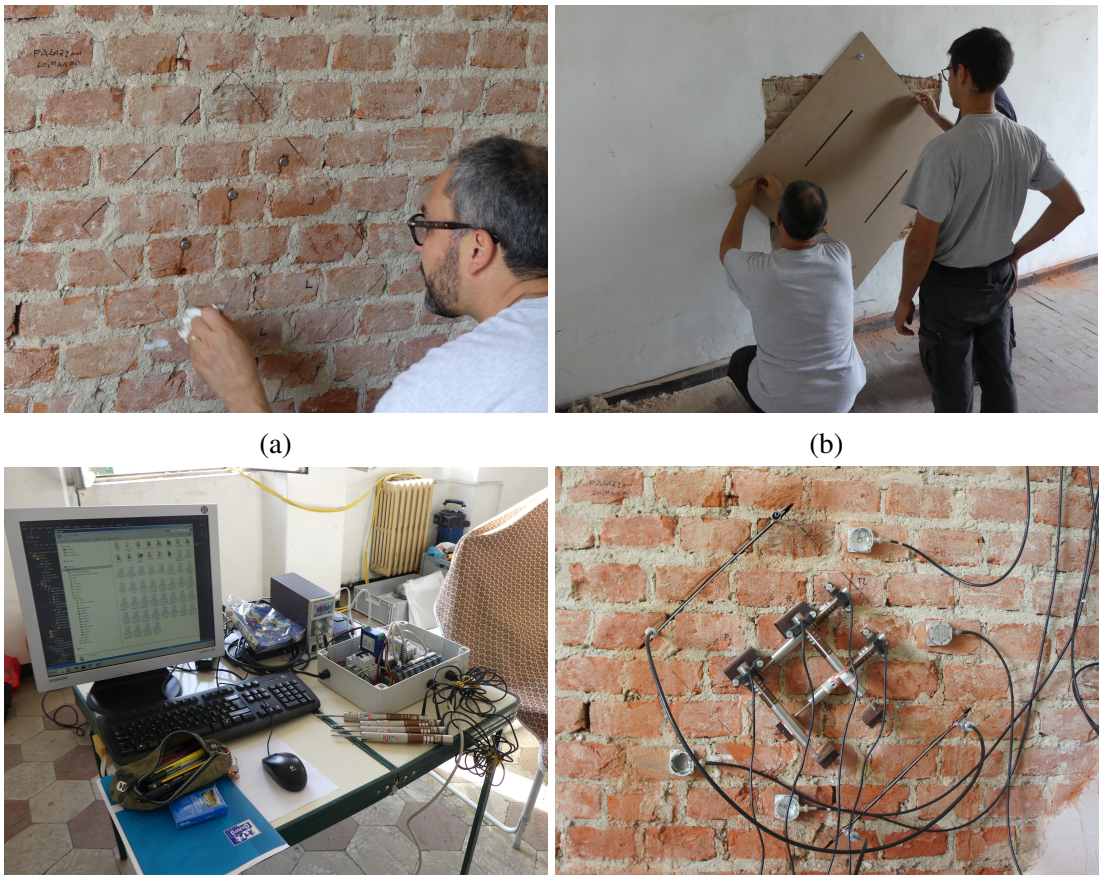

(a) (b)

(c) (d)

Figure 4.2: The pictures illustrate the preliminary phases and the equipment of the shear *FJ* test. The picture 4.2a shows the phase when the measuring points are glued on the sample. The picture 4.2b displays the positioning of the frame that helps during the cuts realization. The automatic acquisition system and the positions of the sensors are presented in pictures 4.2c and 4.2d.

at the first spill of liquid.

The general strain of the sample is evaluated using the following equation:

$$\varepsilon_{i,j} = \frac{d_{i,j} - d_{i,0}}{l_i} \tag{4.3}$$

where: $i = \perp$ refers to the direction perpendicular to the planes of the *FJs* and $i = \parallel$ refers to the direction that is parallel to the same planes; j refers to the general load step when the displacement and the applied stress are recorded ($j = 0$ refers to the moment after the creation of the slots when $\sigma = 0.00$ MPa); $d_{i,j}$ is the distance between the measured points of the basis having direction i and at the step j; l_i is the base length of the measure basis at the moment $j = 0$. It is now possible to evaluate the shear strain as

$$\gamma = \varepsilon_{\parallel} - \varepsilon_{\perp} \tag{4.4}$$

where the subscripts have been omitted.

It results now possible to start the test. The pressure has to be raised slowly in order to let the sample recover the creep deformations. For the same reason, at each load step, the liquid flow has to be stopped for a few moments before measuring the displacements. To evaluate the shear modulus and the inclined Young's modulus, it is recommended to do some cycles (two or three) at low pressure levels. The maximum pressure level of these cycles should be evaluated (maybe using the proposed piecewise linear laws) in order to avoid the plasticization and any damages of the media. For this reason, the principal stresses inside of the sample should be much inferior to the strengths. Once the linear regime of the sample is characterized it results possible to raise the pressure to higher values. These operations have to be performed paying attention to two main things, which are to characterize the transition between the elastic and plastic regime and to avoid large damages of both the sample and of the wall/structure. The number of readings of the deformations should be adequate in order to have a good reconstruction of the curve that represents the sample behavior under test.

The shear modulus has to be evaluated in the linear elastic range of the material under test using the following equation:

$$G = \frac{\tau}{\gamma} = \frac{-\sigma/2}{\gamma} \tag{4.5}$$

Similarly, the inclined Young's modulus has to be evaluated in the same range using this equation:

$$E^* = \frac{\sigma}{\varepsilon_\perp} \tag{4.6}$$

The knowledge of the sample stress status is a key fact. During the test it is possible to have a fast evaluation of this stress status using the piecewise linear laws of Equations 3.18 and 3.19. It results possible to have a better evaluation of the sample stress status. To this purpose it is possible to use two other tools, those are the normalized principal stresses of Table A.2 in the Appendix A and the graphs of Figure 3.24.

After the determination of the sample stress status, it is possible to estimate the tensile strength of the material. The identification of the transition between the elastic and plastic regimes it is not straightforward. In fact, the same problem is present in the evaluation of the compressive strength using the double *FJ* test where many solutions exist. In the present case, it was decided to use a graphical method in order to define this transition. In particular, the proposed method is similar to the one proposed by Vicente et al. [191]. In the proposed method, the intersection between the linear regression of the plastic regime at high strain level and the initial linear regression performed to identify the shear modulus in the elastic regime of the material is adopted in order to identify the shear strain at the linear/non-linear transition (Fig. 4.3). The stress of the experimental curve corresponding to this shear strain is then assumed as the point of transition between the two regimes.

Once the transition point is defined it is possible to evaluate the sample stress status associated to it. Subsequently, it is important to compare the smallest principal stress of the sample with the compressive strength of the media. This is done by assuming an isotropic failure criterion and controlling that the compressive stress does not reach compressive strength. In this case the sample should have had a tensile failure. In order to confirm this fact, the largest principal stress of the sample at the transition point has to

be examined. As highlighted in the previous Chapter, this strength has to be measured in the second tensile branch of the largest principal stress in order to guarantee an optimal inclination of the principal stresses.

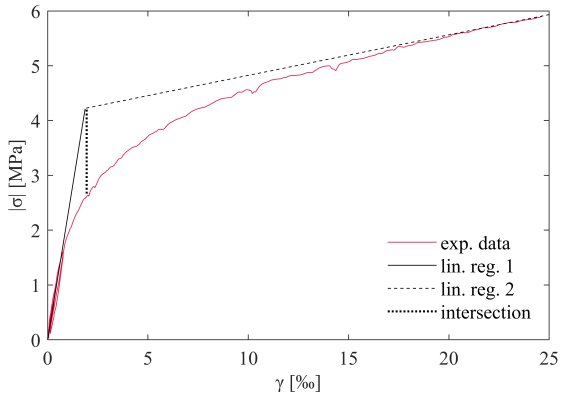

Figure 4.3: The plot illustrates an application of proposed graphical method meant to identify the sample failure.

At the end of the test, the *FJs* should be extracted from the slots and an appropriate material should be employed to repair the slots.

It has to be remarked that it is possible to use *LVDTs* instead of the manual extensometer. In this case, it can be important to measure the displacements due to the creation of the cuts. This can be only performed with the manual equipment because *LVDTs* cannot stay on the sample during the slots creation. In parallel to the *LVDTs*, it is really helpful to use a pressure transducer. In this way, automatic readings can be obtained and it is possible to speed up the test. Peculiar attention has always to be paid to the creep deformations and for this reason the loading of the sample has to be done not too fast. The acquisition system and the sensor positioning are presented in Figures 4.2c and 4.2d. The holes for the *LVDTs* supports should be created before creating the slots in order to avoid eventual displacements of the bricks. Moreover, after the creation of the slots and the measuring of their areas, the *FJs* should be placed as soon as possible. This operation should be performed before starting to fix the supports for the *LVDTs* in order to avoid that creep deformations close the cuts. If the closure of the cuts takes place before placing the actuators, the circular saw has to be re-used to enlarge the slot and every subsequent operations (cleaning, measuring and placing the *FJs*) have to be repeated. Once the *FJs* are in position, it is possible to fix the *LVDTs* on their supports, close the hydraulic system and subsequently start the test.

The characteristics of the sensors used in the executed tests are reported in the Appendix A.

As anticipated, in four of the tests carried out, the *AE* technique was also used with a homemade software (it is possible to observe the sensors in Figure 4.2d). This technique was used in parallel with the automatic acquisition system in order to have more reliable results especially from the synchronization point of view.

4.2 Tests in the "ex Teatro dei Nobili"

The first shear *FJ* test was performed in spring 2017. This test was executed in collaboration with the Cismondi SRL and the ARCOS Engineering SRL. Cismondi SRL is a laboratory authorized by the Italian Ministry of the of Infrastructures and Transportation for the execution and the certification of tests on construction material. ARCOS Engineering SRL is a company specialized in consulting and engineering activities. In addition to the shear *FJ* test, four standard *FJ* tests were carried out.

(a) South side prospect of the structure

(b) Picture of the south side of the building

Figure 4.4: The image gives a picture and prospect of the south side of the "ex Teatro dei Nobili".

The tests were executed in a dismissed theater named "ex Teatro dei Nobili" located in Vercelli (Italy) during a mechanical characterization of the building executed by Cismondi and commissioned by ARCOS. This theater has a long and troubled history that started with its construction in 1787. In 1798 there was a structural collapse and the roof fell on 150 people causing 16 deaths and several injuries. The structure was then

rebuilt creating civil houses but after a few years was abandoned. In 1815 the municipality restored the theater and it became the "Teatro Civico". Unfortunately, in 1923 a fire burned the structure. Some years later the municipality reconstructed the building another time but after a few years of activity it was abandoned for the last time.

This structure (Fig. 4.4) is made of bricks and lime mortar. The building has a rectangular shape and has three main floors. On the ground floor a transverse section of a wall was examined pointing out the good transverse connection. In fact, the whole section is made of bricks and the texture guarantee a single leaf behavior.

The manual equipment was used for these tests.

4.2.1 Standard *FJ* tests

Five tests were performed in this experimental campaign, two couples of single and double flat jack tests and the shear *FJ* test. The first couple of standard *FJ* tests was performed on the ground floor on a perimeter wall (Position 1 in Fig. 4.5b). The other couple of single and double flat jack tests were carried out on the basement (Position 2) near to the location where then the shear *FJ* test was performed (Fig. 4.5a). These two standard *FJ* tests were performed near the shear *FJ* test in order to obtain information about the vertical stress, the Young's modulus and the compressive strength of the wall.

For all these tests, semi-circular *FJs* having a length of 350 mm and a depth of 250 mm were used. The stiffness of the *FJs* (k_m) was evaluated using the data given by the producer. More precisely it was decided to use two constants evaluated with two linear regressions from the data of the *FJs* producer. The first constant is valid for pressures up to 0.6 MPa and the other one from this pressure up to 6.0 MPa (Tab 4.1). This choice was taken considering that a variation of the value of k_m with the increase of the pressure was present.

Recommendations of *RILEM* and *ASTM* [11, 12, 154, 155] were followed. All of the five tests were performed using the same equipment, in particular, the manual one. The cuts were realized with a circular saw. Water was adopted to cool the saw, to reduce the dust and to clean the slots from the debris.

Table 4.1: The table gives characteristics of the flat jacks used in the mechanical characterization of the "ex Teatro dei Nobili".

Charactheristic	Value	Unit
Length	350	mm
Depth	250	mm
A_{FJ}	77506	mm^2
k_m $(0.0-0.6$ MPa$)$	0.873	–
k_m $(0.6-6.0$ MPa$)$	0.902	–

Standard *FJ* tests Position 1

The first test performed was the evaluation of the present stress in Position 1 (Fig. 4.5b). Three measure bases were applied on the sample and after the slot realization a

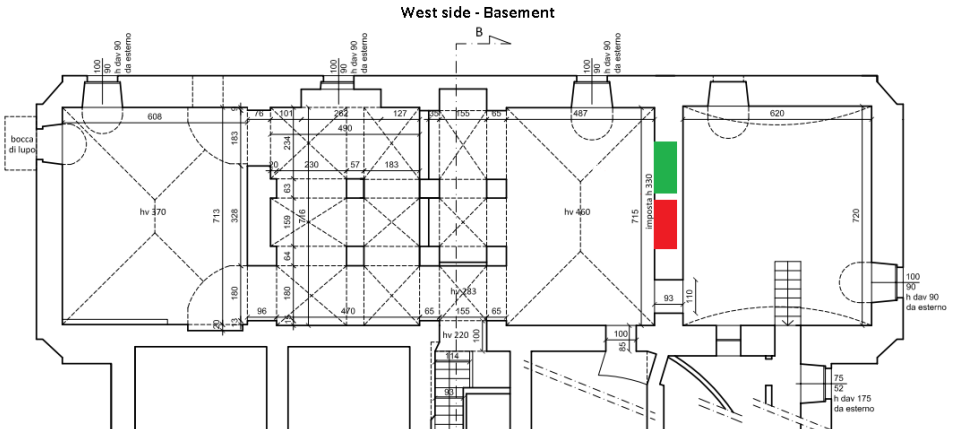

(a) Position of the tests executed on the basement (Position 2)

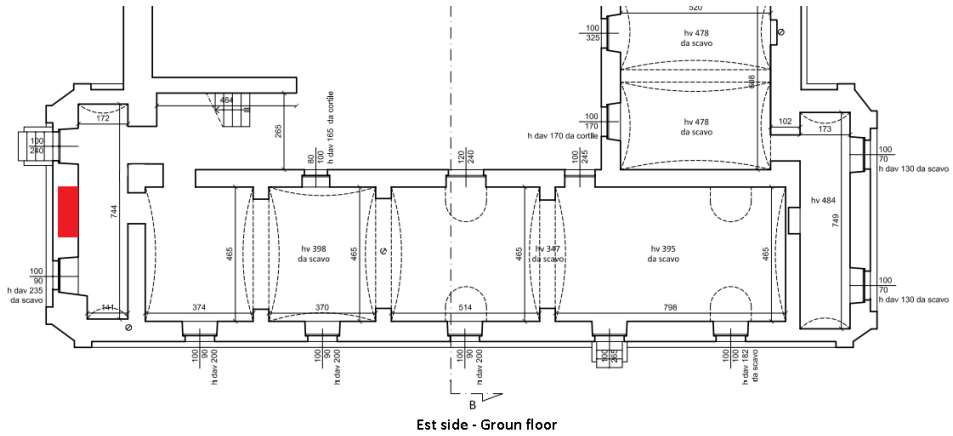

(b) Position of the test executed on the ground floor (Position 1)

Figure 4.5: In the image two layouts of the "ex Teatro dei Nobili" where the tests were executed are reported. In red are marked the position of the standard *FJ* tests and in green the position of the shear *FJ* test.

geometrical ratio of $k_a = 0.950$ was calculated. The pressure was then increased until the three measures of the bases were slightly larger than the first measures taken before the cut creation. The vertical stress evaluated was $\sigma_0 = -0.28$ MPa. This stress led to the recovering of the mean deformation.

After the execution of the single flat jack test, the deformability test was performed in the same position maintaining the cut and the flat jack used in the previous test. For the sake of simplicity, the measuring points for the double *FJ* test were glued at the same time with the ones of the single *FJ* test. For this characterization, three pairs of vertical measure points and one horizontal (positioned, approximately, at the half height of the vertical ones) were used.

A first series of measures was taken before starting the single *FJ* test. The area created was 85600 mm^2. This measure, in combination with the first area, gives a geometrical ratio of $k_a = 0.927$.

The second flat jack was then inserted and connected in series to the first *FJ*. For

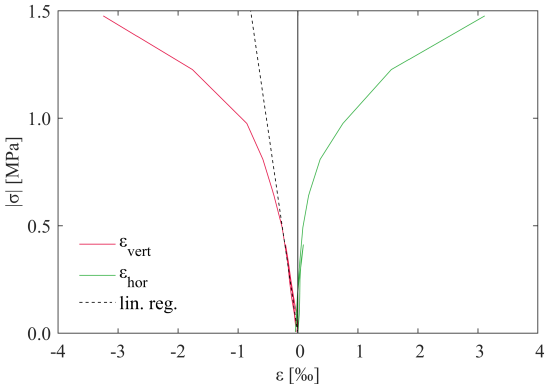

Figure 4.6: The image illustrates the results of the double *FJ* test performed in "ex Teatro dei Nobili" Position 1.

this test, two cycles of load were executed. In the first one, the hydraulic pressure was risen up to 0.50 MPa with increments of 0.10 MPa. After this peak, the sample was unloaded to zero using the same pressure steps. In the second cycle, the pressure was risen up to 1.95 MPa. For this value a detachment of a superficial part of some bricks occurred. In these bricks there were some of the gauge points. For this reason it was not possible to continue the test. However, the non-linear range of the media was already reached giving the possibility of identifying the compressive strength of the wall.

The determination of the Young's modulus was performed using linear regressions in the linear elastic regions of the two cycles (Fig. 4.6). In the second cycle the maximum stress that was chosen as the boundary of the linear elastic branch was $\sigma = -0.64$ MPa. The mean Young's modulus evaluated was $E = 1905$ MPa.

In order to evaluate the compressive strength, what described in Sub-section 2.3.3 was followed. The resulting compressive strength is $f_c = 1.45$ MPa. The method used considers a regression curve that fits the envelope curve in the plastic regime and then the stress associated with a deformation of the 3‰ is considered the compressive strength of the media. In this case, the maximum value of deformation measured in the test was slightly larger than the 3‰ and for this reason, the value of compressive strength is probably a rough estimation.

Standard *FJ* tests Position 2

For this couple of tests, the equipment and the procedure used were the same as the previous one. This characterization was performed on the basement of the building in Position 2 (Fig. 4.5a). For the single flat jack test, the slot area measured was 88275 mm^2 which led to a geometrical ratio $k_a = 0.878$. The present stress measured was $\sigma_0 = -0.25$ MPa and the thickness of the wall was $t = 0.70$ m.

The double flat jack test performed in Position 2 resulted more reliable than the previous one because no detachments occurred. For this test, two cycles of load were performed. In the first, a pressure of 0.39 MPa was reached, in the second cycle it was possible to raise the hydraulic pressure up to 2.30 MPa corresponding to a stress $\sigma = -1.81$ MPa on the sample.

For this test, the determination of the Young's modulus was again performed by

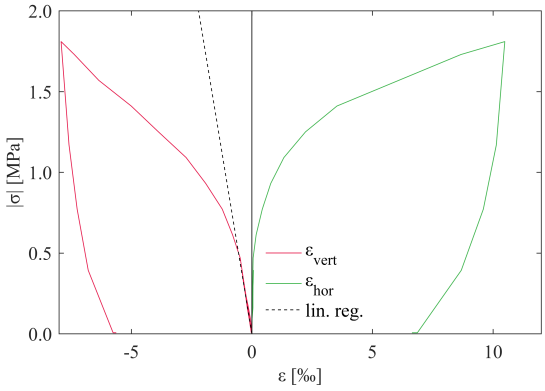

Figure 4.7: The image displays the results of the double *FJ* test performed in "ex Teatro dei Nobili" Position 2.

averaging two linear regressions performed in the linear regions of two load cycles. The mean Young's modulus resulted to be $E = 905$ MPa.

The evaluation of the compressive strength was performed following the methodology described in Sub-section 2.3.3 giving as a result a compressive strength of $f_c = 1.40$ MPa.

Conclusions

The standard test campaign, consisting of two single and two double *FJ* tests, highlighted a discrepancy between the two tested walls. In fact, the Young's modulus obtained on the ground floor is two times greater than the one measured in the basement. This noticeable difference could be correlated to the different exposures to environmental agents. The wall on the basement is in a very high humidity environment and the proximity to the soil could have exposed it to the attack of salts transported by the capillary rise of water. These exposures could have activated a decay of the mechanical properties. Another important thing that has to be remarked is that the Young's modulus of the first test is very similar to the one given by the Italian code (Tab. 2.3). The fact that in the first test there was a detachment can also imply that the strain measured are not correct. It is possible, that the part that detached was not subjected to the *FJ* stress because the detachment started before it was noticed.

The compressive strengths measured in these two tests were more coherent. In fact, the discrepancy between these two values is really small. However, in the Position 1 the value of compressive strength was considered more like as a rough estimation.

The differences between the code and the experimental values highlight the fact that this structure has low mechanical characteristics. Moreover, these results underline the importance of a site campaign for evaluating the mechanical properties of a structure. The suggested values of the Italian code could be used to analyze this structure but in this particular case, they would lead to an overestimation of the compressive strength. In addition, this test campaign highlights the variability of the mechanical characteristics in a single structure. This is an important fact that has to be taken into account in eventual deeper analyses meant to evaluate the safety of the structure.

4.2.2 Shear *FJ* test

As introduced in the previous Sub-section, the shear *FJ* test was performed in the basement of the structure near the location of the second couple of standard *FJ* tests (Position 2 Fig. 4.5a). The position of these two tests was also chosen looking for a wall that had a sufficient vertical load. However, the main features that were taken into account to find the position were the good texture of the masonry and the safe position. In fact, many walls presented a lack of vertical joints and the risk of detachments (as happened in Position 1). In addition, not all of the rooms of the structure were safe because the structure was abandoned for a long time.

The location on the wall of this test was chosen looking principally at the presence of vertical joints in order to avoid interference between the standard *FJ* tests and to have a practical and handy position to perform the test. This last criterion was mostly influenced by the maneuverability of the saw but paying also attention to the possible position of the measure bases. The thickness of this single-leaf wall was about 70 cm.

Methodology

After the position of the test was decided, the locations of the flat jacks were marked on the wall considering a reciprocal distance of 500 mm. This operation was carefully performed in order to obtain the inclination of 45° of the two *FJs* and, at the same time, to have them aligned. Before the realization of the cuts, the positions of the gauge points (and of the measure bases) were chosen. In this test, seven measures bases were used, three perpendicular and four parallel to the *FJs* planes (Fig. 4.8). Measures of the bases were taken before and after the realization of the first cut and then after the realization of the second cut.

The *FJs* employed for the test had the same characteristic of the ones used in the previous tests (Tab. 4.1) as well as the extensometer and the pressure gauges. The area of the lower cut was $A_{low} = 106080$ mm^2 and the other one was $A_{top} = 82275$ mm^2 resulting in a geometrical ratio of $k_a = 0.823$.

When the *FJs* were placed in the corresponding slots the hydraulic system was connected to them as showed in Figure 4.8. Before starting the test, the solvent was pumped inside of the hydraulic system and keeping opened the upper plug of the upper *FJ* in order to take out all the air from the circuit.

The test was performed in four load cycles. It has to be highlighted that the mechanical coefficient k_m for this and the successive tests was not a function of the hydraulic pressure (like the previous tests of the campaign) but a simple value independent of the pressure and taken from the certification of the flat jacks ($k_m = 0.894$). The maximum applied stresses on the masonry in the four cycles were $\sigma = -0.11$, -0.15, -0.29 and -1.91 MPa.

For each pressure step, seven measures of displacements were taken. Every step was decided considering the deformations trend of the previous steps and it was then slowly reached and kept for a few moments with the manual pump before starting the mensuration. This choice was taken in order to recover possible creep deformations. The measures were executed when the pressure was not changing for a time similar to the one required to read the measures (about two minutes).

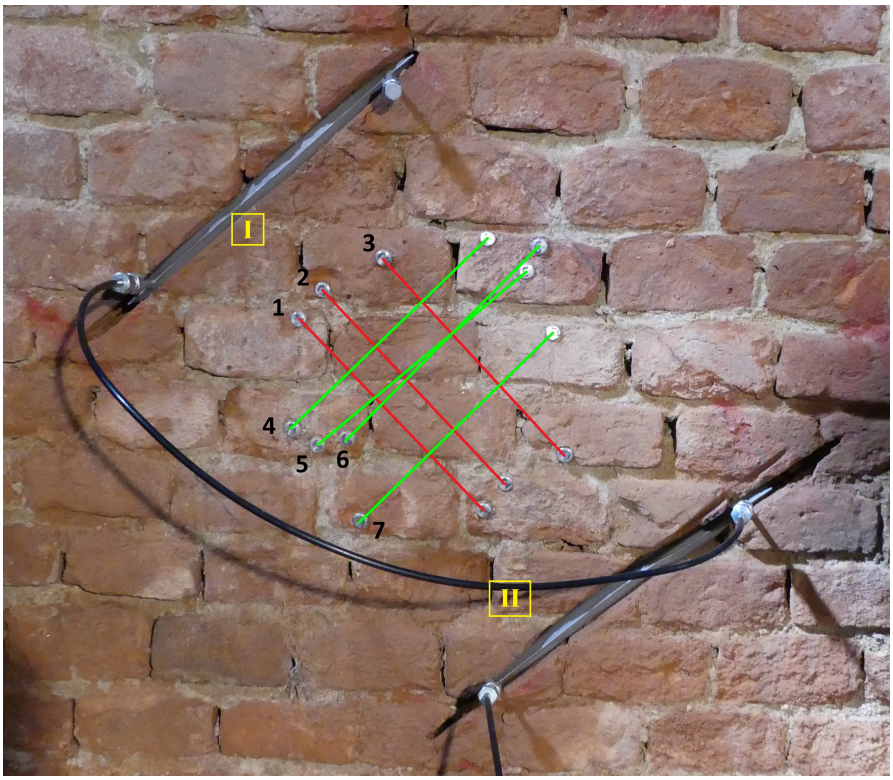

Figure 4.8: The image provides the set-up of the shear *FJ* test performed in "ex Teatro dei Nobili" Position 2. In the picture the measures bases are drawn. In red are highlighted the three measure bases perpendicular to the *FJs* planes and in green the four parallel to the same plane.

Results

It has to be underlined that part of the results of this test were presented in [187].

In Figure 4.9 the results of this shear *FJ* test are reported. In Figure 4.9a the strains perpendicular $\varepsilon_{\perp}$ and the parallel $\varepsilon_{\parallel}$ to the *FJs* planes are plotted. The inclined Young's modulus was evaluated from the elastic linear range of the perpendicular strains with a linear regression. The inclined Young's modulus found is $E^* = 949$ MPa with a standard deviation of 108 MPa (the lowest correlation evaluated is 0.964).

In Figure 4.9b the shear strain and the applied stress are presented as well as the interpolation of the linear elastic range of the material. From a linear regression of the elastic linear range of the shear strain (Fig. 4.9b) it was possible to evaluate the shear modulus. This has a mean value $G = 418$ MPa and a standard deviation of 30 MPa (the lowest correlation is 0.920).

In Figures 4.9c and 4.9d the principal stresses of the sample evaluated with the piecewise linear laws (Eq. 3.18 and 3.19) are reported and in Figures 4.9e and 4.9f the principal stresses evaluated using the normalized principal stresses of Table A.2 (Appendix A) are plotted.

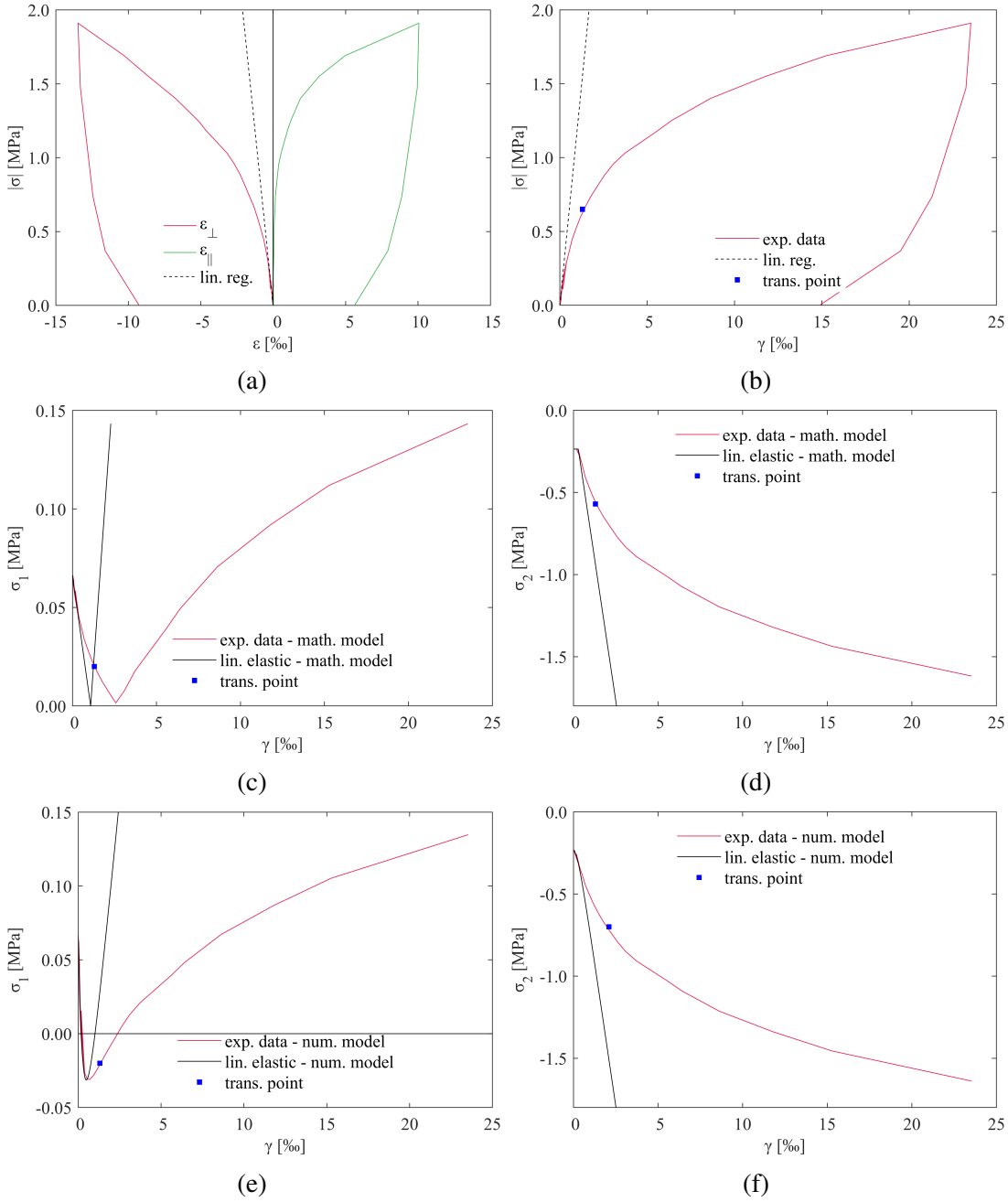

Figure 4.9: The image reveals the results obtained in the shear *FJ* test performed in "ex Teatro dei Nobili", Position 2.

Discussion

This first experimentation highlighted the potential of the test and at the same time pointed out improvements that could be used to better perform the test. In fact, this test was executed as a trial test in order to understand the feasibility of the set-up, to evaluate the possibility of using the standard equipment, to face eventual problematics and to find eventual optimizations.

First of all, this test demonstrated the possibility of the utilization of the same equipment of the standard *FJ* tests. This fact is important in the perspective of further application of the test. In fact, the possibility of using the same equipment of the standard *FJ* tests leads to a marked reduction of costs because the purchasing of specialized equipment is not necessary.

The realization of the cuts was not a simple operation. The lowest cut was the first one to be created. This slot was not matching perfectly the mark due to the non-smooth operation of the saw. As a result, an imperfect inclination of the slot was obtained. In addition, this cut was significantly longer than the mark leading to a bigger slot area. Despite this problem, the difference between the ideal orientation and the one obtained was not too marked. This is verified by the similarity between ε_2 and ε_3 that underlines a homogeneous strain field (Figure A.2 in the Appendix A). The realization of the second cut was performed with a higher precision because the operators were then more able to handle the saw in this unusual position. Another important fact, that had as a result, a better realization of the cut, was that at first the operator carefully cut a line (of about 0.5 cm depth) coincident with the mark on the wall. This incision worked as a guide for the saw during the creation of the slot.

As it can be noticed in the picture (Fig. 4.8), the orientation and the positions of the measure bases were not perfect. The intention was to have these bases perfectly perpendicular and parallel to the cuts. However, this was impossible to obtain due to the thickness of the joints, the position of the bricks, the length of the extensometer and the dimension of the gauge points (diameter $\phi = 1.5$ cm). The positioning phase (of the measure bases) had also a purpose: to cross as close as possible the center of the sample in order to obtain a configuration similar to the numerical models carried out.

Another small issue was underlined at pressures higher than 1.50 MPa. For these cases, it was not possible to keep a constant stress for all the time required to acquire the measures. It was also tried to reach the load step and then to keep the pressure constant (acting on the pump) for a longer time (about 5 min). However, it was not possible to ensure a constant pressure for all the measurements. This change in the pressure level could be correlated to the damaging process to which the sample was subjected and to a not perfect closure of the hydraulic circuit.

A deeper analysis of the results is important. The Young's modulus obtained with the standard *FJ* test is 905 MPa. The Modified Young's modulus measured in the shear *FJ* test is $E^* = 949$ MPa. As numerically evaluated, the ratio E^*/E should be equal to $= 1.06$, in the test this ratio is $E^*/E = 1.05$. It results possible to say that the media shows a good isotropic behavior.

From the measured Young's modulus, it is possible to evaluate the shear modulus by estimating the Poisson's ratio. Supposing $\nu = 0.25$ and using the measured Young's modulus it is possible to evaluate the shear modulus of the sample $G = 362$ MPa. This is calculated supposing an isotropic homogeneous and elastic material and using the well known constitutive equation $G = E/[2(1+\nu)]$. The mean shear modulus measured is $G = 418$ MPa. These two values are close one to the other one which should highlight the ability of the proposed test to measure the shear modulus of the media.

The analysis of the stress status of the sample was performed in two main ways using the piecewise linear laws (Fig. 4.9c and 4.9d) and using Table A.2 of the normalized

principal stresses (Fig. 4.9e and 4.9f). Utilizing the graphical method proposed in the test methodology (Sec. 4.1) and the plot of the shear strain (Fig. 4.9b) it is possible to detect the elastic plastic transition. To this point it correspond a the stress $\sigma = -0.65$ MPa. For this stress, the sample undergoes a strain $\gamma = 1.30‰$ (see the blue square in Fig. 4.9b).

It is now possible to evaluate the sample stress status using the piecewise linear laws by entering with $\gamma = 1.30‰$ in the graphs of Figures 4.9c and 4.9d. The principal stresses associated with this strain are $\sigma_1 = 0.02$ MPa and $\sigma_2 = -0.57$ MPa. For $\gamma = 1.30‰$ the largest principal stress is interpolated with the first branch of the piecewise linear law. As highlighted in the presentation of the piecewise linear laws (Section 3.2), this first branch of the curve does not interpolate perfectly the largest principal stress.

To summarize, the sample is under a bi-axial compressive stress when the plastic regime of the material starts.

Conclusion

This first experimentation gave some encouraging results and at the same time underlined some improvements that were useful to enhance the test and to understand better the behavior of the masonry sample under test. These facts are developed in the following paragraphs.

The position of the shear *FJ* test was forced by the characteristic of both the structure and the masonry. Indeed, it was not simple to find a position where it was possible to perform the shear *FJ* test and the two standard *FJ* tests. The double *FJ* tests underlined the poor quality of the masonry. In fact, both the Young's modulus and the compressive strength are smaller than the values recommended by the Italian codes [86, 87].

From the results obtained with the piecewise linear laws (Fig. 4.9c and 4.9d) the sample seems to fail in a tension-compression status. As underlined previously, for the strain to which corresponds the beginning of the sample plastic range the largest principal stress is interpolated with the first branch of the piecewise linear laws. This does not interpolate perfectly the largest principal stress. This fact is remarked by the results (Fig. 4.9e and 4.9f) of the interpolation obtained with the normalized principal stresses. In these results, it can be noticed that the plastic regime of the sample starts when the sample is in a bi-axial compression status. For this reason, it can be affirmed that the sample fails under a bi-axial compression status.

Nevertheless, it has to be underlined that this experiment was the first shear *FJ* test. When this test was performed the full methodology, proposed in the previous section, was not completely developed yet as well as the full knowledge of the behavior of the sample under test. These modifications/improvements were decided/designed and successively applied in the other tests.

First of all, it was decided to use *LVDTs* in parallel with the classic measuring system as introduced in the test methodology (Sec. 4.1). This choice was made considering two main aspects. The first is the possibility for these transducers of shortening/extending their length of some millimeters. On the contrary, the manual extensometer used in the shear *FJ* test had a fixed length of 250 mm. *LVDTs* can avoid problems on the alignment of the measure bases because the measuring points can easier avoid the joints. The

second advantage that this equipment can guarantee is the possibility of having a continuous monitoring of the displacements during the test. The manual reading requires more time to be performed and, as it has been said before, for high levels of hydraulic pressures it was impossible to keep a constant load so the deformations were changing during the whole time as well as the pressure. The measurements started with the reading of the pressure and then of the displacements but at the end of the recordings, the pressure could have changed. *LVDTs* could also be used to measure creep deformations. One possible disadvantage of the use of these transducers is that, given their own dimensions and that they have to stay mounted on the sample, they have to be placed at different distances (with respect to the sample surface) in order to avoid interferences. To do this, *LVDTs* steel supports were designed (Fig. 4.10). This unavoidable position of the *LVDTs* could be a disadvantage because the measures could be corrupted by eventual small rotations of the sample that are accentuated in the *LVDTs* placed farther from the wall surface. As already said, this measuring system was used in parallel to the classic one because these transducers are delicate and cannot be maintained on the sample during the creation of slots.

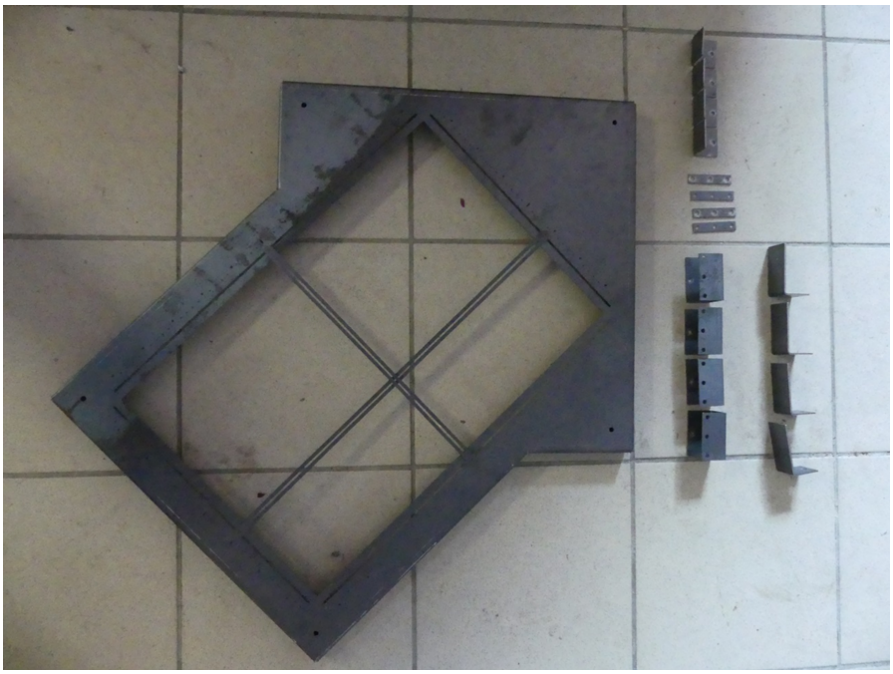

Figure 4.10: The picture shows the steel template designed for the shear *FJ* test. As can be seen the supports for the *LVDTs* are also in the picture.

In parallel to the *LVDTs*, it is necessary to keep a continuous monitoring of the hydraulic pressure. In this way, it is possible to obtain a perfect synchronization of the strains of the sample and the stress applied to it. This is possible using an electronic pressure gauge. The combination of these two types of transducer (*LVDTs* and an electronic pressure gauge) leads to a continuous evaluation of the displacements and the pressure. This fact could be very interesting considering that the usual results of the *FJ* tests are presented only for few pressure steps.

In the preliminary phases of the shear *FJ* test, the location of the *FJs* and of the

measure bases were marked on the sample. This operation was difficult to perform due to the position of the bricks, the thickness of the joints and to the fixed length of the strain gauge. To simplify this task it was decided to design a steel frame to apply on the masonry (Fig. 4.10). In this template, two steel plates were adopted (one crossing the other one) to help the bases positioning. This frame is designed also to help the individuation of the position for the test. In fact, once the template is placed, it is easy to identify a not optimal position for the measure bases and it could be decided to move the steel mask in order to optimize the test location. Moreover, it was also decided to use a wood frame to help the cuts realization.

Another technical decision, regarding the measurements of the deformations and or displacements was explored. This consisted in the possibility of employing the *DIC* technique. This technique has many advantages, for example, it does not interfere with the sample, it allows the evaluation of the absolute displacement, it extends the measures to an area and not only to specific points of the sample, etc. This technique can help in the detection of the shear strain of the sample that is not directly measured and it can also be used to identify the cracks propagation before they are visible at naked eyes. Even the synchronization with the *LVDTs* and with the pressure transducer can be performed very easily. Unfortunately, as it can be noticed in the pictures of the other tests (Fig. 4.14, 4.16, 4.22 and 4.26), this technique cannot be used because the large part of the sample is covered by sensors, cables and tubes.

4.3 Tests in the "Caserma Giovanni Cerutti"

This experimental campaign was conducted in autumn 2018. The tests were performed again with the collaboration of Cosmondi SRL and thanks to the city hall of Boves. In particular, the building under study is owned by the city hall that kindly allowed to perform the tests.

The structure under study is part of a barrack that is named "Caserma Giovanni Cerrutti". This is situated in the city of Boves (Cuneo, Italy). The structures of this barrack were realized just before the second world war, precisely in 1938 and 1939. During the war, the barrack was also used by the 1st SS Panzer Division "Leibstandarte SS Adolf Hitler". The structures present in this barrack show different building techniques. In fact, structures in both reinforced concrete and *URM* are present. The building under test is obviously made of *URM* and it was probably used for the accommodation of the troops and for the commands. Unfortunately, drafts of the barrack were not available.

The tests performed in this barrack were four, a single and a double *FJ* test and two shear *FJ* tests. The two standard *FJ* tests and one shear *FJ* test were executed in the same room on the second last floor of the structure (named Position 1). The other shear *FJ* test was performed in another room but on the same floor of the same structure (Position 2). The choice of performing the test on the same floor was related to the necessity of having a good evaluation of the vertical stress and the specific floor was chosen as the optimal one to perform the test. It has to be said that all of the tested walls have a thickness of 46 cm and that the area of the *FJs* used is reported in Table 4.1.

Moreover, it has to be underlined that the *AE* technique was adopted for the two shear *FJ* tests and for the double flat jack test. Unfortunately, due to a high noise

Figure 4.11: In the image a picture of the "Caserma Giovanni Cerutti" is shown.

present in the structure, a high threshold had to be set. Due to this fact, the acquired data were few and not enough to give acceptable and meaningful results.

4.3.1 Standard *FJ* tests

As introduced also for the test performed before and in the parametric analysis, the knowledge of the vertical stress, the Young's modulus and the compressive strength are important characteristics that can be necessary to understand the behavior of the sample. For this reason, as anticipated, the two standard *FJ* tests were performed in Position 1 next to one of the shear *FJ* test.

After that the plasterwork was removed, it was possible to notice a good quality of the texture and of the masonry. In fact, bricks laid in the direction perpendicular to the wall surface help to have a single-leaf behavior and both vertical and horizontal joints seem to be homogeneous and to have a fine quality. As done for the standard *FJ* tests in Vercelli, the two tests were performed in the same location, using for the double *FJ* test the flat jack used in the single *FJ* test.

Single flat jack test

This standard *FJ* test was performed in the same way as the one executed in Vercelli. The manual equipment was used to measure the displacement. After the creation of the slot its area was measured (88050 mm^2) and a geometrical coefficient $k_a = 0.880$ was evaluated. The mechanical coefficient of the *FJ* used was $k_m = 0.902$. All of the *FJs* utilized in the four tests executed in this building had the same value of the mechanical coefficient because they all came from the same batch of production.

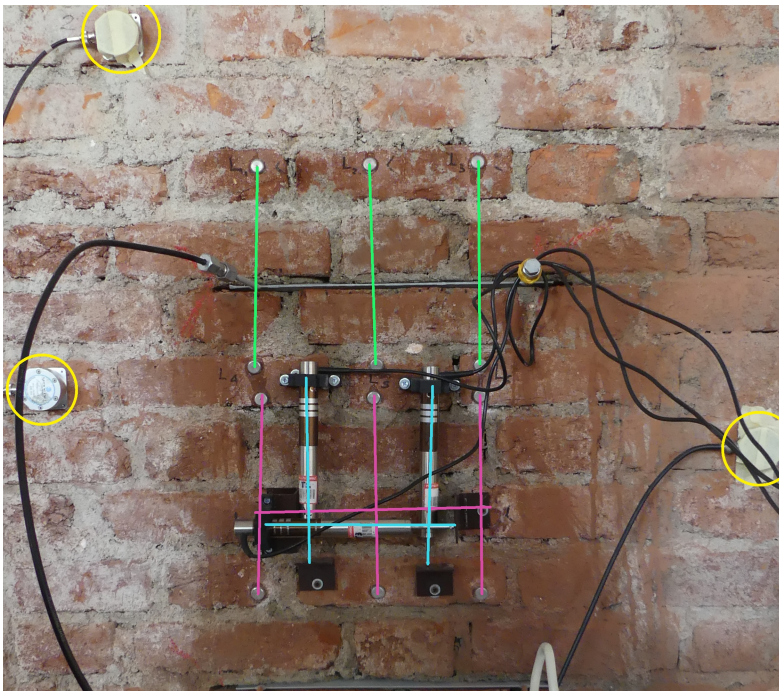

Figure 4.12: The picture displays the positions of sensors and measure bases in the standard *FJ* test. In green are indicated the three measure bases used in the single *FJ* test, in pink the four measures bases (three vertical and one horizontal) used in the first steps of the deformability test, in light blue are highlighted the three *LVDTs* (two vertical and one horizontal) utilized during the second phase of the double *FJ* test and with yellow circles are marked the four *AE* sensors. "Caserma Giovanni Cerutti".

The test was conducted with the same precautions and recommendations discussed previously. The result of this test is a vertical stress $\sigma_0 = -0.55$ MPa. It has to be underlined the position of this test. In fact, the two standard *FJ* tests were performed in a wall that has the main direction parallel to the main direction of the building. It was possible to notice that the floors above the test position are supported by the tested wall. Due to the problem of finding the optimal positions for the shear *FJ* tests, they were performed in two walls that are perpendicular to the one where the standard tests were performed. In fact, in the walls parallel to the one where the standard *FJ* tests were carried out, opening of doors were present. For this reason, these walls seemed to not be able to guarantee sufficient lateral confinement and it was decided to use two walls perpendicular to the main direction of the building where openings are absent.

Considering the disposition of the slabs, of the resisting elements, the above part of the structure and the loads paths it was possible to calculate the vertical stress present in both the positions of the shear *FJ* tests that resulted to be $\sigma_0 = -0.36$ MPa.

Double *FJ* test

As anticipated the double flat jack test was performed in the same position of the single *FJ* test (Fig. 4.12). In this case, the automatic acquisition system was used. After the acquisition, the data were filtered with a Butterworth filter in *MATLAB*.

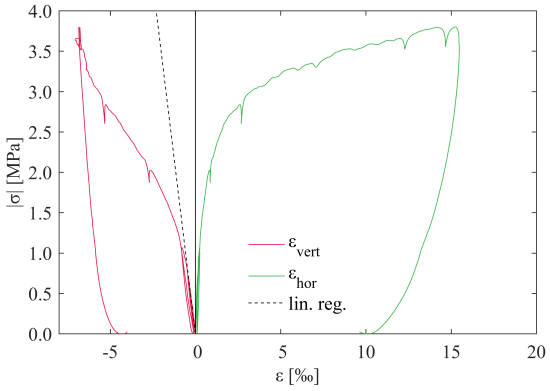

Figure 4.13: The plot summarizes the results of the double *FJ* test performed in "Caserma Giovanni Cerutti" Position 1.

After the creation of the second slot, its area was measured (85338 mm^2). The resulting geometrical coefficient was $k_a = 0.894$.

Subsequently, all the sensors were placed on the sample and the hydraulic system was closed. It was then possible to start the test. The sample was subjected to three cycles of load. The maximum pressures applied in these cycles correspond to stresses $\sigma = -0.72$, -1.07 and -3.80 MPa (Fig. 4.13).

The Young's modulus was evaluated using linear regressions in the first three cycles and for an absolute stress inferior to $|\sigma| = 1.13$ MPa of the third cycle. The mean value of this elastic characteristic is $E = 1739$ MPa, it has a standard deviation of 144 MPa and the lowest correlation measured is 0.994. The value of the Young's modulus underlines a masonry with a good quality and, for this reason, it confirms the visual observations.

The methodology proposed in Sub-section 2.3.3 was followed in order to evaluate the compressive strength of the media. The value of compressive strength found was $f_c = 2.20$ MPa.

Conclusions

The standard tests performed in the "Caserma Giovanni Cerutti" showed a good quality of the masonry. In fact, at the removal of the plasterwork the bricks and the mortar seemed to have an accurate texture and to be made of good materials. This fact was proved by the value of the Young's modulus of the media and its compressive strength.

The position of the single *FJ* test does not give a direct measure of the vertical stress present in the locations where the two shear *FJ* tests were carried out. Nevertheless, with the analysis of the loads and of their paths, it was possible to have an accurate evaluation of the vertical stress.

The characteristics measured and noted until this point of the experimental campaign were promising for what regards the shear *FJ* tests. In fact, the masonry showed a good quality of both the materials and the texture. Moreover, the calculated vertical stress was not too large as well as the thickness of the wall. These two last characteristics are the ones more promising because, as underlined in the numerical analyses of the test configuration, they play an important role in the evaluation of the tensile strength

of the media.

4.3.2 Shear *FJ* test - Position 1

The first shear *FJ* test executed in the "Caserma Giovanni Cerutti" was performed in the same room where the two standard *FJ* tests were carried out. In particular, as mentioned before, this test had to be performed in a wall that has a perpendicular direction with respect to the wall already tested.

At a first view after the plasterwork removal, the masonry showed similar characteristics of the ones observed in the location where the standard *FJ* tests were performed. A good quality of the bricks and of the mortar and a good texture of them were found.

Methodology

The proposed test method with its recommendations was adopted in this experiment. Moreover, the automatic acquisition system. was utilized.

The position of the test was chosen in order to glue the four couples of measuring points for the manual acquisition and to fix the *LVDTs* as much as possible close to the center of the sample. After that the optimal position was found, the *FJs* positions were drawn on the wall in order to help the slots realization. Four *LVDTs* and four manual measure bases were used. Two measure bases and two *LVDTs* were positioned perpendicularly to the *FJs* planes and the other sensors and bases were positioned in the orthogonal direction.

After the creation of the slots their areas were measured resulting $A_{low} = 84733$ mm^2 and $A_{top} = 80600$ mm^2. The obtained geometrical coefficient is $k_a = 0.938$ that means also a really good realization of the cuts. As introduced in the standard *FJ* test, the mechanical coefficient is $k_m = 0.902$.

Subsequently, the sensors were fixed on the sample. In Figure 4.14 it is possible to notice that the positions of the *LVDTs* were slightly not central to the sample. This was considered a negligible issue since this eccentricity was not excessive. In the same image, it is also possible to observe the bases points for the preliminary manual measurements.

The data acquired were then filtered with a Butterworth filter in *MATLAB*.

The test was performed with four load cycles of increasing magnitude. More specifically the maximum applied pressures correspond to stresses $\sigma = -0.49, -0.79, -1.20$ and -4.42 MPa.

Results

The results of the first shear *FJ* test performed in "Caserma Giovanni Cerutti" are presented in Figure 4.15.

The evaluation of the elastic characteristics was performed with linear regressions of the first three load cycles The mean inclined Young's modulus evaluated in the linear elastic regime of the material is $E^* = 3777$ MPa, it has a standard deviation of 255 MPa and the lowest calculated correlation is 0.978 (Fig. 4.15a).

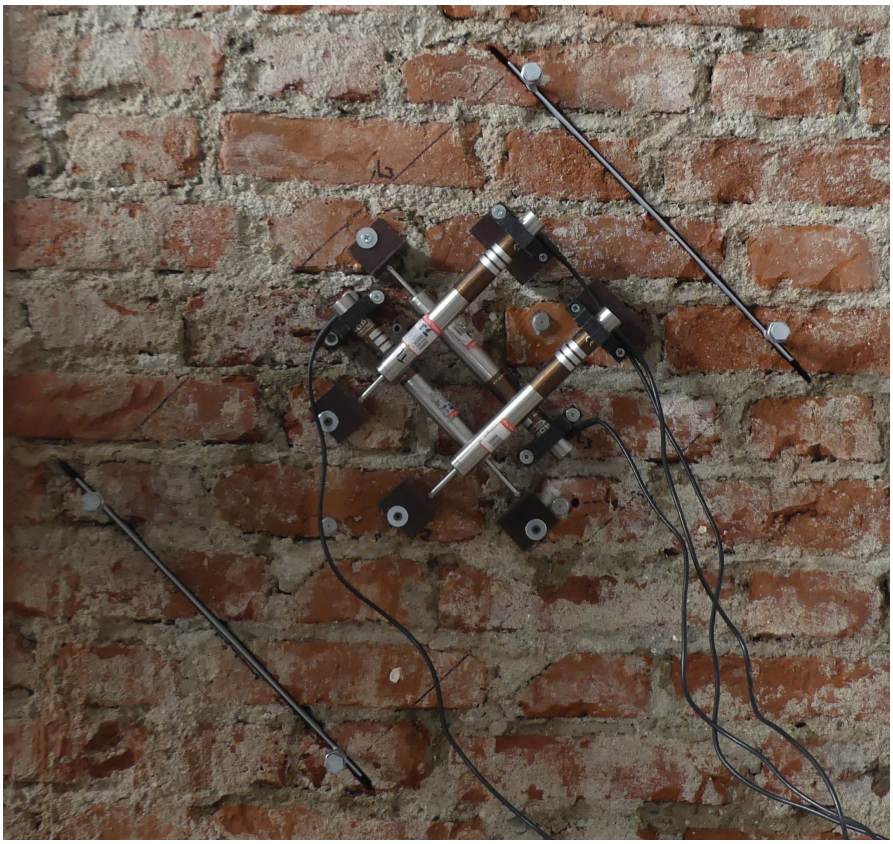

Figure 4.14: The picture shows the test set-up of the shear *FJ* test performed "Caserma Giovanni Cerutti" Position 1.

From the results of the shear strain (Fig. 4.15b) it was possible to evaluate the shear modulus of the sample that results to be $G = 1217$ MPa (standard deviation of 67 MPa, lowest correlation measured 0.985).

The analysis of the sample stress status was performed with both the piecewise linear laws (Eq. 3.18 and 3.19) and the normalized principal stresses (Tab. A.2). The results of this analysis are presented in Figures 4.15c, 4.15d, 4.15e and 4.15f.

Discussion-Conclusion

The test performed in Position 1 of the "Caserma Giovanni Cerutti" was encouraging even before starting it. In fact, the small acting vertical stress, the compressive strength and the limited thickness of the wall were really auspicious.

First of all, in the results obtained (Fig. 4.15) it is possible to notice a large number of acquired points in comparison to the shear *FJ* test performed in the "ex Teatro dei Nobili". This is due to the utilization of the automatic acquisition system that has a sample rate of 1 Hz. This method helps to have a good number of data and in continuous. Attention was paid in order to not load the sample too rapidly giving time to the media for recovering the creep deformations.

The elastic characteristics measured show some discrepancies from the expected ones. Hypothesizing an elastic isotropic homogeneous material, a Poisson's ratio $\nu =$

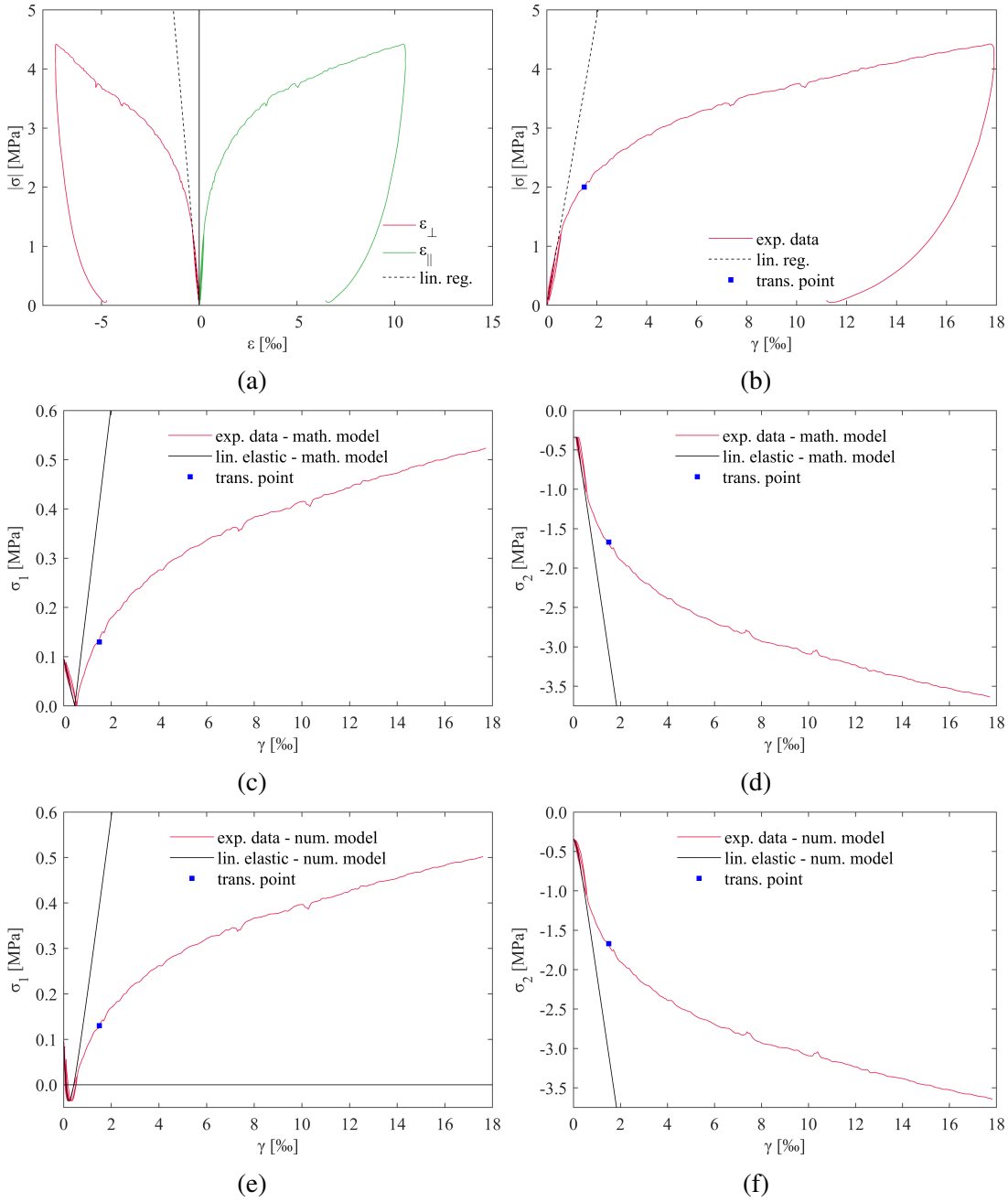

Figure 4.15: The image gives the results obtained in "Caserma Giovanni Cerutti" Position 1.

0.25 and using the measured Young's modulus of $E = 1739$ MPa, the shear modulus results to be $G = 696$ MPa. The shear modulus evaluated with the proposed test is $G = 1217$ MPa.

With regards to the Young's modulus and the inclined Young's modulus, a similar discrepancy was found. The ratio evaluated with the numerical model should be close to the unit ($E^*/E = 1.06$). However, the measured one is $E^*/E = 2.17$.

These two discrepancies can be partially related to the position of the sensors. In

fact, it was not possible to place them perfectly in the center of the sample. However, even this fact cannot be the cause of these discrepancies. A deeper analysis of this issue is presented in the following Chapter.

The proposed piecewise linear laws were then used to evaluate the stress status of the sample. The results obtained are plotted in Figures 4.15c and 4.15d.

For what regards the identification of the transition between the elastic and plastic regimes, the method proposed in Section 4.1 was followed. It results that the transition point is defined by an applied stress $\sigma = -2.00$ MPa and the shear strain associated to this level of stress is $\gamma = 1.50‰$. The two principal stresses associated with this shear strain (Fig. 4.15c and 4.15d) are $\sigma_1 = 0.13$ MPa and $\sigma_2 = -1.67$ MPa. It is important to notice that for this shear strain the largest principal stress is interpolated with the second branch of the piecewise linear laws. This is important because this is the branch where the tensile strength of the media has to be measured. If an isotopic failure criterion of the media is considered, reminding that the evaluated compressive strength is $f_c = 2.20$ MPa and taking into account the stress status of the sample, it is possible to affirm that the failure of the sample was reached in tension. In fact, the smallest principal stress results to be much inferior to the compressive strength ($1.67 < 2.20$ MPa, $|\sigma_2| < f_c$). Identical results are obtained by using the principal stresses evaluated with the normalized principal stresses (Fig. 4.15e and 4.15f).

In addition, the analysis of the sample stress status at the slots realization ($\sigma = 0.00$ MPa) has to be performed. This phase of the test can be problematic. In fact, the failure of the media can be reached because the vertical stress rises high initial stresses inside of the sample. If at the cuts realization one of the principal stresses reaches one of the material strengths at the first pressurization of the *FJs* the sample should immediately show a plastic regime. In the present case it is possible to notice a linear elastic behavior for an absolute stress $|\sigma| < 1.20$ MPa (Fig. 4.15b). Since the linear range of the sample exists it is possible to affirm that the sample did not fail at the slots realization.

To summarize, it is possible to affirm that the evaluated tensile strength is $f_t = 0.13$ MPa and that the measured shear modulus is $G = 1217$ MPa.

4.3.3 Shear *FJ* test - Position 2

The second shear *FJ* test performed in the "Caserma Giovanni Cerutti" was carried out in a room near to the one where the previous three tests were performed. The choice of working in a near room and on the same floor was taken in order to consider more reliable the information given by the standard *FJ* tests. It has to be pointed out that the estimated vertical stress of the point under test is the same as the one evaluated for Position 1 ($\sigma_0 = -0.36$ MPa).

After the removal of the plasterwork in the chosen location, it was possible to notice that the masonry is very similar to the one saw in Position 1 from many points of view (quality of both materials and the texture of them). Since the double *FJ* test was performed in the same building where this shear *FJ* test was carried out and that both materials showed the same visual quality, the Young's modulus and the compressive strength of Position 2 were assumed to be the same of the ones measured in Position 1.

Methodology

The test method used for the shear *FJ* test performed in Position 1 is the one that is proposed at the beginning of this Chapter. Moreover, it was decided to use again the automatic acquisition system (Fig. 4.16) and for this reason, the preliminary phases were identical to the one used in the shear *FJ* test of Position 1.

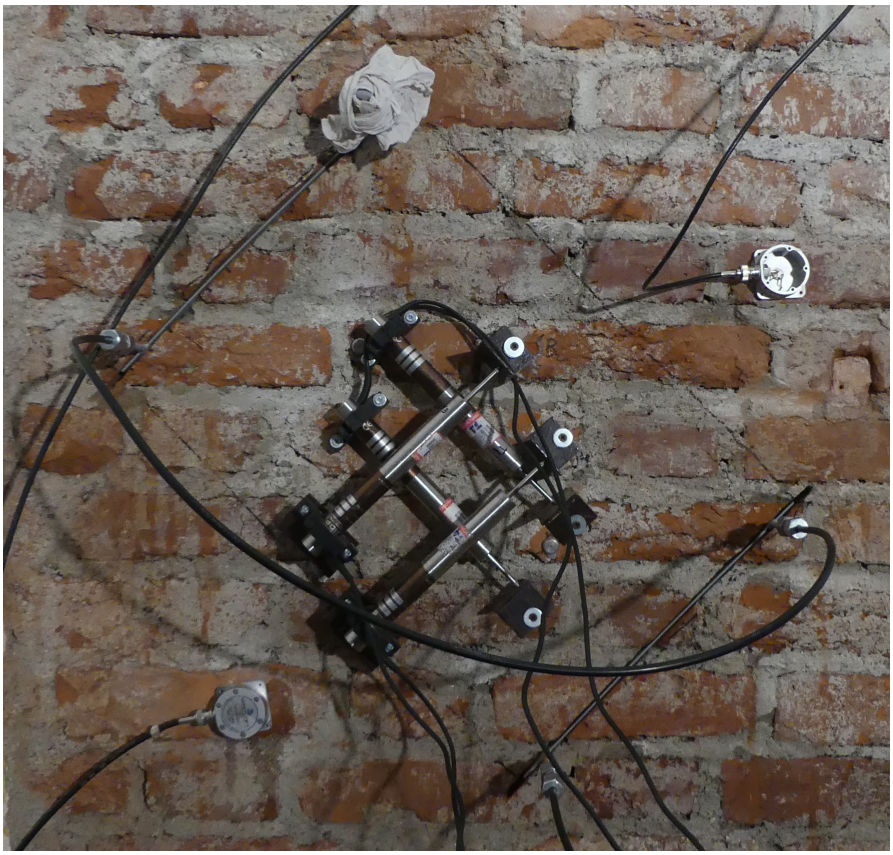

Figure 4.16: The picture shows the shear *FJ* test performed in "Caserma Giovanni Cerutti" Position 2. In the image it is possible to observe the disposition of the *LVDT* and of two *AE* sensors.

Once the location of the test was decided and the other preliminary phases were performed, the cuts were realized. The slots areas were respectively 90615 mm^2 for the lower slot and 86363 mm^2 for the upper slot resulting in a geometrical coefficient of $k_a = 0.876$. The mechanical coefficient of the *FJs* is $k_m = 0.902$.

After these measurements, all of the sensors were placed on the sample surface as well as the *FJs* in the cuts and subsequently the hydraulic circuit was closed. The test was then started. Four cycles of load were applied to the sample. The data acquired were then filtered with a Butterworth filter in *MATLAB*. The maximum absolute stresses applied to each cycle were $|\sigma| = 0.47$, 0.78, 1.23 and 4.02 MPa.

Results

The results of the second shear *FJ* test performed in "Caserma Giovanni Cerutti" are presented in Figure 4.17.

The evaluation of the linear elastic properties of the sample was performed with linear regressions in the linear elastic range of the four cycles performed (in the fourth cycle the max absolute stress considered was $|\sigma| = 1.12$ MPa). The mean shear modulus is $G = 971$ MPa, it has a standard deviation of 153 MPa and the lowest correlation measured is 0.989 (Fig. 4.17b). For what regards the inclined Young's modulus, the mean measured value is $E^* = 2312$ MPa, it has a standard deviation of 230 MPa and the lowest calculated correlation is 0.994 (Fig. 4.17a).

The analysis of the stress status is also presented in Figure 4.17. More precisely, Figures 4.17c and 4.17d display the evaluation of the principal stresses using the piecewise linear laws (Eq. 3.18 and 3.19) and Figures 4.17e and 4.17f the results obtained with the normalized principal stress of Table A.2.

Discussion-Conclusion

As highlighted for the shear *FJ* test carried out in Position 1, the premises for this test were encouraging. In fact, low vertical stress, good quality of the masonry and the mechanical characteristics measured were auspicious for the test.

As done for the test in Position 1, with the measured elastic modulus $E = 1739$ MPa and supposing a Poisson's ratio $\nu = 0.25$ it is possible to evaluate the shear modulus that results to be $G = 696$ MPa. The shear modulus measured with the proposed test is $G = 971$ MPa. There is a discrepancy between these two moduli but it is not too large.

Similarly, the Young's modulus measured with the double *FJ* test ($E = 1739$ MPa) is similar to the inclined Young's modulus measured with the shear *FJ* test ($E^* = 2312$ MPa).

The method proposed in Section 4.1 was followed in order to identify the transition between the elastic and plastic regimes. Therefore, the transition point is defined by an applied stress $\sigma = -1.70$ MPa and the associated strain is $\gamma = 1.50‰$. It results possible to enter with this strain in the results of the piecewise linear laws (Fig. 4.17c and 4.17d) and evaluate the sample stress status for which the sample starts to show plastic deformations. The principal stresses of the sample for $\gamma = 1.50‰$ are $\sigma_1 = 0.09$ MPa and $\sigma_2 = -1.45$ MPa. It is possible to notice that the smallest principal stress is much inferior to the compressive strength measured with the double *FJ* test in Position 1 ($1.45 < 2.20$ MPa, $|\sigma_2| < f_c$). Hypothesizing an isotropic failure criterion and considering that, at the beginning of the sample non-linear regime, the compression stress of the sample is inferior to the material compression strength, it is possible to affirm that the failure of the sample took place in tension and that the tensile strength of the material is $f_t = 0.09$ MPa.

The sample stress status was also evaluated with the normalized principal stresses of Table A.2 and the results are plotted in Figures 4.17e and 4.17f. For the strain related to the beginning of the non-linear regime of the sample ($\gamma = 1.50‰$) the principal stresses evaluated are almost identical to the one evaluated by using the piecewise linear laws. Similarly to what said in the previous paragraph, it is possible to affirm that the sample

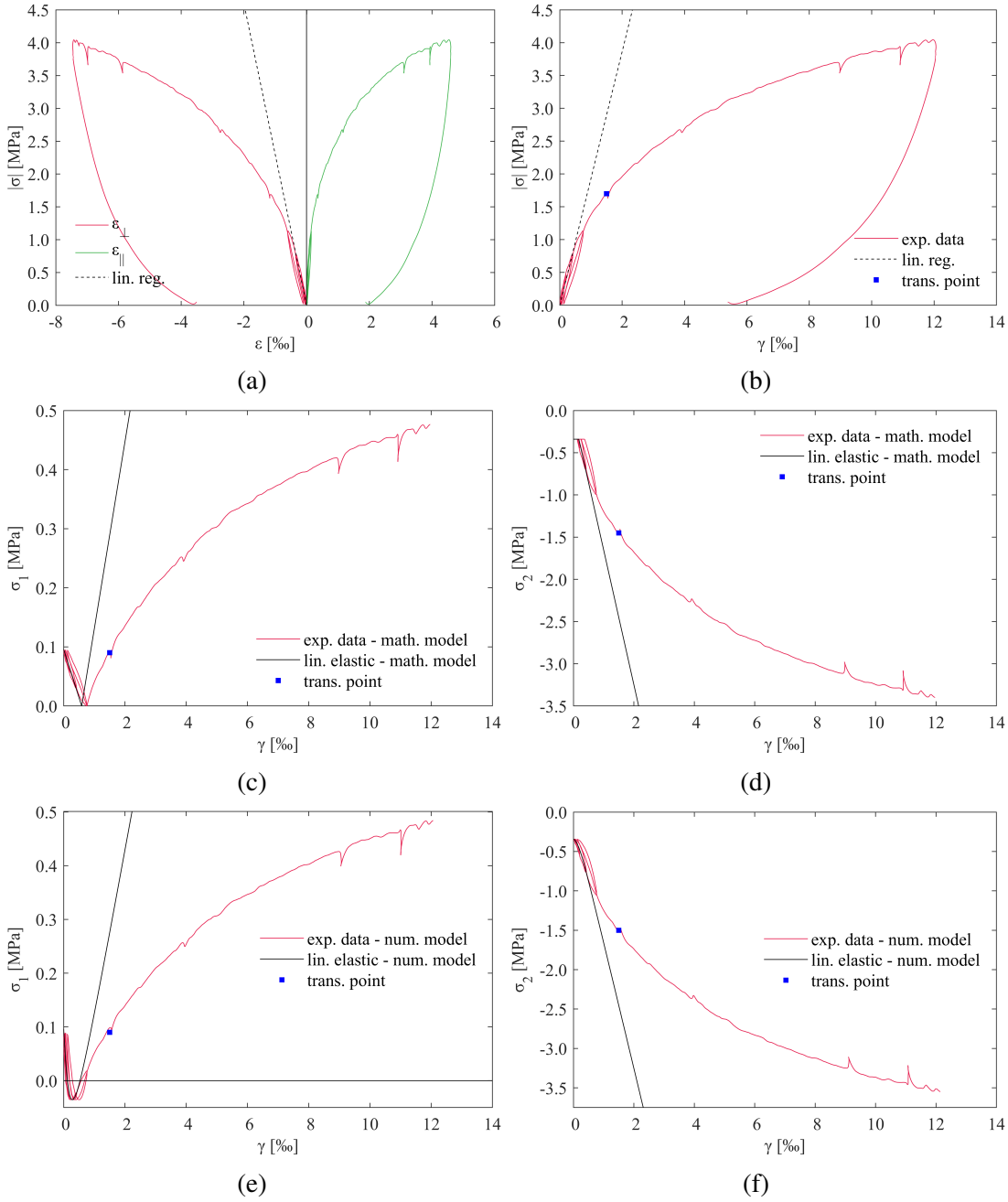

Figure 4.17: The image reports the results obtained in "Caserma Giovanni Cerutti" Position 2.

failed in tension and that the tensile strength of the material is $f_t = 0.09$ MPa.

It is also important to analyze the sample behavior at the slots realization ($\sigma = 0.00$ MPa). In fact, the media can fail at the cuts realization due to the initial stresses caused by the vertical stress. The failure should be verifiable because at the first pressurization of the *FJs* the sample should show immediately a plastic regime if, at the cuts realization, one of the principal stresses reached one of the material strengths. In the test here described it is possible to notice a linear elastic behavior for an absolute

stress $|\sigma| < 1.12$ MPa (Fig. 4.17b). Since the sample plastic regime is not attained for an applied stress close to zero, it is possible to affirm that the sample did not fail at the slots realization.

In conclusion, with the shear *FJ* test performed in Position 2 it was possible to measure a shear modulus $G = 971$ MPa and a tensile strength $f_t = 0.09$ MPa. The measured shear modulus is a bit larger than the expected one. However, the difference is not too high.

4.4 Tests in the "Caserma Valfrè di Bronzo"

This experimentation campaign was conducted in summer 2018. The tests were executed with the collaboration of Cismondi SRL and thanks to the approvals of the "Agenzia del Demanio" and of "Ministero dei Beni e delle Attività Culturali del turismo" (also called *MiBAC*). The "Agenzia del Demanio" is a public Italian agency that is responsible for the management and enhancement of the real estate assets. The *MiBAC* is an Italian ministry that protects and enhances culture, heritage and activities. The approval of these two Italian organisms was necessary because the tests were performed in an ex military barrack under their management in the city of Alessandria.

The "Caserma Valfrè di Bronzo" was designed by Colonel Trincheri and it was realized in six years, from 1885 to 1891. This barrack was built in order to receive the horse artillery and they were used for military purposes until 2002 [193]. The three principal facilities have a U-shaped layout (Fig. 4.18c). In the center the Command building it is present and the two sides of the U are the West and East building for the troops accommodation. In these barracks there were also other facilities that were used as stables, stores, laboratories and to contain the artillery. The structures under test are made of masonry bricks and lime mortar. During the realization of the facilities, a furnace was made in situ in order to provide the bricks necessary for the construction.

The Command building has a rectangular layout with sides of 80.0 and 17.0 m. This structure has three floors above the ground level and a basement. Its height is 17.4 m. The ground floor, as well as the first and second floors, is made of brick masonry vault; on the contrary, the last floor is made of steel beams brick jack-arches.

The two buildings for the troops accommodation have dimensions of 107.0×16.5 m. The central part of these buildings is 17.0 m high and the two lateral parts have a height of 11.0 m. These two structures have a portico that faces in the central courtyard. All of these three buildings have a roof made of wood trusses [193].

Similarly to what was done in Boves, a single and a double *FJ* tests were performed in the West building and in the same room a shear *FJ* test was performed. The area of all the *FJs* used is reported in Table 4.1. A second shear *FJ* test was performed in the Command building.

For what regards the shear *FJ* tests performed in this experimental campaign, it was decided to perform them in positions where a higher vertical stress was present. This choice was made with the purpose of confirming the importance of the role played by the vertical stress in this test configuration.

(a) (b)

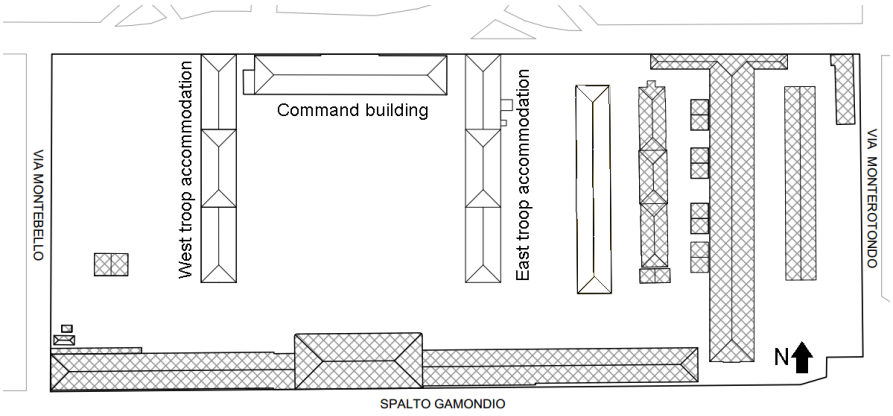

(c)

Figure 4.18: In the image two pictures (the fist of the Command building 4.18a and the second one of the West barrack 4.18a) and the layout (Fig. 4.18c) of the whole "Caserma Valfrè di Bronzo" are presented.

4.4.1 Standard *FJ* tests

In the West building, that was dedicated to the troops accommodation, a single and a double *FJ* tests were performed. These tests were executed in order to measure the Young's modulus, the compressive strength and the vertical stress level. These tests were carried out in the same position, more specifically in an interior wall on the first floor of the West building (Fig. 4.19). This overlap was possible by using the cut of the single *FJ* test for the subsequent double *FJ* test. In the same room, but on the opposite wall, a shear *FJ* test was carried out. The two walls had a thickness of 50 cm.

The equipment used for the evaluation of the vertical stress was the same used for all of the single *FJ* tests. This is the manual equipment. For the other tests, the automatic acquisition system was utilized. This automatic system was employed in parallel with the manual one as described in the test methodology.

Excluding the single flat jack test, four, sensors for the *AE* were mounted in the portion of the wall surrounding the sample. It has to be highlighted that their positions were well studied in order to optimize the results. For this reason, attention was paid to avoid the reciprocal symmetry of the sample and of the sensors. In addition, it was attempted to put the sensors in zones where the cuts did not interfere with the emissions

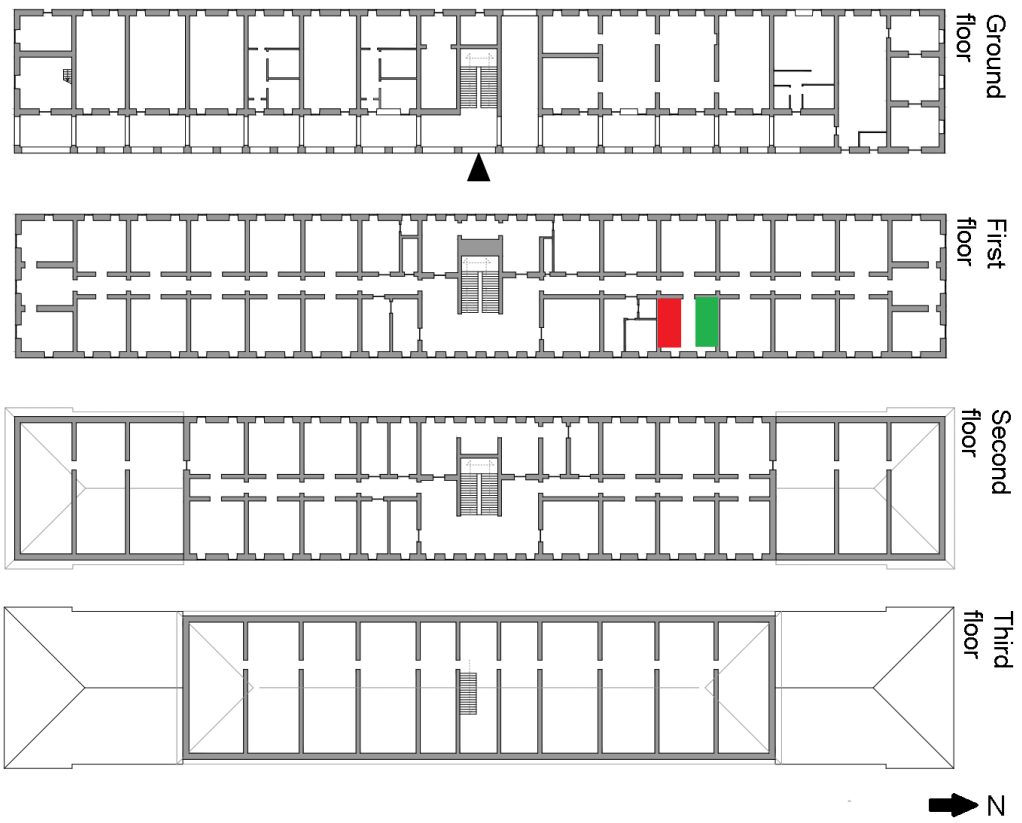

Figure 4.19: The image provides the floor's layouts of the West troop's barrack. In the first floor are marked the positions where one of the shear *FJ* test (in green) and the single and double flat jack test (in red) were performed. "Caserma Valfrè di Bronzo".

paths and that were not too far from the center of the sample.

Single *FJ* test

The single *FJ* test was the first performed in the structure. As introduced, this test and a double *FJ* test were performed in the same position (Fig. 4.20). The position of the test was chosen paying attention to the sample. In fact, the cuts location was decided considering the possibility of having a symmetrical sample for the double flat jack test. The single *FJ* was executed in the location coincident with the lower cut of the double *FJ* test. The operational phases and the recommendations followed were the same that had been used in the other single *FJ* tests performed. During the removal of the plasterwork, it was possible to appreciate the good quality of both bricks and mortar joints.

Before the slot creation, small holes were created in order to fix the supports for the *LVDTs* on the sample. These sensors were used only later in the double *FJ* test. Anyway, in order to not spend too much time to create these holes when the cuts were already realized, it was decided to perform them before the single *FJ* test. In addition, the choice of creating these holes in advance was taken also considering the fact that

when a cut is already created it can be more dangerous to drill because some displacements that can occur. The *LVDTs* supports were placed trying to optimize the sensors. To do this, the relative distance of the holes was decided in order to exploit the linear range of the sensors and their sensibility (Fig. 4.21).

The area created by the circular saw was $A_{slot} = 80800$ mm^2 and the geometrical ratio resulted to be $k_a = 0.959$. The flat jack constant was $k_m = 0.897$. This test was executed using standard manual equipment, therefore the measure bases were glued on the sample and the manual strain extensometer was used (Fig. 4.20). The stress found in this point of the structure was $\sigma_0 = -0.89$ MPa.

Double *FJ* test

A double *FJ* test was performed in order to evaluate the Young's modulus and the compressive strength. The second cut was realized with a distance of 50 cm from the first one. In this point of the structure, the masonry showed a good texture. The same precautions, operational phases and recommendations followed for the other double *FJ* tests were adopted.

The automatic acquisition system was utilized for this test. Before creating of the cuts, standards measure bases were glued on the sample. This choice was taken considering the importance of the information about the sample deformations that occur immediately after the creation of the cuts. Moreover, it is impossible to realize the slots with the electronic equipment mounted on the sample because there is the concrete possibility that the sensors could be damaged in the process.

After the creation of the second slot, its area was measured. It results possible to calculate the geometrical ratio ($k_a = 0.946$) using the area of the second slot ($A_{top} = 83050$ mm^2), the area of the slot created for the single flat jack test and the *FJs* area. *AE* sensors were fixed on the masonry near to the sample and the positions of these sensors were decided considering that the purpose was to monitor the zone in between the two *FJs*. Taking into account the heterogeneity of the media, it was also decided to avoid positions of the *AE* sensors in external zones with respect to the area included between the *FJs*. In this way, it is possible to avoid another heterogeneity represented by the cuts and by the *FJs*. Another important fact to keep in mind for attaching the acoustic emission sensors is that any kind of symmetry between them has to be avoided. Otherwise, if there is an acoustic emission source that is at a symmetrical distance from the sensors, it results impossible to localize the position of the source. In fact, supposing a symmetric sensors disposition and an emission source central to them, there are no differences between the arrival times so it is impossible to evaluate the distance of the sensor from the source and, for the same reason, to localize the source. Accordingly to what explained, semi-random positions of the sensor have to be searched.

For the sake of space, only two *LVDTs* were placed vertically and, as recommended, one was placed horizontally (Fig. 4.20). Distances between the holes (where the supports were fixed) were taken before mounting the supports and the *LVDTs*. These distances were then used as bases length for the determination of the strains.

It was possible to raise the number of acquisitions using this automatic system. In fact, it was decided to save a set of measures every second of the acquisition. The data obtained were then filtered with a Butterworth filter in *MATLAB*.

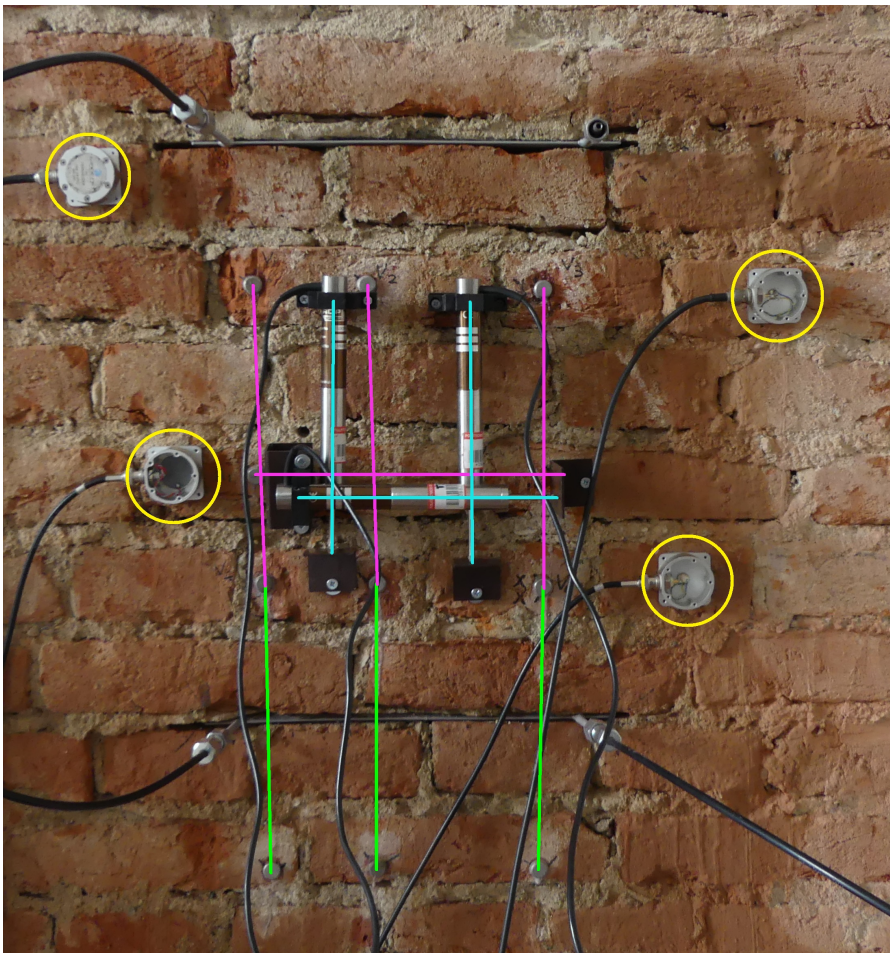

Figure 4.20: The image shows the positions of sensors and of measure bases in the double *FJ* test performed in the West building. In green are indicated the three measure bases used in the single *FJ* test, in pink the four measures bases (three vertical and one horizontal) used in the first steps of the deformability test, in light blue are highlighted the three *LVDTs* (two vertical and one horizontal) used during the second phase of the double *FJ* test and with yellow circles are marked the four *AE* sensors.

In this test, three load cycles were performed before rising the pressure and reaching the plastic regime of the media. In the first cycle the minimum stress applied to the masonry was $\sigma = -1.70$ MPa, in the second was -1.75 MPa and in the third cycle was -5.66 MPa. For this third cycle, the minimum stress analyzed to evaluate the Young's modulus was -1.75 MPa. The mean Young's modulus obtained was $E = 1846$ MPa with a standard deviation of 30 MPa (Fig 4.21). Of the three Young's moduli measured, the lowest correlation found was 0.997.

The methodology proposed in Sub-section 2.3.3 was followed in order to evaluate the compressive strength of the media. A value $f_c = 3.20$ MPa of compressive strength was found.

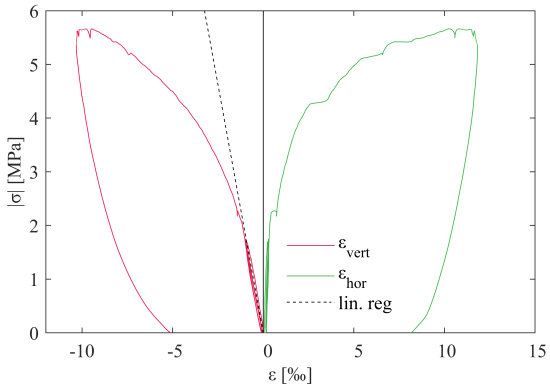

Figure 4.21: The image displays the results of the double *FJ* test performed in the West building.

Conclusions

The two standard tests were carried out in the West barrack. After the removal of the plasterwork of the wall, it was already possible to appreciate the good quality of the masonry. This quality was also confirmed by the double *FJ* test performed.

The single flat jack test pointed out the large vertical stress acting on this point of the structure. In fact, the vertical stress found was $\sigma_0 = -0.89$ MPa.

The double flat jack test proved the good quality of the material. The measured Young's modulus was $E = 1846$ MPa. Moreover, the measured compressive strength of $f_c = 3.20$ MPa is noticeably good.

The *AE* data were processed with a homemade software and the obtained results were compared with the results obtained with another software (presented in [189]). For the sake of brevity, the *AE* results of the double *FJ* test are not presented.

4.4.2 Shear *FJ* test - West building

One shear *FJ* test was conducted in the West building. As introduced, the test was performed in the same room where the two standard tests were carried out. After the removal of the plasterwork, it was possible to appreciate that the masonry was very similar to the one found in the previous tests. In fact, the texture, the quality of the resisting elements and of the joints were identical. The thickness of the wall was again 50 cm.

Methodology

As for the shear *FJ* tests performed in Boves, the test methodology followed was the one that is proposed at the beginning of this Chapter and the automatic acquisition system was used.

After the plasterwork removal, the first operation performed was to draw the position of the flat jacks on the wall. This position was chosen in order to have the possibility of gluing the four measuring points and to fix the four *LVDTs* as much as possible close to the sample center.

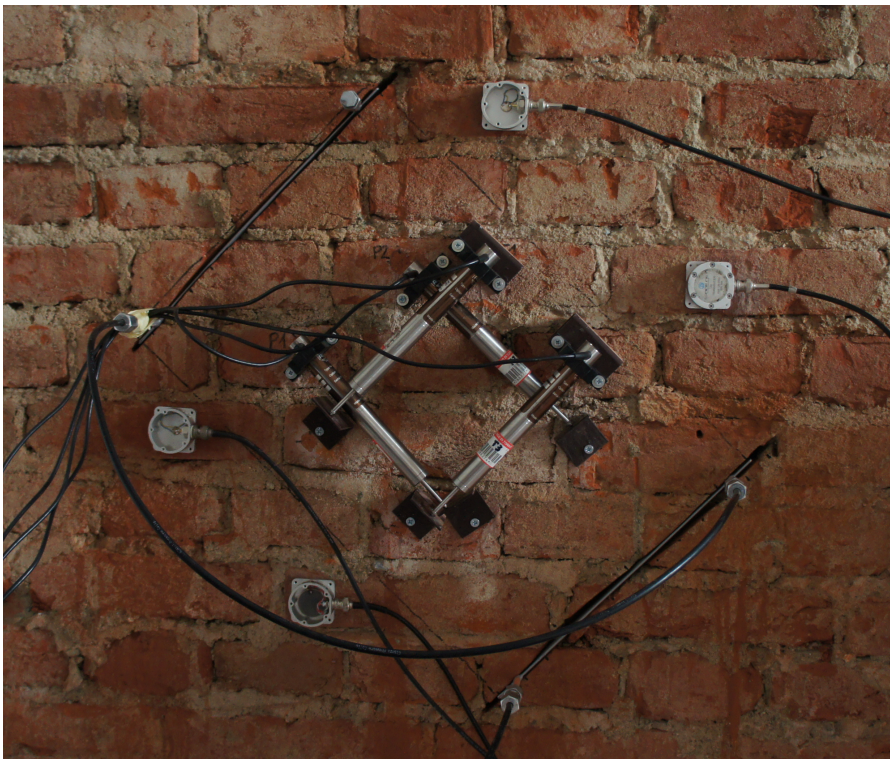

Figure 4.22: The picture shows the test set-up of the shear *FJ* test performed in the West building. In the image it is possible to notice the disposition of the *LVDTs* and of the *AE* sensors.

After this preliminary phase, it was possible to realize the cuts. The slots areas were then measured as introduced in the test method. The geometrical ratio found was $k_a = 0.919$ ($A_{top} = 84677$ mm^2 and $A_{low} = 84088$ mm^2). The mechanical constant for the flat jacks was taken from the certificates of the producer and it was $k_m = 0.897$.

At this point, the *FJs* were inserted into the cuts but were not yet connected to the hydraulic system. The *LVDTs* were then fixed on the sample and the *AE* sensors were glued on the wall following the same procedure used for the double flat jack test. Once that all the preliminary phases were completed, it was possible to connect the hydraulic system and to start the test.

Three loading cycles were performed in this test. The first two cycles were performed at low levels of stress ($\sigma = -0.42$ and -0.62 MPa) in order to have a better characterization of the elastic regime of the masonry. Then the pressure was risen up to a corresponding stress $\sigma = -5.78$ MPa. It was not possible to rise more the pressure because it was already higher than the full scale of the manual pressure gauge. Nevertheless, the plastic regime of the sample was already reached. After the reach of this peak value, the pressure was slowly decreased to a zero value.

The data acquired were then filtered with a Butterworth filter in *MATLAB*.

Results

The execution of the first shear *FJ* test of this experimental campaign allowed to understand different peculiarities of the masonry. As already noticed with the double flat jack test, it was possible to raise the pressure to high levels. In fact, the stress applied to the sample was almost three times the one applied in the test performed in the "ex Teatro dei Nobili" in Vercelli.

The results of the test are reported in Figure 4.24. As for the other tests described before, in the test here presented it was possible to attain both the elastic and the plastic regime of the sample (Fig. 4.23a and 4.23b). Both the inclined Young's modulus and the shear modulus were evaluated with linear regression of the linear elastic regime of the sample that was present in the three load cycles. More precisely the linear regressions were performed in the first two cycles and for an absolute stress inferior to 0.66 MPa of the third cycle.

The mean inclined Young's modulus found is $E^* = 3492$ MPa with a standard deviation of 5 MPa (the smallest correlation was 0.990). The mean shear modulus is $G = 1562$ MPa and it has a standard deviation of 60 MPa (the smallest correlation was 0.976).

The analysis of the sample stress status was performed with both the piecewise linear laws (Eq. 3.18 and 3.19) and the normalized principal stresses (Tab. A.2). The results of the piecewise linear laws are presented in Figures 4.23c and 4.23d. In Figures 4.23e and 4.23f the principal stresses evaluated with the normalized principal stresses are reported.

The *AE* results are presented in Figure 4.24. These results were obtained with a homemade software and they were compared with the results obtained using another software (presented in [189]). In particular, the evolution over time of the cumulative *AE* counts is plotted with the time evolution of the applied stress in Figure 4.24a and with the time evolution of the shear strain Figure 4.24b.

Discussion-Conclusion

It has to be underlined that this test was performed in a room where a high vertical stress was present ($\sigma = -0.89$ MPa). As discussed where the piecewise linear laws and the test method were presented, the place where the shear *FJ* test has to be performed should be decided in order to have a small vertical stress. In the present test and in the one performed in the Command building it was decided to understand if the vertical stress played the important role found in the parametric analysis of the previous Chapter. For this reason, a higher vertical stress was sought.

The first things that have to be discussed are the elastic characteristics of the materials. The shear modulus and the inclined Young's modulus are much larger than the expected ones. In fact, the Young's modulus found with the double *FJ* test is $E = 1849$ MPa. The ratio between the inclined Young's modulus and the Young's modulus is $E^*/E = 1.89$. Hypothesizing an isotropic behavior of the sample, as shown in the parametric analysis, the ratio should be close to one. Moreover, supposing a Poisson's ratio $\nu = 0.25$, taking the Young's modulus measured with the double *FJ* tests and using the constitutive equation $G = E/[2(1+\nu)]$, the shear modulus obtained is

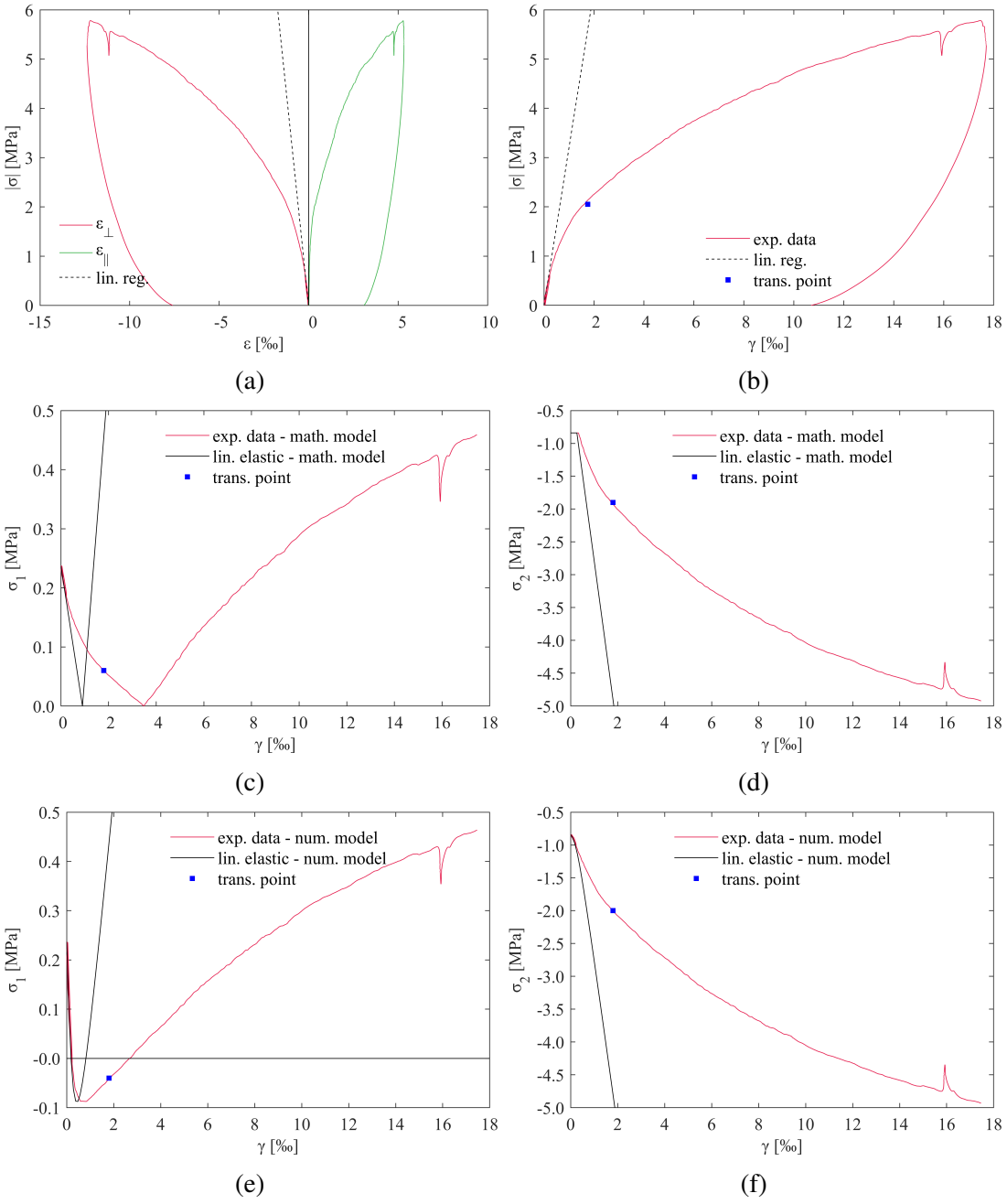

Figure 4.23: The image gives the results of the shear *FJ* test performed in the West building.

$G = 740$ MPa. The shear modulus measured with the presented test is $G = 1562$ MPa. Since the moduli measured are quite different from the expected ones, a deeper analysis is necessary and it is proposed in the following Chapter.

Following the method proposed in Section 4.1 it was possible to identify the transition between the elastic and plastic regimes. This consists in of an absolute applied stress $|\sigma| = 2.00$ MPa and a shear strain $\gamma = 1.80‰$.

It is possible to examine the principal stresses of the sample corresponding to the

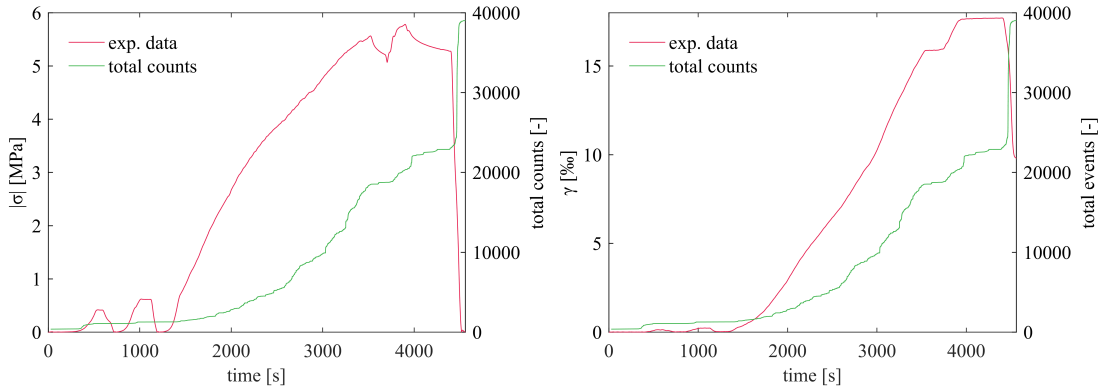

Figure 4.24: The image contains the *AE* results of the shear *FJ* test performed in the West building.

shear strain for which the sample starts to show its plastic regime. The piecewise linear laws give the largest principal stress $\sigma_1 = 0.06$ MPa and the smallest is $\sigma_2 = -1.80$ MPa (Fig. 4.23c and 4.23d). It is important to notice that the largest principal stress is interpolated with the first branch of the piecewise linear law. As highlighted previously this branch of the model does not reproduce perfectly the stresses numerically evaluated. The sample stress status evaluated for $\gamma = 1.80‰$ with the normalized principal stresses (Fig. 4.23e and 4.23f) is almost identical to the one evaluated with the numerical results. With this method, the largest principal stress is $\sigma_1 = -0.04$ MPa and the smallest is equal to the one evaluated before ($\sigma_2 = -1.80$ MPa). Therefore, it is possible to affirm that when the media plastic regime starts the sample is under a bi-axial compression.

Since a large vertical stress is acting on the tested wall, the realization of the cuts leads to high initial principal stresses inside of the sample (for $\sigma = 0.00$ MPa). In fact, the largest principal stress is $\sigma_1 = 0.24$ MPa and the smallest is $\sigma_2 = -0.84$ MPa. The tensile stress acting on the sample is noticeably high. In fact, a typical tensile strength for reinforced historical masonry should range in between $0.03 < f_t < 0.20$ MPa (Tab 2.3 and 2.4). In the present test, after the slots realization, it was possible to perform a few load cycles in which a linear elastic behavior of the sample was noticed. If at the slots realization one of the principal stresses reaches one of the media strengths, at the first *FJs* pressurization the sample would show a linear elastic behavior. So, it is possible to affirm that the cuts realization did not lead to the sample failure.

For what regards the *AE* results, it is interesting to notice that in the first $\simeq 1500$ s only few counts were recorded even if the first two load cycles and the beginning of the third one were already performed (Fig. 4.24a). These counts were recorded in the first $\simeq 500$ s. For this reason, these acoustic emissions were related to the *FJs* adjustment inside of the cuts. Since in these first 1500 s there are two load cycles and that the counts of the sample do not increase it is possible to affirm that there is a Kaiser-effect. Moreover, as highlighted in the introduction Chapter, the *AE* counts are a measure of the energy emitted during the events and, for this reason, they are a measure of the damaging process of the sample. Since in the first 1500 s there are a few counts, it is

possible to affirm that there is no damage of the sample. This fact underlines the linear elastic behavior of the sample under these load cycles.

The cumulative *AE* counts curve starts to increase after the first 1500 *s* indicating that the damaging process starts to take place. In Figure 4.24a it is possible to notice that to this time it corresponds an applied stress $|\sigma| \simeq 1.00$ MPa. Moreover, this stress corresponds to a first small deviation from the tangent fit of the experimental results (Fig. 4.23b) which underline the firsts plastic deformations.

A second and more marked increase of the cumulative *AE* counts curve is noticeable after the first 2200 s. This fact underlined the growth of the sample damaged zone. The same consideration can be observed in the experimental data (Fig. 4.23b) where, for stresses larger than 3.50 MPa (corresponding to $t > 2200$ s), the plastic deformations are remarkable.

Another evidence that it is important to highlight is the presence of a Felicity-Ratio $FR < 1$ that is noticeable between the stress peak at 3500 s ($|\sigma| = 5.60$ MPa) and the subsequent same level of stress.

The last important fact that it is noticeable is the high number of counts that were recorded in the last 200 s when the unloading phase started. This growth of the curve can be associated with the fact that at the peak load the sample is damaged in compression with an orientation of the principal stress. When the unloading phase takes place the principal stresses rotate back and the sample keeps damaging due to this rotation.

In conclusion, with the shear *FJ* test performed in the West building it was possible to measure a shear modulus $G = 1562$ MPa and it results possible to affirm that the failure of the sample occurred when the sample was under a bi-axial compression. The measured shear modulus is larger than the expected one and a detailed analysis of it is presented in the following Chapter.

4.4.3 Shear *FJ* test - Command building

This shear *FJ* test was carried out in another building of the "Caserma Valfrè di Bronzo", to be more specific in the Command building (Fig. 4.19). This building was reserved for the troops with the highest rank and there were also present offices.

In the same manner as the West building, it was decided to verify the role played in the test by a higher vertical stress. For this reason, the shear test was performed on the first floor. This position was decided in order to have an easier evaluation of the vertical stress starting from the one measured in the West building. In fact, it was not possible to perform another set of standard *FJ* tests and for this reason the vertical stress had to be evaluated starting from the one measured in the West building and considering that the typology of roof and floors was the same and that the spans of them were similar. The presented vertical stress calculated is $\sigma = -0.74$ MPa and the thickness of the wall is again 50 cm.

For what regards the Young's modulus and the compressive strength, these were assumed to be the same as the ones measured in the West building. This assumption was taken because the wall showed the same quality of both resisting elements and mortar joints, the two buildings were made in the same construction fields and the bricks were made using the same furnace.

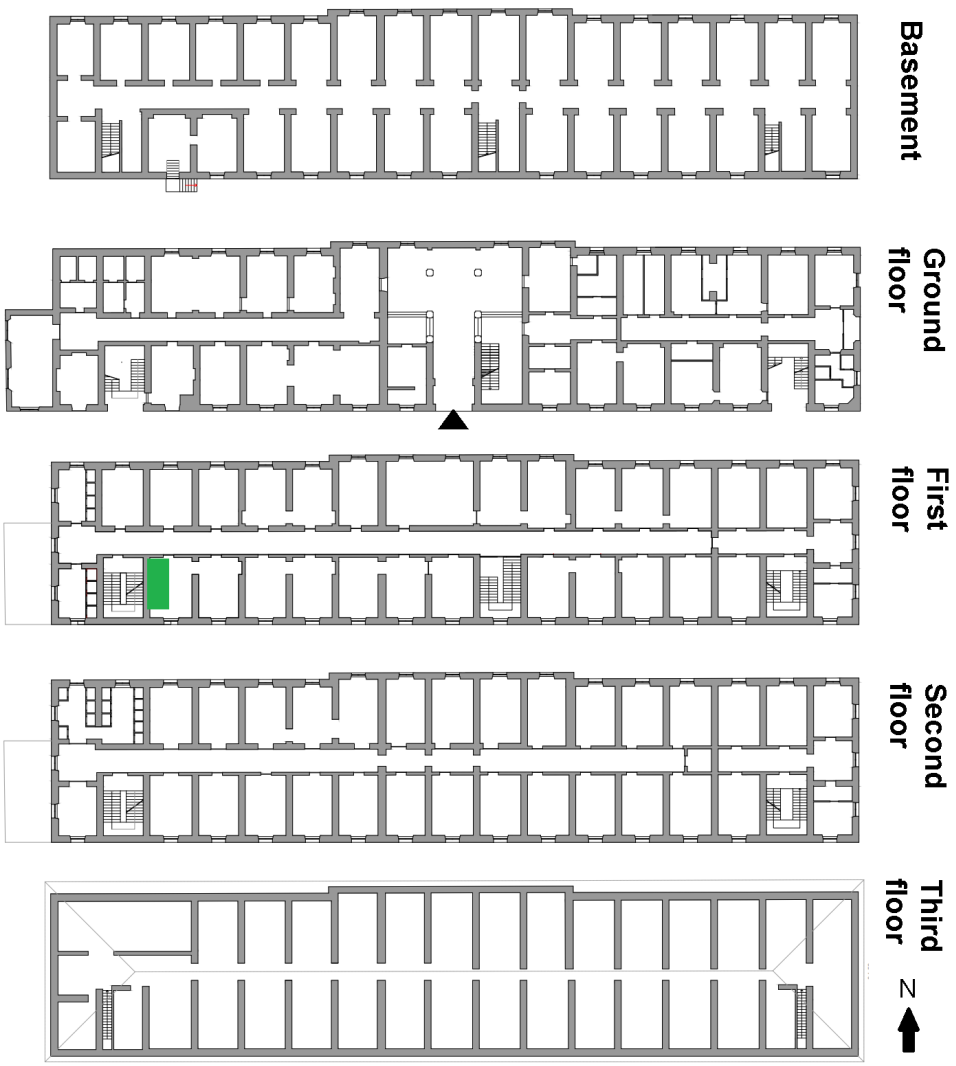

Figure 4.25: The image reports the floor's layouts of the Command building. In green is highlighted the position of the shear *FJ* test.

Methodology

The test was performed with the same methodology of the one carried out in the West building and according to the proposed methodology. In Figure 4.26 it is possible to notice that the automatic acquisition system and the *AE* technique were adopted.

After the removal of the plasterwork, the positions of the *FJs* were drawn on the bricks, the manual gauge points were glued and the holes for the supports of the *LVDTs* were created. After this first operation, the cuts were executed and their areas were measured ($A_{low} = 84990$ mm^2 $A_{top} = 84275$ mm^2). The resulting geometrical ratio is $k_a = 0.916$ and the mechanical coefficient of the *FJs* is $k_m = 0.896$. It was then possible to place the *FJs* inside of the slots, take the measure bases of the *LVDTs*, mount the supports for these sensors, place both the *LVDTs* and the *AE* sensors and, finally, close the hydraulic system.

Four cycles of load were carried out in this test. The maximum pressures applied to

the *FJs* in these cycles correspond to $\sigma = -0.20$, -0.37, -0.70 and -4.01 MPa.

The data acquired were then filtered with a Butterworth filter in *MATLAB*.

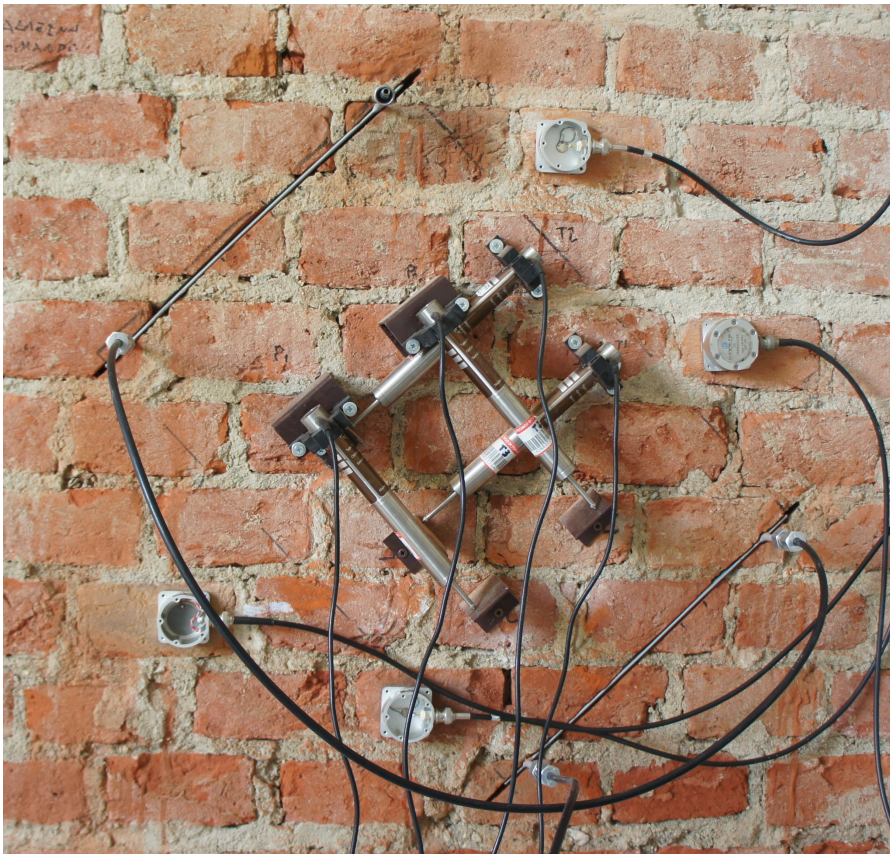

Figure 4.26: The image displays the set-up of the shear *FJ* test performed in the Command building.

Results

The experimental results of this test are summarized in Figure 4.27. As obtained for the tests described previously, in Figures 4.27a and 4.27b a linear and a non-linear regime of the sample were attained.

For what concerns the elastic characteristics, these were evaluated in the linear elastic regime of the media that coincided with the first three cycles and the initial part of the fourth cycle for an absolute stress up to $|\sigma| = 0.82$ MPa. The evaluation of these characteristics was performed with linear regressions of the obtained data in these four cycles.

The calculated mean shear modulus is $G = 715$ MPa with a standard deviation of 82 MPa (the smallest correlation was 0.979). The mean inclined Young's modulus is $E^* = 1620$ MPa and it has a standard deviation of 156 MPa (with the lowest correlation of 0.987).

The analysis of the stress status of the sample was performed with both the piecewise linear laws (Eq. 3.18 and 3.19) and the normalized principal stresses (Tab. A.2).

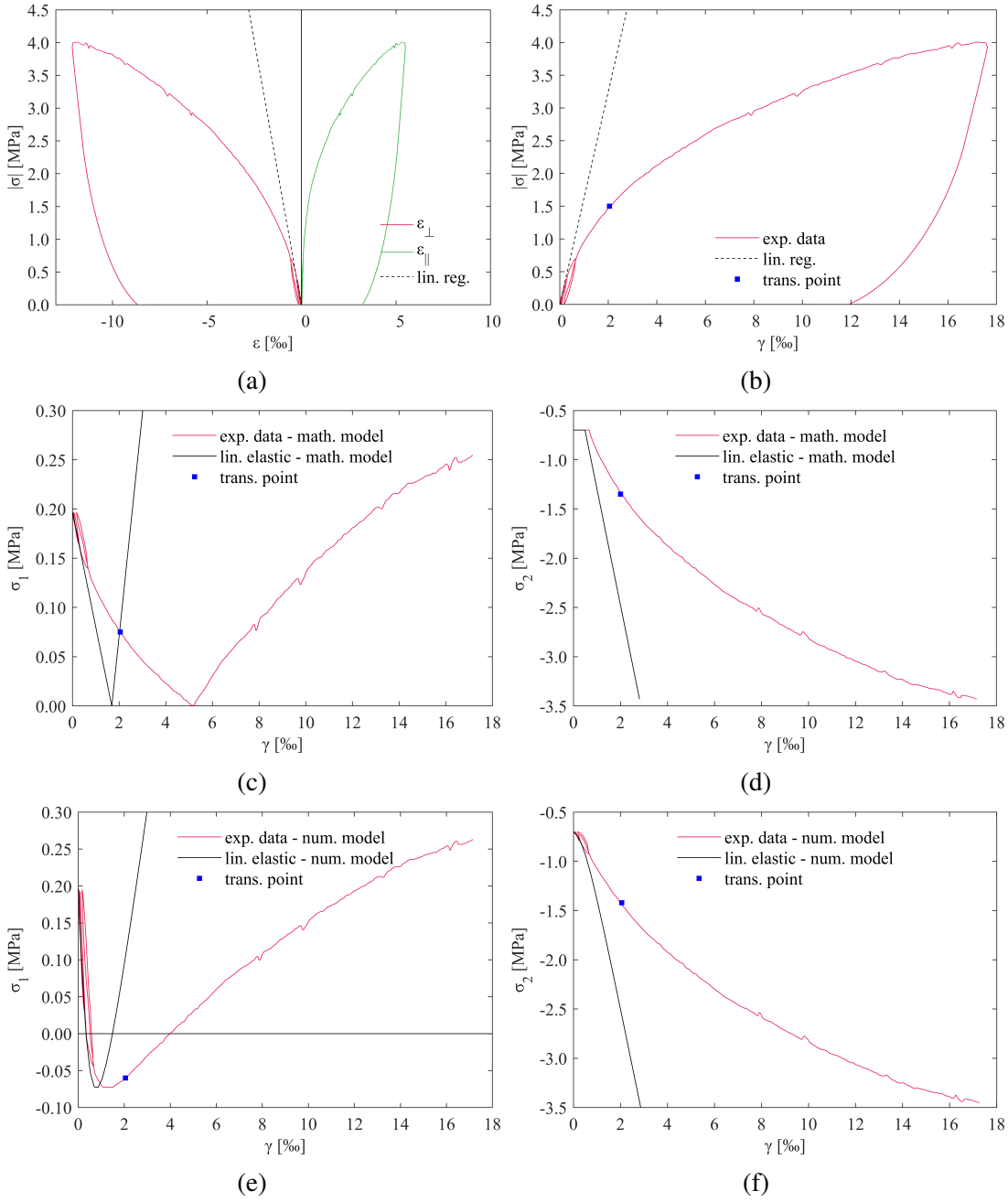

Figure 4.27: The plots summarize the results of the shear *FJ* test performed in the Command building.

More precisely, the results of the piecewise linear laws are reported in Figures 4.27c and 4.27d and the results obtained with the normalized principal stresses are reported in Figures 4.27e and 4.27f.

The *AE* data were processed with a homemade software and the results are plotted in Figure 4.24. These results were compared with the results obtained using another software (presented in [189]). In Figure 4.24a the evolution over time of the cumulative

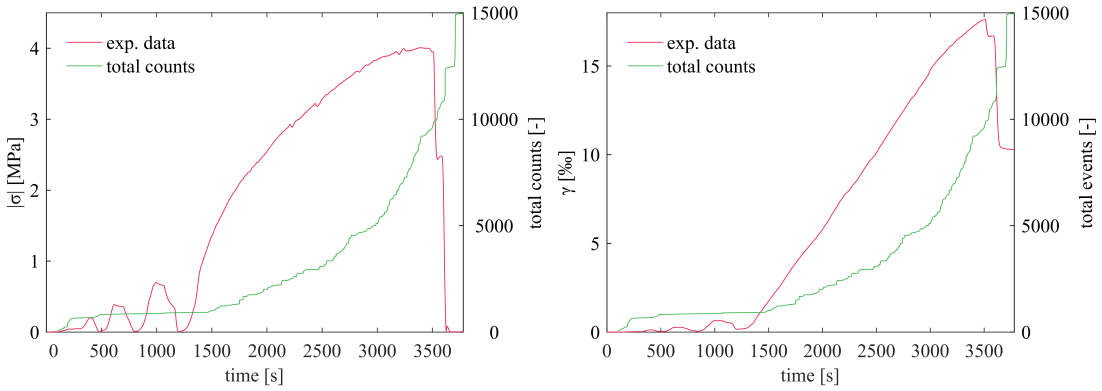

Figure 4.28: The image displays the *AE* results of the shear *FJ* test performed in the Command building.

AE counts is plotted with the time evolution of the applied stress. Similarly, the evolution over time of the cumulative *AE* counts with the time evolution of the shear strain are presented in Figure 4.24b.

Discussion-Conclusion

The test performed in this building allowed to underline some differences and some similarities with the test performed in the West building. First of all the disposition of the bricks in the two walls is different. In the Command building, the bricks were laid with their longer axes perpendicular to the wall plane (Fig. 4.26). In the West building, two different layers are present. In the first one, the disposition of the bricks coincides with the one of the Command building. In the other layer, the major axes of the bricks are parallel to the wall plane.

The vertical stress is also not equal to the one measured in the West building. Anyway, a high vertical stress ($\sigma_0 = -0.74$ MPa) was sought. In fact, in shear *FJ* tests performed in the "Caserma Valfrè di Bronzo" it was decided to verify the important role of the vertical stress already highlighted in the parametric analysis.

In this test, the measured elastic characteristics are closer to the expected ones compared to the test performed in the West building. The inclined Young's modulus is $E^* = 1620$ MPa. Supposing a perfect isotropic behavior of the media the inclined Young's modulus should be equal to the Young's modulus measured with the double *FJ* test ($E = 1846$ MPa). The two values are quite close and this fact highlights a good isotropic behavior of the media. Using the Young's modulus measured with the double *FJ* test, supposing a Poisson's ratio $\nu = 0.25$, hypothesizing a homogeneous linear elastic isotropic material and using the equation $G = E/[2(1+\nu)]$ it is possible to evaluate the shear modulus $G = 738$ MPa. The shear modulus measured with the proposed test is $G = 715$ MPa. Therefore, also the shear moduli are noticeably similar and this fact highlights an isotropic behavior of the media.

The transition point between the elastic and plastic regimes was defined as proposed in the test methodology (Sec, 4.1). This point corresponds to an absolute applied stress

$|\sigma| = 1.50$ MPa and a shear strain $\gamma = 2.00‰$.

It is possible to examine the sample stress status associated with the beginning of the plastic regime of the material. Entering in the results obtained with the piecewise linear laws (Fig. 4.27c and 4.27d) with $\gamma = 2.00‰$ it is possible to notice that the largest principal stress is $\sigma_1 = 0.08$ MPa and the smallest is $\sigma_2 = -1.35$ MPa. It has to be underlined that the largest principal stress is interpolated with the first branch of the piecewise linear law which does not reproduce perfectly the numerical results. This fact is noticeable comparing Figures 4.27c and 4.27e. By entering with $\gamma = 2.00‰$ in the results obtained with the normalized principal stresses (Fig. 4.27e) the largest principal stress results to be $\sigma_1 = -0.06$ MPa and the smallest principal stress is almost equal to the one evaluated with the piecewise linear laws ($\sigma_2 = -1.42$ MPa). It is possible to conclude that the beginning of the media plastic regime starts when the sample is under a bi-axial compressive stress. Moreover, it was supposed that the masonry has the compressive strength measured in the West building ($\sigma_c = 3.20$ MPa). With this, hypothesis and considering an isotropic failure criterion, it is possible observe that both the principal stresses at the beginning of the plastic regime are inferior to this strength. For this reason, the failure of the material is not clear.

As introduced in the numerical analyses of the test configuration, a high vertical stress induces high stresses in the sample at the cuts realization ($\sigma = 0.00$ MPa). In the present case, at the cut realization, the largest principal stress inside of the sample is $\sigma_1 = 0.20$ MPa and the smallest is $\sigma_2 = -0.70$ MPa. It is possible to observe that the tensile stress is noticeably high since the usual tensile strengths are inferior to 0.20 MPa. If one of the material strengths was reached at the cuts realization the sample would have shown plastic deformations at the first *FJs* pressurization. However, the load cycles performed at a low stress level highlighted a linear elastic range of the material which confirms the fact that the sample principal stresses did not reach the material strengths at the slots realization.

The *AE* technique gave some interesting results. In Figure 4.28a it is possible to observe that in the first 1500 s three complete cycles of load were performed and the fourth one was started. In these initial parts of the test the cumulative counts recorded were just a few and almost no *AE* activity was present in the first 300 s. In these first moments of the test, not even a single load cycle was performed but it was started to pump the hydraulic liquid inside of the *FJs*. For these reasons the counts recorded in these 300 s are associated with the adjustment of the *FJs* inside of the slots. Since in the first 1500 s three cycles were performed but almost no counts were recorded it is possible to affirm that a Kaiser effect is present.

After these first 1500 s the cumulative counts curve increases noticeably. In Figure 4.28a it is possible to notice that the applied absolute stress at 1500 s from the beginning of the test is $|\sigma| = 1.40$ MPa. As underlined in a previous paragraph, the plastic regime of the sample starts for an absolute applied stress $|\sigma| = 1.50$ MPa. It is possible to notice that the *AE* activity highlights the beginning of the sample damaging process for an applied stress that is almost the same as the one taken at the beginning of the sample plastic behavior. This should highlight that the method given for the identification of the elastic-plastic transition is correct.

After the first 2500 s the *AE* data show a second large increase of counts (Fig. 4.28).

At this point of the test the stress applied to the sample is $\sigma = -3.30$ MPa. In Figure 4.27b it is possible to observe that the plastic deformations are noticeable which confirms the progress of the damaging process.

Another interesting fact that is possible to observe from the *AE* results of Figure 4.28 is the last large increase of counts that is present in the last 400 s of the test. This increase coincides with the unloading phase of the sample and can be associated with the fact that at the maximum applied stress the sample is damaged in compression with a specific orientation of the principal stresses. When the unloading phase starts the principal stresses rotate back and they keep damaging the media.

In conclusion, the test performed in the Command building gave as results a shear modulus ($G = 715$ MPa) and an inclined Young's modulus ($E^* = 1620$ MPa) that are really close to the expected shear modulus and to the Young's modulus measured in the West building. This fact should highlight a good isotropic behavior of the sample. The beginning of the sample plastic regime becomes clear for an applied stress of about -1.50 MPa. The transition between the linear elastic regime and the plastic one is also underlined by a first increase of the *AE* activity. At the beginning of the plastic regime the sample is subjected to a bi-axial compression.

4.5 Summary

The experimental campaign carried out was not too extensive. This is due to the fact that it is not so simple to find a structure where the owner(s) allows to perform the test. Nevertheless, five shear *FJ* tests were performed. Moreover, in parallel to these five tests, other six standard *FJ* tests were carried out in order to have a better characterization of the materials mechanical behavior and of the vertical stresses acting on the samples. All the experiments were executed in three different structures from three different centuries: end of '700 for the "ex Teatro dei Nobili", end of '800 for the "Caserma Valfrè di Bronzo" and of the middle of the '900 for the "Caserma Giovanni Cerutti".

When the first test was performed (the one of the "ex Teatro dei Nobili") the whole methodology and the numerical parametric analysis were not yet completed. Moreover, in this test the manual acquisition system was used. Nevertheless, this test gave encouraging results and it helped to improve the test methodology.

The proposed methodology was applied and the automatic acquisition system was used for the other four shear *FJ* tests.

For what regards the evaluation of the tensile strength the best results were obtained in the "Caserma Giovanni Cerutti". The positions of the tests carried out in this building were chosen in order to have a low vertical stress acting on the samples. In these tests it was possible to appreciate that the plastic regime of the samples starts when a tensile principal stress is present and, at the same time, the compression stress is much smaller than the media compressive strength. For this reason, it is possible to affirm that the failure of the sample is due to the fact that the largest principal stress reaches the tensile strength of the material.

In the two shear *FJ* tests performed in the "Caserma Valfrè di Bronzo" a larger vertical stress acting on the samples was searched in order to verify its important role

that was already found in the numerical models. This large vertical stress leads to high initial principal stresses inside of the samples. However, the failure of the samples did not occur at this first stage. In particular, the plastic regimes of the media were attained for a bi-axial compression of the sample when both the principal stresses were inferior to the compressive strength of the media. This fact is studied in the next Chapter.

For what regards the elastic characteristics, in three tests the inclined Young's moduli are close to the Young's moduli measured with the double *FJ* tests as well as the measured shear moduli are close to the shear moduli evaluated with the constitutive equation $G = E/[2(1+\nu)]$, supposing a Poisson's ration $\nu = 0.25$ and using the Young's modulus measured with the double *FJ* tests. For the shear *FJ* tests performed in the West building and in Position 1 of the "Caserma Giovanni Cerutti" the discrepancy between the measured characteristics and the expected ones is larger. This fact is further investigated in the following Chapter by means of micro-models and linear analyses.

With the aim of analyzing the obtained data, non-linear numerical analyses were performed using macro-models. These analyses are presented in the following Chapter. More precisely, these analyses aim at understanding the failure mechanism.

Chapter 5

FEM analyses

In this Chapter, the non-linear *FEM* numerical analyses of the shear *FJ* tests are presented as well as the linear analyses performed with micro-models. All of these analyses were performed using the commercial software *DIANA* [65] starting from the results obtained during the experimental campaign.

The linear micro-models were created with the purpose of understanding the discrepancies between the elastic characteristics measured with the shear *FJ* tests and the ones expected from the results of the double *FJ* tests.

The *FEM* non-linear analyses were performed in order to understand the behavior of the sample under the proposed experimental set-up. For this reason, the objective of these analyses was the reproduction of the results obtained with the five experimental shear *FJ* tests using non-linear models and the data obtained with the standard *FJ* tests.

These non-linear analyses were carried out using the approach adopted for the numerical models of the parametric analysis (Sub-section 3.2.2). The media was considered isotropic and homogeneous. The thickness of the wall was the only geometrical parameter that was adjusted for each model adapting it for each experiment performed. The modeled walls had dimensions of 4.0×3.0 m and the models used were similar to the one adopted in the analyses of the test configuration of Chapter 3. For these non-linear analyses, the elements utilized were linear tetrahedrons named TE12L [65] (Fig. 5.1). The elements sizes were adapted for each geometrical part of the wall as for the models used for the linear analyses. The smallest elements have a size of 15 mm and they were used for the slots. This size was chosen in order to avoid high aspect ratios. The seeding sizes were then increased from the center of the sample (30 mm) to the edges of the wall (250 mm).

For these non-linear analyses the constitutive model used is called Total Strain Rotating Crack Model [65]. In this constitutive model a single stress-strain relationship is used to describe the material behavior both in compression and in tension [65], assuming isotropy. The definition of both tensile and compressive non-linear behaviors can be performed using predefined functions or customized subroutines. In the analyses performed the non-linear behavior in tension of the masonry was modeled as tension softening with an exponential softening curve (Fig. 2.20a). The compression behavior of the masonry was modeled with a parabolic function (Fig. 2.20b). For the models created, the crack bandwidths were automatically evaluated as described by Rots [159]. With this method, the bandwidths were proportional to the volumes of the elements

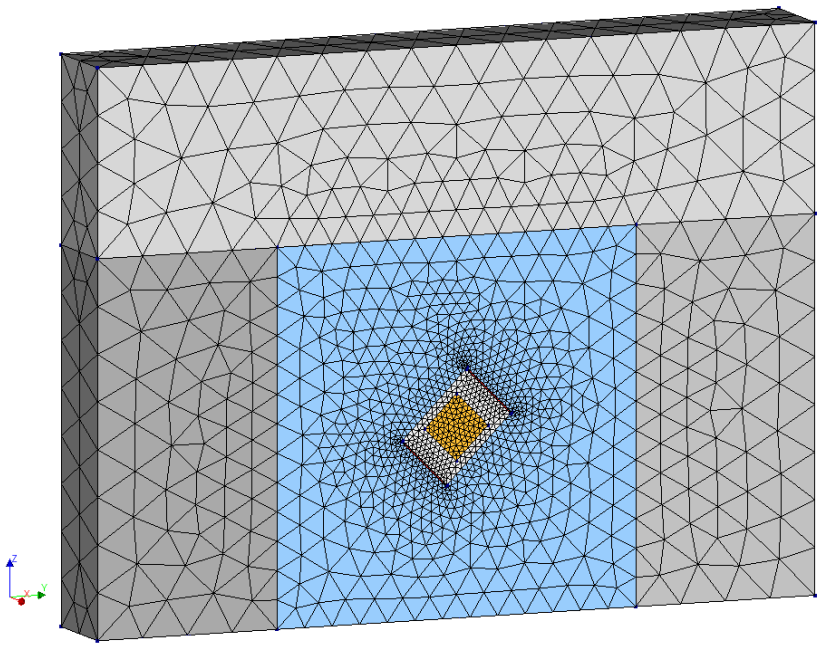

Figure 5.1: The image displays the mesh of a model used in a non-linear *FEM* analysis.

used (they would be proportional to the areas for 2D models).

In the performed analyses the unloading phases were not modeled because they were not considered interesting for the purposes of the work.

These non-linear analyses were performed with the phases and the boundary conditions described in Chapter 3. A Newton-Raphson iterative method with a maximum number of iterations of 300 was used. It was established to use the arc-length control and, for the convergence criterion, it was decided to monitor the energy norm ratio and fix the tolerance to 0.001. The number of elements utilized was ranging between 56000 and 71000 depending on the thicknesses of the wall modeled.

Some of the results obtained in the present Chapter will be published in a manuscript that is currently under preparation [190].

5.1 "ex Teatro dei Nobili"

The model used to analyze the results obtained in the "ex Teatro dei Nobili" had a thickness $t = 0.70$ m. The mechanical characteristics measured with the standard tests and the shear *FJ* test are summarized in Table 5.1.

The Young's modulus and the vertical stress used in the analyses were the ones measured with the standard *FJ* tests performed near to the position where the shear *FJ* test was executed (Tab. 5.1). The Poisson's ratio set was $\nu = 0.20$. For the firsts trial analyses, the compressive strength assumed was the one obtained in the double *FJ* test performed nearby. The first trial tensile strength was estimated using the Italian code [86] ($f_t = 0.15$ MPa). Similarly, the first fracture energies were estimated following what said in Sub-section 2.8.2.

The numerical result that fitted better the experimental results was obtained with the

Table 5.1: The table summarizes the mechanical characteristics obtained in Position 2 in the "ex teatro dei Nobili".

Characteristic	Symbol	MPa
Vertical present stress	σ_0	-0.25
Young's modulus	E	905
Compressive strength	f_c	1.42
Inclined Young's modulus	E^*	949
Shear modulus	G	418

Table 5.2: The table shows the mechanical properties used in the *FEM* non-linear analyses that fitted the experimental results of the shear *FJ* test performed in the "ex teatro dei Nobili".

Characteristic	Symbol	Value	Unit
Young's modulus	E	905	MPa
Tensile strength	f_t	0.15	MPa
Tensile fracture energy	G_{ft}	15	N/m
Compressive strength	f_c	0.60	MPa
Compressive fracture energy	G_{fc}	300	N/m

mechanical characteristics reported in Table 5.2.

A sensitivity analysis was performed to understand the influence of each single parameter that could affect the non-linear behavior of the media. For this reason, both strengths (compressive and tensile) and both fracture energies (compression and tension) were varied. The results of this sensitivity analysis are reported in Figure 5.2.

From the numerical results, the mechanical characteristics adopted and the sensitivity analysis it is possible to draw some first conclusions. The best fit obtained does not cover the whole experimental curve. However, the part reproduced by the numerical model properly replicates the results. This best fit was obtained with the Young's modulus that coincides with the one measured with the double *FJ* test (that was anyway close to the inclined Young's modulus). However, the compressive strength that leads to this best fit is quite different from the measured one.

The sensitivity analysis underlines the fact that changes in the results are mainly dominated by variations of the compressive strength and of the compressive fracture energy (Fig. 5.2c and 5.2d). In opposition, changes of the $\pm 30\%$ of the tensile strength lead to small and almost inappreciable variations of the numerical results (Fig. 5.2a) as well as changes of the tensile fracture energy (Fig. 5.2b).

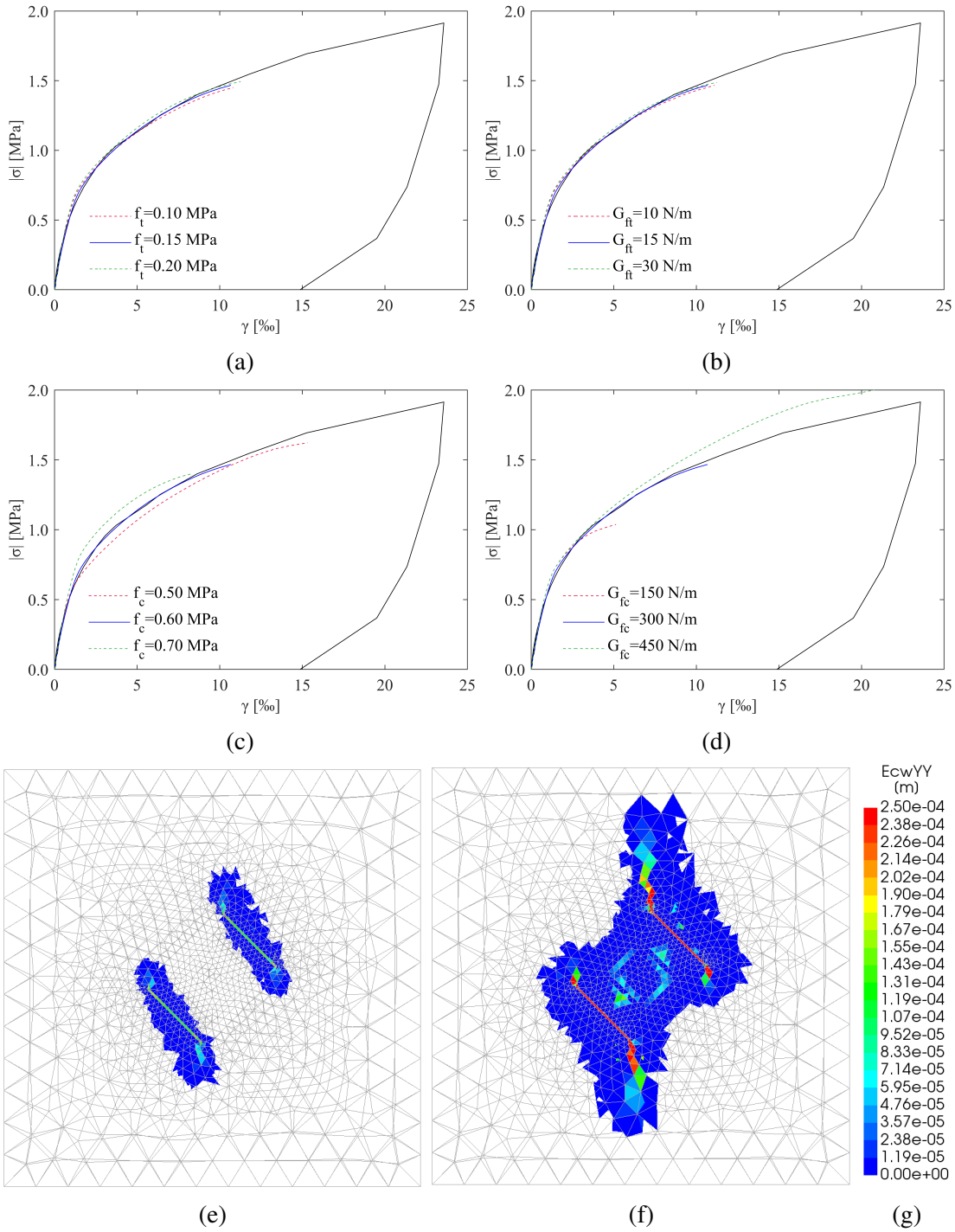

Figure 5.2: The images 5.2a, 5.2b, 5.2c and 5.2d show the numerical results of the sensitivity analysis carried out for the shear *FJ* test performed in the "ex teatro dei Nobili". The best fit is reproduced with the blue continuous line. The images 5.2e and 5.2f show the crack widths in the horizontal direction parallel to the wall plane of the best fit obtained for the shear *FJ* test performed in "ex teatro dei Nobili". In particular, 5.2e are the results obtained at the transition point ($\sigma = 0.65$ MPa), the results for the last point of convergence are plotted in 5.2f and in 5.2g the legend is presented.

Figures 5.2e and 5.2f show two contour plots of the crack widths as well as their legend. These were obtained with the model that fitted better the experimental results. Figure 5.2e refers to the transition point and Figure 5.2f to the last load step when convergence was found. It is possible to observe in both images that it is present damage at the corners of the slots. In fact, in these points an intensification of stresses is present. In Figure 5.2f it is possible to notice that the center of the sample is also damaged.

5.2 "Caserma Giovanni Cerutti"

In this Section the non-linear *FEM* results of the analyses performed to study the shear *FJ* tests carried out in the "Caserma Giovanni Cerutti" are presented. The tested walls have in common the thickness ($t = 46$ cm) and the vertical stress ($\sigma_0 = -0.36$ MPa).

5.2.1 Position 1

The mechanical characteristics measured with the standard and the shear *FJ* tests are summarized in Table 5.3. These characteristics measured with the standard *FJ* tests were obtained in a wall close to Position 1 where one shear *FJ* test was carried out.

Table 5.3: The table summarizes the mechanical characteristics measured in "Caserma Giovanni Cerutti" Position 1.

Characteristic	Symbol	MPa
Vertical present stress	σ_0	-0.36
Young's modulus	E	1739
Compressive strength	f_c	2.20
Tensile strength	f_t	0.13
Inclined Young's modulus	E^*	3777
Shear modulus	G	1217

In the first analyses, the Young's modulus used for the numerical models was the one obtained in the double *FJ* test performed on a wall near to the position of the experimental test. Due to a not perfect matching with the experimental results, it was decided to use the inclined Young's modulus (E^*) measured with the shear *FJ* tests (Tab. 5.3). The modeled vertical stress was evaluated starting from the one measured with the single *FJ* test. The Poisson's ratio adopted was $\nu = 0.20$, the first trial compressive strength was the one obtained in the double *FJ* test and the first trial tensile strength was the one evaluated with the shear *FJ* test. The trial fracture energies were also estimated as proposed in Sub-section 2.8.2.

The numerical curve that fitted better the experimental results was obtained with the mechanical characteristics reported in Table 5.4.

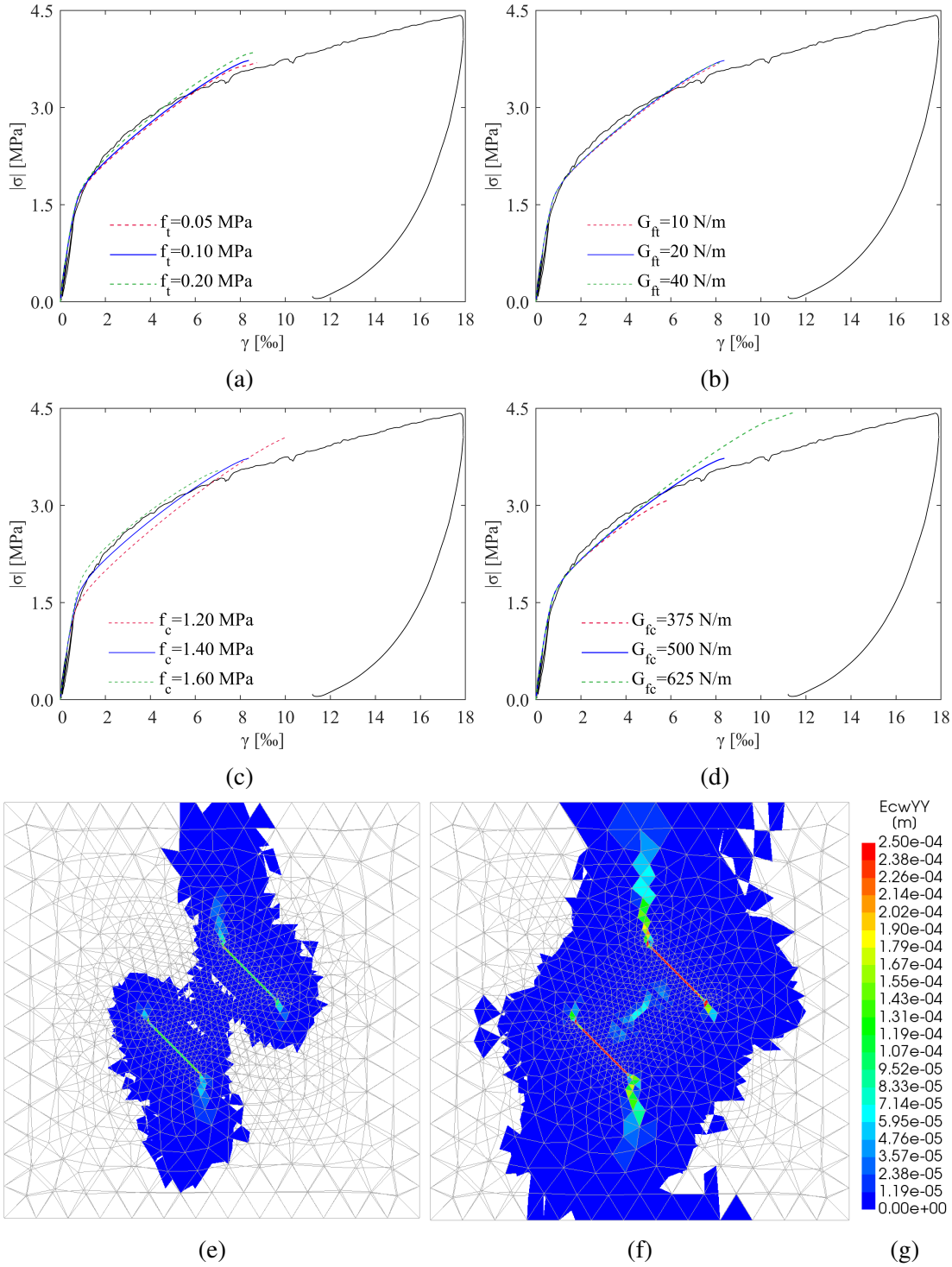

Figure 5.3: The images 5.3a, 5.3b, 5.3c and 5.3d report the numerical results of the sensitivity analysis carried out for the shear *FJ* test performed in "Caserma Giovanni Cerutti" Position 1. The best fit is reproduced with the blue continuous line. The images 5.3e and 5.3f show the crack widths in the horizontal direction parallel to the wall plane of the best fit. In particular, in 5.3e are the results obtained at the transition point ($\sigma = 2.00$ MPa), the results for the last point of convergence are plotted in 5.3f and in 5.3g the legend is presented.

Table 5.4: The table summarizes the mechanical properties used in the *FEM* non-linear analyses that best fitted the experimental results of the shear *FJ* test performed in "Caserma Giovanni Cerutti" Position 1.

Characteristic	Symbol	Value	Unit
Young's modulus	E	3780	MPa
Tensile strength	f_t	0.15	MPa
Tensile fracture energy	G_{ft}	20	N/m
Compressive strength	f_c	1.60	MPa
Compressive fracture energy	G_{fc}	625	N/m

The results obtained in the non-linear analyses lead to some conclusions. The best fit obtained does not cover the whole experimental curve. However, where both curves exist, the numerical curve fits really well the experimental one (Fig. 5.3). The curve that best replicates the experimental results was obtained with the inclined Young's modulus (Tab. 5.6). For these tests, the two measured Young's moduli were really different one from the other. This discrepancy is analyzed in the following Section 5.4. The compressive strength that leads to the best fit is different from the measured one but this difference is less marked in comparison to what was found for other analyses.

The sensitivity analysis underlined that changes in the compressive strength are the only ones that significantly influence the numerical results (Fig. 5.3c). The other characteristic that modifies appreciably the results is the compressive fracture energy (Fig. 5.3d). This influence is more appreciable only for high strain. For what regards the tensile strength, variations of $\pm 50\%$ of this characteristic produces small differences in the results (Fig. 5.3a). Moreover, variations of the tensile fracture energy do not lead to significant changes in the numerical results (Fig. 5.3b). These results are in contrast to what was expected.

Some other numerical results are presented in Figures 5.3e and 5.3f. This image displays two contour plots of the crack widths (as well as their legend) obtained with the model that fitted better the experimental results. Figure 5.3e refers to the transition point and Figure 5.3f to the last load step when convergence was found. In accordance with the results obtained in the "ex teatro dei Nobili", the corners of the cuts show high damages. In Figure 5.3f it is possible to observe that the center of the sample is also damaged. In particular, it is important to notice an opening of a crack in a line in the center of the sample that crosses it in its longer axis of symmetry. This should highlight the tensile failure of the sample that was sought.

5.2.2 Position 2

The mechanical characteristics measured with the standard and the shear *FJ* tests are summarized in Table 5.5. The mechanical characteristics measured with the standard *FJ* tests were the ones measured in Position 1.

The Young's modulus adopted was the one obtained in the double *FJ* test performed in Position 1. The modeled vertical stress was evaluated starting from the one measured with the single *FJ* test carried out in Position 1. Similarly to what was done in the

Table 5.5: The table summarizes the mechanical characteristics obtained in "Caserma Giovanni Cerutti" Position 2. ([1]) measured in Position 1, ([2]) estimated from the value measured in Position 1.

Characteristic	Symbol	MPa
Vertical present stress [2]	σ_0	-0.36
Young's modulus [1]	E	1739
Compressive strength [1]	f_c	2.20
Tensile strength	f_t	0.09
Inclined Young's modulus	E^*	2312
Shear modulus	G	971

previous analyses, the Poisson's ratio adopted was $\nu = 0.20$. For the first trial analyses, the compressive strength assumed was the one obtained in the double *FJ* test and the tensile strength was estimated with the shear *FJ* test. As already done before, the initial fracture energies were estimated following what said in Sub-section 2.8.2.

The numerical result that better reproduces the experimental results was obtained with the mechanical characteristics summarized in Table 5.6.

Table 5.6: The table summarizes the mechanical properties used in the *FEM* non-linear analyses that gave the best fit of the experimental results of the shear *FJ* test performed in "Caserma Giovanni Cerutti" Position 2.

Characteristic	Symbol	Value	Unit
Young's modulus	E	1739	MPa
Tensile strength	f_t	0.15	MPa
Tensile fracture energy	G_{ft}	20	N/m
Compressive strength	f_c	1.85	MPa
Compressive fracture energy	G_{fc}	2000	N/m

Thanks to the analyses performed and to the data reported above, it results possible to draw some conclusions. The numerical curve that best fitted the experimental curve covers the whole experimental curve. As for the other models, the unloading phase was not modeled. This numerical result reproduces quite well the experimental one. This best fit was obtained with the Young's modulus that is almost coincident with the one measured with the double *FJ* test. It has to be underlined that the difference between the Young's modulus and the inclined Young's modulus was not so large for this test.

The sensitivity analysis underlines that the compressive strength is the parameter that influences more the results (Fig. 5.4c). It has to be noticed that the compressive strength used in the best fit curve is quite close to the one measured with the double *FJ* test. The sensitivity analysis (Fig. 5.4) highlights that the two fracture energies partially vary the numerical curves (Fig. 5.4d and 5.4b). Similarly, tensile strength variations of $\pm 25\%$ slightly change the numerical results (Fig. 5.4a). This outcome is again in contrast to what was supposed.

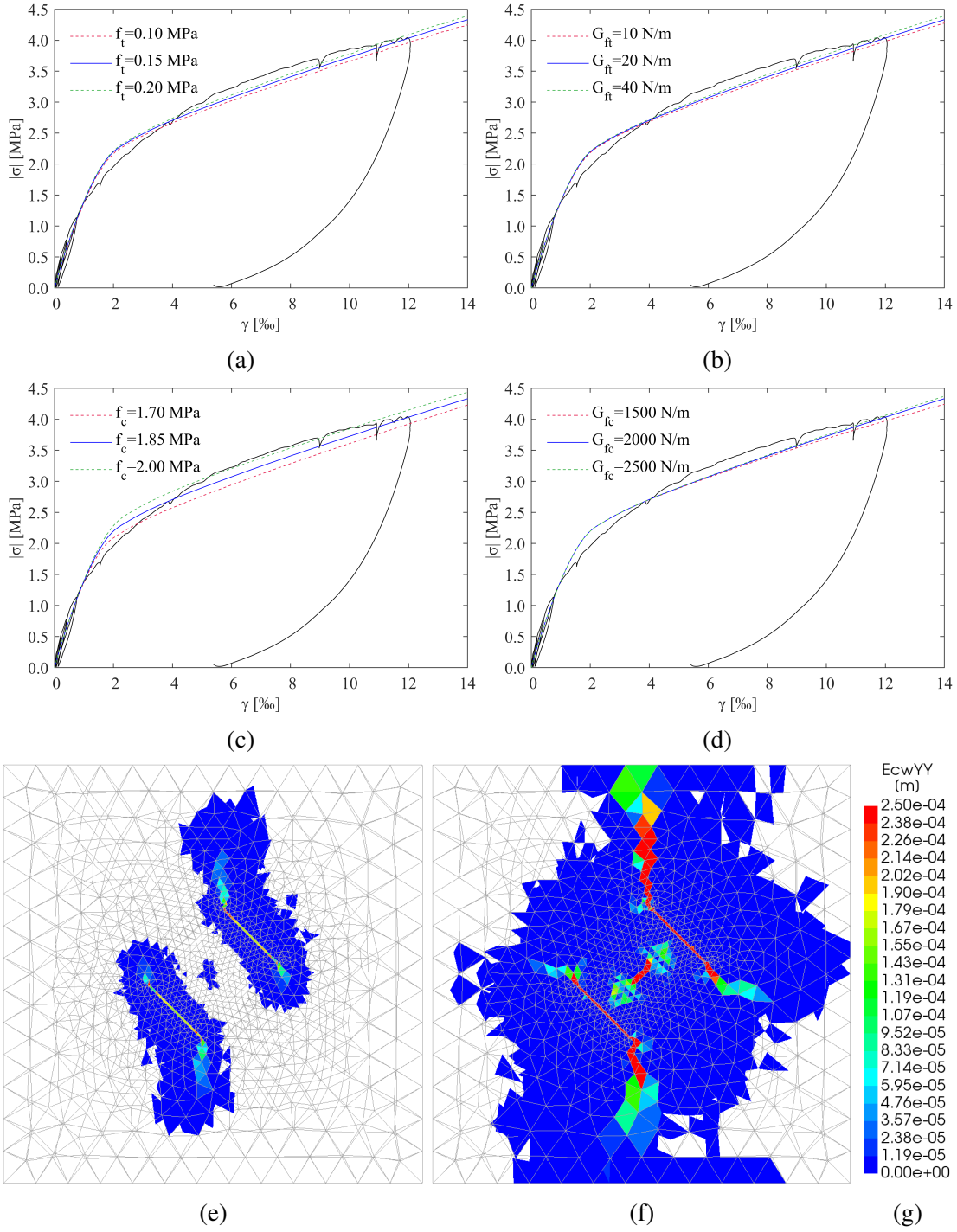

Figure 5.4: The Images 5.4a, 5.4b, 5.4c and 5.4d provide the sensitivity analysis carried out for the shear *FJ* test performed in "Caserma Giovanni Cerutti" Position 2. The best fit is reproduced with the blue continuous line. The images 5.4e and 5.4f show the crack widths in the horizontal direction parallel to the wall plane of the best fit. In particular, 5.4e are the results obtained at the transition point ($\sigma = 1.70$ MPa), the results for the last point of convergence are plotted in 5.4f and in 5.4g the legend is presented.

Two plots, obtained from the numerical model that best fitted the experimental results, are presented in Figures 5.4e and 5.4f. In this image, two contour plots of the crack widths, as well as their legend, are presented. Figure 5.4e refers to the transition point and Figure 5.4f to the last load step when convergence was found. In agreement with what it was already found, the corners of the cuts show high damages due to the stress intensification. In Figure 5.4f it is possible to observe that the center of the sample is also damaged. It is very interesting to observe a crack in a line which crosses the sample center in its longer axis of symmetry. This crack opening should underline the tensile failure of the sample that was sought.

5.3 "Caserma Valfrè di Bronzo"

In this Section, the non-linear *FEM* results of the analyses performed to study the two shear *FJ* tests carried out in the "Caserma Valfrè di Bronzo" are presented.

5.3.1 West building

The model used to analyze the results obtained in the West building had a thickness $t = 0.50$ m. The mechanical characteristics measured with the standard tests and the shear *FJ* test are summarized in Table 5.7.

Table 5.7: The table summarizes the mechanical characteristics obtained in the West building.

Characteristic	Symbol	MPa
Vertical present stress	σ_0	-0.89
Young's modulus	E	1846
Compressive strength	f_c	3.20
Inclined Young's modulus	E^*	3492
Shear modulus	G	1562

In the first numerical analyses, the Young's modulus utilized was the one obtained in the double *FJ* test performed nearby the shear *FJ* test. Since in the linear range the numerical results were not matching the experimental ones, it was decided to use a value of the Young's modulus close to the inclined Young's modulus (E^*) measured with the shear *FJ* test (Tab. 5.7). The modeled vertical stress was the one measured with the single *FJ* test. The Poisson's ratio utilized was $\nu = 0.20$ and, in the first trial analysis, the assumed compressive strength was the one obtained in the double *FJ* test. The firsts trial tensile strength was estimated using the Italian code [86] ($f_t = 0.15$ MPa). As for the other non-linear analyses the initial fracture energies were estimated following Sub-section 2.8.2.

The numerical result that better fitted the experimental curve was obtained with the mechanical characteristics reported in Table 5.8.

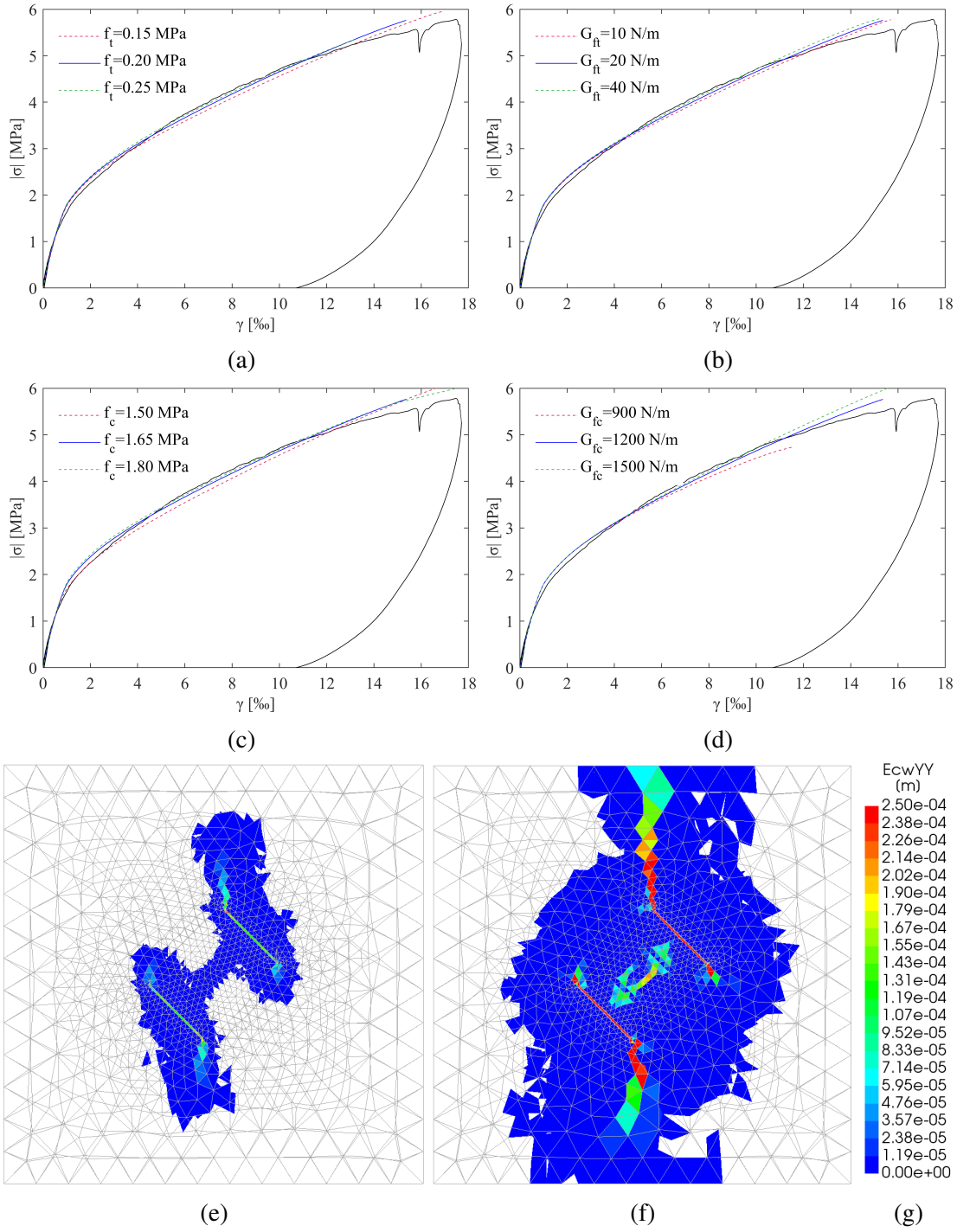

Figure 5.5: The images 5.5a, 5.5b, 5.5c and 5.5d give the numerical results of the sensitivity analysis carried out for the shear *FJ* test performed in the West building. The best fit is reproduced with the blue continuous line. The images 5.5e and 5.5f show the crack widths in the horizontal direction parallel to the wall plane of the best fit. In particular, the results obtained at the transition point ($\sigma = 2.00$ MPa) are presented in 5.5e, the results for the last point of convergence are plotted in 5.5f and in 5.5g the legend is presented.

A sensitivity analysis was also carried out with the aim of understanding the influence of each parameter. To perform this analysis both strengths (compressive and tensile) and both fracture energies (compressive and tensile) were varied. The result of this sensitivity analysis are reported in Figure 5.5.

Some conclusions can be drawn from the results reported in Figure 5.5. The best fit curve obtained covers the experimental curve. The numerical curve reproduces quite well the experimental one. This best fit was obtained with the Young's modulus that almost coincides with the inclined Young's modulus. This fact should highlight an anisotropy of the media. Anyway, a deeper analysis to understand this issue is developed in Section 5.4. The Compressive strength that leads to the best fit is substantially different from the measured one.

Table 5.8: The table reports the mechanical properties used in the *FEM* non-linear analyses that gave the best fit of the experimental results of the shear *FJ* test performed in West building.

Characteristic	Symbol	Value	Unit
Young's modulus	E	3490	MPa
Tensile strength	f_t	0.20	MPa
Tensile fracture energy	G_{ft}	20	N/m
Compressive strength	f_c	1.65	MPa
Compressive fracture energy	G_{fc}	1200	N/m

The sensitivity analysis underlines that variations of the compressive strength do not cause large changes (Fig. 5.5c) in the results as well as for the tensile fracture energy (Fig. 5.5b). The compressive fracture energy (Fig. 5.5d) modifies the results only for high strain. For what regards the tensile strength (Fig. 5.5a), it was varied of $\pm 30\%$ but a large influence is not obtained in contrast to what was expected.

Two contour plots are presented in Figures 5.5e and 5.5f. These were obtained from the numerical model that best fitted the experimental results. These plots display the crack widths as well as their legend. In particular, Figure 5.5e refers to the transition point and Figure 5.5f to the last load step when convergence was found. Accordingly with the results shown before, damages are found in the slots corners were the stress intensification is present. In both Figures 5.5e and 5.5f, it is possible to observe that the center of the sample is damaged. It is possible to see that the damage is aligned and almost coincided with the longer axis of the sample. This large crack widths should underline the tensile failure of the sample.

5.3.2 Command building

The model used to analyze the results obtained in the Command building had a thickness $t = 0.50$ m. The mechanical characteristics measured with the standard and the shear *FJ* tests are summarized in Table 5.9.

As for the numerical analyses of the West building, the Young's modulus used in the first trial analyses was the one obtained in the double *FJ* test performed in the

Table 5.9: The table summarizes the mechanical characteristics obtained in the Command building. $(^1)$ measured in the West building, $(^2)$ estimated from the value measured in the West building.

Characteristic	Symbol	MPa
Vertical present stress [2]	σ_0	-0.74
Young's modulus [1]	E	1846
Compressive strength [1]	f_c	3.20
Inclined Young's modulus	E^*	1620
Shear modulus	G	715

West building. Since the numerical results in the linear range were not matching the experimental ones, it was decided to use the value of the inclined Young's modulus (E^*) measured with the shear *FJ* test (Tab. 5.9). The modeled vertical stress was evaluated starting from the vertical stress measured in the West building (Tab. 5.9). As for the other non-linear analyses, the adopted Poisson's ratio was $\nu = 0.20$. In the firsts trial analyses the compressive strength assumed was the one obtained in the double *FJ* test in the West building. In these analyses, the tensile strength was at first estimated using the Italian code [86] ($f_t = 0.15$ MPa). The trial fracture energies were estimated as already done for the previous analyses (following Lourenço [106, 108]).

The numerical result that best fitted the experimental results was obtained with the mechanical characteristics reported in Table 5.10.

Table 5.10: The table gives the mechanical properties used in the *FEM* non-linear analyses that best fitted the experimental results of the shear *FJ* test performed in the Command building.

Characteristic	Symbol	Value	Unit
Young's modulus	E	1620	MPa
Tensile strength	f_t	0.20	MPa
Tensile fracture energy	G_{ft}	20	N/m
Compressive strength	f_c	1.60	MPa
Compressive fracture energy	G_{fc}	2000	N/m

The results obtained (Fig 5.6) help to give some first conclusions. The best fit obtained covers the whole of the experimental curve obtained loading the sample. This numerical curve reproduces appreciably well the experimental one. This best fit was obtained with the Young's modulus that almost coincides with the inclined Young's modulus. It has to be underlined that the difference between these two measured elastic characteristic is not so large. The compressive strength that leads to the best fit is again substantially different from the measured one.

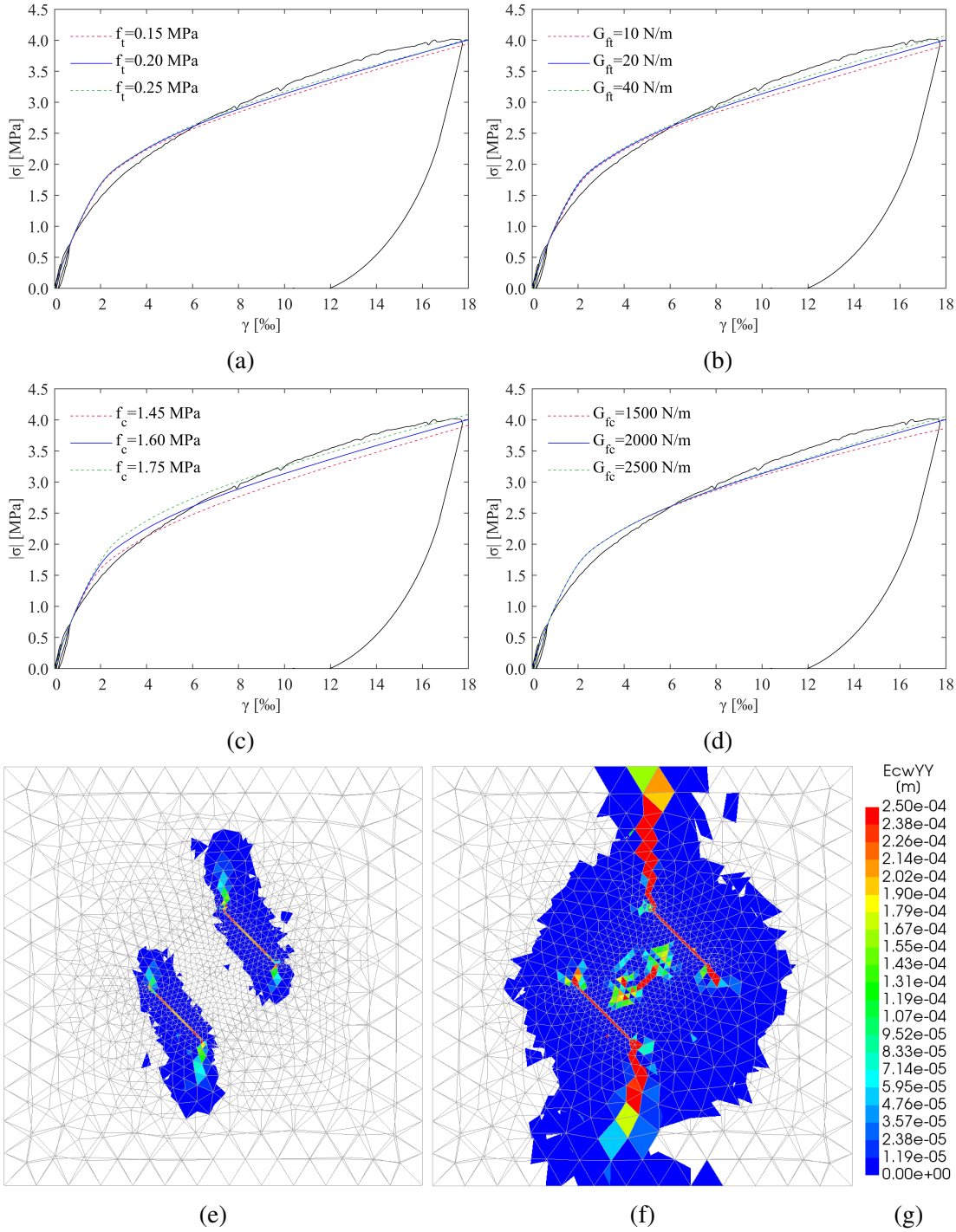

Figure 5.6: The images 5.6a, 5.6b, 5.6c and 5.6d provide the numerical results of the sensitivity analysis carried out for the shear *FJ* test performed in the Command building. The best fit is reproduced with the blue continuous line. The images 5.6e and 5.6f show the crack widths in the horizontal direction parallel to the wall plane of the best fit. In particular, the results obtained at the transition point ($\sigma = 1.50$ MPa) are presented 5.6e, the results for the last point of convergence are plotted in 5.6f and in 5.6g the legend is presented.

The sensitivity analysis underlines that changes in the compressive strength lead to large variations in the results (Fig. 5.6c). The fracture energies partially vary the numerical curves but only for high strain (Fig. 5.6d and 5.6b). For what regards the tensile strength, variations of its value of $\pm 25\%$ yielded to small differences in the results (Fig. 5.6b) on the contrary of what was expected.

Figures 5.6e and 5.6f show two images that were exported from the numerical results that fitted better the experimental results. These plots displays the crack widths as well as their legend. In particular, Figure 5.6e refers to the transition point and Figure 5.6f to the last load step when convergence was found. These images are in agreement with the ones that were found before. In fact, damages are found in the slots corners were the stress intensification is present. In addition, it is possible to observe that in Figure 5.6f the center of the sample is damaged. As noticed before, it is possible to observe that the damage is in the center of the sample and aligned with the longer axis of the sample. These large crack widths should underline the tensile failure of the sample in agreement with the purpose sought.

5.4 Micro-models

Micro-models were used to study the differences between the expected and the measured moduli. In specific, were studied differences between the Young's modulus and the inclined Young's modulus and the shear modulus evaluated starting from the Young's modulus and the shear modulus measured with the shear *FJ* tests. Only linear analyses were performed using these models.

These numerical models, the methods used and the results obtained are presented. More specifically these models were used to analyze the result obtained in the West building of "Caserma Valfrè di Bronzo".

Methodology

As anticipated in the literature review at the beginning of this thesis, in the micro-modeling method both the resisting elements and the mortar joints are modeled separately. In some micro-models even the interface between the two materials is modeled. In the present case, the interfaces were not taken into account since they are usually the planes were non-linearities take place and considering that the analyses performed are meant to understand the linear behavior of the sample.

The knowledge of the mechanical characteristics of both materials is needed. Since the problem that is under examination is the difference between linear elastic characteristics, it was decided to work with linear elastic micro-models. The unknowns are drastically reduced with this simplification.

The elastic properties of both bricks and joints have to be known in order to create a micro-model. These properties were not evaluated in the experimental campaigns. However, it is possible to estimate the Young's moduli of both materials starting from the Young's modulus of the masonry (Fig. 5.7).

It is possible to suppose a masonry wall with a regular disposition of bricks (Fig. 5.7a) that has a vertical Young's modulus E (for example measured with a double *FJ* test). It

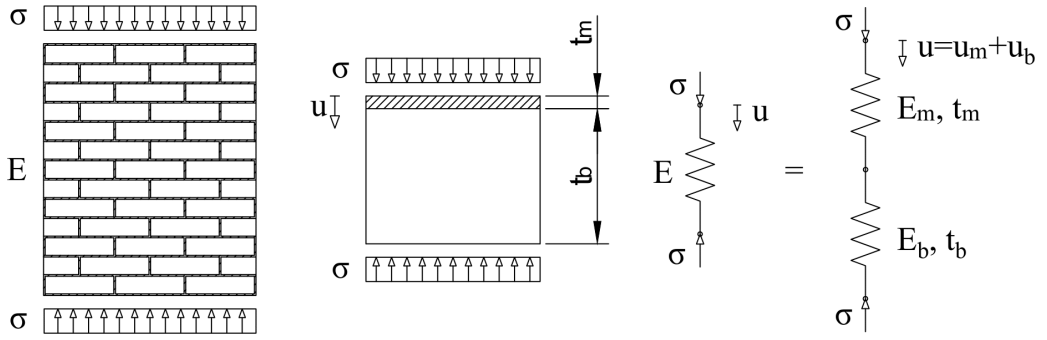

(a) (b) (c)

Figure 5.7: The images display the scheme used to estimate the elastic properties of bricks and mortar.

is assumed that the bricks have a Young's modulus E_b, regular dimensions and height t_b. Similarly, the thickness of the bed joints t_m is considered constant and the mortar Young's modulus is E_m. If the vertical joints are not taken into account and a stress σ is supposed to act on the wall (Fig. 5.7a), the homogenized vertical strain field of this wall is almost equivalent to the homogenized vertical strain field of a single bed joint laid on the top of a brick subjected to the same stress (Fig. 5.7b).

If this simplified model of Figure 5.7b is subjected to a stress σ a vertical displacement u takes place:

$$u = \varepsilon(t_b + t_m) = \frac{\sigma}{E}(t_b + t_m) \tag{5.1}$$

This displacement is the sum of the displacements that take place in the mortar u_m and in the brick u_b (Fig. 5.7c). For this reason, it is possible to write the following equivalence:

$$u = u_b + u_m \tag{5.2}$$

From the equations above (Eq. 5.1 and 5.2) it results possible to write the following equivalence that is often adopted in literature (e.g. [3, 58, 99]):

$$\frac{\sigma}{E}(t_b + t_m) = \frac{\sigma}{E_b}(t_b) + \frac{\sigma}{E_m}(t_m) \tag{5.3}$$

In historical walls, bricks and mortar joints do not have homogeneous dimensions. From the analysis of measures taken in place, it was possible to create two uniform textures (Fig. 5.8). For this reason, it was possible to obtain two thicknesses of the bed joints ($t_{m,1} = 16.4$ mm and $t_{m,2} = 15.0$ mm) and one brick thickness ($t_b = 60.0$ mm). The number of unknowns of Equation 5.3 drops to two (E_b and E_m) thanks to these two geometrical characteristics and the Young's modulus of the wall. If, for example, the Young's modulus of the brick is supposed (or measured) it is possible to evaluate the Young's modulus of the mortar:

$$E_m = \frac{t_m}{(t_b + t_m)/E - t_b/E_b} \tag{5.4}$$

This methodology was applied for the test performed in the West building of the "Caserma Valfrè di Bronzo" in order to create a micro-model of the shear *FJ* test. The

Young's modulus measured in this building was $E = 1846$ MPa. However, both the Young's moduli of bricks and mortar were not measured.

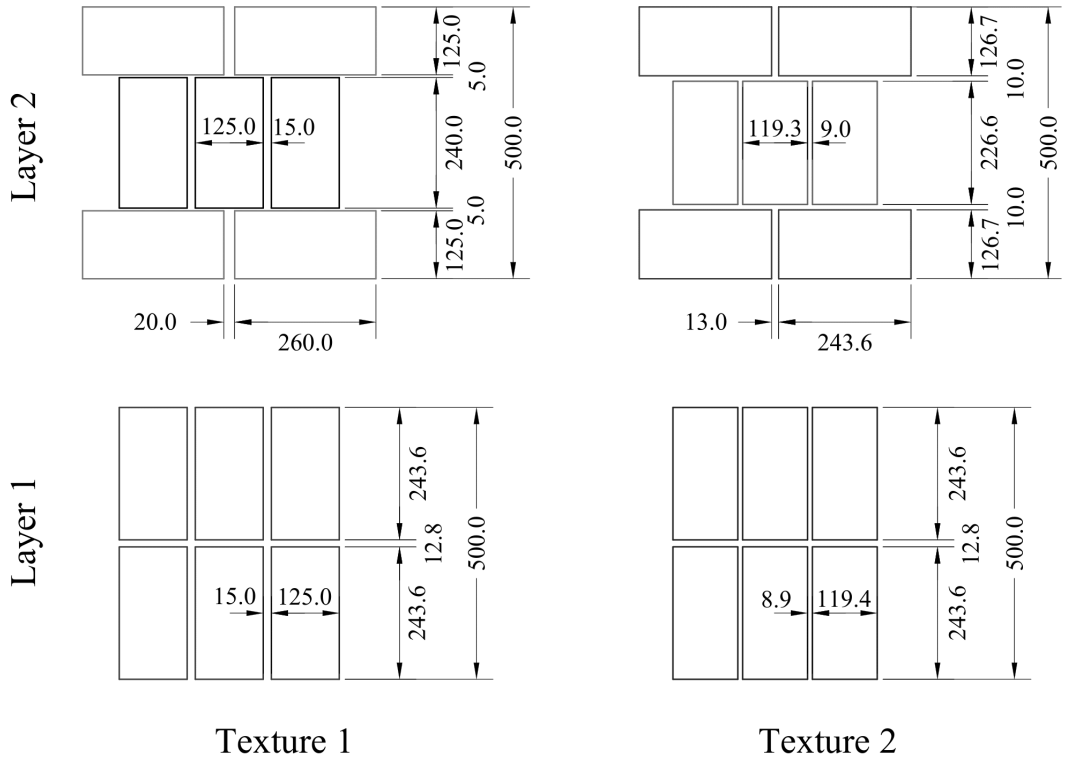

Figure 5.8: The image shows the two texture utilized in the micro-models.

Many authors performed evaluations of historical bricks Young's modulus [8, 18, 22, 64, 84, 121, 127, 160]. For what regards Italian historical bricks, usual Young's moduli range between 2000 and 6000 MPa. For the micro-models created it was decided to use two bricks Young's moduli belonging to this rage that were $E_{b,1} = 3000$ MPa and $E_{b,2} = 5000$ MPa. The intention was to eventually adapt these values if the results of the micro-models were significant.

Thanks to these two values, to the two bed-joints thicknesses and to Equation 5.4 it is possible to evaluate four mortar Young's moduli. For this reason the models created were four. For sake of simplicity a summary of the models is reported in Table 5.11. The Poisson's ratio utilized was $\nu = 0.20$.

Table 5.11: The table summarizes the characteristics utilized for the micro-models.

Model	Texture	t_m mm	E_m MPa	E_b MPa
A	1	16.4	767	3000
B	1	16.4	558	5000
C	2	15.0	727	3000
D	2	15.0	524	5000

The walls modeled had dimensions of $4.0 \times 3.0 \times 0.5$ m and the phases of the analysis (imposition of the vertical stress, cuts realization, etc.) were exactly the ones used for all the previous analyses. For each wall only a part of it was modeled using the micro-modeling technique that coincides with the central part of the wall that had dimensions of $2.0 \times 2.0 \times 0.5$ m (Fig. 5.9). The part surrounding this central prism was modeled using the macro-model technique considering a homogeneous, isotropic linear and elastic material having the Young's modulus coincident with the one measured using the double *FJ* test. The choice of dividing the geometry was taken considering the possibility of enlarging the elements in the surrounding part and for this reason to limit the computational efforts. In fact, the models had 640000 elements therefore even for simple linear elastic analyses the computational times were noticeable. The elements adopted were quadratic tetrahedron (CTE30 [65]).

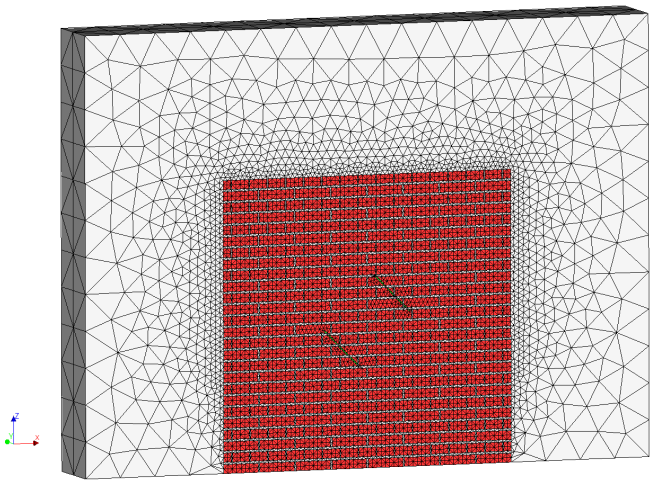

Figure 5.9: The image shows the mesh of one of the micro-models used.

Results

As introduced, the linear analyses performed using the micro models were four. The differences between these models were the Young's moduli of both bricks and mortars and textures as summarized in Table 5.11.

The results of one model are displayed in Figure 5.10. In particular the image shows the field of displacement due to a *FJs* stress $\sigma = 6.00$ MPa of the Model B.

Table 5.12: Summary of the results obtained with the micro-models, the expected results and the measured characteristics.

	Theoretical MPa	Experimental MPa	Model A MPa	Model B MPa	Model C MPa	Model D MPa
G	771	1561	711	731	683	695
E^*	1850	3492	1536	1593	1850	1598

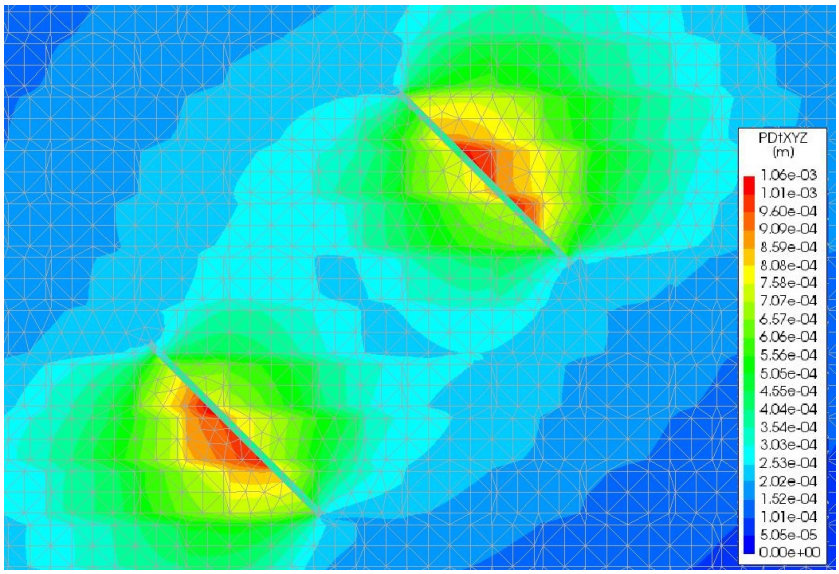

Figure 5.10: The image shows a detail of the Model B. In particular the is shows the countour plot of the total displacements for an applied stress $\sigma = 6.00$ MPa.

The inclined Young's moduli and the shear moduli of both models were evaluated starting from the numerical results.

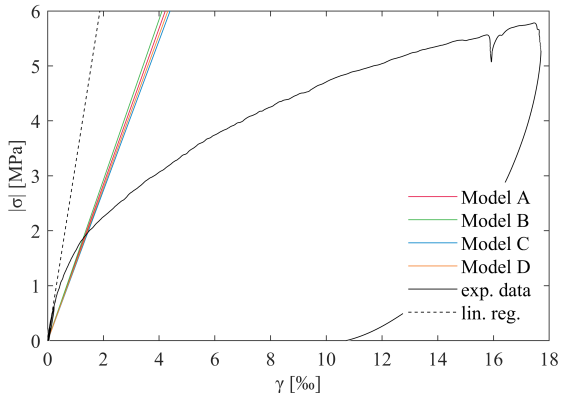

Figure 5.11: The images displays the results of the analyses performed using micro-models.

From Figure 5.11 and Table 5.12 it is possible to notice that not a single shear modulus evaluated using the micro-models were close to the measured one. In contrast, both the mechanical properties and textures give shear moduli that are close to the theoretical shear modulus calculated starting from the measured Young's modulus, the Poisson's ratio and considering the material linear elastic and isotropic ($G = E/[2(1+\nu)]$). In fact, the maximum difference is about the 13%.

The comparison between the inclined Young's moduli measured in the experimental result and the ones measured in the numerical models shows that the discrepancies are noticeable large. The inclined Young's modulus measured using the micro-models results close to the expected one that coincides with the Young's modulus of the media

(1850 MPa). In particular, the inclined Young's modulus of Model C perfectly coincides with this value. The other values are inferior to the expected one of about the 20%.

Therefore, it is possible to affirm that the textures and the mechanical properties investigated do not lead to a large anisotropic behaviors as measured with the shear *FJ* test.

Conclusion

Four numerical analyses carried out using micro-models were performed to study the high values of the inclined Young's modulus and of the shear modulus measured on field tests.

The numerical results do not show correspondence with the experimental results. Two possible causes can be related to the estimation of the material properties and to the texture assumptions. Nevertheless, these hypotheses do not seem to be the causes since four different models were explored. So, the question related to the discrepancies found between the expected shear moduli and inclined Young's moduli remains open. Small discrepancies between the numerical results and the results obtained considering the masonry as a homogeneous, isotropic linear and elastic material were found. Therefore, it can be affirmed that the textures and the mechanical properties utilized to create the micro-models do not lead to a pronounced anisotropic behavior of the wall.

Since there is a good match between the theoretical and numerical measured elastic characteristics, it is expected to find the same good pairing for all the tests in which a good match between the expected and measured elastic properties was found. The author will try to verify this hypothesis in future works.

5.5 Summary and discussion

This Section gives a summary and the discussion of the results obtained in the present Chapter. For this reason, the two main arguments treated are the non-linear *FEM* analyses and the micro-models.

The non-linear *FEM* analyses, as well as the performed sensitivity analyses, gave useful information about the proposed shear *FJ* test.

First of all, to have the best match of the linear range of the experimental results in some analyses it was necessary to use the inclined Young's modulus. The discrepancy between the two measured Young's moduli were analyzed in Section 5.4.

An interesting fact is that the best fits were almost always obtained for compression strengths different from the one measured with the double *FJ* tests. This fact can underline that the hypothesis of an isotropic failure criterion for this media and in this specific case could not valid.

The sensitivity analyses underline different facts:

- The fracture energies (both compressive and tensile) slightly influence the numerical results and mainly for high levels of strains;
- The compressive strength is the mechanical characteristic that influences more the numerical results;

- The tensile strength does not significantly influence the numerical results.

This last point can be important. It seems to evidence that the numerical results are not so in agreement with the thesis for which the proposed test method can be a tool for evaluating the tensile strength of masonry. However, a cause of this mismatch can be related to the material model. The problem under study is a mixed-mode fracture. Moreover, the failure of the sample is dependent on the micro-structure of the material. For these reasons, it seems interesting the possibility of studying the experimental results with models that consider the micro-structure of the material. It could be of noticeable importance the adoption of the discrete element method that is showing increasing attention (e.g. [89, 144, 145]).

The micro-models were made with the purpose of studying the differences between the estimated moduli and the moduli measured with the shear *FJ* tests. In particular, the discrepancies measured in the West building of the "Caserma Valfrè di Bronzo" were analyzed.

The results of these analyses show that in the case studied, the behavior of the tested wall under the shear *FJ* test is not reproduced with the micro-model. The micro-models gave as results a material behavior that is almost totally considerable as isotropic. For this reason, it is expected that the micro-models would confirm the good results obtained in the tests were a good match between the expected and measured elastic characteristics was found.

The possible causes of the discrepancies measured can be related to the hypotheses taken.

First of all, as assumed for the standard single and double *FJ* tests, in the proposed test the stress transferred by contact to the masonry sample by the *FJs* is considered uniform. However, due to their shape the *FJs* they cannot transfer a perfect uniform stress.

In the proposed test the cuts intersect both resisting elements and mortar joints. Due to the difference between the stiffness of these materials the stress might be transferred more to the elements that are most rigid. This fact should lead to a stress field that is not completely uniform. However, the same issue should be also present testing rubble stone masonry but it is not unusual to perform standard *FJ* tests in this media.

One of the recommendations of the standard *FJ* tests is to place shims in between the *FJ* and the masonry. This operation is made with the intention of protecting the actuator and, more important, distributing more uniformly the stresses. The circular saw used for the shear *FJ* tests creates cuts that have a thickness slightly larger than the *FJs* thickness. It was decided to avoid enlarging the slots to have space for the shims. This choice was made considering the risks of enlarging the slot too much and disturbing the specimen. This last risk can be due to cuts not perfectly perpendicular to the surface of the wall, to the water used to cool down the saw and to the vibrations that the saw can cause. The risk of enlarging too much the cuts can lead to not optimal expansion of the *FJs*. This can cause a non-uniform distributions of the stresses and the risk that *FJs* enlarge too much.

Another possible issue comes from the hypothesis that assumes a homogeneous sample. This hypothesis might not be valid for the proposed tests. In this case, noticeable discrepancies between the readings of the bases should be present. However,

these large differences were not measured. Moreover, it is possible to appreciate that the differences between the readings of the bases measured in the shear *FJ* tests and the ones of the double *FJ* tests have the same magnitude. The hypothesis of a homogeneous media is taken in both tests. Since the strains in both tests have a similar behavior, the hypothesis of a homogeneous media must be valid (or not) for both the tests.

Chapter 6

Conclusions

In this work the necessity of evaluating the shear modulus and the tensile strength of unreinforced masonry (*URM*) was highlighted. These characteristics are at the moment evaluated only using *DT* tests. This is why the main aim of the thesis is the creation, design, test and analysis of a new *MDT* test (called shear flat jack test) meant to evaluate the shear modulus and the tensile strength of *URM*. In order to create this test, it was decided to use the Flat Jack (*FJ*) technique.

The design of the shear *FJ* test started with numerical analyses of six different configurations of slots, *FJs* positions and dimensions. To understand which of the configurations was the best one, a series of criteria were defined. In particular, the destructiveness, costs, and the effectiveness were examined in order to define the best layout.

Once that the best geometrical configuration was found, a deep and comprehensive parametric analysis was carried out. The effects of constraints, elastic characteristics, vertical stress and wall thickness on the sample strain/stress statuses were evaluated. The first result of this parametric analysis is that the chosen configuration seems to be able to evaluate both the shear modulus and the tensile strength. Some tools were created in order to evaluate the principal stresses of the sample. In particular, a piecewise law, two graphs and a table were produced.

At this point, since the theoretical validity of the test was proven, the test method was designed. Attention was paid to all the aspects of the test. It has to be remarked that the test was designed in order to be as much as possible accessible. For this reason, the most diffuse equipment for *FJ* testing was adopted. The tests performed in situ proved the good design of the test method.

The shear *FJ* test was applied in five experiments. These were carried out in four different structures made of brick and lime mortar. One test was performed in the "ex Teatro dei Nobili" (Vercelli), a structure of the 18^{th} century. In this building two single *FJ* tests and two double *FJ* tests were also performed. Two shear *FJ* tests, one single *FJ* test and a double *FJ* test were carried out in two buildings of the barrack "Caserma Valfrè di Bronzo". This barrack is situated in Alessandria and it was built in the 19^{th} century. Similarly to what done in "Caserma Valfrè di Bronzo", two shear *FJ* tests, one single *FJ* test and a double *FJ* test were carried out in the barrack "Caserma Giovanni Cerutti". This is the structure that is more recent and was built in the 20^{th} century. In the experimentation carried out, it was decided to analyze the effect of the vertical stress in the results. For this reason, different levels of vertical stress were looked for.

Moreover, for four tests the Acoustic Emission (*AE*) technique was adopted in order to monitor the damage progress of the sample. In the tests, the inclined Young's modulus was measured in parallel to the shear modulus. This characteristic should be close to the Young's modulus of the material otherwise it should highlight an eventual anisotropy of the media.

For two of the tests performed, it was possible to evaluate the tensile strength of the material. In the other three cases the failure of the sample was not clear. For what regards the elastic characteristics, it was expected to find values of inclined Young's moduli close to Young's moduli measured with the double *FJ* tests and values of shear moduli close to the ones calculated starting from the Young's moduli (hypothesizing a linear elastic isotropic material, $\nu = 0.25$ and using $G = E/[2(1+\nu)]$). A good correspondence between the expected and the found elastic characteristics was found in three tests.

To analyze the failure of the samples, macro-models were created and non-linear analyses were carried out. The best fits of the experimental curves were searched with these analyses. Once the best fitting curves were found, sensitivity analyses were carried out to understand the role played by the singular mechanical characteristic (compressive strength, tensile strength, tensile fracture energy and compressive fracture energy).

These best fits were obtained for values of compressive strengths that in some cases were not so close to the measured ones. This fact underlines that a non-isotropic failure criterion should be taken into account. For the two tests in which it was possible to measure the tensile strength, the best fits were obtained with values of this characteristic close to the measured ones.

The sensitivity analyses evidenced a noticeable influence of the sample behavior in the compressive strength. In contrast, the fracture energies seemed to influence only marginally the results and mainly for high strains.

The main aspect that stems from the sensitivity analyses is that the results are not so dependent on the values of the tensile strength. This fact is against one of the main purposes of the work. However, the nature of the failure of the material is a mixed-mode fracture and other material models should be explored in order to have a deeper comprehension of the specimen failure.

Micro-models were adopted in order to study the discrepancies found in terms of expected and evaluated elastic characteristics. For this reason, linear elastic analyses were carried out with micro-models in order to study the experimental results of West building of the "Caserma Valfrè di Bronzo". In particular, the targets of the analyses were the inclined Young's modulus and the shear modulus. In the micro-model technique both resisting elements and joints are modeled separately. Since the properties of these materials were not measured they were estimated. For this reason, four different micro-models having two textures, two brick Young's moduli and four mortar Young's moduli were created.

The analyses highlighted that both textures and material properties cannot be the cause of the discrepancies found. Possible explanations can be addressed to the hypotheses taken. For example, in *FJ* testing it is usual to consider uniform the stress transferred by the actuators. Shims could be used in order to obtain a more uniform stress. A second possible issue is related to the fact that the slots are made in both

bricks and mortars. Since these materials have different stiffnesses, it is understandable that the stiffer material is going to be subjected to a higher stress. A third reason can be addressed to the hypothesis of a homogeneous material. Due to the sample dimensions, this hypothesis could not be valid.

Some aspects of the shear *FJ* test have to be investigated better. In future works, the author has the intention of studying uniform in-scale specimens in order to understand fully the sample behavior. In parallel to the in scale specimens, a full characterization of the material would be performed in order to understand and analyze better the experimental results. Moreover, a deeper analysis of the *AE* data will be performed to characterize better the recorded signals and to localize the *AE* sources. Moreover, in the contour plots were present regions, close to the cuts corners, where high stresses are present. It is expected that the same high stresses are present in single and double *FJ* testing. The author together with a supervisor is working in a method meant to reduce these stresses in the double *FJ* tests and in the shear *FJ* tests.

Appendix A

Appendix

A.1 Sensors characteristics

For sake of completeness the characteristics of the used sensors are here presented.

A.1.1 Manual instruments

- Pressure gauges.
  The first pressure gauge has a range of $0-1.60$ MPa and its sensitiveness is 0.01 MPa.
  The second pressure gauge has a range of $0-6.00$ MPa with a sensitiveness of 0.05 MPa.

- Extensometer.
  It has a base length of 250 mm and the sensitiveness is 1 μm.

A.1.2 Automatic instruments

It has to be highlighted that the characteristics of the *LVDT* and of the pressure transducer depend on the acquisition system. For the tests performed with this equipment, it consists of a Beckoff *PLC*. The instrumentation has eight channels with a maximum voltage entrance of 12 V and the readings are performed with 16 bit. The resolution of the *PLC* results to be 366 μV. The frequency of acquisition was set at 1 Hz. In the characteristics here by reported the sensitiveness already takes in to account the acquisition.

- Pressure transducer.
  The range of the instrument is $0-10$ MPa, the linearity is 0.20% and the output range is $0-10$ V. Considering the *PLC* characteristics, the sensitivity results to be 0.37 kPa.

- *LVDT*. The characteristics of the *LVDTs* are summarized in Table A.1.

Table A.1: Characteristics of *LVDT*.

LVDT	Serial n.	Sensitivity mV/mm	Linear range mm	Linearity %	Calibration uncertainty μm
T1	152426	179.65	±12.5	0.40	6.2
T2	152424	181.22	±12.5	0.25	6.2
T3	152425	179.46	±12.5	0.14	6.2
T4	152427	180.46	±12.5	0.18	6.2

From these data and the characteristics of the *PLC* the sensitiveness of the instruments results to be 2 μm.

A.2 "ex Teatro dei Nobili"

In the following some of the results of the shear *FJ* tests performed in "ex Teatro dei Nobili". In particular, in Figure A.1 are displayed the results of the double *FJ* test performed in Position 1, in Figure A.2 the one performed in Position 2 and in Figure A.3 the results of the shear *FJ* test.

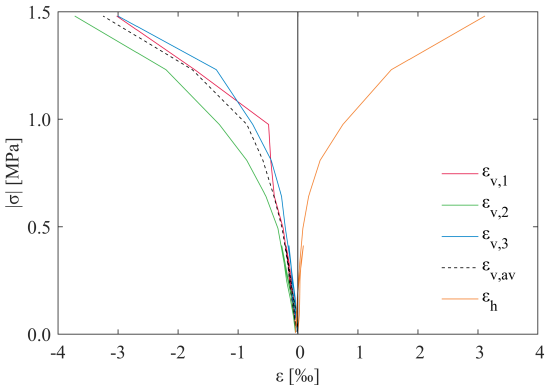

Figure A.1: The image shows the measured strains in the double *FJ* test on Position 1 of the "ex Teatro dei Nobili".

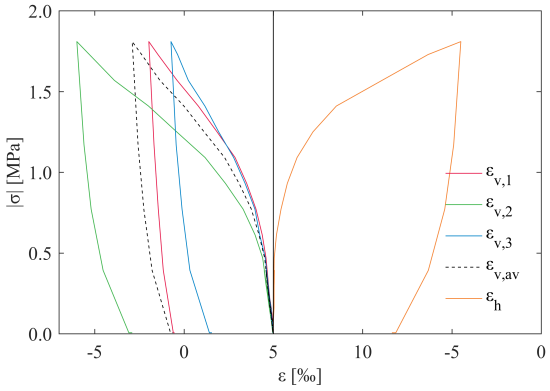

Figure A.2: The image shows the measured strains in the double *FJ* test on Position 2 of the "ex Teatro dei Nobili".

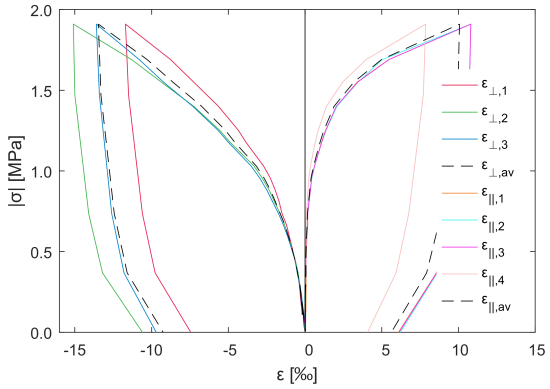

Figure A.3: The image shows the measured strains obtained in the shear *FJ* test in "ex Teatro dei Nobili". In particular are plotted the three perpendicular strains $\varepsilon_{\perp 1,2,3}$ and their average, the four parallel strains $\varepsilon_{||1,2,3,4}$ and their average.

A.3 "Caserma Giovanni Cerutti"

In the following some of the results of the shear *FJ* tests performed in "Caserma Giovanni Cerutti". In particular, in Figure A.6 are displayed the results of the double *FJ* test performed in Position 1, in Figure A.5 the results of the shear *FJ* test performed in Position 1 and in Figure A.6 the results of the shear *FJ* test carried out in Position 2.

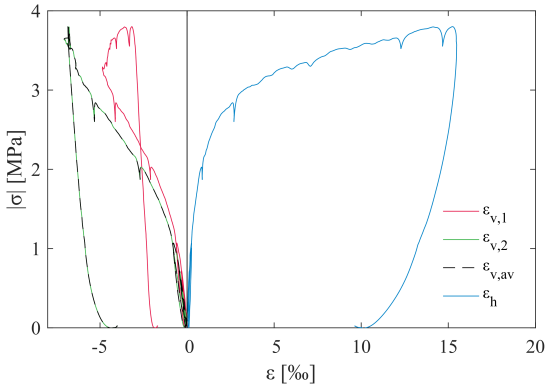

Figure A.4: The image shows the measured strains obtained in the double *FJ* test performed in "Caserma Giovanni Cerutti" Position 1.

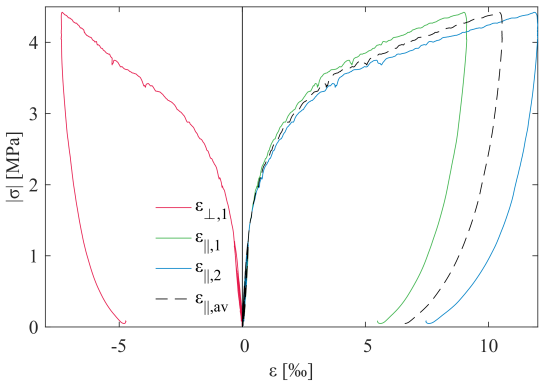

Figure A.5: The image shows the measured strains obtained in the shear *FJ* test executed in "Caserma Giovanni Cerutti" Position 1. In particular are plotted one perpendicular strain $\varepsilon_{\perp 1}$, the two parallel strains $\varepsilon_{||1,2}$ and their average.

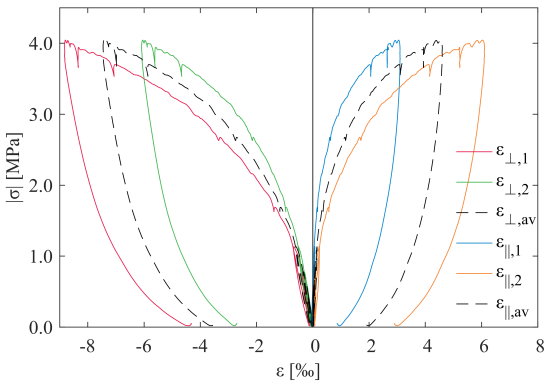

Figure A.6: The image shows the measured strains obtained in the shear *FJ* test executed in "Caserma Giovanni Cerutti" Position 2. In particular are plotted the two perpendicular strains $\varepsilon_{\perp 1,2}$, their average, the two parallel strains $\varepsilon_{||1,2}$ and their average.

A.4 "Caserma Valfrè di Bronzo"

In the following some of the results of the shear *FJ* tests performed in "Caserma Valfrè di Bronzo". In particular, in Figure A.7 are displayed the results of the double *FJ* test, in Figure A.9 the results of the shear *FJ* test performed in the West Building and in Figure A.9 the results of the shear *FJ* test performed in the Command building.

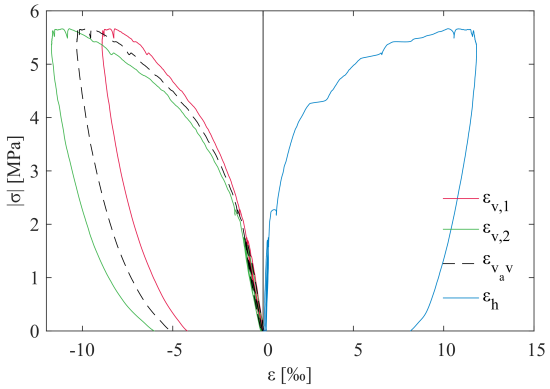

Figure A.7: The image shows the measured strains obtained in the double *FJ* test performed in the West building of "Caserma Valfrè di Bronzo".

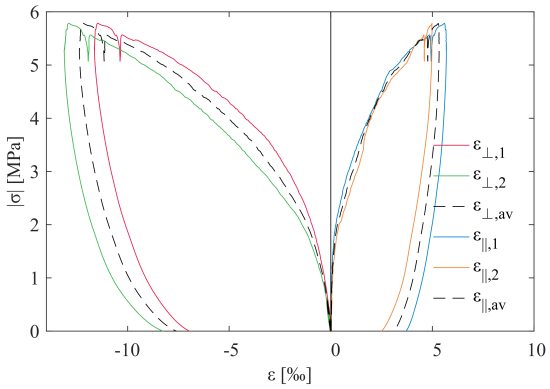

Figure A.8: The image shows the measured strains obtained in the shear *FJ* test executed in the West. In particular are plotted the two perpendicular strains $\varepsilon_{\perp 1,2}$ and their average, the two parallel strains $\varepsilon_{||1,2}$ and their average.

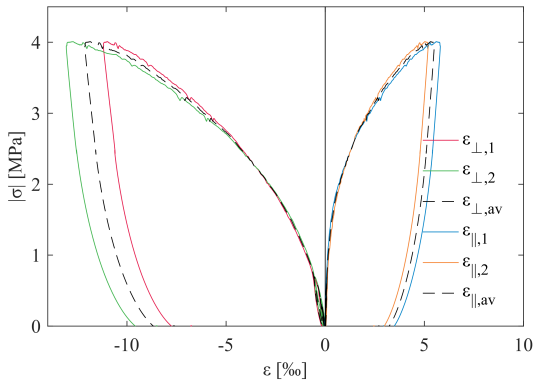

Figure A.9: The image shows the measured strains obtained in the shear *FJ* test executed in the Command building. In particular are plotted the two perpendicular strains $\varepsilon_{\perp 1,2}$ and their average, the two parallel strains $\varepsilon_{||1,2}$ and their average.

A.5 Normalized stresses

In this Section is presented a tool which is useful for evaluating the sample principal stresses. This evaluation can be crucial to understand the failure mechanism of the sample. Table A.2 summarizes the normalized principal stresses $\sigma_1/|\sigma_0|$ and $\sigma_2/|\sigma_0|$ in function of the normalized applied stress σ/σ_0 and the wall thickness t.

Table A.2: The table reports the normalized principal stresses as function of the normalized stress applied by *FJs* for different wall thickness.

σ/σ_0	$t = 0.40$ m		$t = 0.50$ m		$t = 0.75$ m		$t = 1.00$ m		$t = 1.50$ m	
	$\sigma_1/\lvert\sigma_0\rvert$	$\sigma_2/\lvert\sigma_0\rvert$	$\sigma_1/\lvert\sigma_0\rvert$	$\sigma_2/\lvert\sigma_0\rvert$	$\sigma_1/\lvert\sigma_0\rvert$	$\sigma_2/\lvert\sigma_0\rvert$	$\sigma_1/\lvert\sigma_0\rvert$	$\sigma_2/\lvert\sigma_0\rvert$	$\sigma_1/\lvert\sigma_0\rvert$	$\sigma_2/\lvert\sigma_0\rvert$
0.00E+00	2.72E-01	-9.54E-01	2.66E-01	-9.44E-01	2.66E-01	-9.26E-01	2.67E-01	-9.19E-01	2.68E-01	-9.15E-01
1.67E-01	1.86E-01	-9.79E-01	1.81E-01	-9.70E-01	1.79E-01	-9.55E-01	1.79E-01	-9.50E-01	1.79E-01	-9.47E-01
3.33E-01	1.12E-01	-1.01E+00	1.06E-01	-1.01E+00	1.02E-01	-9.96E-01	1.01E-01	-9.92E-01	1.01E-01	-9.89E-01
5.00E-01	4.98E-02	-1.06E+00	4.41E-02	-1.06E+00	3.76E-02	-1.05E+00	3.57E-02	-1.05E+00	3.47E-02	-1.04E+00
6.67E-01	2.57E-04	-1.12E+00	-5.77E-03	-1.12E+00	-1.48E-02	-1.11E+00	-1.78E-02	-1.11E+00	-1.95E-02	-1.11E+00
8.33E-01	-3.70E-02	-1.20E+00	-4.36E-02	-1.19E+00	-5.53E-02	-1.19E+00	-5.95E-02	-1.19E+00	-6.19E-02	-1.19E+00
1.00E+00	-6.30E-02	-1.28E+00	-7.05E-02	-1.28E+00	-8.50E-02	-1.28E+00	-9.05E-02	-1.28E+00	-9.36E-02	-1.28E+00
1.17E+00	-7.93E-02	-1.38E+00	-8.79E-02	-1.37E+00	-1.05E-01	-1.37E+00	-1.12E-01	-1.37E+00	-1.16E-01	-1.38E+00
1.33E+00	-8.76E-02	-1.48E+00	-9.73E-02	-1.47E+00	-1.18E-01	-1.48E+00	-1.26E-01	-1.48E+00	-1.31E-01	-1.48E+00
1.50E+00	-8.93E-02	-1.59E+00	-1.00E-01	-1.58E+00	-1.24E-01	-1.59E+00	-1.34E-01	-1.59E+00	-1.40E-01	-1.59E+00
1.67E+00	-8.58E-02	-1.70E+00	-9.82E-02	-1.69E+00	-1.25E-01	-1.70E+00	-1.37E-01	-1.71E+00	-1.43E-01	-1.71E+00
1.83E+00	-7.81E-02	-1.82E+00	-9.20E-02	-1.81E+00	-1.23E-01	-1.82E+00	-1.35E-01	-1.83E+00	-1.43E-01	-1.83E+00
2.00E+00	-6.71E-02	-1.94E+00	-8.25E-02	-1.93E+00	-1.17E-01	-1.95E+00	-1.31E-01	-1.95E+00	-1.39E-01	-1.96E+00
2.17E+00	-5.33E-02	-2.06E+00	-7.03E-02	-2.06E+00	-1.08E-01	-2.07E+00	-1.24E-01	-2.08E+00	-1.33E-01	-2.08E+00
2.33E+00	-3.74E-02	-2.19E+00	-5.60E-02	-2.18E+00	-9.73E-02	-2.20E+00	-1.15E-01	-2.21E+00	-1.25E-01	-2.21E+00
2.50E+00	-1.98E-02	-2.32E+00	-3.99E-02	-2.31E+00	-8.48E-02	-2.33E+00	-1.04E-01	-2.34E+00	-1.15E-01	-2.34E+00
2.67E+00	-6.66E-04	-2.45E+00	-2.24E-02	-2.44E+00	-7.10E-02	-2.46E+00	-9.14E-02	-2.47E+00	-1.04E-01	-2.48E+00
2.83E+00	1.96E-02	-2.58E+00	-3.76E-03	-2.57E+00	-5.60E-02	-2.59E+00	-7.80E-02	-2.60E+00	-9.11E-02	-2.61E+00
3.00E+00	4.10E-02	-2.71E+00	1.59E-02	-2.70E+00	-4.00E-02	-2.72E+00	-6.36E-02	-2.74E+00	-7.77E-02	-2.74E+00
3.17E+00	6.31E-02	-2.84E+00	3.64E-02	-2.83E+00	-2.32E-02	-2.86E+00	-4.84E-02	-2.87E+00	-6.35E-02	-2.88E+00
3.33E+00	8.60E-02	-2.98E+00	5.76E-02	-2.96E+00	-5.73E-03	-2.99E+00	-3.26E-02	-3.01E+00	-4.85E-02	-3.01E+00
3.50E+00	1.09E-01	-3.11E+00	7.94E-02	-3.10E+00	1.24E-02	-3.13E+00	-1.61E-02	-3.14E+00	-3.30E-02	-3.15E+00
3.67E+00	1.33E-01	-3.25E+00	1.02E-01	-3.23E+00	3.10E-02	-3.26E+00	9.09E-04	-3.28E+00	-1.70E-02	-3.29E+00
3.83E+00	1.58E-01	-3.38E+00	1.25E-01	-3.36E+00	5.00E-02	-3.40E+00	1.83E-02	-3.41E+00	-5.69E-04	-3.42E+00
4.00E+00	1.83E-01	-3.52E+00	1.48E-01	-3.50E+00	6.94E-02	-3.53E+00	3.61E-02	-3.55E+00	1.63E-02	-3.56E+00
4.17E+00	2.08E-01	-3.65E+00	1.71E-01	-3.63E+00	8.92E-02	-3.67E+00	5.43E-02	-3.69E+00	3.34E-02	-3.70E+00
4.33E+00	2.34E-01	-3.79E+00	1.95E-01	-3.77E+00	1.09E-01	-3.81E+00	7.27E-02	-3.83E+00	5.09E-02	-3.84E+00
4.50E+00	2.59E-01	-3.92E+00	2.19E-01	-3.90E+00	1.30E-01	-3.94E+00	9.14E-02	-3.96E+00	6.86E-02	-3.98E+00
4.67E+00	2.85E-01	-4.06E+00	2.43E-01	-4.04E+00	1.50E-01	-4.08E+00	1.10E-01	-4.10E+00	8.66E-02	-4.12E+00
4.83E+00	3.12E-01	-4.20E+00	2.68E-01	-4.18E+00	1.71E-01	-4.22E+00	1.30E-01	-4.24E+00	1.05E-01	-4.25E+00
5.00E+00	3.38E-01	-4.33E+00	2.93E-01	-4.31E+00	1.92E-01	-4.36E+00	1.49E-01	-4.38E+00	1.23E-01	-4.39E+00
5.33E+00	3.91E-01	-4.61E+00	3.43E-01	-4.58E+00	2.34E-01	-4.63E+00	1.88E-01	-4.66E+00	1.60E-01	-4.67E+00
5.67E+00	4.45E-01	-4.88E+00	3.93E-01	-4.86E+00	2.77E-01	-4.91E+00	2.28E-01	-4.94E+00	1.98E-01	-4.95E+00
6.00E+00	5.00E-01	-5.16E+00	4.44E-01	-5.13E+00	3.21E-01	-5.19E+00	2.68E-01	-5.22E+00	2.36E-01	-5.23E+00
6.33E+00	5.55E-01	-5.43E+00	4.95E-01	-5.40E+00	3.64E-01	-5.47E+00	3.08E-01	-5.49E+00	2.75E-01	-5.51E+00
6.67E+00	6.10E-01	-5.71E+00	5.47E-01	-5.68E+00	4.09E-01	-5.74E+00	3.49E-01	-5.77E+00	3.14E-01	-5.79E+00
7.00E+00	6.65E-01	-5.99E+00	5.99E-01	-5.95E+00	4.53E-01	-6.02E+00	3.90E-01	-6.05E+00	3.53E-01	-6.07E+00
7.33E+00	7.21E-01	-6.26E+00	6.51E-01	-6.23E+00	4.98E-01	-6.30E+00	4.32E-01	-6.33E+00	3.92E-01	-6.35E+00

Continued on next page

Table A.2 – continued from previous page

σ/σ_0	$t = 0.40$ m		$t = 0.50$ m		$t = 0.75$ m		$t = 1.00$ m		$t = 1.50$ m	
	$\sigma_1/\lvert\sigma_0\rvert$	$\sigma_2/\lvert\sigma_0\rvert$	$\sigma_1/\lvert\sigma_0\rvert$	$\sigma_2/\lvert\sigma_0\rvert$	$\sigma_1/\lvert\sigma_0\rvert$	$\sigma_2/\lvert\sigma_0\rvert$	$\sigma_1/\lvert\sigma_0\rvert$	$\sigma_2/\lvert\sigma_0\rvert$	$\sigma_1/\lvert\sigma_0\rvert$	$\sigma_2/\lvert\sigma_0\rvert$
7.67E+00	7.76E-01	-6.54E+00	7.04E-01	-6.50E+00	5.42E-01	-6.58E+00	4.73E-01	-6.61E+00	4.32E-01	-6.63E+00
8.00E+00	8.32E-01	-6.82E+00	7.56E-01	-6.78E+00	5.87E-01	-6.86E+00	5.15E-01	-6.89E+00	4.72E-01	-6.92E+00
8.33E+00	8.89E-01	-7.09E+00	8.09E-01	-7.05E+00	6.32E-01	-7.14E+00	5.57E-01	-7.17E+00	5.11E-01	-7.20E+00
8.67E+00	9.45E-01	-7.37E+00	8.62E-01	-7.33E+00	6.78E-01	-7.41E+00	5.99E-01	-7.46E+00	5.51E-01	-7.48E+00
9.00E+00	1.00E+00	-7.65E+00	9.15E-01	-7.61E+00	7.23E-01	-7.69E+00	6.41E-01	-7.74E+00	5.92E-01	-7.76E+00
9.33E+00	1.06E+00	-7.93E+00	9.68E-01	-7.88E+00	7.69E-01	-7.97E+00	6.83E-01	-8.02E+00	6.32E-01	-8.04E+00
9.67E+00	1.11E+00	-8.20E+00	1.02E+00	-8.16E+00	8.14E-01	-8.25E+00	7.26E-01	-8.30E+00	6.72E-01	-8.32E+00
1.00E+01	1.17E+00	-8.48E+00	1.07E+00	-8.43E+00	8.60E-01	-8.53E+00	7.68E-01	-8.58E+00	7.13E-01	-8.61E+00
1.03E+01	1.23E+00	-8.76E+00	1.13E+00	-8.71E+00	9.06E-01	-8.81E+00	8.10E-01	-8.86E+00	7.53E-01	-8.89E+00
1.07E+01	1.28E+00	-9.04E+00	1.18E+00	-8.99E+00	9.51E-01	-9.09E+00	8.53E-01	-9.14E+00	7.94E-01	-9.17E+00
1.10E+01	1.34E+00	-9.32E+00	1.23E+00	-9.26E+00	9.97E-01	-9.37E+00	8.96E-01	-9.42E+00	8.34E-01	-9.45E+00
1.13E+01	1.40E+00	-9.59E+00	1.29E+00	-9.54E+00	1.04E+00	-9.65E+00	9.38E-01	-9.70E+00	8.75E-01	-9.73E+00
1.17E+01	1.46E+00	-9.87E+00	1.34E+00	-9.81E+00	1.09E+00	-9.93E+00	9.81E-01	-9.99E+00	9.16E-01	-1.00E+01
1.20E+01	1.51E+00	-1.01E+01	1.40E+00	-1.01E+01	1.14E+00	-1.02E+01	1.02E+00	-1.03E+01	9.57E-01	-1.03E+01
1.23E+01	1.57E+00	-1.04E+01	1.45E+00	-1.04E+01	1.18E+00	-1.05E+01	1.07E+00	-1.05E+01	9.98E-01	-1.06E+01
1.27E+01	1.63E+00	-1.07E+01	1.50E+00	-1.06E+01	1.23E+00	-1.08E+01	1.11E+00	-1.08E+01	1.04E+00	-1.09E+01
1.30E+01	1.68E+00	-1.10E+01	1.56E+00	-1.09E+01	1.27E+00	-1.10E+01	1.15E+00	-1.11E+01	1.08E+00	-1.11E+01
1.33E+01	1.74E+00	-1.13E+01	1.61E+00	-1.12E+01	1.32E+00	-1.13E+01	1.20E+00	-1.14E+01	1.12E+00	-1.14E+01
1.37E+01	1.80E+00	-1.15E+01	1.66E+00	-1.15E+01	1.37E+00	-1.16E+01	1.24E+00	-1.17E+01	1.16E+00	-1.17E+01
1.40E+01	1.86E+00	-1.18E+01	1.72E+00	-1.18E+01	1.41E+00	-1.19E+01	1.28E+00	-1.20E+01	1.20E+00	-1.20E+01
1.43E+01	1.91E+00	-1.21E+01	1.77E+00	-1.20E+01	1.46E+00	-1.22E+01	1.32E+00	-1.22E+01	1.24E+00	-1.23E+01
1.47E+01	1.97E+00	-1.24E+01	1.83E+00	-1.23E+01	1.50E+00	-1.24E+01	1.37E+00	-1.25E+01	1.28E+00	-1.26E+01
1.50E+01	2.03E+00	-1.27E+01	1.88E+00	-1.26E+01	1.55E+00	-1.27E+01	1.41E+00	-1.28E+01	1.33E+00	-1.28E+01
1.53E+01	2.09E+00	-1.29E+01	1.93E+00	-1.29E+01	1.60E+00	-1.30E+01	1.45E+00	-1.31E+01	1.37E+00	-1.31E+01
1.57E+01	2.14E+00	-1.32E+01	1.99E+00	-1.31E+01	1.64E+00	-1.33E+01	1.50E+00	-1.34E+01	1.41E+00	-1.34E+01
1.60E+01	2.20E+00	-1.35E+01	2.04E+00	-1.34E+01	1.69E+00	-1.36E+01	1.54E+00	-1.36E+01	1.45E+00	-1.37E+01
1.63E+01	2.26E+00	-1.38E+01	2.10E+00	-1.37E+01	1.74E+00	-1.38E+01	1.58E+00	-1.39E+01	1.49E+00	-1.40E+01
1.67E+01	2.32E+00	-1.40E+01	2.15E+00	-1.40E+01	1.78E+00	-1.41E+01	1.63E+00	-1.42E+01	1.53E+00	-1.43E+01
1.70E+01	2.37E+00	-1.43E+01	2.20E+00	-1.42E+01	1.83E+00	-1.44E+01	1.67E+00	-1.45E+01	1.57E+00	-1.45E+01
1.73E+01	2.43E+00	-1.46E+01	2.26E+00	-1.45E+01	1.88E+00	-1.47E+01	1.71E+00	-1.48E+01	1.61E+00	-1.48E+01
1.77E+01	2.49E+00	-1.49E+01	2.31E+00	-1.48E+01	1.92E+00	-1.50E+01	1.76E+00	-1.51E+01	1.66E+00	-1.51E+01
1.80E+01	2.55E+00	-1.52E+01	2.37E+00	-1.51E+01	1.97E+00	-1.53E+01	1.80E+00	-1.53E+01	1.70E+00	-1.54E+01
1.83E+01	2.60E+00	-1.54E+01	2.42E+00	-1.53E+01	2.02E+00	-1.55E+01	1.84E+00	-1.56E+01	1.74E+00	-1.57E+01
1.87E+01	2.66E+00	-1.57E+01	2.47E+00	-1.56E+01	2.06E+00	-1.58E+01	1.89E+00	-1.59E+01	1.78E+00	-1.60E+01
1.90E+01	2.72E+00	-1.60E+01	2.53E+00	-1.59E+01	2.11E+00	-1.61E+01	1.93E+00	-1.62E+01	1.82E+00	-1.62E+01
1.93E+01	2.78E+00	-1.63E+01	2.58E+00	-1.62E+01	2.16E+00	-1.64E+01	1.97E+00	-1.65E+01	1.86E+00	-1.65E+01
1.97E+01	2.83E+00	-1.66E+01	2.64E+00	-1.65E+01	2.20E+00	-1.67E+01	2.01E+00	-1.67E+01	1.90E+00	-1.68E+01
2.00E+01	2.89E+00	-1.68E+01	2.69E+00	-1.67E+01	2.25E+00	-1.69E+01	2.06E+00	-1.70E+01	1.94E+00	-1.71E+01

Nomenclature

Greek Symbols

α_τ	Coefficient for evaluation of the shear strength in diagonal compression tests
α_f	Coefficient for evaluation of the tensile strength in diagonal compression tests
δ_E	Relative displacement of the middle point of the panel in shear compression test considering it in a linear elastic regime
Δ_i	Displacement in the i diagonal in diagonal testing
δ_u	Relative displacement of the middle point of the panel in shear compression test at the maximum horizontal force P_{su}
γ	Shear strain
$\gamma_{1/3}$	Shear strain at $1/3$ of the peak load
ν	Poisson's ratio
ϕ	Diameter
ψ	Angle of principal stress orientation
σ	Stress applied by the flat jacks to the masonry
σ_0	Vertical stress in FJ testing/Imposed compression stress in the shear compression test
σ_1	Largest principal stress
σ_2	Smallest principal stress
σ_i	Stress in the direction i (i=x,y,z)
τ	Shear stress
$\tau_{d,1/3}$	Shear stress evaluated at $1/3$ of the peak load of the diagonal compression test
$\tau_{d,F}$	Shear strength measured using the diagonal compression test evaluated following Frocht M.

$\tau_{d,std}$ Shear strength measured using the diagonal compression test evaluated following the standards *ASTM* and *RILEM*

τ_{ij} Shear stress on the acting in the direction i,j (i,j=x,y,z)

τ_s Shear strength measured using the diagonal compression test evaluated following the *NTC08*

$\varepsilon_{\parallel}$ Strain parallel to the *FJs* planes

$\varepsilon_{\perp}$ Strain perpendicular to the *FJs* planes

ε_h Horizontal strain

ε_v Vertical strain

Superscripts

A_d Net area of the specimen in the diagonal compression test

A_i Area of the slot *i* in double flat jack test

A_s Cross area of the specimen in the shear compression test

A_{av} Averaged area of the slots in flat jack testing

A_{dB} Amplitude of *AE* event in decibel

A_{FJ} Area of the flat jack

A_{slot} Area of the slot

$d_{i,j}$ Distance between measuring points of the basis having direction *i* at the load step *j*

d_{uc} Ductility index

E Young's modulus

E^* Inclined Young's modulus

E_b Brick Young's modulus

E_m Mortar Young's modulus

E_s Secant modulus of elasticity

E_t Tangent modulus of elasticity

$f_{c,exp}$ Experimental compression strength

$f_{c,m}$ Average compression strength

$f_{c,teo}$ Theoretical compression strength

f_c Compression strength

$f_{t,d,B}$ Tensile strength evaluated with the diagonal compression test following Brignola et al. [31]

$f_{t,d,F}$ Tensile strength evaluated with the diagonal compression test following Frocht M.

$f_{t,d,std}$ Tensile strength evaluated with the diagonal compression test following the standards *ASTM* and *RILEM*

$f_{t,d}$ Tensile strength evaluated with the diagonal compression test following the *NTC08*

$f_{t,s}$ Tensile strength evaluated with the shear compression test following the *NTC08*

f_t Tensile strength

G Shear Modulus

g Base length in diagonal testing

$G_{1/3}$ Secant shear modulus for a $1/3$ of the peak load

G_{fc} Fracture energy in compression

G_{ft} Fracture energy in tension

h Height of the specimen for the diagonal compression test

k_a Ratio between the area of the flat jack and the area of the slot

k_m Flat jack constant, also named jack calibration constant

l Width of the specimen in the diagonal compression test and in the shear compression test

l_i Length of the measure basis having direction i

m Magnitude of seismic events

N Cumulative number of oscillations

n Percent of the gross area of the unit that is solid, expressed as a decimal

$N(\geq m)$ Cumulative number of seismic events having magnitude $\geq m$

$N(A_{dB})$ Cumulative number of *AE* events having amplitude A_{dB}

N_c Oscillations counter

N_{AE} Events counter

p Hydraulic pressure

P_d Force on the diagonal compression test

P_s Horizontal force on the shear compression test

P_{du} Maximum force on the diagonal compression test

P_{su} Maximum horizontal force on the shear compression test

r Ratio between the shear strength evaluated using the shear compression test and the diagonal test

t Thickness of the wall in shear *FJ* testing/ thickness of the specimen in the diagonal compression test and in the shear compression test

t_b Brick thickness

t_m Mortar thickness

u Total vertical displacement

u_b Brick vertical displacement

u_m Mortar vertical displacement

w Specific weight

FC Felicity ratio

Acronyms / Abbreviations

AE Acoustic Emission

ASTM American Society for Testing Materials

DIC Digital Image Correlation

DT Destructive Testing

FC (From the name in Italian) Confidential factor

FEMA Federal Emergency Management Agency

FEM Finite Element Method

FJ Flat jack

GPR Ground Penetrating Radar

ISTAT National (Italy) institute of statistic

LC (From the name in Italian) Level of knowledge of the structure

LVDT Linear Variable Displacement Transducer

MDT Minor Destructive Testing

MiBAC Ministero dei beni e delle attività culturali del turismo

NDT Non Destructive Testing

NTC08 (From the name in Italian) Technical code for constructions of the 2008

NTC18 (From the name in Italian) Technical code for constructions of the 2018

ReLUIS Laboratories University Network of seismic engineering

RILEM (From the name in French) The International Union of Laboratories and Expert in Construction Materials

URM Unreinforced Masonry

XFEM eXtended Finite Element Method

Bibliography

[1] C. Abdunur. "Stress and deformability in concrete and masonry". In: *IABSE Symposium on Strengthening of Building Structures-Diagnostic and Therapy, Venice, Italy*. 1983.

[2] Daniel P. Abrams and Nirav Shah. *Cyclic load testing of unreinforced masonry walls*. Tech. rep. DTIC Document, 1992.

[3] D. Abruzzese, L. Miccoli, and J. Yuan. "Mechanical behavior of leaning masonry Huzhu Pagoda". In: *Journal of Cultural Heritage* 10.4 (2009), pp. 480–486. ISSN: 1296-2074. DOI: https://doi.org/10.1016/j.culher.2009.02.004. URL: http://www.sciencedirect.com/science/article/pii/S1296207409000818.

[4] Daniela Addessi, Domenico Liberatore, and Renato Masiani. "Force-based beam finite element (FE) for the pushover analysis of masonry buildings". In: *International Journal of Architectural Heritage* 9.3 (2015), pp. 231–243.

[5] Daniela Addessi et al. "Modeling approaches for masonry structures". In: *Open Civil Engineering Journal* 8.1 (2014), pp. 288–300.

[6] Naida Ademovic, Mustafa Hrasnica, and Daniel V. Oliveira. "Pushover analysis and failure pattern of a typical masonry residential building in Bosnia and Herzegovina". In: *Engineering Structures* 50 (2013). Engineering Structures: Modelling and Computations (special issue IASS-IACM 2012), pp. 13–29. ISSN: 0141-0296. DOI: https://doi.org/10.1016/j.engstruct.2012.11.031. URL: http://www.sciencedirect.com/science/article/pii/S0141029612005974.

[7] Sk Sekender Ali and Adrian W. Page. "Finite element model for masonry subjected to concentrated loads". In: *Journal of structural engineering* 114.8 (1988), pp. 1761–1784.

[8] M. Angelillo and R. S. Olivito. "Experimental analysis of masonry walls loaded horizontally in plane". In: *Masonry International* 8.3 (1995), pp. 91–100.

[9] Anna Anzani et al. "Use of Sonic and GPR tests to control the effectiveness of grout injections of stone masonry". In: *ECNDT 2006* 3 (2006), pp. 1–7.

[10] Panagiotis G. Asteris et al. "Numerical Modeling of Historic Masonry Structures". In: *Handbook of Research on Seismic Assessment and Rehabilitation of Historic Structures* (2015), pp. 213–256.

[11] ASTM International. “ASTM C1196-14a Standard Test Method for In Situ Compressive Stress Within Solid Unit Masonry Estimated Using Flatjack Measurements”. In: (2014), pp. 1–6.

[12] ASTM International. “ASTM C1197-14a Standard Test Method for In Situ Measurement of Masonry Deformability Properties Using the Flatjack Method”. In: (2014), pp. 1–7. DOI: 10.1520/C1197-09.2.

[13] ASTM International. “ASTM C1232-15a Standard Terminology of Masonry”. In: (2015), pp. 1–7. DOI: 10.1520/C1232-15A.2.

[14] ASTM International. “ASTM C1531-03 Standard Test Method for In Situ Measurement of Masonry Mortar Joint Shear Strength”. In: (2003), pp. 1–7. DOI: 10.1520/C1531-03.

[15] ASTM International. “ASTM E519/E519M-15 Standard Test Method for Diagonal Tension (Shear) in Masonry Assemblages”. In: (2015), pp. 1–5. DOI: 10.1520/E0519.

[16] R. H. Atkinson et al. “Response of Masonry Bed Joints in Direct Shear”. In: *Journal of Structural Engineering* 115.9 (1989), pp. 2276–2296. DOI: 10.1061/(ASCE)0733-9445(1989)115:9(2276).

[17] N. Augenti and A. Romano. “Seismic design of masonry buildings through macro-elements”. In: *Proceedings of the XIV International Brick and Block Masonry Conference, Sydney*. 2008.

[18] S. Bati and G. Ranocchiai. “A critical review of experimental techniques for brick material”. In: *10th international brick/block masonry conference, Calgary*. 1994, pp. 1247–1255.

[19] Arash Behnia, Hwa Kian Chai, and Tomoki Shiotani. “Advanced structural health monitoring of concrete structures with the aid of acoustic emission”. In: *Construction and Building Materials* 65 (2014), pp. 282–302. DOI: https://doi.org/10.1016/j.conbuildmat.2014.04.103. URL: http://www.sciencedirect.com/science/article/pii/S0950061814004292.

[20] Luisa Berto et al. “Shear behaviour of masonry panel: parametric FE analyses”. In: *International journal of solids and structures* 41.16 (2004), pp. 4383–4405.

[21] Z. T. Bieniawski. “Determining rock mass deformability: experience from case histories”. In: *International Journal of Rock Mechanics and Mining Sciences & Geomechanics Abstracts*. Vol. 15. 5. Elsevier. 1978, pp. 237–247.

[22] L. Binda, G. Mirabella Roberti, and C. Tiraboschi. “Problemi di misura dei parametri meccanici della muratura e dei suoi componenti”. In: *Atti del Convegno Nazionale La Meccanica delle Murature tra Teoria e Progetto, Messina* (1996).

[23] L. Binda and A. Saisi. *State of the art of research on historic structures in Italy*. 2001.

[24] L. Binda, A. Saisi, and C. Tiraboschi. "Investigation procedures for the diagnosis of historic masonries". In: *Construction and Building Materials* 14.4 (2000), pp. 199–233. ISSN: 0950-0618. DOI: http://dx.doi.org/10.1016/S0950-0618(00)00018-0. URL: http://www.sciencedirect.com/science/article/pii/S0950061800000180.

[25] L. Binda et al. "Repair and investigation techniques for stone masonry walls". In: *Construction and Building Materials* 11.3 (1997), pp. 133–142.

[26] Luigia Binda and Antonella Saisi. *Il ruolo delle indagini nella diagnostica strutturale*. 2003.

[27] Luigia Binda and Claudia Tiraboschi. "Flat-Jack Test: A slightly destructive technique for the diagnosis of brick and stone masonry structures". In: *Restoration of Buildings and Monuments* 5.5 (1999), pp. 449–472.

[28] A. Borri, M. Corradi, and A. Vignoli. "Nuove sperimentazioni per la valutazione della resistenza a taglio delle murature prima e dopo il rinforzo". In: *XI Congresso Nazionale "L'ingegneria Sismica in Italia", Genova*. 2004, pp. 25–29.

[29] Antonio Borri, Giulio Castori, and Marco Corradi. "Determination of shear strength of masonry panels through different tests". In: *International Journal of Architectural Heritage* 9.8 (2015), pp. 913–927.

[30] Antonio Borri et al. "A method for the analysis and classification of historic masonry". In: *Bulletin of Earthquake Engineering* 13.9 (2015), pp. 2647–2665.

[31] Anna Brignola et al. "Identification of shear parameters of masonry panels through the in-situ diagonal compression test". In: *International Journal of Architectural Heritage* 3.1 (2008), pp. 52–73.

[32] S. Caddemi et al. "An original discrete macro-elemen method for the analysis of historical structures". In: *Proceedings of the 16th European conference on earthquake engineering*. Vol. 195. 2018.

[33] Bruno Calderoni et al. "Problematiche di modellazione strutturale di edifici in muratura esistenti soggetti ad azioni sismiche in relazione all'utilizzo di software commerciali". In: *Proceedings of XVI Convegno ANIDIS, L'ingegneria sismica in Italia*. ANIDIS L'Aquila. 2015.

[34] I. Caliò. "La prova di scorrimento con martinetto piatto". In: *Proceedings of the XIV ANIDIS (Italian Nacional Association of Earthquake Engineering)* (2011), p. 157.

[35] I. Caliò, M. Marletta, and B. Pantò. "A simplified model for the evaluation of the seismic behaviour of masonry buildings". In: *Proceedings of the 10th international conference on civil, structural and environmental engineering computing. Stirlingshire, UK: Civil-Comp Press, Paper*. Vol. 195. 2005.

[36] Francesco Cannizzaro. "Un nuovo approccio di modellazione della risposta sismica degli edifici storici". PhD thesis. Università degli Studi di Catania, 2011.

[37] Nicholas J. Carino, Mary Sansalone, and Nelson N. Hsu. "A point source-point receiver, pulse-echo technique for flaw detection in concrete". In: *Journal Proceedings*. Vol. 83. 2. 1986, pp. 199–208.

[38] Alberto Carpinteri, Stefano Invernizzi, and Giuseppe Lacidogna. "Cracking simulation of brick-masonry elements subjected to the double flat-jack test". In: *Proceedings of the 6th International Conference on Structural Analysis of Historic Construction*. 2008, pp. 367–374.

[39] Alberto Carpinteri, Stefano Invernizzi, and Giuseppe Lacidogna. "In situ damage assessment and nonlinear modelling of a historical masonry tower". In: *Engineering Structures* 27.3 (2005), pp. 387–395.

[40] Alberto Carpinteri and Giuseppe Lacidogna. "Damage evaluation of three masonry towers by acoustic emission". In: *Engineering structures* 29.7 (2007), pp. 1569–1579.

[41] Alberto Carpinteri, Giuseppe Lacidogna, and Amedeo Manuello. "Damage mechanisms interpreted by acoustic emission signal analysis". In: *Key Engineering Materials*. Vol. 347. Trans Tech Publ. 2007, pp. 577–582.

[42] Alberto Carpinteri, Giuseppe Lacidogna, and Gianni Niccolini. "Critical behaviour in concrete structures and damage localization by acoustic emission". In: *Key Engineering Materials*. Vol. 312. Trans Tech Publ. 2006, pp. 305–310.

[43] Alberto Carpinteri, Giuseppe Lacidogna, and Gianni Niccolini. "Fractal analysis of damage detected in concrete structural elements under loading". In: *Chaos, Solitons & Fractals* 42.4 (2009), pp. 2047–2056.

[44] Alberto Carpinteri, Giuseppe Lacidogna, and Simone Puzzi. "From criticality to final collapse: Evolution of the "b-value" from 1.5 to 1.0". In: *Chaos, Solitons & Fractals* 41.2 (2009), pp. 843–853.

[45] J. Carvalho et al. "Safety analysis of modern heritage masonry buildings: Box-buildings in Recife, Brazil". In: *Engineering Structures* 80 (2014), pp. 222–240. ISSN: 0141-0296. DOI: https://doi.org/10.1016/j.engstruct.2014.09.004. URL: http://www.sciencedirect.com/science/article/pii/S0141029614005276.

[46] CEN. *Eurocode 6: Design of masonry structures - Part 1-1: General rules for reinforced and unreinforced masonry structures*. 2005.

[47] E. Cescatti et al. "Analysis and evaluations of flat jack test on a wide existing masonry buildings sample". In: *Proceedings of 16th International Brick & Block Masonry Conference*. CRC press London. 2016, pp. 1485–91.

[48] Sandro Chiostrini, Luciano Galano, and Andrea Vignoli. "On the determination of strength of ancient masonry walls via experimental tests". In: *Proc. of 12th World Conf. Earthquake Engrg*. 2000.

[49] T. C. Chu, W. F. Ranson, and Mr. A. Sutton. "Applications of digital image correlation techniques to experimental mechanics". In: *Experimental mechanics* 25.3 (1985), pp. 232–244.

[50] Baran Cobanoglu et al. "Seismic performance assessment of masonry buildings using in situ material properties". In: *Journal of Performance of Constructed Facilities* 31.4 (2017), p. 04017033.

[51] CEB-FIP Model Code et al. “Comite euro-international du beton”. In: *Bulletin d’information* 213 (1993), p. 214.

[52] Ing S Colombo, IG Main, and MC Forde. “Assessing damage of reinforced concrete beam using “b-value” analysis of acoustic emission signals”. In: *Journal of materials in civil engineering* 15.3 (2003), pp. 280–286.

[53] RILEM Technical Committee et al. “Recommendation of RILEM TC 212-ACD: acoustic emission and related NDE techniques for crack detection and damage evaluation in concrete”. In: *Materials and Structures* 43.9 (2010), p. 1183 1186.

[54] V. Compán et al. “Structural safety assessment of geometrically complex masonry vaults by non-linear analysis. The Chapel of the Würzburg Residence (Germany)”. In: *Engineering Structures* 140 (2017), pp. 1–13. ISSN: 0141-0296. DOI: https://doi.org/10.1016/j.engstruct.2017.03.002. URL: http://www.sciencedirect.com/science/article/pii/S0141029617307022.

[55] M. Corradi, A. Borri, and A. Vignoli. “Experimental study on the determination of strength of masonry walls”. In: *Construction and Building Materials* 17.5 (2003), pp. 325–337. ISSN: 0950-0618. DOI: http://dx.doi.org/10.1016/S0950-0618(03)00007-2.

[56] Marco Corradi et al. “Experimental evaluation of shear and compression strength of masonry wall before and after reinforcement: deep repointing”. In: *Construction and building materials* 22.4 (2008), pp. 463–472.

[57] Massimo Dalla Benedetta. “Qualificazione di murature storiche: procedure sperimentali in sito e calibrazione in laboratorio.” Phd Thesis. Università degli Studi di Padova, 2012.

[58] A. Drougkas, P. Roca, and C. Molins. “Compressive strength and elasticity of pure lime mortar masonry”. In: *Materials and Structures* 49.3 (Mar. 2016), pp. 983–999. ISSN: 1871-6873. DOI: 10.1617/s11527-015-0553-2. URL: https://doi.org/10.1617/s11527-015-0553-2.

[59] A. Elvin and H. C. Uzoegbo. “Response of a full-scale dry-stack masonry structure subject to experimentally applied earthquake loading: technical paper.” In: *Journal of the South African Institution of Civil Engineering= Joernaal van die Suid-Afrikaanse Instituut van Siviele Ingenieurswese* 53.1 (2011), pp. 22–32.

[60] Luca Facconi et al. “Improving shear strength of unreinforced masonry walls by nano-reinforced fibrous mortar coating”. In: *Materials and Structures* 48.8 (Aug. 2015), pp. 2557–2574. DOI: 10.1617/s11527-014-0337-0. URL: https://doi.org/10.1617/s11527-014-0337-0.

[61] D. Faiella, G. Manfredini, and P. P. Rossi. *In situ flat jack tests: analysis of results and critical assessment*. ISMES, 1983.

[62] Federal Emergency Management Agency. *Guidelines for the seismic rehabilitation of buildings*. 1997.

[63] W. A. Ferguson and J. Skandamoorthy. "The screw pull-out test for the in-situ measurement of the strength of masonry materials". In: *Proceedings of the Tenth International Brick/Block Masonry Conference*. 1994, pp. 1257–66.

[64] F. M. Fernandes, P. B. Lourenço, and F. Castro. "Ancient Clay Bricks: Manufacture and Properties". In: *Materials, Technologies and Practice in Historic Heritage Structures*. Ed. by Maria Bostenaru Dan, Richard Přikryl, and Ákos Török. Dordrecht: Springer Netherlands, 2010. Chap. 3, pp. 29–48. ISBN: 978-90-481-2684-2. DOI: 10.1007/978-90-481-2684-2_3. URL: https://doi.org/10.1007/978-90-481-2684-2_3.

[65] Denise Ferreira and Jonna Manie. *DIANA FEA BV - User's Manual - Release 10.2*. 2017.

[66] Dario Foppoli and Alessandro Armanasco. "Laboratory and In Situ Calibrations of New Flat Jack Method for Assessing Masonry Shear Characteristics". In: *Structural Analysis of Historical Constructions*. Cham: Springer International Publishing, 2019, pp. 513–522. ISBN: 978-3-319-99441-3.

[67] Dario Foppoli and Alessandro Armanasco. "Laboratory Calibration and In Situ Application of Test Methods to Assess Masonry Shear Characteristics thought Flat Jack (FJ-SCT Method)". In: *Atti del XVII Convegno ANIDIS L'ingegneria Sismica in Italia*. Pisa University Press, 2017, pp. 104–114.

[68] Dario Foppoli, Anselmo Pulcini, and Foppoli Moretta. "A New Method to Test Masonry Shear Characteristics Thought Flat Jack (FJ-SCT Method)". In: *19th World Conference on Non-Destructive Testing 2016 A* November (2016), pp. 1–9. URL: http://www.ndt.net/article/wcndt2016/papers/mo2c1.pdf.

[69] Max Mark Frocht. "Recent advances in photoelasticity and an investigation of the stress distribution in square blocks subjected to diagonal compression". In: *Trans. ASME* 53 (1931), pp. 135–153.

[70] Claude Froidevaux, Christian Paquin, and Marc Souriau. "Tectonic stresses in France: in situ measurements with a flat jack". In: *Journal of Geophysical Research: Solid Earth* 85.B11 (1980), pp. 6342–6346.

[71] Luca Gambirasio, Giulio Mirabella Roberti, and Egidio Rizzi. "Numerical simulations of flat-jack test setups for the local shear characterization of masonry panels". In: *International Journal of Masonry Research and Innovation* 1.4 (2016), pp. 306–329.

[72] T. N. Ganju. "Non-linear finite element analysis of clay brick masonry". In: *Proc. 6th Australasian Conf. on Mech. of Structures and Materials*. 1977, pp. 59–65.

[73] Tomasz Garbowski, Giulio Maier, and Giorgio Novati. "Diagnosis of concrete dams by flat-jack tests and inverse analyses based on proper orthogonal decomposition". In: *Journal of Mechanics of Materials and Structures* 6.1 (2011), pp. 181–202.

[74] MPS GdL. *Redazione della mappa di pericolosità sismica prevista dall'Ordinanza PCM 3274 del 20 marzo 2003, Rapporto Conclusivo per il Dipartimento della Protezione Civile, INGV, Milano-Roma, aprile 2004, 65 pp.+ 5 appendici*. 2004.

[75] Domenico Giardini, Jochen Wössner, and Laurentiu Danciu. "Mapping Europe's Seismic Hazard". In: *EOS* 95.29 (2014), pp. 261–262. DOI: 10.12686/SED-00000001-SHARE. URL: http://www.efehr.org:8080/jetspeed/portal/hazard.psml.

[76] Carbonara Giovanni. *Restauro Architettonico*. Vol. II. UTET, 1996.

[77] Michele Godio et al. "Quasi-static shear-compression tests on stone masonry walls with plaster: Influence of load history and axial load ratio". In: *Engineering Structures* 192 (2019), pp. 264–278. ISSN: 0141-0296. DOI: https://doi.org/10.1016/j.engstruct.2019.04.041.

[78] Paweł Gregorczyk and Paulo B. Lourenço. "A review on flat-jack testing". In: (2000).

[79] C. U. Grosse and M. Ohtsu. *Acoustic emission testing*. Springer Science & Business Media, 2008.

[80] Beno Gutenberg and Charles F. Richter. "Frequency of earthquakes in California". In: *Bulletin of the Seismological Society of America* 34.4 (1944), pp. 185–188.

[81] H. Hao and B. G. Tarasov. "Experimental Study of Dynamic Material Properties of Clay Brick and Mortar at Different Strain Rates". In: *Australian Journal of Structural Engineering* 8.2 (2008), pp. 117–132. DOI: 10.1080/13287982.2008.11464992.

[82] TG Hughes and R Pritchard. "An investigation of the significance of flatjack flexibility in the determination of in situ stresses". In: *Proceedings of the Tenth International Brick/Block Masonry Conference*. 1994, pp. 569–78.

[83] International Conference of Building Officials. *Uniform code for building conservation*. International Conference of Building Officials, 1991.

[84] M. Ispir et al. "Material Characterization of the Historical Unreinforced Masonry Akaretler Row Houses in Istanbul". In: *Journal of Materials in Civil Engineering* 22.7 (2010), pp. 702–713. DOI: 10.1061/(ASCE)MT.1943-5533.0000071. eprint: https://ascelibrary.org/doi/pdf/10.1061/. URL: https://ascelibrary.org/doi/abs/10.1061/.

[85] Italian Code. *Aggiornamento delle «Norme Tecniche per le Costruzioni», Decreto Ministeriale del 17/1/2018, Suppl. ord. n. 42 alla G.U. n. 42 del 20/2/2018.* 2018.

[86] Italian Code. *Circolare 2 febbraio 2009, n. 617 - Istruzioni per l'applicazione delle 'Nuove norme tecniche per le costruzioni' di cui al decreto ministeriale 14 gennaio 2008. (GU n. 47 del 26-2-2009 - Suppl. Ordinario n.27)*. 2008.

[87] Italian Code. *Circolare 21 gennaio 2019 - Istruzioni per l'applicazione dell'« Aggiornamento delle norme tecniche per le costruzioni» di cui al decreto ministeriale 17 gennaio 2018. (GU n. 35 del 11-2-2019 - Suppl. Ordinario n.27)*. 2019.

[88] Italian Code. *Norme Tecniche per le Costruzioni, Decreto Ministeriale del 14/1/2008, Suppl. ord. n. 30 alla G.U. n. 29 del 4/2/2008.* 2008.

[89] Pina-Henriques J. and Lourenço Paulo B. "Masonry compression: a numerical investigation at the meso-level". In: 23.4 (Jan. 2006), pp. 382–407. ISSN: 0264-4401. DOI: 10.1108/02644400610661163. URL: https://doi.org/10.1108/02644400610661163.

[90] Lorenzo Jurina. "La caratterizzazione meccanica delle murature parte seconda: martinetti piatti". In: *Proceedings of the International Conference CIAS*. 2007, pp. 133–150.

[91] Lorenzo Jurina, Paolo Bonaldi, and Pier Paolo Rossi. "Indagini sperimentali e numeriche sui dissesti del palazzo della regione di Milano". In: 1980.

[92] J. Kaiser. "An investigation into the occurrence of noises in tensile tests, or a study of acoustic phenomena in tensile tests". PhD thesis. 1950.

[93] Fillitsa V. Karantoni and Michael N. Fardis. "Computed versus observed seismic response and damage of masonry buildings". In: *Journal of Structural Engineering* 118.7 (1992), pp. 1804–1821.

[94] Meta Kržan et al. "Acquiring reference parameters of masonry for the structural performance analysis of historical buildings". In: *Bulletin of earthquake engineering* 13.1 (2015), pp. 203–236.

[95] J. Kubica. "Investigation of the stress–Strain relationship of unreinforced masonry". In: *Proceedings of the Seventh North American Masonry Conference, University of Notre Dame, Indiana*. 1996.

[96] S. Lagomarsino and S. Podestà. "Seismic Vulnerability of Ancient Churches: I. Damage Assessment and Emergency Planning". In: *Earthquake Spectra* 20.2 (2004), pp. 377–394. DOI: 10.1193/1.1737735. eprint: https://doi.org/10.1193/1.1737735. URL: https://doi.org/10.1193/1.1737735.

[97] S. Lagomarsino and S. Podestà. "Seismic Vulnerability of Ancient Churches: II. Statistical Analysis of Surveyed Data and Methods for Risk Analysis". In: *Earthquake Spectra* 20.2 (2004), pp. 395–412. DOI: 10.1193/1.1737736. eprint: https://doi.org/10.1193/1.1737736. URL: https://doi.org/10.1193/1.1737736.

[98] José V. Lemos. "Discrete Element Modeling of Masonry Structures". In: *International Journal of Architectural Heritage* 1.2 (2007), pp. 190–213. DOI: 10.1080/15583050601176868.

[99] T. Li and S. Atamturktur. "Fidelity and Robustness of Detailed Micromodeling, Simplified Micromodeling, and Macromodeling Techniques for a Masonry Dome". In: *Journal of Performance of Constructed Facilities* 28.3 (2014), pp. 480–490. DOI: 10.1061/(ASCE)CF.1943-5509.0000440.

[100] I. Lombillo. "Theoretical-experimental research about minor destructive tests (MDT) applied to the mechanical on-site characterization of historical masonry structures". PhD thesis. University of Cantabria, Santander, 2010.

[101] I. Lombillo, L. Villegas, and J. Elices. *Non (Minor) Destructive methodlogies applied to study and diagnosis of masonry structures of building heritage: a state of the art*. Building Technology R+ D Group of the University of Cantabria, ETS de Ingenieros de Caminos, Canales y Puertos. Santander, Spain. 2009.

[102] I. Lombillo et al. "In situ mechanical investigation of rammed earth: Calibration of minor destructive testing". In: *Construction and Building Materials* 51 (2014), pp. 451–460.

[103] I. Lombillo et al. "Mechanical characterization of rubble stone masonry walls using non and minor destructive tests". In: *Construction and Building Materials* 43 (2013), pp. 266–277.

[104] Paoulo B. Lourenço and J. A. Roque. "Simplified indexes for the seismic vulnerability of ancient masonry buildings". In: *Construction and Building Materials* 20.4 (2006). Structural Masonry and Earthquakes, pp. 200–208. ISSN: 0950-0618. DOI: https://doi.org/10.1016/j.conbuildmat.2005.08.027. URL: http://www.sciencedirect.com/science/article/pii/S0950061805002679.

[105] Paulo B. Lourenço. *A user/programmer guide for the micro-modeling of masonry structures*. 1996.

[106] Paulo B. Lourenço. "Computational strategies for masonry structures". PhD thesis. TU Delft, Delft University of Technology, 1996.

[107] Paulo B. Lourenço. "Computations on historic masonry structures". In: *Progress in Structural Engineering and Materials* 4.3 (2002), pp. 301–319.

[108] Paulo B. Lourenço. "Recent advances in masonry modelling: micromodelling and homogenisation". In: *Multiscale Modeling in Solid Mechanics*. 2010. Chap. -, pp. 251–294. DOI: 10.1142/9781848163089_0006.

[109] LUSAS. *Theory Manual Volume 1*. Version 15.2 : Issue 1.

[110] LUSAS. *Theory Manual Volume 2*. Version 15.2 : Issue 1.

[111] Eduarda Luso and Paulo B. Lourenço. "Experimental characterization of commercial lime based grouts for stone masonry consolidation". In: *Construction and Building Materials* 102 (2016), pp. 216–225. ISSN: 0950-0618. DOI: https://doi.org/10.1016/j.conbuildmat.2015.10.096. URL: http://www.sciencedirect.com/science/article/pii/S0950061815305183.

[112] G. Magenes. *Simplified models for the seismic analysis of masonry building*. G.N.D.T. Report (in Italian). 1999.

[113] G. Magenes and G. M. Calvi. "In-plane seismic response of brick masonry walls". In: *Earthquake Engineering & Structural Dynamics* 26.11 (1997), pp. 1091–1112.

[114] G. Magenes and A. D. Fontana. "Simplified non-linear seismic analysis of masonry buildings". In: *Proc. Br. Masonry Soc. No. 8*. 1998, pp. 190–195.

[115] Vincenzo Mallardo et al. "Seismic vulnerability of historical masonry buildings: A case study in Ferrara". In: *Engineering Structures* 30.8 (2008), pp. 2223–2241.

[116] Elizabeth Campbell Manning. "Enhancement of the tube-jack non-destructive test method for historical structural masonry diagnosis". Phd Thesis. Universidade do Minho, Portugal, 2016.

[117] Elizabeth Campbell Manning, Luıés F Ramos, and FM Fernandes. "Tube-jack testing: Semi-irregular masonry wall testing". In: *Structural Analysis of Historical Constructions: Anamnesis, diagnosis, therapy, controls*. CRC Press, 2016, pp. 732–739.

[118] Elizabeth Manning, Luıés F Ramos, and Francisco M Fernandes. "Tube-Jack Testing for Irregular Masonry Walls: Regular Masonry Wall Testing". In: *Journal of Nondestructive Evaluation* 35.3 (2016), pp. 1–13.

[119] Giancarlo Marcari et al. "In-plane shear performance of masonry panels strengthened with FRP". In: *Composites Part B: Engineering* 38.7 (2007), pp. 887–901. ISSN: 1359-8368. DOI: https://doi.org/10.1016/j.compositesb.2006.11.004. URL: http://www.sciencedirect.com/science/article/pii/S1359836806001570.

[120] Rui Marques and Paulo B Lourenço. "Unreinforced and confined masonry buildings in seismic regions: Validation of macro-element models and cost analysis". In: *Engineering Structures* 64 (2014), pp. 52–67.

[121] G. A. Marzahn, R. Jahnel, and N. V. Tue. "Finite element analysis of two ancient groined masonry vaults". In: *13th International Brick/Block Masonry Conference*. 2004, pp. 147–156.

[122] Nicola Mazzon. "Infuence of Grout Injection on the Dynamic Behaviour of Stone Masonry Buildings". Phd Thesis. Università degli Studi ti Padova, 2010.

[123] D. M. McCann and M. C. Forde. "Review of *NDT* methods in the assessment of concrete and masonry structures". In: *NDT & E International* 34.2 (2001), pp. 71–84. ISSN: 0963-8695. DOI: http://dx.doi.org/10.1016/S0963-8695(00)00032-3. URL: http://www.sciencedirect.com/science/article/pii/S0963869500000323.

[124] Carosena Meola. "Infrared thermography of masonry structures". In: *Infrared Physics & Technology* 49.3 (2007). Workshop on Advanced Infrared Technology and Applications, pp. 228–233. ISSN: 1350-4495. DOI: http://dx.doi.org/10.1016/j.infrared.2006.06.010.

[125] Gabriele Milani, Paulo Lourenço, and Antonio Tralli. "Homogenization approach for the limit analysis of out-of-plane loaded masonry walls". In: *Journal of structural engineering* 132.10 (2006), pp. 1650–1663.

[126] Michael Mistler, Christoph Butenweg, and Konstantin Meskouris. "Modelling methods of historic masonry buildings under seismic excitation". In: *Journal of Seismology* 10.4 (2006), pp. 497–510.

[127] C. Modena et al. "Design choices and intervention techniques for repairing and strengthening of the Monza cathedral bell-tower". In: *Construction and Building Materials* 16.7 (2002), pp. 385–395. ISSN: 0950-0618. DOI: https://doi.org/10.1016/S0950-0618(02)00041-7.

[128] Archana Nair and CS Cai. "Acoustic emission monitoring of bridges: Review and case studies". In: *Engineering structures* 32.6 (2010), pp. 1704–1714.

[129] Lucio Nobile et al. "Micro-Destructive Flat-Jack Test for the Diagnosis of Historic Masonry". In: *Advances in Fracture and Damage Mechanics VIII*. Vol. 417. Key Engineering Materials. Trans Tech Publications Ltd, Jan. 2010, pp. 741–744. DOI: 10.4028/www.scientific.net/KEM.417-418.741.

[130] J. L. Noland, R. H. Atkinson, and M. P. Schuller. "A review of the flat-jack method for nondestructive evaluation". In: *Proceedings, Conference on Nondestructive Evaluation of Civil Structures and Materials, Boulder, 00*. 1990.

[131] J. L. Noland, G. R. Kingsley, and R. H. Atkinson. "Utilization of nondestructive techniques into the evaluation of masonry". In: *Proceedings of the 8 th International Brick/Block Masonry Conference Dublin, Ireland, 19-21 September 1988*. 1988, pp. 1693–1703.

[132] James L. Noland, Gregory R. Kingsley, and Richard H. Atkinson. "Nondestructive evaluation of masonry: An update". In: *Masonry: Components to Assemblages*. ASTM International, 1990.

[133] Javier Ortega et al. "Assessment of the efficiency of traditional earthquake resistant techniques for vernacular architecture". In: *Engineering Structures* 173 (2018), pp. 1–27. ISSN: 0141-0296. DOI: https://doi.org/10.1016/j.engstruct.2018.06.101. URL: http://www.sciencedirect.com/science/article/pii/S0141029618304000.

[134] Javier Ortega et al. "Assessment of the influence of horizontal diaphragms on the seismic performance of vernacular buildings". In: *Bulletin of Earthquake Engineering* 16.9 (2018), pp. 3871–3904.

[135] Bing Pan et al. "Two-dimensional digital image correlation for in-plane displacement and strain measurement: a review". In: *Measurement science and technology* 20.6 (2009), p. 062001.

[136] Bartolomeo Panto et al. "Non-linear modeling of masonry churches through a discrete macro-element approach". In: *Earthquakes and Structures* 12.2 (2017), pp. 223–236.

[137] E. Papa. "Damage and failure models". In: *Computational modelling of masonry brickwork and blockwork structures. Stirling, Scotland: Saxe-Coburg Publications* (2001), pp. 1–26.

[138] S Parivallal et al. "Evaluation of in-situ stress in masonry structures by flat jack technique". In: *Proc. of the National Seminar and Exhibition of Non-Destructive Evaluation*. 2011.

[139] Vasco Peixoto de Freitas et al. "Minor destructive techniques applied to the mechanical characterization of historical rubble stone masonry structures". In: *Structural Survey* 28.1 (2010), pp. 53–70.

[140] W. H. Peters and W. F. Ranson. "Digital imaging techniques in experimental stress analysis". In: *Optical engineering* 21.3 (1982), pp. 213427–213427.

[141] Madalena Ponte, Rita Bento, and Silva Daniel Vaz. "A Multi-Disciplinary Approach to the Seismic Assessment of the National Palace of Sintra". In: *International Journal of Architectural Heritage* 0.0 (2019), pp. 1–22. DOI: 10.1080/15583058.2019.1648587. eprint: https://doi.org/10.1080/15583058.2019.1648587. URL: https://doi.org/10.1080/15583058.2019.1648587.

[142] J. S. Popovics. "NDE techniques for concrete and masonry structures". In: *Progress in Structural Engineering and Materials* 5.2 (2003), pp. 49–59. ISSN: 1528-2716. DOI: 10.1002/pse.146. URL: http://dx.doi.org/10.1002/pse.146.

[143] Presidente del Consiglio dei Ministri 9 febbraio 2011. *Valutazione e riduzione del rischio sismico del patrimonio culturale con riferimento alle Norme tecniche per le costruzioni di cui D.M. 14/01/2008 (GU n. 47 del 26-2-2011 - Suppl. Ordinario n.54)*. 2011.

[144] Bora Pulatsu et al. "Discontinuum analysis of the fracture mechanism in masonry prisms and wallettes via discrete element method". In: *Meccanica* 55.3 (2020), pp. 505–523. ISSN: 1572-9648. DOI: 10.1007/s11012-020-01133-1. URL: https://doi.org/10.1007/s11012-020-01133-1.

[145] Bora Pulatsu et al. "Simulation of uniaxial tensile behavior of quasi-brittle materials using softening contact models in DEM". In: *International Journal of Fracture* 217.1 (2019), pp. 105–125. ISSN: 1573-2673. DOI: 10.1007/s10704-019-00373-x. URL: https://doi.org/10.1007/s10704-019-00373-x.

[146] Giovanni Punzo. "Modellazione e analisi non lineare di murature esistenti". PhD thesis. Alma Mater Studiorum – Università di Bologna, 2016.

[147] W. Qinglin and W. Xiuyi. "The evaluation of compressive strength of brick masonry in-situ. 8 th Int". In: *Proceedings of the 8 th International Brick/Block Masonry Conference Dublin, Ireland, 19-21 September 1988*. 1988.

[148] Luıés F. Ramos and Ziba Sharafi. “Tube-jack testing for irregular masonry walls: first studies”. In: *Advanced Materials Research*. Vol. 133. Trans Tech Publ. 2010, pp. 229–234.

[149] Luıés F. Ramos et al. “Tube-jack testing for irregular masonry walls: Prototype development and testing”. In: *NDT & E International* 58 (2013), pp. 24–35.

[150] ReLUIS. *SubTask 3b.3 Misura in situ delle proprietà elastiche mediante l’uso di martinetto piatto doppio*. 2007.

[151] ReLUIS. *SubTask 3b.3 Misura in situ dello stato di sforzo mediante l’uso di martinetto piatto singolo*. 2007.

[152] RILEM TC 127-MS. “MS-D.6 In situ measurement of masonry bed joint shear strenght”. In: *Materials and Structures* 29.October 1996 (1996), pp. 459–475.

[153] RILEM TC 127-MS. “Test for masorny materials and structures - D.9: Determination of mortar strenght by the screw (helix) pull-out method”. In: *Materials and Structures* 30.July 1997 (1997), pp. 325–327.

[154] RILEM TC 177-MDT. “Masonry durability and on-site testing - D.4: In-situ stress tests based on the flat jack”. In: *Materials and Structures* 37.September 2004 (271 2004), pp. 491–496.

[155] RILEM TC 177-MDT. “Masonry durability and on-site testing - D.5: In-situ stress - strain behaviour tests based on the flat jack”. In: *Materials and Structures* 37.September 2004 (271 2004), pp. 497–501.

[156] RILEM TC LUM B6. “Diagonal tensile strength tests of small wall specimens, 1991”. In: *RILEM Recommendations for the testing and use of constructions materials* (1994), pp. 488–489.

[157] Pier Paolo Rossi. “Analysis of mechanical characteristics of brick masonry by means of non-destructive in-situ tests”. In: *Proc 6th international brick masonry conference. Rome*. 1982, pp. 77–85.

[158] Pier Paolo Rossi. “Prove distruttive e non distruttive per la caratterizzazione meccanica dei materiali”. In: *ISMES Bollettino* 130 (1980).

[159] Jan Gerrit Rots. “Computational modeling of concrete fracture”. PhD thesis. Delft University of Technology, 1988.

[160] T. Rotunno et al. “Experimental Study of Bond Behavior of CFRP-to-Brick Joints”. In: *Journal of Composites for Construction* 19.3 (2015), p. 04014063. DOI: 10.1061/(ASCE)CC.1943-5614.0000528.

[161] M. A. Saadeghvaziri and S. S. Metha. “An analytical model for URM structures”. In: *Proc. 6th North American Masonry Conf., Ed. AA Hamid and HG Harris, Philadelphia, Pennsylvania*. 1993, pp. 409–418.

[162] G. Sacchi Landriani and A. Taliercio. “Numerical analysis of the flat jack test on masonry walls”. In: *Journal de mécanique théorique et appliquée* 5.3 (1986), pp. 313–339.

[163] R. Vidya Sagar and B. K. Raghu Prasad. "A review of recent developments in parametric based acoustic emission techniques applied to concrete structures". In: *Nondestructive Testing and Evaluation* 27.1 (2012), pp. 47–68.

[164] R. Vidya Sagar, B. K. Raghu Prasad, and R. K. Singh. "Kaiser effect observation in reinforced concrete structures and its use for damage assessment". In: *Archives of Civil and Mechanical Engineering* 15.2 (2015), pp. 548–557. ISSN: 1644-9665. DOI: https://doi.org/10.1016/j.acme.2014.05.004. URL: http://www.sciencedirect.com/science/article/pii/S1644966514000831.

[165] A. Salmanpour and N. Mojsilovic. "Application of Digital Image Correlation for strain measurements of large masonry walls". In: *Conference Proceedings. APCOM & ISCM, Singapore*. 2013.

[166] Michael P Schuller. "FLAT JACK METHODS FOR DIAGNOSIS OF MODERN MASONRY". In: *PRO 26: International RILEM Workshop on On Site Control and Evaluation of Masonry Structures and Materials*. Vol. 26. RILEM Publications. 2003, p. 167.

[167] Michael P. Schuller. "Nondestructive testing and damage assessment of masonry structures". In: *Progress in Structural Engineering and Materials* 5.4 (2003), pp. 239–251. DOI: 10.1002/pse.160.

[168] Ramakrishnan Senthivel and Paulo B. Lourenço. "Finite element modelling of deformation characteristics of historical stone masonry shear walls". In: *Engineering structures* 31.9 (2009), pp. 1930–1943. ISSN: 0141-0296. DOI: https://doi.org/10.1016/j.engstruct.2009.02.046.

[169] P. R. Sheorey et al. "Schmidt hammer rebound data for estimation of large scale in situ coal strength". In: *International Journal of Rock Mechanics and Mining Sciences & Geomechanics Abstracts* 21.1 (1984), pp. 39–42. ISSN: 0148-9062. DOI: http://dx.doi.org/10.1016/0148-9062(84)90008-1. URL: http://www.sciencedirect.com/science/article/pii/0148906284900081.

[170] Peter Sheppard. *In-situ test of the shear strength and deformability of an 18th century stone-and-brick masonry wall*. 1985.

[171] Tomoki Shiotani. "Evaluation of long-term stability for rock slope by means of acoustic emission technique". In: *Ndt & E International* 39.3 (2006), pp. 217–228.

[172] Rui A. Silva et al. "Mechanical characterisation of dry-stack masonry made of {CEBs} stabilised with alkaline activation". In: *Construction and Building Materials* 75 (2015), pp. 349–358. ISSN: 0950-0618. DOI: http://dx.doi.org/10.1016/j.conbuildmat.2014.11.038.

[173] A. Simões et al. "Mechanical Characterization of Masonry Walls With Flat-Jack Tests". In: *Experimental Techniques* 40.3 (June 2016), pp. 1163–1178. ISSN: 1747-1567. DOI: 10.1007/s40799-016-0114-9. URL: https://doi.org/10.1007%20s40799-016-0114-9.

[174] B. Stafford Smith and C. Carter. "Distribution of stresses in masonry walls subjected to vertical loading". In: *Proc. 2nd Int. Brick Masonry Conference*. 1970, pp. 119–124.

[175] M. Solla et al. "GPR evaluation of the Roman masonry arch bridge of Lugo (Spain)". In: *NDT & E International* 44.1 (2011), pp. 8–12.

[176] B. Stafford Smith and K. M. K. Rahman. "The variations of stress in vertically loaded brickwork walls." In: *Proceedings of the Institution of Civil Engineers* 51.4 (1972), pp. 689–700.

[177] M. A. Sutton and J. Anderson. "Application of digital correlation methods to rigid body mechanics". In: *Optical Engineering* 22.6 (1983), pp. 738–742.

[178] M. A. Sutton et al. "Application of an optimized digital correlation method to planar deformation analysis". In: *Image and Vision Computing* 4.3 (1986), pp. 143–150.

[179] Theodosius P. Tassios and Nina Avramidou. *Meccanica delle murature*. Liguori, 1988.

[180] S. Tercelj, P. Sheppard, and V. Turnsek. "The influence of frequency on the shear strength and ductility of masonry walls in dynamic loading tests". In: *Proceedings of the Fifth International Conference on Earthquake Engineering*. Vol. 3. 1969, pp. 2292–9.

[181] Miha Tomaževič. "Shear resistance of masonry walls and Eurocode 6: shear versus tensile strength of masonry". In: *Materials and Structures* 42.7 (Aug. 2009), pp. 889–907. ISSN: 1871-6873. DOI: 10.1617/s11527-008-9430-6. URL: https://doi.org/10.1617/s11527-008-9430-6.

[182] Miha Tomaževič. "The computer program POR". In: *Report ZRMK* (1978).

[183] V. Turnšek and F. Čačovič. "Some experimental results on the strength of brick masonry walls". In: *Proceedings of the 2nd international brick-masonry conference. British Ceramic Society, Stoke-on-Trent*. 1971, pp. 149–156.

[184] Ali Ural et al. "Seismic performance of masonry buildings during the 2007 Bala, Turkey earthquakes". In: *Natural Hazards* 60.3 (Feb. 2012), pp. 1013–1026. ISSN: 1573-0840. DOI: 10.1007/s11069-011-9887-4. URL: https://doi.org/10.1007/s11069-011-9887-4.

[185] G. Vasconcelos and Paulo B. Lourenço. "In-plane experimental behavior of stone masonry walls under cyclic loading." In: *Journal of structural engineering* 135.10 (2009), pp. 1269–1277.

[186] Els Verstrynge et al. "Monitoring and predicting masonry's creep failure with the acoustic emission technique". In: *NDT & E International* 42.6 (2009), p. 518 523.

[187] N. Viale and G. Ventura. "A New Experimental Test for the Characterisation of Masonry Shear Parameters". In: *Proceedings* 2.8 (2018). ISSN: 2504-3900. DOI: 10.3390/ICEM18-05369. URL: https://www.mdpi.com/2504-3900/2/8/464.

[188] N. Viale and G. Ventura. "Shear Flat Jack Test for Evaluating Shear Characteristics on Unreinforced Masonry Structures". In: *International Journal of Architectural Heritage* (2020). DOI: 10.1080/15583058.2020.1734687.

[189] N. Viale et al. "AE Characterization of Brick Masonry Walls Mechanical Behavior: The Case-Study of Alessandria and Boves Barracks". In: *Mechanics of Masonry Structures Strengthened with Composite Materials III*. Vol. 817. Key Engineering Materials. Trans Tech Publications Ltd, Oct. 2019, pp. 563–570. DOI: 10.4028/www.scientific.net/KEM.817.563.

[190] N. Viale et al. "Linear and Non-linear FEM Analyses of Shear Flat Jack Tests Performed In Situ". Manuscript in preparation. 2020.

[191] R. Vicente et al. "In Situ Flat-Jack Testing of Traditional Masonry Walls: Case Study of the Old City Center of Coimbra, Portugal". In: *International Journal of Architectural Heritage* 9.7 (2015), pp. 794–810. DOI: 10.1080/15583058.2013.855840. eprint: https://doi.org/10.1080/15583058.2013.855840. URL: https://doi.org/10.1080/15583058.2013.855840.

[192] D. Woodham and M. Schuller. "Development of a flexible flatjack for quantitative evaluation of masonry". In: *Proceedings of the 9th North American Masonry Conference, Clemson, South Carolina*. 2003, pp. 990–1011.

[193] Emanuele Zamperini. "Caserme delle regioni nord-occidentali". In: *Le caserme e la città: i beni immobili della Difesa tra abbandoni, dimissioni e riusi*. Ed. by Franco Storelli and Francesca Turri. Palombi Editori, 2014, pp. 292–305.

[194] A. Zucchini and P. B. Lourenço. "A micro-mechanical model for the homogenisation of masonry". In: *International Journal of Solids and Structures* 39.12 (2002), pp. 3233–3255.

This Ph.D. thesis has been typeset by means of the TEX-system facilities. The typesetting engine was pdfLATEX. The document class was `toptesi`, by Claudio Beccari, with option `tipotesi=scudo`. This class is available in every up-to-date and complete TEX-system installation.